Titolo

State-of-Art and selection of techniques in multiphase flow measurement

Ente emittente   CIRTEN

PAGINA DI GUARDIA

Descrittori

Tipologia del documento: Rapporto tecnico/ Technical Report

Collocazione contrattuale: Accordo di programma ENEA-MSE: tema di ricerca "Nuovo nucleare da fissione"

Argomenti trattati: Reattori ad acqua leggera/Light Water Reactors

Sommario

That report has been issued in the frame of the second research programme of ENEA-MSE agreement and it is one of the deliverables of the task C "IRIS integral testing – special instrumentation selection" of the work-programme 2 "Evolutionary INTD reactors" of the research theme on "Nuovo Nucleare da Fissione".

The report deals with the instrumentation to be used for measuring two-phase flow. The analysis has been focused on instruments to be able to resist to all working conditions foreseen in the SPES-3 facility.

Note

Copia n.   **In carico a:**

				NOME			
2				FIRMA			
1				NOME			
				FIRMA			
0	EMISSIONE	28-09-2010		NOME	F. Bianchi		S. Monti
				FIRMA			
REV.	DESCRIZIONE	DATA			CONVALIDA	VISTO	APPROVAZIONE
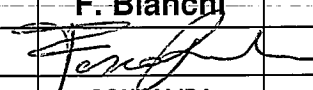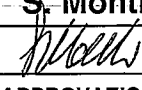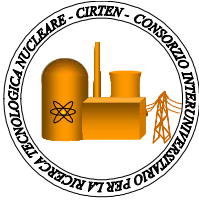
CIRTEN

Consorzio Interuniversitario
per la Ricerca Tecnologica Nucleare

POLITECNICO DI TORINO
DIPARTIMENTO DI ENERGETICA

State of art and Selection of techniques in Multiphase Flow Measurement

Cristina Bertani, Mario De Salve, Mario Malandrone, Grazia Monni,

Bruno Panella

1

Summary

List of Figures

5

List of Tables:

1. Introduction

The measurement of two-phase flow quantities is essential for the understanding of many technical processes, especially reactor system behaviour under accident conditions, and is also a prerequisite for proper code modelling and verification.

More than 25 years have been spent on developing various solutions for measuring two-phase flow with the aim to:

- obtain local or integral information,

- build very sensitive (but usually also fragile) instruments and try to improve the precision of the more rigid sensors as well, and

- apply techniques that are simple to use and to interpret and to install highly sophisticated instruments.

In spite of these efforts, there is no and perhaps never will be a Standard or Optimum Instrumentation. Measuring two-phase flow will always require experienced researchers using special solutions for each required purpose.

Successful application of a measuring system in a two-phase test setup does not automatically guarantee its applicability for nuclear reactor conditions, or even for other test loops if environmental conditions such as radiation levels or even simply water quality change. In addition, two-phase measuring techniques in many cases do not measure directly the two-phase properties

(such as local shear, velocities of the single phases etc.) needed to verify the two-phase models so that indirect comparison of calculated and measured data is needed.

Despite these not very encouraging facts, the large reactor safety research programs performed in the last decade as well as the detailed development work carried out at numerous universities and research institutions have significantly increased our knowledge of two-phase flow measurement techniques.

But the key to fundamental understanding of two-phase flow is still careful development of specialized instrumentation, in particular for special and complex geometrical applications.

In addition, development of special algorithms is sometimes necessary to interpret the measurement signals under many possible two-phase conditions.

2. TWO PHASE FLOW PARAMETERS

Multiphase flow is a complex phenomenon which is difficult to understand, predict and model. Common single-phase characteristics such as velocity profile, turbulence and boundary layer, are thus inappropriate for describing the nature of such flows.

The flow structures are classified in flow regimes, whose precise characteristics depend on a number of parameters. The distribution of the fluid phases in space and time differs for the various flow regimes, and is usually not under the control of the designer or operator.

Flow regimes vary depending on operating conditions, fluid properties, flow rates and the orientation and geometry of the pipe through which the fluids flow. The transition between different flow regimes may be a gradual process.

The parameters used to characterise the two phase flow are:
- Mass flow and velocity
- Temperature
- Void fraction
- Local void fraction
- Critical heat flux
- Liquid level and film thickness
- Flow regimes
- Wall shear stress and turbulence
- Velocity distribution

The determination of flow regimes in pipes in operation is not easy. Analysis of fluctuations of local pressure and/or density by means of for example gamma-ray densitometry has been used in experiments and is described in the literature. In the laboratory, the flow regime may be studied by direct visual observation using a length of transparent piping. Descriptions of flow regimes are therefore to some degree arbitrary, and they depend to a large extent on the observer and his/her interpretation.

The main mechanisms involved in forming the different flow regimes are transient effects, geometry effects, hydrodynamic effects and combinations of these effects.

For a complete review on flow pattern see Rouhani et Sohal (1982).

Transients occur as a result of changes in system boundary conditions. This is not to be confused with the local unsteadiness associated with intermittent flow. Opening and closing of valves are examples of operations that cause transient conditions.

Geometry effects occur as a result of changes in pipeline geometry or inclination.

In the absence of transient and geometry effects, the steady state flow regime is entirely determined by flow rates, fluid properties, pipe diameter and inclination. Such flow regimes are seen in horizontal straight pipes and are referred to as "hydrodynamic" flow regimes.

All flow regimes however, can be grouped into dispersed flow, separated flow, intermittent flow or a combination of these (see Fig. 1 and Fig. 2)

• Dispersed flow is characterised by a uniform phase distribution in both the radial and axial directions. Examples of such flows are bubble flow and mist flow.

• Separated flow is characterised by a non-continuous phase distribution in the radial direction and a continuous phase distribution in the axial direction. Examples of such flows are stratified and annular .

• Intermittent flow is characterised by being non-continuous in the axial direction, and therefore exhibits locally unsteady behaviour. Examples of such flows are elongated bubble, churn and slug flow. The flow regimes are all hydrodynamic two-phase gas-liquid flow regimes.
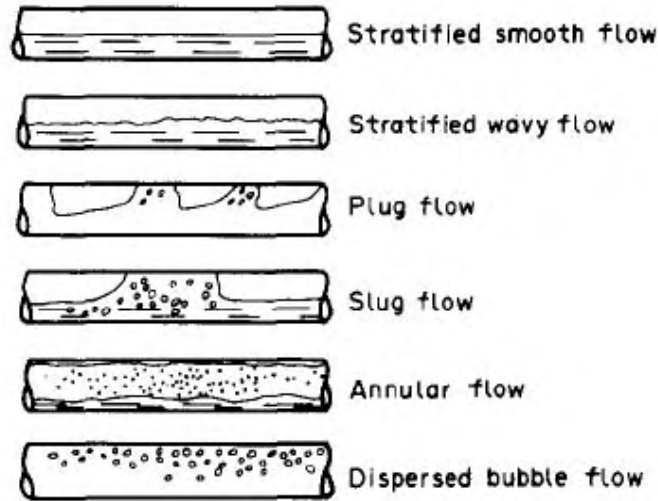
Fig. 1: Schematics of horizontal flow regimes
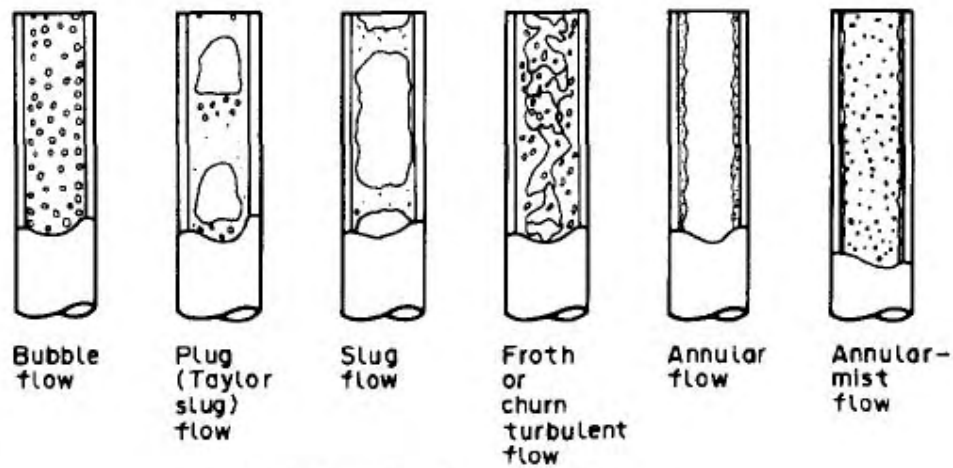
Fig. 2: Schematics of vertical flow regimes

For a quantitative description of the conditions which lead to the transition of flow regimes from one pattern to another it is necessary to define a set of parameters or parameter groups which show a direct bearing on such transitions. In a simplistic approach two of the main flow parameters may be used to define a coordinate system in which the boundaries between different flow regimes may be charted. This would then represent a flow regime map.

One such simplistic two-dimensional coordinate system could be defined by mass velocities of vapor and liquid in the channel, or by using the so called superficial phase velocities of vapor and liquid (mass flow rate of the particular phase divided by its density and total flow area). Such a simple coordinate system is

11

perhaps adequate for identifying the operating conditions that specify various regimes for a given fluid in a fixed geometry (pipe diameter and wall surface nature). But it would not be useful for making any generalization to other fluids or other geometries regarding the conditions which would cause flow regime transitions. This is because many different parameters affect the occurrence of various flow regimes and it is not possible to represent flow regime transition criteria in terms of only two simple variables.

Baker (1954) was one of the first ones to use some relevant groups of flow variables as flow regime
description coordinates. Baker's flow regime map was based on observations on cocurrent flow of gaseous and condensate petroleum products in horizontal pipes The diagrams in Fig. 3 is   qualitative illustrations of how flow regime transitions are dependent on superficial gas and liquid velocities in vertical multiphase flow. In Fig. 4 is illustrate the Taitel and Dukler' map for horizontal flow, and in Fig. 5 a comparison is made for vertical flow, with Ishii and Mishima's map.
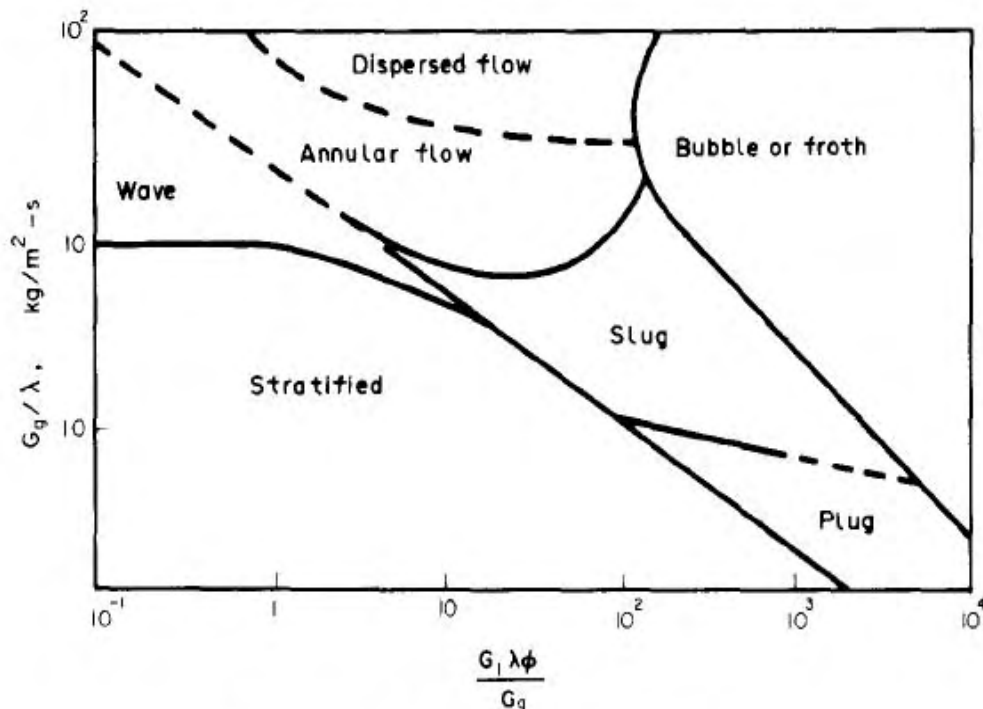
Fig. 3: Baker's horizontal flow pattern map

Although Baker's flow map coordinates includes these apparently relevant variables for scaling a variety of different conditions, later investigations showed that this map did not adequately predict horizontal flow regimes in all situations. There are many other coordinate systems for flow regime maps suggested by different investigators. A few of these are summarized in Tab. 1.

Abscissas	Ordinates	Suggested/Used by
$\psi = \dfrac{\text{Gas Vol. Flow}}{\text{Total Vol. Flow}}$	$Fr_m \approx \dfrac{(V_{gs} + V_{\ell s})^2}{g D_h}$	
V_{gs}	$V_{\ell s}$	Griffith and Wallis (1961)
$\rho_g V_{gs}^2$	$\rho_\ell V_{\ell s}^2$	Hewitt and Roberts (1969)
G_{tot}	X (steam weight fraction)	Bergles *et al.* (1968)

<div align="center">

Tab. 1: Some of flow pattern map coordinates

</div>

<div align="center">
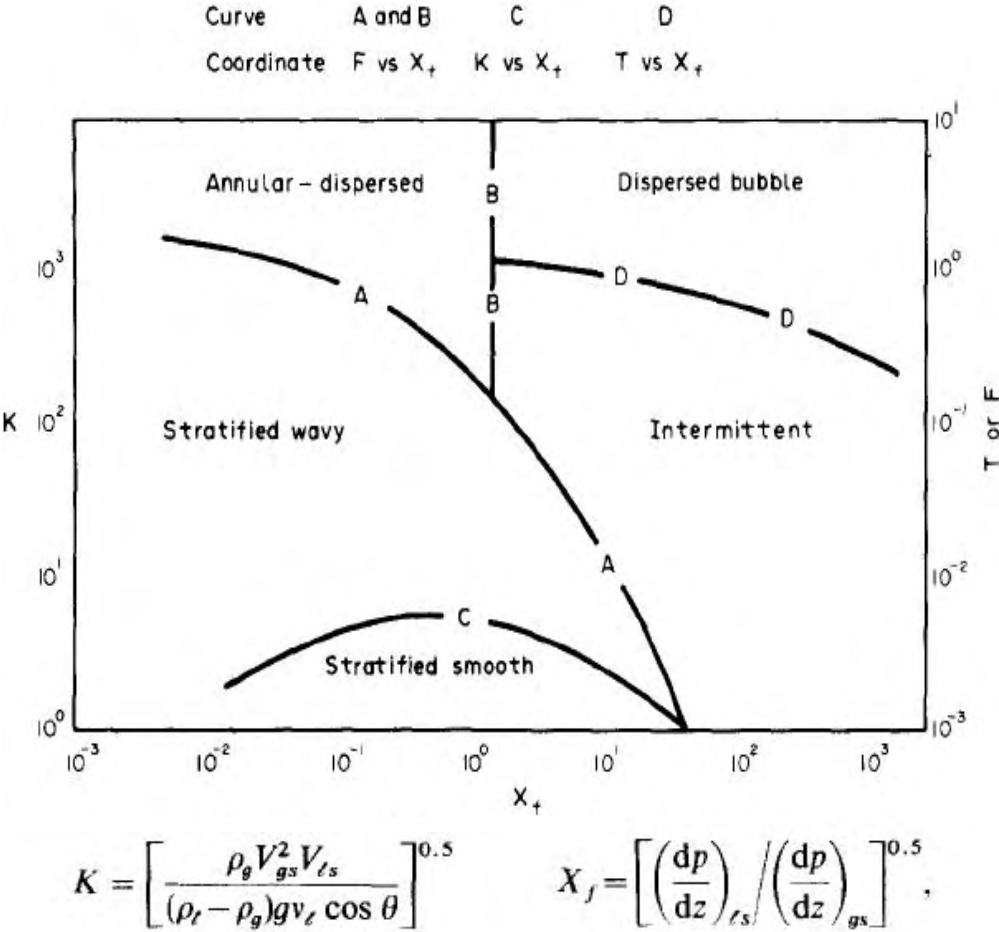
Fig. 4: Taitel and Dukler's (1976) horizontal flow map

</div>

$$K = \left[\frac{\rho_g V_{gs}^2 V_{\ell s}}{(\rho_\ell - \rho_g) g v_\ell \cos\theta}\right]^{0.5} \qquad X_f = \left[\left(\frac{\mathrm{d}p}{\mathrm{d}z}\right)_{\ell s} \Big/ \left(\frac{\mathrm{d}p}{\mathrm{d}z}\right)_{gs}\right]^{0.5},$$
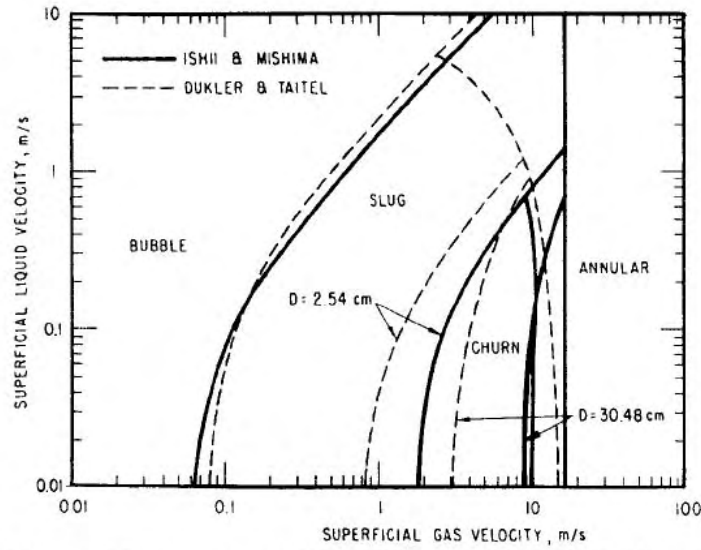
Fig. 5: Comparison of the verical flow pattern maps of Ishii and Mishima (1980) with of Taitel and Dukler.

Another way to classify multiphase flow, apart from the classification according to the flow pattern, is by the void fraction value of the flow. This method of classification is relevant to multiphase metering; a meter measuring predominately liquid with just a few percent gas would be significantly different from one designed to operate in what is generally understood as a wet gas application. Four classes are defined in Tab. 2

Class	Indicative GVF range	Comment
Low GVF	0 - 25%	This Low GVF range of multiphase flow could also be termed 'gassy liquid'. In the lower end of this range traditional single-phase meters could in many cases provide the sufficient measurement performance. Increasing measurement uncertainty, and also risk of malfunctioning must be expected as the GVF increases.
Moderate GVF	25% - 85%	The Moderate GVF can be considered as the 'sweet spot' of multiphase meters, i.e. the range where they have their optimum performance, and where at the same time traditional single-phase meters are not a viable option.
High GVF	85% - 95%	Entering this High GVF range the uncertainty of multiphase meters will start to increase, with a rapid increase towards the upper end of the range. This increase in uncertainty is not only linked to more complex flow patterns at high gas fraction, but also because the measurement uncertainty will increase as the relative proportion of the fraction of the component of highest value (in this case the oil) decreases. In some cases partial separation (see 7.1.2.2) is used to move the GVF back into the Moderate GVF range.
Very high GVF	95% - 100%	This upper end of the multiphase range could also be termed the 'wet gas' range. In the lower end of the very high GVF range the measurement performance of in-line multiphase meters may still be sufficient for well testing, production optimisation and flow assurance. For allocation metering, in particular at the high end of this range, often gas is the main 'value' component, and a wet gas meter would be the preferred option. This corresponds to a Lockhart-Martinelli (LM) value in the range from 0 to approximately 0.3.

Tab. 2: Classification of Multiphase flow, based on void fraction value (HMPF (2005))

3. INSTRUMENTS CLASSIFICATIONS

The needs of the chemical, petrochemical, gas and oil pipeline, and nuclear industries and the availability of advanced signal-processing techniques stimulate rapid developments in instrumentation applicable to two-phase flow measurements.

The objective of multiphase flow metering is to determine the flow rates of the individual components, for example water and gas or water and steam.

Unfortunately there is no single instrument, which will measure these parameters directly and it is necessary to combine several devices in an instrument package and to calculate the specific flow rates from the combined readings. There are many possible combinations, and the number of instruments required depends upon whether or not the components can be mixed together upstream of the instrumentation (homogeneous flow). If homogeneity of flow can be achieved, then only three instruments are required, each measuring a characteristic of the mixed fluid flow; if not, then individual component velocities and concentrations have to be determined.

Excellent reviews have been written on the state of the art of two-phase flow instrumentation. See, for example, Baker (2000), Hewitt (1978), and Miller (1996).

In the previously paragraph the parameters that characterized the two phase flow has been defined.

For measurement purpose an instrument classification can be made considering which parameter can be measured and through which physical principle the instrument operate.

The following main categories can be applied:

• In-line meters

• Separation type meters

    − Full two-phase gas/liquid separation

    − Partial separation

    − Separation in sample line

In-line meter performed directly in the multiphase flow line, hence, no separation and/or sampling of the fluids are required.

The volume flow rate of each phase is represented by the area fraction multiplied by the velocity of each phase. This means that a minimum of six parameters has to be measured or estimated (*T, p, v, W, x, alph*a or *ρ*).

Meter classification considering the parameter measured is:

- Density(*ρ*) meter
- Velocity (*v*) meter
- Momentum (ρv^2) meter
- Mass flow (ρv) meter

The physical principles of the different flow meter are:

- Mechanical
- Hydraulic
- Acoustic
- Electrical
- Gamma and X-ray
- Neutrons
- Microwave attenuation
- Infrared spectroscopy

The different physical working principle are used to measure different parameters (Baker (2000)):

Measurement of density (*ρ*)

- Gamma-ray (*γ*) absorption
- Neutron (*n*) interrogation
- Weighing of tube
- Hot film anemometer
- Capacitance / Conductance probes
- Ultrasonic flowmeter

Measurement of velocity (*v*)

- Pulsed-neutron activation
- Electromagnetic flow meter
- Turbine flowmeter
- Gamma-ray cross correlation
- Neutron cross correlation
- Acoustic cross correlation

- Capacitance/conductivity cross correlation

- Laser Doppler velocimeter

Measurements of mass flow (ρv)

- True mass flow meter

- Vibrating tube

- Differential pressure flowmeters

Measurements of momentum flux (ρv^2)

- Venturi meter

- Drag Disk

The choice of a meter (involving at least two separate measuring devices) to measure flow rates in two-phase flow (Hewitt 1978) depends on the purpose for which the measurement is made, and the accuracy required. It also depends on the nature of the flow field and the two phases involved.

The devices employed can be either nonintrusive (external to the flow field or, at most, part of the pipe/fluid interface) or intrusive (thus distorting the flow geometry at the place of measurement).

Nonintrusive devices can use tomographic techniques to sense local characteristics of the motion. Some intrusive devices provide global measurements, and some (local optical, electrical, or pressure probes) provide local phase flow rates.

The relative magnitudes of the instrumental length scales (pipe diameter, probe tip radius, piezoelectric crystal diameter), the dispersed phase length scale (particle, drop or bubble "diameters," film thickness), and the wave length of the sensing radiation (whether electromagnetic or acoustic) restrict the nature of the information provided by any device and hence affect how fluxes are deduced.

It is almost always helpful to have overall kinematic information about phase distributions and phase velocities when selecting a measurement technique for a particular flow.

The measurement of two-phase mass flow rate is of primary importance in experimental programs involving loss-of-coolant studies. Because of the severe environments present during blowdown, relatively few instrument types have gained widespread acceptance; these include turbine meters, gamma densitometers, and drag flowmeters. (Pressure and temperature measurements are

also required for reduction of data from the other instruments.) located in a relatively short piping segment called a spool piece. The design of spool pieces is important because intrusive meter may seriously alter the flow regime. On the other hand, location of all the instruments in close proximity is desirable because of the often unsteady and inhomogeneous nature of two phase flow.

In the last few years many efforts were made by scientists all over the world to understand the physics of the chain 'pipe configuration-disturbed flow profile-change in flowmeter behaviour and to find out effective methods and techniques to minimise these installation effects.

The relation between disturbed flow profile and change of flowmeter behaviour alone already presents a huge field of problems. Installation effects basically depend on the technical principle and construction of the flowmeter itself. The resulting problems are therefore unique for every type of flowmeter.

One truly two-phase fluid is steam. Superheated steam may be treated as a gas and its properties are well tabulated. However, it is increasingly important to measure the flow of wet steam made up, say, of about 95 per cent (by mass) vapour and about 5 per cent liquid. The droplets of the liquid are carried by the vapour, but will not follow the vapour stream precisely.

The measurement of such a flow causes major problems, since the pressure and temperature remain constant while the dryness fraction changes. It is therefore not possible to deduce the dryness fraction or density from the pressure and temperature, and in addition the droplets will cause an error in the flowmeter's registration.

These complex flows have been extensively studied, and flow pattern maps have been developed to indicate the conditions under which the various flow regimes occur.

However, these tend to be limited in their application to particular fluid combinations and pipe sizes.

The response of a meter in two-phase flow tends to be high sensitive to the flow pattern and to the upstream configuration and flow history. The best practice is to calibrate the instruments with known phase flow rates and with an exact simulation of the upstream pipework. The flow pattern is likely to be also time dependant in transient tests.

Though the ideal is to use in situ calibration, the more usual method is to interpret the measurement from an instrument in terms of a theory whose validity is tested by conducting separate experiments. Very often these experiments are conducted for very different flow conditions and fluids: instruments used for steam/water flows are frequently calibrated using air/water flows.

The response of a flowmeter may be different in transient situation and it's better to find a way to correct for this.

The basis of proper meter selection is a general awareness of flow measurement science and a clear understanding of specific application requirements.

General Meter Selection Factors

For end users, there are a number of specific issues to keep in mind when choosing a flow-metering instrument. Different flowmeters are designed for optimum performance in different fluids and under different operating conditions. That's why it is important to understand the limitations inherent to each style of instrument. Measuring the flow of liquid and gases (two- phase flow) demands superior instrument performance. In the reactor studies context this measurement is complicated by the fact that during the transient, the fluid becomes a nonhomogeneous mixture of liquid water and steam at. or very near saturation. In addition, materials from which the transducer is fabricated must be carefully chosen for their ability to survive the destructive effects of the water chemistry and radiation.

Process Conditions

In high-pressure flow applications, the "water hammer" effect can severely damage conventional flow measurement devices. Water hammer (or, more generally, fluid hammer) is a pressure surge or wave caused by the kinetic energy of a fluid in motion when it is forced to immediately stop or change direction. For example, if a valve is closed suddenly at an end of a pipeline system, a water hammer wave propagates in the pipe. Ideally, an industrial flowmeter, whether it employs mechanical or electromagnetic principles, should respond instantly and consistently to changes in water velocity. Meters, however, are not perfect instruments and may not accurately register velocity in all measurement conditions encountered. Turbulent or pulsating flows can cause registration errors in meters. In recent years, instrument suppliers have developed new PD meter

configurations for pulsating flow streams encountered in batch applications. These meters, employing a bearingless design and non-intrusive sensors.

Flowmeter Accuracy

In situations where flowmeters are used to give an indication of the rate at which a liquid or gas is moving through a pipeline, high accuracy is not crucial. But for batching, sampling and dispensing applications, flowmeter accuracy can be the deciding factor between optimum quality and wasted product. Typically, flowmeter accuracy is specified in percentage of actual reading (AR), in percentage of calibrated span (CS), or in percentage of full-scale (FS) units. Accuracy requirements are normally stated at minimum, normal, and maximum flow rates. The flowmeter's performance may not be acceptable over its full range.

Response time is another key flowmeter performance criteria.

Fluid Compatibility

For special applications flowmeters can be constructed with specialized materials. In addition to 316 stainless steel and Hastelloy, standard flowmeter wetted parts are manufactured from Tantalum, Monel, Nickel, Titanium, Carbon Steel, and Zirconium. Flowmeter manufacturers have invested considerable time and resources to develop meter designs utilizing thermoplastic materials able to handle corrosive liquids and gases. For example, all-plastic PD meters are ideal for aggressive liquid flow applications, including acids, caustics, specialty chemicals, and DI water. Ultrasonic flowmeters have no moving or wetted parts, suffer no pressure loss, and provide maintenance-free operation— important advantages over conventional mechanical meters such as vortex meters, and also, in many cases, coriolis mass meters. Clamp-on ultrasonic meters are mounted completely external to the pipe wall, so they are not affected by corrosive or erosive liquids, and are not damaged by solids, gases or particles in the process liquid.

Pipe Size, Configuration

When evaluating a flowmeter installation, the flow direction, pipe size, pipe material, flange-pressure rating, accessibility, up or downstream turns, valves, regulators, and available straight-pipe run lengths must be evaluated. The amount

of available installation space may dictate the choice of flowmeter technology. Where there is limited room, larger instrument designs like Coriolis meters may not be feasible. Vortex, turbine and PD meters, as well as a handful of other technologies, are a wiser choice under these circumstances. Nearly all flow instruments must be installed with a significant run of straight pipe before and after the location of the meter. Elbows, reducers, chemical injection ports, filters, screens and valves can cause radial, tangential and axial swirling effects within the pipe. In combination, these changes can rapidly distort the velocity profile, degrading the flowmeter's accuracy and repeatability. Many flow measurement instruments require straightening vanes or straight upstream piping to eliminate distorted patterns and swirls. This involves the installation of additional diameters of straight pipe run before the flow straightener, and between the straightener and the flowmeter itself.

Maintenance Needs

Flowmeters with few or no moving parts require less attention than more complex instruments. Meters incorporating multiple moving parts can malfunction due to dirt, grit and grime present in the process fluid. Meters with impulse lines can also plug or corrode, and units with flow dividers and pipe bends can suffer from abrasive media wear and blockages. Moving parts are a potential source of problems, not only for the obvious reasons of wear, lubrication and sensitivity to coating, but also because they require clearance spaces which sometimes introduce "slippage" into the flow being measured. Even with well-maintained and calibrated meters, this unmeasured flow varies with changes in fluid viscosity and temperature. Temperature changes also change the meters internal dimensions and require compensation.

Flow-meter selection criteria for the SPES 3 facility

The most important criteria that the flow-meter has to satisfy, are listed below, with a brief explanation:

Two phase flow handling capability and easy modelling

Existing experimental evidence the meter design can effectively handle two-phase flow is a required prerequisite, since new meter concepts cannot be explored in industrial testing. First approximated modelling capability of the meter response is as well required. Two-phase flow metering is not standardized, so that meters response has to be somewhat tailored for every application. In this respect, a highly sophisticated instrument that is to be taken as a black box is not suited for practical use.

High Span (minimal number of parallel lines)

The break flow is expected to vary in a wide range, so that the capability of the meter to cover a huge span is a good prerequisite. If a wide range meter is not available, the only solution is to build a proper number of parallel lines in order to use more than one meter for different mass flow rates.

Good Repeatability and Accuracy

The repeatability of the instruments has to be as good as possible in order to guarantee the correspondence of values collected in different times, but in the same operation condition.

Minimal Installation Constraints (straight pipe length between the meter and the disturbance source) -A minimal straight pipe length is required in front and after the instrument in order to avoid disturbance to the velocity profile.

A distorted profile (different from the complete developed profile) could cause an error in the instrument response.

Simplicity of Calibration; effects of calibration and operation temperature differences (different fluid properties, flow-meter material expansion)

The meter has to be as independent as possible from the temperature difference between the calibration and the operation condition. Calibration in cold conditions is easier, while specific facilities are required in hot conditions and the costs increases. If the calibration of the instrument in hot condition was not possible, some simple correction, with known expressions, would have to be applied to the collected data.

Capability of Handling Different Flow Regimes (temperature range, pressure range)

There are some cases in which the flow is far away from being homogeneous, because particular temperature and pressure conditions could cause the separation of the two phases. These different types of flow regime could cause a misleading response of the flow-meter, because not all the flow-meters are able to spanning all the pipe section to detect average values of the measured quantity.

Transient Operation Capability (time response)

Since the break discharged flow is not steady state, a good transient capability is a required prerequisite. The capability to follow fast transient is required, or at least the capability to mathematically model the dynamic response of the meter so as to correct the signal for dynamic effects.

Bi-directional Operation Capability

Both Reactor Pressure Vessel discharge into the Containment and possible reverse flow from the Containment into the Reactor Pressure Vessel have to be measured.

Minimal Regulatory Requirements

The process that leads to the installation of the instruments has to be as fast as possible, according with the current legislation.

Suitable Physical Dimension

Instrumentation dimensions and weight need to be consistent with the available space and support facilities. The instruments dimensions are likely to be the more critical issue.

Minimal Disturbance to the Flow

In order to avoid any significant alteration of the thermal-hydraulic coupling between the Reactor Pressure Vessel and the Containment that could drive somewhat the testing and that the testing is intended to explore, the disturbance to the discharged flow caused by the meter should be as low as possible.

Simplicity of Data Acquisition

The instrumentation needed to collect the data generated by the flow-meter has to operate independently from the fluid conditions and the necessary power supply and electrical equipment has to cope with the SIET available facilities.

Capability of Operating in Different Assembling Orientation (horizontal, vertical, inclined)- Some meters require particular assembling orientation in order to avoid inhomogeneous configuration of the flow pattern and entrapment of

gas bubbles near to the sensors position, both leading to an incorrect measurement of the fluid flow. This constraint could be an issue for the design of the SPES3 pipelines, because of the spatial orientation of the pipes.

Cavitation

The cavitation phenomenon should be avoided.

In the 2003 Yeung and Ibrahim proposed a selection of multiphase sensors based on the following criteria:

1. known behaviour in oil/water/gas flows
2. frequency (or dynamic response)
3. complexity of sensor output processing
4. commercial availability
5. cost
6. non-intrusive design
7. reproducibility
8. ruggedness/complexity

Based on the analysis of previous works they built the following table:

Sensor	Criteria							
	i	ii	iii	iv	v	vi	vii	viii
Absolute pressure	A	A	A	A	A	A	A	A
Differential pressure	A	A	A	A	A	A	A	A
Conductance	A	A	A	B	B	A	A	A
Impedance	A	A	A	B	B	A	A	A
Gamma	A	B	A	A	B	A	A	B
X-ray	A	B	B	B	C	A	A	B
Ultrasonic	B	B	B	B	B	A	B	B
Microwave	B	B	B	B	B	A	B	B
Infrared/optical	B	C	C	B	B	A	B	B

Tab. 3: Selection of sensor (Yeung and Ibrahim, 2003)

The present work would give insight into the topic, analyse concepts and problems that span a range of meter types and consider some of the approaches to the design of meters for two phase flows.

This searches could miss relevant papers and many papers are necessarily covered only very briefly.

It is not possible to cover the subject exhaustively here, so we restrict the analysis at only few instruments. The reader is referred to the books by Baker (2000) for more information.

4. TURBINE METERS

The turbine-meter is essentially a turbine rotor which rotates as the fluid passes through its blades. The turbine output, registering a pulse for each passing blade, can be used to calculate the fluid velocity and the Volumetric flux; is actually the most important volumetric meter.

According to the installed direction of a rotor shaft, two types of turbine flowmeter are available: axial type turbine flowmeter and tangential type turbine flowmeter, and the axial type turbine flowmeter is usually called a turbine flowmeter now.

The original tangential type turbine flowmeter (Stine (1977)) was invented in 1961 and is used to measure micro-flow rate. This type of the meter does not have wide application because of its unformed structure. However, some performances of a tangential type turbine flowmeter are still better than a turbine flowmeter, such as lower limit of measurement range, higher sensitivity and faster dynamic response. In general, the research on tangential type flowmeters is still limited now.

The modern axial turbine flowmeter, when properly installed and calibrated, is a reliable device capable of providing high accuracies (of about 0.2%) for both liquid and gas volumetric flow measurement.
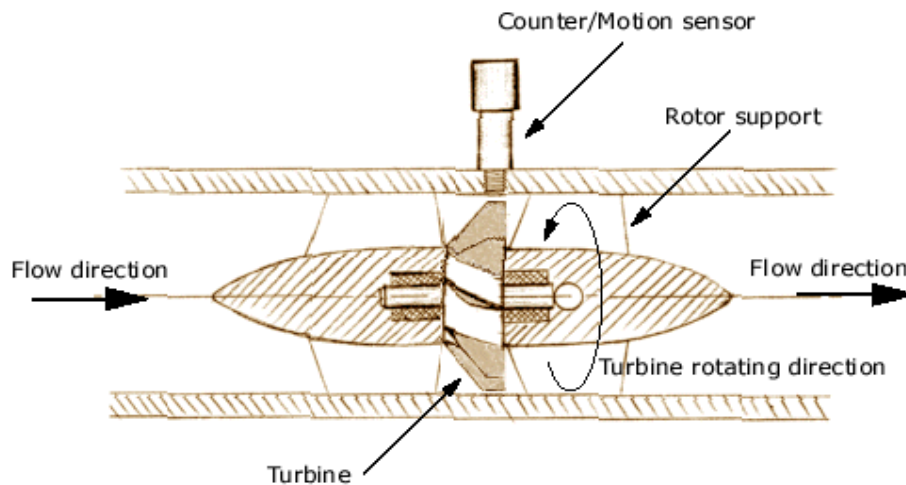
Fig. 6: Axial turbine flowmeter

General performance characteristics

Axial turbines perform best when measuring clean, conditioned, steady flows of gases and liquids with low kinematic viscosities (below about 10^{-5} m^{2}s^{-1}, 10 cSt, although they are used up to 10^{-4} m^{2}s^{-1}, 100 cSt), and are linear for subsonic, turbulent flows. Under these conditions the inherent mechanical stability of the meter design gives rise to excellent repeatability performance.

The main performance characteristics are:

- Sizes, (internal diameter) range from 6 to 760 mm , (1/4" - 30").
- Maximum measurement capacities range from 0.025 Am^3/hr to 25,500 Am^3/hr, (0.015 ACFM to 15,000 ACFM), for gases and 0.036 m^3/hr to 13,000 m^3/hr, (0.16 gpm to 57,000 gpm or 82,000 barrels per hour), for liquids, where A denotes actual.
- Typical measurement repeatability is $\pm$ 0.1% of reading for liquids and $\pm$ 0.25% for gases with up to $\pm$ 0.02% for high accuracy meters. Typical linearities, (before electronic linearization), are between $\pm$ 0.25% to $\pm$ 0.5% of reading for liquids and $\pm$ 0.5% and $\pm$ 1.0% for gases. High accuracy meters have linearities of 0.15% for liquids and 0.25% for gases, usually specified over a 10:1 dynamic range below maximum rated flow.
- Rangeability, when defined as the ratio of flow rates over which the linearity specification applies, is typically between 10:1 and 100:1.
- Operating temperature ranges span -270°C to 650°C, (-450°F to 1200°F).
- Operating pressure ranges span coarse vacuum to 414 MPa, (60,000 psi).
- Pressure drop at the maximum rated flow rate ranges from around 0.3 kPa (0.05 psi) for gases to in the region of 70 kPa (10 psi) for liquids.

Theory

Tangential type

The principal configuration of the tangential type turbine flowmeter is shown in Fig. 1. Annotation 1 is the jet, 2 is the rotor-blade, and 3 is the magnetic pickup. When fluid flow through the rotor-blade is in the tangential direction, fluid drives the rotor-blade to rotate anti-clockwise. In order to improve the driving force, the jet is installed at the inlet of the meter, and the measurement range can be changed by altering the diameter of the jet outlet aperture. The rotational speed of the rotor-blade can be obtained by the magnetic pickup.
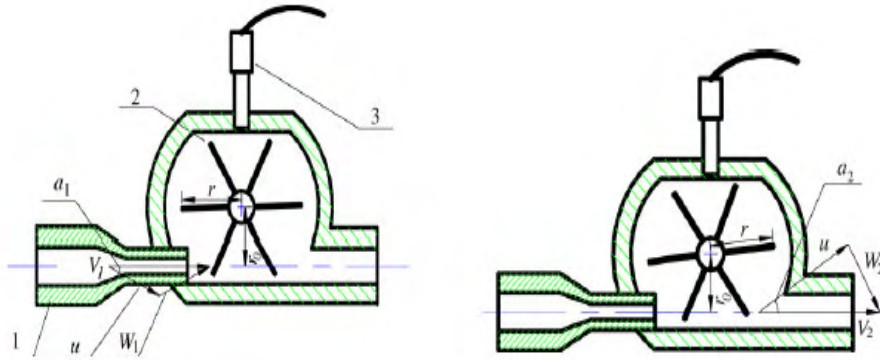
Fig. 7: a. Inlet velocity triangle of tangential type turbine flowmeter, b.Outlet velocity triangle of tangential type turbine flowmeter.

The velocity vector triangle of a tangential type turbine flowmeter at inlet and outlet is shown in Fig. 7, where W_1 is inlet relative velocity, W_2 is outlet relative velocity which is tangential with the outlet rotor blade, U_1 and U_2 are circular velocity, and r0 is the distance between the shaft and the axis of jet outlet.

The equation of the meter performance is developed from a torque balance on the rotor-blade as below (Zheng and Tao (2007)):

$$T_r - T_{rm} - T_{rf} - T_{re} = 0$$

where T_r is the rotor driving torque, T_{rm} is journal bearing retarding torque, T_{rf} is rotor-blade retarding torque due to fluid drag, and T_{re} is retarding torque due to the attractive force of the magnetic pickup.

At the beginning of rotor-blade rotation, T_r mainly overcomes the mechanical friction retarding torque, and T_{rf} is very small at that time. With the increase of the

rotor's rotational speed, T_{rf} becomes bigger. When the rotor is in the steady operation situation, $T_{rm} \ll T_{rf}$ is taken. So T_{rf} plays an important position while T_{rm} is neglected.

Usually T_{re} is very small and can be regarded as zero, so T_{re} is neglected. Under steady flowing condition, the rotor is in the balance of rotating. The main factor affecting meter performance is T_{rf}, so a new equation for the meter performance is developed from a torque balance on the rotor as below:

$$T_r - T_{rf} = 0$$

When the fluid is flowing through the meter, usually, under the turbulence flow condition, T_{rf} is represented as follows:

$$T_{rf} = C\rho Q^2 \text{ where C is constant.}$$

According to the momentum equation, the rotor driving torque T_r is represented as follows:

$$T_r = \rho Q \left(V_1 r \cos\alpha_1 - V_2 r \cos\alpha_2 \right)$$

where ρ is fluid density, Q is volumetric flow rate, r is radius of rotor, α_1 is the angle between V_1 and U_1, and α_2 is the angle between V_2 and U_2.

The fluid absolute velocity V_1 at jet outlet is presented as follows:

$$V_1 = \frac{Q}{A}$$

where A is the area of jet outlet aperture.

According to the outlet velocity triangle, the following equation can be presented

$$V_2 r \cos\alpha_2 = u = 2\pi r_0 n$$

where n is rotor rotary speed.

According to Fig. 7, r_0 is presented as:

$$r_0 = r \cos\alpha_1$$

Substituting into the first equation to obtain the rotor driving torque T_r :

$$T_r = \rho Q \left(\frac{Q}{A} r_0 - 2\pi r^2 n \right)$$

The tangential type turbine flowmeter performance is described by a volumetric meter factor K as follows:

$$K = \frac{f}{Q}$$

where f is pulse frequency,

$$f = Z \cdot n$$

where Z is the number of rotor blades.

Combining the equations, the tangential type turbine flow meter performance equation is given as:

$$K = \frac{Z}{2\pi r^2}\left(\frac{r_0}{A} - C\right)$$

The following conclusions can be obtained from the above equation: meter factor K is only affected by the meter structural parameter, while it is not affected by volumetric flow rate, density, etc. So K can be regarded as a constant value (Zheng and Tao (2007)).

Axial type

There are two approaches described in the current literature for analyzing axial turbine performance.

The first approach describes the fluid driving torque in terms of momentum exchange, while the second describes it in terms of aerodynamic lift via airfoil theory (Thompson (1970)). The former approach has the advantage that it readily produces analytical results describing basic operation, some of which have not appeared via airfoil analysis.

The latter approach has the advantage that it allows more complete descriptions using fewer approximations. However, it is mathematically intensive and leads rapidly into computer generated solutions. One prominent pioneer of the momentum approach is Lee (1965) who, using this approach, later went on to invent one of the few, currently successful, dual rotor turbine flowmeters, while Thompson and Grey (1970) provided one of the most comprehensive models currently available using the airfoil approach, which for instance, took into account blade interference effects. In the following, it is used the momentum exchange approach to highlight the basic concepts of the axial turbine flowmeter.

In a hypothetical situation, where there are no forces acting to slow down the rotor, it will rotate at a speed which exactly maintains the fluid flow velocity vector at the blade surfaces.
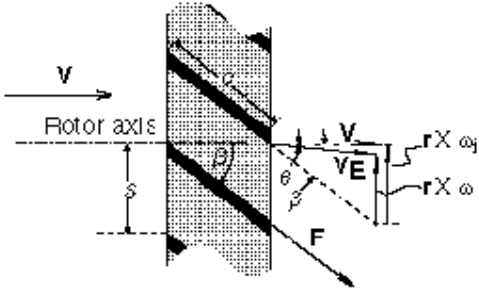
Fig. 8: Vector diagram for a flat-bladed axial turbine rotor. The difference between the ideal (subscript *i*) and actual tangential velocity vectors is the rotor slip velocity and is caused by the net effect of the rotor retarding torques.

This gives rise to linearity errors and creates swirl in the exit flow. V incident fluid velocity vector; V_E exit fluid velocity vector; θ exit flow swirl angle due to rotor retarding torques; β blade pitch angle, same as angle of attack for parallel flow; ω rotor angular velocity vector; r rotor radius vector; F flow induced drag force acting on each blade surface; c blade chord; s blade spacing along the hub; c/s rotor solidity factor.

Fig. 8 is a vector diagram for a flat bladed rotor with a blade pitch angle equal to β. Assuming that the rotor blades are flat and that the velocity is everywhere uniform and parallel to the rotor axis, then referring to Fig. 8:

$$r\omega_i = V \tan \beta$$

When one introduces the total flow rate this becomes:

$$\frac{\omega_i}{Q} = \frac{\tan \beta}{\bar{r}A}$$

Where ω_i is the 'ideal' rotational speed, Q is the volumetric flow rate, A is the area of the annular flow cross section and $\bar{r}$ is now the root-mean-square of the inner and outer blade radii, (R, a). Eliminating the time dimension from the left hand

32

side quantity reduces it to the number of rotor rotations per unit fluid volume, which is essentially the flowmeter *K* factor specified by most manufacturers. Hence, according to the second equation, in the ideal situation the meter response is perfectly linear and determined only by geometry. In some flowmeter designs the rotor blades are helically twisted to improve efficiency. This is especially true of blades with large radius ratios, (R/a). If the flow velocity profile is assumed to be flat, then the blade angle in this case may be described by *tanβ =constant · r*. This is sometimes called the 'ideal' helical blade. In practice, there are instead a number of rotor retarding torques of varying relative magnitudes. Under steady flow the rotor assumes a speed which satisfies the following equilibrium:

Fluid driving torque = rotor blade surfaces fluid drag torque + rotor hub and tip clearance fluid drag torque + rotation sensor drag torque + bearing friction retarding torque

Referring again to Fig. 8, the difference between the actual rotor speed, $r\omega$, and the ideal rotor speed, $r\omega_i$, is the rotor slip velocity due to the combined effect of all the rotor retarding torques as described in the equilibrium equation above, and as a result of which the fluid velocity vector is deflected through an exit or swirl angle, θ. Denoting the radius variable by *r*, and equating the total rate of change of angular momentum of the fluid passing through the rotor to the retarding torque, one obtains:

$$\int_a^R \frac{\rho Q 2\pi r^2 \left(r\omega_i - r\omega\right)}{\pi\left(R^2 - a^2\right)} . dr = N_T$$

which yields:

$$\overline{r}^2 \rho Q(\omega_i - \omega) = N_T$$

Where ρ is the fluid density and N_T is the total retarding torque. Combining this equation with the first and rearranging, yields:

$$\frac{\omega}{Q} = \frac{\tan\beta}{\overline{r}A} - \frac{N_T}{\overline{r}^2 \rho Q^2}$$

The trends evident in the obtained equation reflect the characteristic decline in meter response at very low flows and why lower friction bearings and lower drag pickups tend to be used in gas versus liquid applications and small diameter meters. In most flowmeter designs, especially for liquids, the latter three of the four retarding torques described in the equilibrium equation are small under normal operating conditions compared with the torque due to induced drag across the blade surfaces. As shown in Fig. 8, the force, F, due to this effect acts in a direction along the blade surface and has a magnitude given by:

$$F = \frac{\rho V^2}{2} \cdot C_D \cdot S$$

where C_D is the drag coefficient and S is the blade surface area per side. Using the expression for drag coefficient corresponding to turbulent flow, selected by Pate et al. (1984) and others, this force may be estimate by:

$$F = \rho V^2 0.074 \, \text{Re}^{-0.2} \, S$$

where Re is the flow Reynolds number based on the blade chord shown as dimension c in Fig. 8. Assuming θ is small compared with β, then after integration, the magnitude of the retarding torque due to the induced drag along the blade surfaces of a rotor with n blades is found to be:

$$N_D = n(R+a)\rho V^2 0.037 \, \text{Re}^{-0.2} \, S \sin \beta$$

Combining whit:

$$\frac{\omega}{Q} = \frac{\tan \beta}{\bar{r}A} - \frac{N_T}{\bar{r}^2 \rho Q^2}$$

and rearranging yields:

$$\frac{\omega}{Q} = \frac{\tan \beta}{\bar{r}A} - \frac{0.036n(R+a)\text{Re}^{-0.2} \, SA^2 \sin \beta}{\bar{r}^2}$$

34

That is an approximate expression for *K* factor because it neglects the effects of several of the rotor retarding torques, and a number of important detailed meter design and aerodynamic factors, such as rotor solidity and flow velocity profile. Nevertheless, it reveals that linearity variations under normal, specified operating conditions are a function of certain basic geometric factors and Reynolds number. These results reflect general trends which influence design and calibration. Additionally, the marked departure from an approximate ρV^2 (actually $\rho^{0.8} V^{1.8} \mu^{-0.2}$ via Re) dependence of the fluid drag retarding torque on flow properties under turbulent flow, to other relationships under transitional and laminar flow, gives rise to major variations in the *K* factor versus flow rate and media properties for low flow Reynolds numbers. This is the key reason why axial turbine flowmeters are generally recommended for turbulent flow measurement.

Dynamic response of axial turbine flowmeter in single phase flow

Turbine flowmeters are essentially instruments for metering steady flows, but it is often argued that their responsiveness makes them suitable for metering flows in which a degree of unsteadiness is present.

The dynamic response of turbine flowmeters in low density (gas) flows is relatively well understood and methods are available for the correction of errors due to over-registration in pulsating flows. The work of Ovodov et al. (1989) on liquid nitrogen indicated problems of predicting transient behaviour without knowing the dynamic characteristics of the meter.

Some items of plant can cause approximately sinusoidal pulsations, such as reciprocating pumps or unstable control valves in a pipeline. The dynamic response of turbine flowmeters in low-pressure gas flows (where the rotational inertia of the fluid is negligible) is well understood and methods for correcting meter signals for a lack of response are available. Turbine flowmeters in liquid flows are expected to be subject to similar errors although the relevant ranges of pulsation frequency and amplitude are expected to be different.

In a flow system, if the flow is pulsating sinusoidally with a relative pulsation amplitude α_p, the time dependent true volume flow rate, $\dot{V}_a(t)$, is given by:

$$\dot{V}_a(t) = \dot{V}_a \left(1 + \alpha_p \sin 2\pi f_p t \right)$$

where $\dot{V}_a$ is the mean volume flow rate and f_p is the pulsation frequency. When the meter is subjected to $\dot{V}_a$, the rotor responds and rotates with angular velocity $\omega(t)$, and the meter indicated volume flow rate, $\dot{V}_m$, can then be evaluated. It is of interest to investigate this time dependent response of the meter to the driving flow rate.

According to BS ISO TR 3313 (1998), when a turbine flowmeter is operating within a pulsation cycle, the inertia of the rotor (and possibly of the fluid contained within the rotor envelope) can cause the rotor speed to lag behind the steady state condition in an accelerating flow and to exceed it in a decelerating flow.

The response of a meter to accelerating and decelerating flows is not linear, the influence of a decelerating flow is greater than that of an accelerating one, so that the mean speed of a flowmeter subjected to pulsation becomes greater than that corresponding to the mean flow rate. This effect leads to two problems in turbine flowmetering. Firstly the mean flow indicated, $\dot{V}_m$, is higher than that which would occur with the corresponding true mean flow, $\overline{\dot{V}_a}$; secondly there is a difference between the peak-to-peak pulsation amplitude indicated by the meter, ϕ_m, and the true peak-to-peak pulsation amplitude, ϕ_a. These two effects are commonly termed "over-registration", OR, and "amplitude attenuation", AA, respectively. In extreme cases, over-registration error can be as high as 60% for meters in gas flow (McKee (1992)). These effects are expressed algebraically as follows:

$$OR = \frac{\overline{\dot{V}_m} - \overline{\dot{V}_a}}{\overline{\dot{V}_a}} \times 100\%$$

$$AA = \frac{\varphi_a - \varphi_m}{\varphi_a} \times 100\%$$
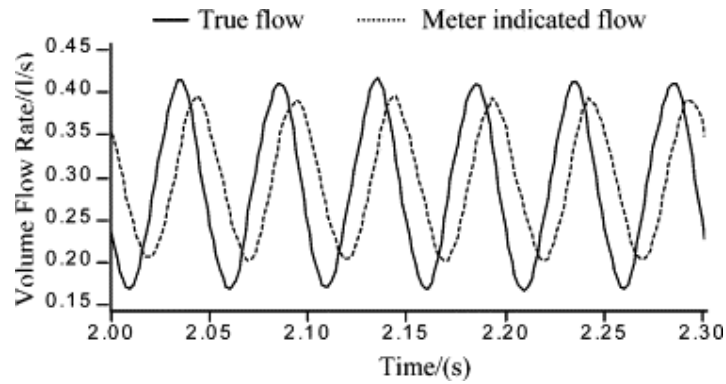
Fig. 9: Comparison of the true flow rate with the meter indicated flow rate, meter B, 40% relative pulsation amplitude at 20 Hz.

The occurrence of these errors has been known for nearly 70 years, and a number of workers (Ower (1937), Lee et all (1975), Bronner et all (1992)) have published suggestions of possible procedures for the estimation of correction factors for meters operating in gas flows. However, in pulsating liquid flows, there is a lack of experimental data on the meter dynamic response.

A literature survey revealed the only experimental study on pulsating liquid flow effects was published by Dowdell and Liddle (1953) and their results did not show any significant over-registration error. They tested three water meters in the size range of 6–8-in with pulsation frequencies not higher than 2 Hz. For these pulsation conditions no significant errors would be expected, particularly for larger size meters. They also did not independently measure the actual flow pulsations to which the meter was subjected; hence, the results were not conclusive.

"Small" turbine meters are expected to behave differently from "large" meters for a number of reasons. A smaller meter would generally have: (1) a larger percentage of tip clearance leakage flow; (2) less fluid momentum between the meter blading; and, (3) greater contribution of fluid friction forces on the effective surface area.

Lee et all. (2004) investigated the response of small turbine meters to pulsating liquid flows and provided a method for correction. In this research project, arbitrarily, meters up to size 25 mm were defined as small; and within this study, meters of size 6–25 mm (1/4–1-in) were investigated under pulsating water flows. Lee et al. in a previous work (2000) have reported some preliminary experimental results for pulsation frequencies of 5–300 Hz, although the mean flow rates

indicated by the meters did not show the large levels of 'over-registration' associated with intermittent gas flow, there was significant attenuation of the amplitudes of pulsations.

Theoretical model for transient single phase flow

The theoretical model presented here attempts to provide a physical basis for the meter response observed in the experimental work. The published theories of transient meter response in gas flows are all very similar (Grey (1956), Lee and Evans (1970), Cheesewright et al. (1994)), and these treatments assume, either implicitly or explicitly, that the rotational inertia of the fluid contained within the turbine rotor is negligible compared to that of the rotor itself. In some cases (McKee (1992), Cheesewright et al. (1996)), there are no friction effects included.

Fig. 10 shows a velocity vector diagram for a cascade of blades with a helix blade angle β_r at a general radius, r. For a typical meter rotor the angle of the blade varies with radius to accommodate the velocity profile across the pipe but in order to simplify the analysis of meter response it is usually assumed that the average flow condition around the blade exists at the root mean square radius $\bar{r}$. In all cases, it is assumed that the fluid leaving the blades is aligned with the blade. However, the fluid entering the blades will not be aligned with the blade. This is shown in Fig. 10. In the case of a pulsating flow, the incidence angle will change with the flow. Assuming that Fig. 10 can be applied at $\bar{r}$, it is clear that the tangential velocity of the fluid has changed from zero at entry to the blades to $U_x \tan \beta_{\bar{r}} - \omega \bar{r}$ at outlet.
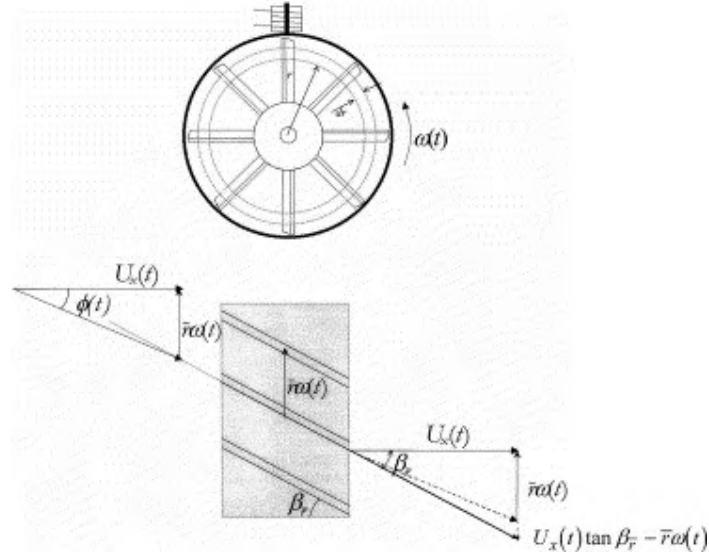
Fig. 10 . Cascade diagram for flow through turbine blades.

Dijstelbergen (1970), suggested that, the "gas equation" is only valid when the moment of inertia of the medium between the rotor blades is negligibly small compared with the inertia of the rotor. For the case of high-density fluid flow, he suggested that the total angular momentum involved in the dynamics will be the sum of that of the rotor and the liquid that it carries round. The torque required to accelerate both the rotor and the fluid surrounding it can be expressed, to a first approximation, as:

$$T_d = I_R \frac{d\omega}{dt} + I_f \frac{d(\omega - U_x \tan \beta_{\overline{r}} / \overline{r})}{dt}$$

where I_R is the rotational inertia of the turbine rotor and I_f is the rotational inertia of the appropriate body of fluid (rotating with the turbine rotor).

Since T_d is also equated to the change of angular momentum flux (neglecting any frictional forces in the bearings of the meter), the "high density fluid equation" now becomes:

$$I_R \frac{d\omega}{dt} + I_f \frac{d(\omega - U_x \tan \beta_{\overline{r}} / \overline{r})}{dt} = \rho U_x A \overline{r}(U_x \tan \beta_{\overline{r}} - \omega \overline{r})$$

and Cheesewright and Clark showed that, following the same generalisation as used by Atkinson (1992), the equation leads to:

$$V_a^2 - V_m V_a = b \left(1 + \frac{I_f}{I_R}\right) \frac{d \dot{V}_m}{dt} - b \frac{I_f}{I_R} \frac{d \dot{V}_a}{dt}$$

39

where $b = \left(I_R / \rho r^{-2} \right)$.

This equation implies that b and I_f/I_R need to be known separately.

For turbine meters used in flows where the fluid inertia is negligible, b is usually determined by step response tests following the procedure described by Atkinson (1992). For the case of significant fluid inertia, Cheesewright and Clark in the 1997 have reported a theoretical solution to the equation for the response to a step change in flow. However, they go on to conclude that the part of their solution relevant to the period immediately after the initiation of the step may not correspond to what is observed in experiments because it would require the flow to separate from the blades thus invalidating the equation. The part of their solution which is valid further away from the step corresponds to a solution to the equation when $d\dot{V}_a/dt$ is set equal to zero. This solution is in the form of an exponential decay similar to that observed in the step response for fluids of negligible inertia except that the time constant is given by:

$$t_c = \frac{b(1 + I_f / I_R)}{\dot{V}_a}$$

rather than by:

$$t_c = \frac{b}{\dot{V}_a}$$

values of b and I_f/I_R can be calculated from dimensions given on the meter manufacturers drawings and the value of I_f could be calculated by assuming that only the fluid contained within the envelope of the rotor contributed.

It should be noted that although the validity of the

$$\dot{V}_a^2 - \dot{V}_m \dot{V}_a = b\left(1 + \frac{I_f}{I_R}\right) \frac{d\dot{V}_m}{dt} - b\frac{I_f}{I_R}\frac{d\dot{V}_a}{dt}$$

with $I_f=0$ for turbine meters with fluids of negligible inertia can be considered to be well established, there are no known published reports of experimental validations, for cases of significant fluid inertia. It should also be noted that the neglect of the $d\dot{V}_a/dt$ term for the case of a step change does not automatically imply that its effect will be negligible in the case of a pulsating flow.

Other published reports of work on the response of turbine meters in liquid flows deal with the response to a flow which starts (instantaneously) from zero and it is

doubtful whether the exact mechanism of the response to such a change will be the same as that for either small step changes or sinusoidal flow pulsations. The step response tests reported by Cheesewright and Clark (1997) did not include start-up from zero but did include steps to zero and in that case it was demonstrated that the whole mechanism of the response was different because the forces on the turbine rotor are dominated by disk friction effects rather than by fluid dynamic forces on the blades.

In the work of Lee et all (2004) the authors show that all the meters suffer from significant pulsation amplitude errors over a range of pulsation amplitudes and frequencies. The pulsation amplitude error increases significantly with increasing pulsation frequency but it shows a relatively weak dependence on pulsation amplitude. The over-registration error is proportionately much smaller than the pulsation amplitude error. It increases both with increasing pulsation frequency and with increasing pulsation amplitude, but for all meters tested there was a range of amplitude and frequency over which the error was less than the measurement uncertainty quoted by the meter manufacturers. However, for all the meters there were ranges of experimental conditions for which the error was significant.

There are two ways in which the results of the experiments can be compared with the above theory. Firstly, approximate expressions for the amplitude attenuation, AA, and the over-registration, OR, can be derived from the theory and the functional dependencies of these errors on the pulsation amplitude and the pulsation frequency, contained within the approximate expressions, can be compared to the functional dependencies noted above in the experimental data. Secondly, the theory can be used as the basis for an attempt to correct the experimentally measured pulsation profiles. In both of these comparisons, it is necessary to neglect the influence of the last term on the right hand side of the equation.

For any one cycle of the flow pulsation, we can write:

$$AA = 1 - \frac{(\dot{V}_m)_{max} - (\dot{V}_m)_{min}}{2\bar{\dot{V}}_a \alpha_p}$$

To obtain an insight into the physical factors which influence AA and OR, an approximate expression for $\dot{V}_m$ can be obtained in terms of the corresponding $\dot{V}_a$

41

terms from the approximate solution to the abbreviated equation (abbreviated by the omission of the last term),of

$$V_a^2 - V_m V_a = b\left(1 + \frac{I_f}{I_R}\right)\frac{d\dot{V}_m}{dt} - b\frac{I_f}{I_R}\frac{d\dot{V}_a}{dt}$$

as for example:

$$(\dot{V}_m)_{max} = (\dot{V}_a)_{max}\left(1 - \frac{b(1 + (I_f/I_R))}{(V_a)_{max}^2}\frac{d\dot{V}_a}{dt}\right)$$

where the $d\dot{V}_m/dt$ term has been approximated by $d\dot{V}_a/dt$ (it should be noted that when the $d\dot{V}_a/dt$ terms are evaluated they will have opposite signs for the $(\dot{V}_m)_{max}$ and $(\dot{V}_m)_{min}$ expressions). When the abbreviated equation and the corresponding equation for $(\dot{V}_m)_{min}$ are substituted into the AA formula and the $d\dot{V}_a/dt$ terms are approximated by the maximum and minimum values obtained from the prescribed time dependence of $\dot{V}_a$ (first equation of the model), the functional dependence of AA is given by:

$$AA = \frac{2\pi f_p\, b(1 + (I_f/I_R))}{\overline{V}_a(1 - (\alpha_p^2/4))}$$

It should be noted that in the derivation of the above expression of AA, both the numerator and the denominator were divided through by α_p, so that it cannot be expected to be correct in the limit $\alpha_p=0$.

Strictly, OR is given by:

$$OR = \frac{f_p}{\overline{V}_a}\int_0^{L/f_p} V_m dt - 1$$

but it is convenient to approximate it by:

$$OR = \frac{(\dot{V}_m)_{max} + (V_m)_{min}}{2\overline{V}_a} - 1$$

when OR expression is approximated in a similar way to AA equation, the functional dependence of OR is given by:

$$OR = \frac{2\pi f_p\, b(1 + (I_f/I_R))}{\overline{V}_a}\frac{\alpha_p^2}{(1 + (\alpha_p^2/4))}$$

42

It will be seen that the proposed expression of AA suggests that AA is proportional to the pulsation frequency but only weakly dependent on the pulsation amplitude. The proposed expression of OR suggests that OR is also proportional to the pulsation frequency but is much more strongly dependent on the pulsation amplitude than was the case for AA.

In any attempt to compare the theory to the experiments by using the theory as a basis for the correction of the experimental meter output, it must be remembered that while I_R is a well defined quantity which can be calculated with reasonable accuracy from drawings of the meter rotor and material properties, I_f is not well defined and estimated values of it may be significantly inaccurate. With this in mind, it is reasonable Lee et al. (2004) did a comparison by checking the validity of a correction based on I_R only. The correction is based on solving:

$$(\dot{V}_m)_{max} = (\dot{V}_a)_{max} \left(1 - \frac{b(1+(I_f/I_R))}{(\dot{V}_a)^2_{max}} \frac{\mathrm{d}\dot{V}_a}{\mathrm{d}t} \right)$$

for each experimental value of $\dot{V}_m$ using a central difference estimate of $d\dot{V}_m/dt$. The authors showed that the correction was inadequate to explain the difference between the 'true' flow and the meter output.

Fig. 11 shows the same comparison but with the correction based on I_R and I_f with the latter being obtained by a calculation based on the fluid contained within the meter rotor. It can be seen that while the correction does not provide a complete explanation of the difference between the 'true' flow and the meter output, it does provide a worthwhile improvement. It is not clear whether the remaining discrepancy (which is present for all the tests on all five meters) is due to inaccuracies in the values of I_f, or to the neglect of the last term of:

$$\dot{V}_a^2 - \dot{V}_m \dot{V}_a = b \left(1 + \frac{I_f}{I_R} \right) \frac{\mathrm{d}\dot{V}_m}{\mathrm{d}t} - b\frac{I_f}{I_R} \frac{\mathrm{d}\dot{V}_a}{\mathrm{d}t},$$

or to some other inadequacy in the model.
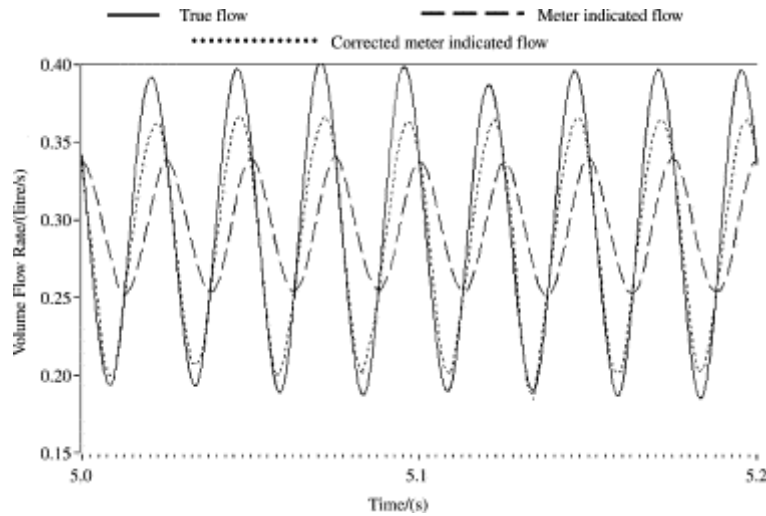
Fig. 11. Comparison of the output of meter B with the 'true' flow rate and the output corrected on the basis of I_R and I_f. (Lee et al. (2004))

From the analytical solution to the truncated form of the basic equation, it can be seen that the condition for the absence of significant error at any point in a measurement is that

$$4b(1 + (I_f / I_R))\mathrm{d}\dot{V}_m / \mathrm{d}t \ll \dot{V}_m^2$$

and for negligible error the $\dot{V}_m$ can be replaced by $\dot{V}_t$, giving

$$4b(1 + (I_t / I_R))\mathrm{d}\dot{V}_a / \mathrm{d}t \ll \dot{V}_a^2$$

Calibration, installation and maintenance

Turbine flowmeters have a working dynamic range of at least 10:1 over which the linearity is specified. The maximum flow rate is determined by design factors related to size versus maximum pressure drop and maximum rotor speed. The minimum of the range is determined by the linearity specification itself. Due to small, unavoidable, manufacturing variances, linearity error curves are unique to individual meters and are normally provided by the manufacturer. However, although recommended where possible, the conditions of the application cannot usually and need not necessarily duplicate those of the initial or even subsequent calibrations.

In case more than one meter is required, they cannot share the same pipe, in order to protect the lower span turbine from rotor overspeed, so that an active control system to place in line the proper meter during the test and valve off all the others is required.

44
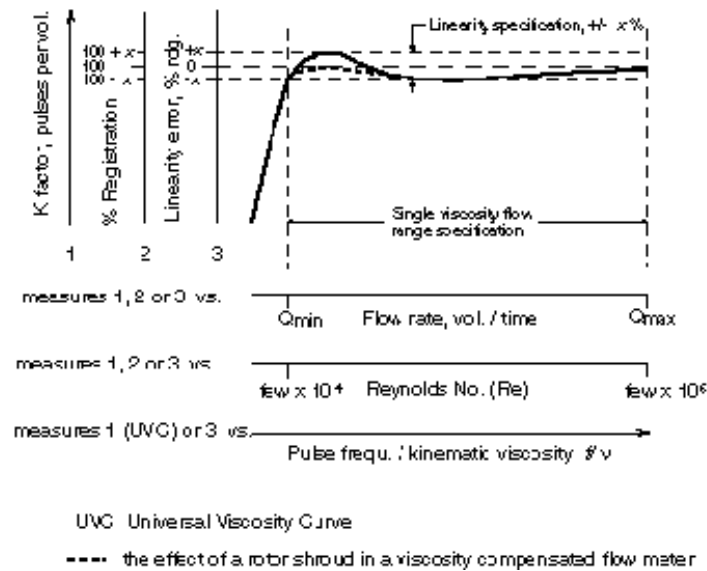
Fig. 12: typically shaped calibration curve of linearity versus flow rate for axial turbine
meter (Wadlow (1998))

A typical single rotor axial turbine linearity error, or calibration, curve for a low
viscosity fluid showing the main alternative presentations in current use.

Higher accuracy specifications usually correspond to a 10:1 flow range down
from Q_{max}, while extended operating ranges usually correspond to reduced
accuracies. The hump in the depicted curve is a characteristic feature caused by
flow velocity profile changes as Re approaches the laminar region. This feature
varies in magnitude between meters. Sensitivity and repeatability performance
degrades at low Re. Percent registration is only used with meters which have
mechanical pickups. All other meters have a K factor. UVC and Re calibrations
remain in effect at different known media viscosities provided Re or f/v stays
within the specified range. Re is referenced to the connecting conduit diameter
and is less within the flowmeter. The Re range shown is therefore approximate
and can vary by an order of magnitude depending on the meter. Linearity error
may also be expressed in terms of Strouhal number (fD/V) versus Re (VD/v) or
Roshko number $(fD^2/v$), when instead D is a flowmeter reference diameter,
(Wadlow (1998)).

Fig. 12 depicts a typically shaped calibration curve of linearity versus flow rate
expressed in terms of multiple alternative measures, various combinations of
which may be found in current use. The vertical axis thus represents either the

45

linearity error as a percentage of flow rate, a *K* factor expressed in terms of the number of pulses from the rotation sensor output per volume of fluid or the deviation from 100% registration; the latter only applying to flowmeters with mechanical pickups. The horizontal axis may be expressed in terms of flow rate in volume units/time, Reynolds number, (Re), or pulse frequency (from the rotation sensor for non-mechanical) divided by kinematic viscosity, (*f/v*), in units of Hz per m^2s^{-1} , (Hz/cSt or Hz/SSU; 10^{-6} m^2s^{-1} = 1 centistoke $\cong 31.0$ seconds Saybolt Universal), and where kinematic viscosity is the ratio of absolute viscosity (*u*) to density.

Calibrations are preferably expressed versus Re or *f/v*, which is proportional to Re. The hump shown in the curve is a characteristic frequently observed at lower Re and is due to velocity profile effects. K factor versus *f/v* calibration curves are specifically called universal viscosity curves (UVC) and for most meters are available from the manufacturer for an extra charge.

A key utility of UVC is that where media type and properties differ significantly from those of the original calibration, accuracies much greater than the overall linearity error can still readily be obtained via the flowmeters UVC if the kinematic viscosity of the application is known. An alternative, advanced calibration technique (Wadlow (1998)) (Olivier (1992)), is to provide response in terms of Strouhal number versus Re or Roshko number. This approach is not widely adopted, but it is particularly relevant to high accuracy and extreme temperature applications because it further allows correct compensation for flowmeter thermal expansion errors.

The accuracy of axial turbine flowmeters is reduced by unconditioned flow, especially swirl. An installation incorporating flow conditioners along with specific upstream and downstream straight pipe lengths is generally recommended, (ISA-RP 31.1 (1997)). Some axial turbine flowmeters can be purchased with additional large flow straighteners that mount directly ahead of the flowmeter body or conditioning plates which are integral to the body. The manufacturer is the first source of information regarding installation. Errors due to flow velocity pulsations are another concern, particularly in certain gas installations. However no standard technique for effectively counteracting this source of error has yet been adopted. Periodic maintenance, testing and

recalibration is required because the calibration will shift over time due to wear, damage or contamination.

Both one-directional and bidirectional designs are currently available, but a calibration for each flow direction is necessary.

Calibration of the flow-meter together with surrounding pipework and straighteners is recommended to eliminate the effect of upstream flow effect. ANSI/API suggested an upstream length of 20D and a downstream length of 5D. Baker (2000) shows an example of suggested upstream spacing from manufacturer, for elbow and bends effects on installation.

Temperature differences between calibration and operation cause dimensional changes, viscosity changes, density changes and velocity pattern shift and then affect the turbine meter signal.

Design and construction

There are numerous, often proprietary, designs incorporating variations in rotors, bearings, pickups and other components in format and materials which are tailored to different applications. Meter bodies are available with a wide range of standard end-fittings. Within application constraints, the primary objective is usually to optimize the overall mechanical stability and fit in order to achieve good repeatability performance. Design for performance, application and manufacture considerations impact every internal component, but most of all the rotor with respect to blade shape and pitch, blade count, balance and rigidity versus, drag, stress and inertia, bearings with respect to precision versus friction, speed rating and durability and rotation pickup versus performance and drag (Wadlow (1998)).

Most low radius ratio blades are machined flat, while high ratio blades tend to be twisted. The blade count varies from about 6 to 20 or more depending on the pitch angle and blade radius ratio so that the required rotor solidity is achieved. Rotor solidity is a measure of the 'openness' to the flow such that higher solidity rotors are more highly coupled to the flow and achieve a better dynamic range. The pitch angle, which primarily determines the rotor speed, is typically 30° to 45° but may be lower in flowmeters designed for low density gas applications. Rotor assemblies are usually a close fit to the inside of the housing. In large diameter meters the rotor often incorporates a shroud around the outer perimeter for

enhanced stability. Also, since large meters are often used for heavy petroleum products, via selection of a suitable wall clearance, the fluid drag resulting from this clearance gap is often designed to offset the tendency at high media viscosities for the meter to speed up at lower Reynolds numbers. The materials of construction range from non magnetic to magnetic steels to plastics (Wadlow (1998)).

Stainless steel ball bearings tend to be used for gas meters and low lubricity liquids such as cryogenic liquids and freon, while combination tungsten carbide or ceramic journal and thrust bearings are often considered best for many other liquid meters depending on the medium lubricity. Fluid bearings (sometimes called 'bearingless' designs) are often used in conjunction with the latter, but also sometimes with gases, for reducing the drag. They operate by various designs which use flow induced forces to balance the rotor away from the shaft ends. Bearing lubrication is either derived from the metered medium or an internal or external system is provided. The more fragile, jeweled pivot bearings are also used in certain gas sensor are magnetic applications and small meters.

The most common types of rotation, modulated carrier and mechanical, while optical, capacitative and electrical resistance are also used. In research, a modulated nuclear radiation flux rotation sensor for use in certain nuclear reactors has also been reported (Van Der Hagen (1993). Mechanical pickups, which sometimes incorporate a magnetic coupling, are traditional in some applications, can have high resolution and one advantage that they require no electrical power. However the pickup drag tends to be high. The magnetic and modulated carrier types utilize at least a coil in a pickup assembly which screws into the meter housing near the rotor. In magnetic inductance types, which are now less common, the blades or shroud carry magnetized inserts, and signals are induced in the coil by the traversing magnetic fields. In the more prevalent magnetic reluctance type, the coil is wrapped around a permanent magnet or magnet pole piece in the pickup assembly which is mounted next to a high magnetic permeability bladed rotor (or machined shroud). The latter is then typically made of a magnetic grade of stainless steel such as 416, 430 or 17-4Ph. As the rotor turns, the reluctance of the magnetic circuit varies producing signals at the coil. In the more expensive modulated carrier types, the rotor need only be electrically conductive. The coil is part of a radio frequency, (RF), oscillator circuit and

proximity of the rotor blades changes the circuit impedance giving rise to modulation at a lower frequency which is recovered. The RF types have much lower drag, higher signal levels at low flow and can operate at temperatures above the Curie point of typical ferromagnetic materials. They are preferred for wide dynamic range and high temperature applications. Bi-directional flowmeters, usually have two magnetic pickups to determine flow direction. Multiple magnetic pickups are also used in some designs to provide increased measurement resolution. Regarding output, various pulse amplifiers, totalizers, flow computers for gas pressure and temperature correction, along with 4-20 mA and other standard interface protocols, are available to suit particular applications. As an example of advanced transmitters, at least one manufacturer provides a real-time, miniature, reprogrammable, 'smart' transmitter which is integrated into the pickup housing along with a meter body temperature sensor, for full viscosity compensation and UVC linearization. These are for use in dedicated applications, where the medium viscosity-temperature relationship is known (Wadlow (1998)).

Frequency conversion methods

There are different methods to obtain rotor speed (Baker 2000):

1) Inductive

2) Variable reluctance (the magnetic reluctance can be thought of as having an analogous function to resistance in an electrical circuit; is the resistance opposed by a certain material to the passage of the magnetic flux).

3) Radiofrequency.

4) Photoelectric.

5) Magnetic reed switch.

The signal needs to be amplified and screened from external magnetic and voltage sources. There could be an influence due to a magnetic pickup device (referred presumably to type 1), 2) and 5)) on the velocity of the rotor due to the drag force; at 1/6 FDS (full-scale deflection) it provokes an error of 4% (Ball (1977)).

Ohlmer and Schulze (1985) verified the slowing down effect of two types of pick off devices (magnetic pick-off and eddy current pick-off); they stated that the influence of the brake effect of the pick off system is evident just for velocities below 1% of the maximum velocity, when the turbine is given a certain rotational speed, and then is allowed to run freely in the stagnant air.

Two-phase flow measurement capability and modelling

Metering are currently available. The basic model is the following:

$$\Gamma = K\rho_{TP}\omega$$

Γ Two-phase mass flow rate [kgs^{-1}]

ω Rotational frequency [Hz]

ρ_{TP} two-phase mixture density [kgm^{-3}]

$$\rho_{TP} = \alpha\rho_g + (1-\alpha)\rho_l \quad \text{photographic density}$$

$$\rho_{TP}^{-1} = \left[\frac{x^2}{\alpha\rho_g} + \frac{(1-x)^2}{(1-\alpha)\rho_l}\right]^{-1} \quad \text{momentum density}$$

ρ_l Liquid density [kgm^{-3}]

ρ_g Vapor density [kgm^{-3}]

α Two-phase mixture void fraction

Rouhani (1964) has shown that the appropriate density for the turbine meter is the momentum density.

The calculation of the two-phase mixture density ρ_{TP} requires, in principle, the side measurement of the void fraction α (typically performed in academic research). Acceptable results can be obtained with existing empirical correlations for the void fraction α deduced for channel flow (which normally requires the knowledge of the local pressure and the local mixture quality, whose accessibility is to be evaluated).

The proportionality constant K can be extrapolated from single-phase flow literature (provided the meter is single-phase standard design) and tailored on the basis of preliminary in-situ testing.

Parameters description

In principle for steady flow the meter factor *K* of a specific meter depends on dimensionless parameters such as:

• the Reynolds number Re

• the Mach number M

• the ratio of mechanical friction torque, to the driving fluid torque

The manufacturer uses steady flow calibrations at different pressures to distinguish between Reynolds number effects and the influence of mechanical friction. In general the Mach number dependency is a small correction due to a Mach number effect in the temperature measurements at high flow rates.

In unsteady condition the response of the meter will also depend on:

• the Strouhal number Sr

• the amplitude of the perturbations

• the ratio of fluid density, ρ, and rotor material density, ρ_m,

Ideally, the volume flow is proportional to the rotation speed. However, slight deviations are observed as a function of the Reynolds number. In designing a flow meter, the object is to make the dependence on the Reynolds number as small as possible and to create a robust meter, not sensitive to wear nor damage. In "Dynamics of turbine flow meters" (2007) is described a two-dimensional analytical model to predict the deviation of the rotation speed of the rotor from the rotation speed of an ideal helical rotor in an ideal flow, without mechanical friction or fluid drag. By comparing the results of the model with calibration data of turbine flow meters, the author find that the theory can explain global effects of the inlet velocity profile, the pressure drag of the wake and other friction forces; for a more accurate model it is necessary to include realistic tip clearance effects and the additional lift induced by the shape of the trailing edge.

Another important source of systematic errors are time dependent perturbations in the flow. In the same work, the author investigate the effect of pulsations at high frequencies on the rotation speed of the rotor. Above a critical frequency, determined by the inertia of the rotor, the turbine meter will not be able to follow the variations in volume flow in time. Instead an average rotation speed will be

established. Due to non-linearities of the forces exerted by the flow on the turbine blades this rotation speed corresponds to a higher steady volume flow than the actual time-averaged flow. By assuming quasi-steady behaviour of the flow for the model obtained for ideal steady flow, the relative error in volume flow is equal to the root-mean-square of the ratio of acoustical to main flow velocities. The range of validity of this prediction has been explored experimentally for harmonic pulsations. Although significant deviations from the quasi-steady model were found, the quadratic dependence on the velocity amplitude appears to remain valid for all measurements. The exact quadratic dependence is a function of the Strouhal number of the pulsations. In the range of Strouhal numbers below 2.5, based on the blade chord length at the tip of the rotor blade and the flow velocity at the rotor inlet plane, we find a slow decrease of the error with increasing Strouhal number following a power 1/5 of Strouhal. Measurements at high Strouhal numbers were not reliable enough to confirm this dependence for higher Strouhal numbers. The deviation obtained for the superposition of two harmonic perturbations can be predicted by addition of the deviations caused by the two individual perturbations.

The Structural damage due to two phase flow is another important parameter to take in account; cavitation is recognized as a destructive phenomenon in turbine flowmeters. The intermittent impact of liquid in a liquid/gas flow may damage the internals of the meter. It is possible that erosion and abrasion may occur around sharp edges.

Cavitation could cause overreading also. The safe rule to avoid cavitation is that the back pressure has to be at least twice the pressure drop across the meter, plus the absolute vapour pressure times 1.25 (Baker (2000)).

Two phase Performances

The maximum applied pressure used in two phase experiments with turbine meter is 240-400 bar for threaded design, the maximum temperature is 310ºC (Baker (2000)).

Chen and Felde (1982) experiments were conducted in a pressure range of 5.5-13.8 MPa.

They demonstrated (comparing the Kamath and Lahey model to the homogeneous model) that the variation of the correlation coefficients may lead to great changes in the mass flux evaluation, especially for fast transients. The correlations coefficients are defined (Chen and Felde, (1982), Kamath and Lahey (1977)) by the following formulas:

$$C_l = \frac{\langle (1-\alpha) V_l^2 \rangle}{\langle (1-\alpha) \rangle \langle V_l^2 \rangle} \ \text{(for liquid)}$$

$$C_l = \frac{\langle \alpha V_v^2 \rangle}{\langle \alpha \rangle \langle V_v^2 \rangle} \ \text{(for gas)}$$

They depend on the flow regimes and are adjustment to homogeneous model input for non homogeneous flow effects.

Also the variation of the slip ratio could cause great changing in the mass flux evaluation (the higher the slip ratio, the smaller the magnitude and the earlier is the peak in the mass flux).

A good knowledge of the expected flow regimes is therefore necessary to calculate the mass flux with the lower uncertainty.

The quality range they observed during their experiments was 0.8-1.4 quality for steam and water.

Ohlmer and Schulze (1985) used a model of turbine flow-meter studied at the CENG (Centre D'Etudes Nucleaires Grenoble) to measure the two-phase flow in the LOCE (Loss of Coolant Experiments) test. The test facility reproduced the operation condition of a PWR reactor and the turbines had to face conditions of high pressure and temperature: pressure of 158 bar and coolant temperature up to 327ºC.

Hardy (1982) tested a turbine flow meter coupled with a string probe for all the flow patterns from bubble to annular $(0 \leq \alpha \leq 1)$. The mass flow rate was obtained correlating the two-phase density from the string probe to the velocity sensed by the turbine with the following formula:

$$m = \rho_{TP} v_T$$

where ρ_{sp} is the density from the string probe and V_T is the velocity from the turbine. The data, represented in a graph that related the mass flow rate ($\dot{M}$) to the product ρ_{sp} V_T, shown a high scatter especially for $M < 2$ kg/s.
The curve was fitted using two different exponential functions, one for $M < 5 kg/s$ and one for $M > 5 kg/s$.

Hewitt (1978) stated that the interpretation of the performance of a turbine flow meter in two phase flow is difficult for flow regimes other than those close to homogeneous. For example, the response in annular flow, for a certain mass flux and void fraction, is likely to be different from that for homogenized flow with the same characteristics (mass flow rate and void fraction).

Two Phase flow Models for steady- state and transient flow conditions

The measurement of two-phase flow by a turbine meter usually incorporates an evaluation model which relates the metered velocity to the actual velocities of the gas and liquid phases.

Some models developed to interpret the response of a turbine flow meter and relate it to the true mass flow rate are lists below:

Volumetric model (Silverman and Goodrich, (1977)):

$$\overline{V} = \alpha V_g + (1-\alpha) V_l,$$

This model is based in the assumption that the velocity measured is equal to the volumetric flow rate divided the cross sectional area.

Aya's model (Aya, (1975)):

$$C_{tg} \alpha \rho_g \left(V_g - \overline{V} \right)^2 = C_{tl} (1-\alpha) \rho_g \left(\overline{V} - V_l \right)^2$$

where C_{tg} and C_{tl} are the mono-phase calibration coefficients. The model has been derived from the assumption that the force that the gas flow exerts upon the turbine blades is equal to the force that the blades are exerting on the liquid flow.

Rouhani's model (Rouhani, (1964)):

$$\overline{V} = xV_g + (1-x)V_l$$

Also this model is based on a momentum balance calculation, as the previous one, but the authors used different ways of expressing the momentum terms.

According to Hsu (1978) (Hetsroni (1982)), some experiments at the Oak Ridge National Laboratory showed that the first model is working better for down flow with slip ratio<1, while Aya and Rouhani model predict the turbine velocity more accurately for horizontal flow or for down flow with slip ratio>1.

The turbine meter has been largely used in experiments to model nuclear plant operating a long way from normal conditions; in unsteady flow a valid model to analyse the output turbine signal is the Kamath and Lahey model (1977 and 1980):.

Kamath and Lahey have developed analytical models for the dynamic response of free-field turbine-meters and drag-disks. These models have been combined with various density and velocity profile models to synthesize a predictive technique for global mass flux and void fraction.

Comparison of this model with the data taken at Wyle Labs has indicated that a DTT rake is capable of predicting global mass flux trends.

Parametric studies indicate that for a typical blowdown transient, dynamic effects such as rotor inertia can be important for the turbine-meter. In contrast, for the drag-disk, a frequency response analysis showed that the quasi-steady solution is valid below a forcing frequency of about 10 Hz, which is faster than the time scale normally encountered during blowdown.

A detailed derivation of the equation can be find in Kamath and Lahey (1980).

Kamath and Lahey's Model

In the model the turbine flowmeter dynamic equation was derived from the principle of angular momentum conservation.

The equation accounts for effects of non-uniformity of velocity and void profiles in conduit, imperfect guidance of the fluid by the rotor blades, rotor inertia, slip ratio, bearing friction, and windage losses.

$$\frac{dV_{zl}}{dt} = |V_{zl}|\left[\frac{\omega\kappa}{\Delta x}\right] - V_{zl}\left[\frac{1}{S+R_1}\left(\frac{R_1}{\rho_l}\frac{d\rho_l}{dt} + \frac{S}{\rho_v}\frac{d\rho_v}{dt}\right) + \left(\frac{S-R_2}{S+R_1}\right)\frac{1}{\alpha}\frac{d\alpha}{dt}\right] +$$

$$-\left[\frac{C_{lt}R_1 + C_v S^2}{(S+R_1)\Delta x}\right]V_{zl}\cdot|V_{zl}| + \omega\kappa\left[\frac{1}{(S+R_1)}\left(\frac{R_1}{\rho_l}\frac{d\rho_l}{dt} + \frac{S}{\rho_v}\frac{d\rho_v}{dt}\right) + \left(\frac{S-R_2}{S+R_1}\right)\frac{1}{\alpha}\frac{d\alpha}{dt}\right] +$$

$$+\kappa\frac{d\omega}{dt}\left[\frac{1+R_1}{S+R_1} + \frac{I_{rotor}(1+\eta_v)}{A_{xs}\Delta x R_v^2 \rho_v \alpha(S+R_1)}\right] +$$

$$+\frac{\rho_l^{0.57}|\omega|^{0.57}\omega\eta_l^{0.43}(1+\eta_v)\kappa}{A_{xs}\Delta x R_v^2 \rho_v \alpha(S+R_1)}\left[0.039(Ct_B N)R_T^{2.57}(R_B - R_T)^{-0.43} + 0.078\left(L_{jb}R_s^{3.57}\right)(R_{h1} - R_s)^{-0.43}\right]$$

Where:

$$R_1 = \frac{R_l^2}{R_v^2}\frac{\rho_l}{\rho_v}\frac{1-\alpha}{\alpha}\frac{1+\eta_v}{1+\eta_l} \qquad\qquad R_2 = \frac{R_l^2}{R_v^2}\frac{\rho_l}{\rho_v}\frac{1+\eta_v}{1+\eta_l}$$

R_B DTT shroud radius

R_h turbine hub radius

R_{h1} turbine bearing radius

R_s effective journal radius

R_T blade-tip radius

S slip ratio

$\kappa = \dfrac{R}{tg\beta} = \text{constant}$

R pipe radius

R_k radius at which the effect of phase k can be assumed to be concentrated, it is dependent on the velocity and void profile.

η_k the flow deviation factor for the phase k, it's a measure of the imperfect guidance of the fluid by the blading.

A_{xs} flow area through the turbine blading

The results of a parametric study show that the velocity and void profiles, which determine the correlation coefficients and the effective radii, have a significant effect on the mass flux calculation, especially for transients. The effect of the moment of inertia is also appreciable for fast transient: the Kamath-Lahely model precedes the homogeneous model by 50 ms in some portion of the transient, resulting in a significant mass flux difference.

Hence, since the quasi-steady approach is not accurate in general, the transient mass flux calculation scheme given in the above equations is recommended for turbine-meter evaluations.

Chen and Felde (1982) obtained a good time response of at least 50 ms in their experiments, comparing the results from the homogeneous model with those from the Kamath and Lahey model.

They reported some interesting result of the measurement of two phase mass flow at the ORNL THTF (Oak Ridge National Laboratory, Thermal-Hydraulic Test Facility) using two different spool pieces design with mass flux in the range 195-830 *Kg/(m² s)*:

- Thermocouple, absolute pressure tap, turbine meter for volumetric flow or velocity, single beam gamma densitometer for the average density, drag disk for the momentum flux.
- Thermocouple, absolute pressure tap, turbine meter for volumetric flow or velocity, three beams gamma densitometer for the average density, drag disk for the momentum flux.

It need to highlight that in steady state conditions this model is equivalent to Rouhani model.

The same authors evaluated the error in using the homogeneous flux model and the Kamath and Lahey model (Chen and Felde, (1982), Kamath and Lahey (1977)) to measure the mass flux in steady state, two phase flow regime and obtained uncertainty bands of less than ±50% of reading (95% confidence level) for both the models.

Hewitt (1978) suggests being very careful in evaluating the transient response of a turbine flow-meter, because of the inertia of the turbine rotor. Fig. 13 shows the influence of the rotor inertia on the evaluation of the flow rate. The figure is based on Kamath and Lahey (1977) calculation. The turbine tends to over predict the flow rate in the first part of the transient and to under predict it

in the second part because of the increasing and decreasing of the angular momentum. The effect is more evident as the inertia increases.
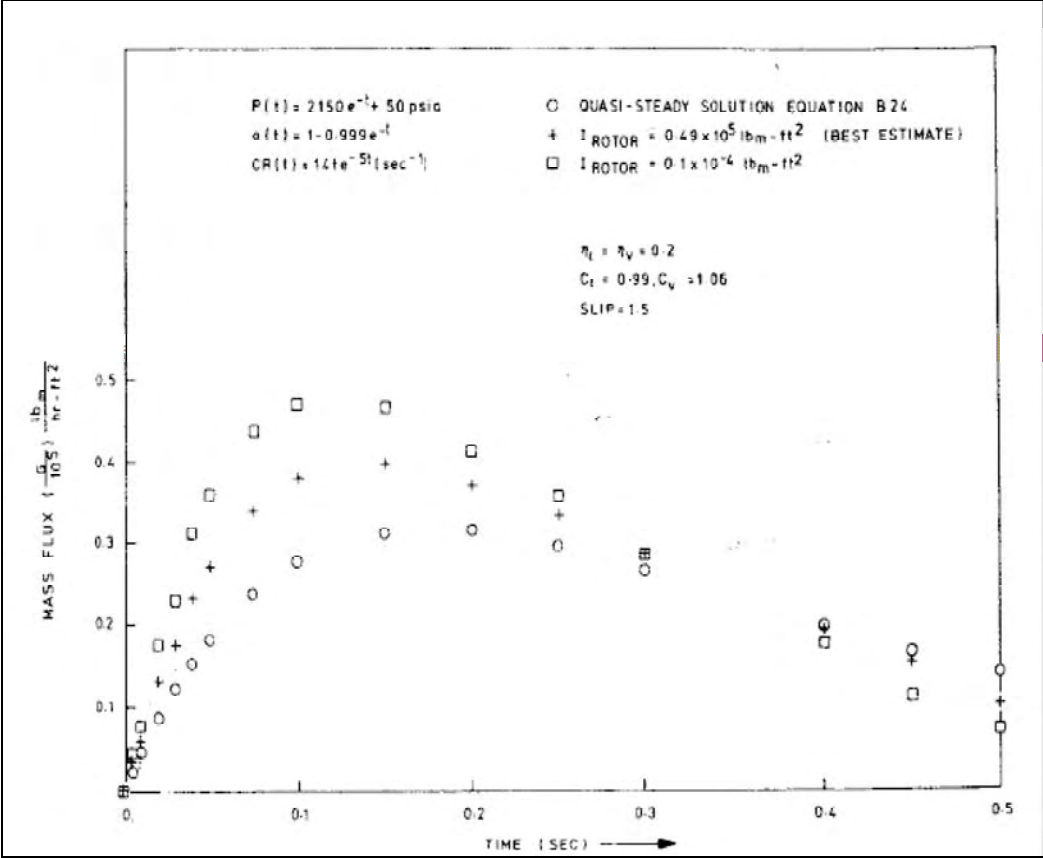
Fig. 13: Variation of the turbine meter response as a function of the rotor inertia (Hewitt (1978), based on Kamath and Lahey (1977) calculations)

Ohlmer and Schulze (1985) also, used turbine meter in experiments to model incidental conditions in a nuclear plant.

The instruments were just calibrated in a water-only or air-only loop with velocities up to 12 m/s and 100 m/s, respectively. The turbine meters presented a very good linearity down to 1% of the nominal range. The relation between the turbine meters reading and the mass flow rate was simply: $\dot{m} = A \cdot \rho \cdot v$, where $\dot{m}$ is the mass flow rate, v is the mixture velocity detected by the turbine, A is the

59

cross sectional area of the pipe and ρ is the average mixture density detected by a two-beam gamma densitometer.

The values obtained were compared to the mass flow rates measured by a reference TMFM (True Mass Flow Meter, in fact a Coriolis flow-meter, and showed a remarkably good agreement.

Two different types of tests were implemented: LB (large break) and SL (small leak) tests. In the first one the fluid velocities in the intact loop remained below 10 *m/s* and decreased under 1 *m/s* at the end of the tests, while in the location closer to the break position they reached values around 100 *m/s* . In the Small Leak test the intact loop velocities were around 0.5 *m/s.* During the first ones very high flow velocities (up to 100 m/s at the break location) occurred and the thermohydraulic transients were very strong; the second ones were characterized by lower flow velocities and much longer transients (one hour and more). The failure rate for the instrument used in the SL was higher, because the of the longer operation time at temperatures above 120ºC (this value has been chosen as the discriminating parameter).

In the Small Leak tests they verified that the linear calibration curve remained unvaried for measurements above 10% of nominal flow rate, while in the lower region a mean deviation up to 25% of the reading was observed (the standard deviation was about 1% of the reading). The error increase was due to the bearing alterations. The two authors underlined also the usefulness of the rundown check to infer about the state of the turbine meter bearings. The turbine rotor is given a certain speed and then it is allowed to run in the air till the brake effect of the pick-off device, the drag of the air and the bearing friction will make it stop. The changes in the position of the stop point in the rotational frequency-time curves can help in the detection of a turbine failure.

Heidrick et al. (1978) (in Baker (1991)) tested a turbine meter together with pitot tubes and gamma densitometer and concluded that steady flow and slow transients were measurable with reasonable accuracy.

Kinghorn and McHugh (1981) in Baker (1991)) obtained some widely varying results for horizontal water/air flows which do more to warn of the unpredictability than to offer hope of high precision.

Baker and Deacon (1983) tested a turbine flow-meter in a vertical upward air/water flow up to $\alpha = 0.06$. They obtained in almost all cases a positive error (the flow rate measured by the turbine was bigger than the actual flow rate) with respect to the reference flow rate (previously measured with single phase flow instruments). The maximum error rises up to 20%. They used two plates with holes in order to introduce the air to the test rig. In order to monitor the turbine response in non homogenized flow conditions, they did not use a mixing device. The flow patterns were mostly bubble and plug flow. A surprising hysteresis effect was noticed in the turbine output for $\alpha \cong 0.05$. This may have been due to the particular meter or the flow circuit, but it raised speculation as to whether vortex structures in the vicinity of the ball-bearing fluid access path could be entrapping air and holding it in the bearing after the external air content in the flow had dropped. A small increase in air content from about 4 per cent to about 5 per cent caused an error increase of about 15 per cent, and this was not immediately removed by reducing the air content back to 4 per cent. A possible explanation was that a vortex structure within the meter had trapped air and caused it to be drawn into the bearing.

Millington and King (1986, 1988) described tests in a kerosene-like liquid and air flow with upstream jet mixing which reduced errors from 20 to below 8 per cent, and Mark et al. (1990) described some interesting data and theoretical modelling. In a further paper Mark et al. (1990) claim that the level of signal turbulence is directly proportional to the void fraction in a water/air flow. They made some attempt to explain the overspeeding noted by them and others.

Hardy (1982) described the performance of a string probe and a turbine flow meter to measure steady two-phase flow (steam and entrained water) at the vent valve location of the Cylindrical Core Test Facility (CCTF) in Japan, in the range of mass flow rates 0.1-16 *kg/s*. 80% of all the measurements fall within ±30% of the known flow rate for velocities >2 *m/s*, for lower flow rates the error rises to ±70%, because of the low sensitivity of the homogeneous model at low flow rates. Hardy (1982) demonstrated that the turbine flow-meter response is sensitive to the variation in the flow pattern (see Fig. 14). The dotted lines in the figure delimits the regions of the graph characterized by different flow patterns.
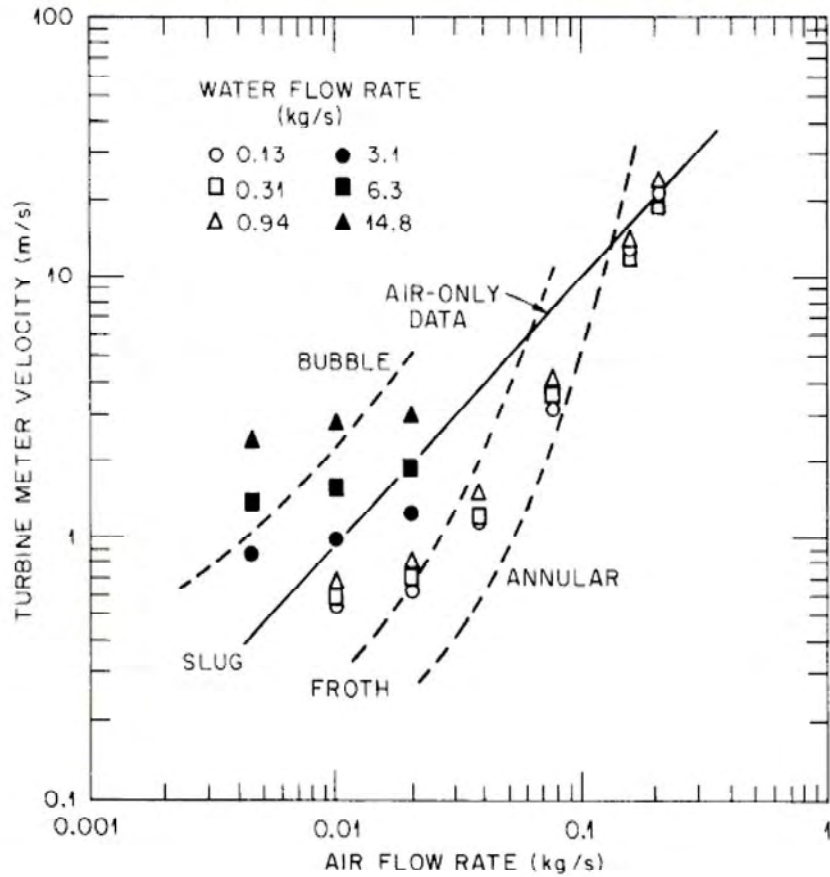
Fig. 14: Turbine meter velocities as a function of the air flow rate in two-phase vertical upflow, Hardy (1982)

For the lowest values of liquid flow rate (empty symbols), the velocity sensed by the turbine is lower than the air only line (continuous line in Fig. 14).The turbine response is dominated by the water velocity: the introduction of liquid tends to slow down the flow-meter. For increasing values of the air flow rate, the turbine velocity approaches the air only line (empty symbols) and finally, in the case of annular-mist flow regime, the turbine response is dominated by the air flow. At low air flows and high water rates the liquid phase is continuous and the turbine response is dictated by the water flow (black symbols).

Later on Hardy and Hylton (1983) confirmed that the response of a turbine flow-meter is likely to be more sensitive to the gas phase at high-void condition, while

at low-void flows they tend to react more to the liquid phase. In intermediate void fraction condition, like. slug flow regime, their behaviour is not well understood.

To attend sufficient accuracy in two phase flow is clear that the turbine flowmeter must to be use with an auxiliary sensor. This may either be a void fraction sensor or a pressure drop device such as a venturimeter or drag disk, of which the pressure drop approach appears to be technically more promising. A differential pressure producing flowmeter such as a venturimeter in series with a turbine is known to be a technically appropriate and straightforward method for measuring the volumetric and mass flow rates.

Two techniques currently studied do not require an auxiliary in-line sensor. The first uses the turbine meter itself as the drag body and combines the output of the turbine with that of a small differential pressure sensor connected across the inlet and outlet regions. This technique requires a homogenizer ahead of the turbine and measurement accuracies of $\pm 3\%$ for the volumetric flow rates of both phases have recently been reported for air/water mixtures up to a void fraction of 80%, (Abdul-Razzak et al. (1995)). The second technique is based entirely on analysis of the turbine output signal and has provided significant correlations of the signal fluctuations with void fraction. Accuracies of water volumetric flow rate measurement of $\pm 2\%$ have been reported when using air/water mixtures with void fractions of up to 25%, (Johnson et al. (1995)).

A new method for measuring the volumetric flow rate of each phase for two-phase, air and water, flowing upwardly in a vertical tube is developed by Shim (1997). The Two Turbine Flow Meter System (TYFMS), is composed of two turbine flow meters, a valve, two thermocouples, and two pressure transducers. For a given two-phase flow, the rate of rotation of the turbine flow meter is found to depend only upon the volumetric flow rates of gas and liquid at the point of measurement.

Axial-flow type turbine flow meter (TFM) was used for this study.

The frequency output signal (commonly pulses), f, of the turbine flow meter is conveniently expressed in units of volumetric flow rate, and the turbine flow meter output expressed as the variable S is defined as the product Kf, where K is the flow coefficient of the instrument obtained in single phase liquid flow. For the given two-phase flow in the vertical channel and at a fixed temperature, the rate of

rotation of the turbine flow meter was, to a good approximation, found to depend only upon the volumetric flow rates of gas and liquid at the point of measurement.

$$S = f\left(Q_g, Q_l\right)$$

This rate of rotation was nearly a linear function of the volumetric flow rate of the gas phase, and when the gas flow rate was zero, the turbine flow meter output (S) should only read the liquid flow rate.

For a fixed water flow rate, S is linearly related to the volumetric flow rate of gas:

$$S = k_1 + k_2 Q_g$$

where Qg represents the volumetric flow rate of gas, and k_1 and k_2 are constants that depend only on the water flow rate.

When the volumetric flow rates of gas are corrected to actual cubic meters per hour (acmh) at the locations of each Turbine flow meter, the TFM output values, S, show approximately a linear relationship to the gas flow rate. Both at the top and the bottom TFM values collapse into a single line for a given liquid flow rate. Therefore

$$S = k_1 + k_2 Q_{g,acmh}$$

where $Q_{g,\ acmh}$ represents the volumetric flow rate of gas in acmh. Assuming that k_2 is a linear function of liquid flow rate, Q_t, and the second term represents the liquid-gas interactions,

$$k_2 = k_3 + k_4 Q_l$$

Where k_3 and k_4 are constants.

Thus

$$S = k_1 + \left(k_3 + k_4 Q_l\right) Q_{g,acmh}$$

When the gas flow rate is zero $k_1 = Q_l$

From the equation of state:,

$$Q_{g,acmh} = \frac{p_{standard}}{T_{standard}} \frac{T}{p} Q_g$$

$$p_{standard} = 101.3 \text{ KPa}$$

$$T_{standard} = 21.1°C$$

Substituting:

$$S = Q_l + 0.027747 \left(k_3 + k_4 Q_l\right) \frac{T}{p} Q_g$$

This equation is the general equation governing TI'FMS for upflow.

It is used for the top (t) TFM and the bottom (b) TFM, by correcting for pressures and temperatures at the corresponding locations of turbine flow meters. The equations are,

$$S = Q_l + 0.027747(k_3 + k_4 Q_l)\frac{T_t}{p_t}Q_g$$

$$S = Q_l + 0.027747(k_3 + k_4 Q_l)\frac{T_b}{p_b}Q_g$$

Rearranging the equations to find the volumetric flow rate of liquid phase:

$$Q_l = \frac{S_t p_t T_b - S_b p_b T_t}{p_t T_b - p_b T_t}$$

And for the gas flow rate:

$$Q_l = \frac{(S_t - S_b) p_b p_t}{0.027747(k_3 + k_4 Q_l)(p_b T_t - p_t T_b)}$$

The constants are curve fitted with the following results,

$$S = k_1 + (k_3 + k_4 Q_l)Q_{g,acmh} = 1.050941 Q_l + 0.034519 Q_l Q_{g,acmh} + 0.248743 Q_{g,acmh}$$

Note, k_l value is not exactly equal to Qt as it was assumed in the model, and a correction factor should be included in the equation for Q_l:

$$Q_l = \frac{1}{1.050941}\left(\frac{S_t p_t T_b - S_b p_b T_t}{p_t T_b - p_b T_t}\right)$$

Therefore, by having a TITMS system one can calculate both Qt and Qg, volumetric flow rate of each phase of liquid and gas simultaneously, assuming pressures and temperatures are available at each location of the turbine flow meter.
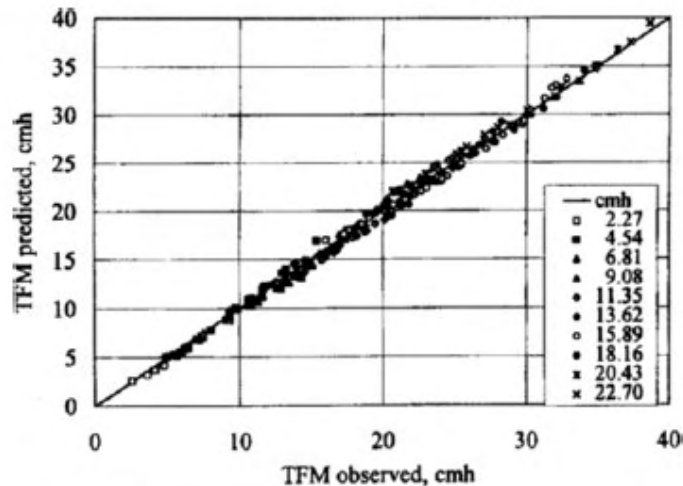
Fig. 15: Top Turbine flow meter (TFM) output predicted vs. observed values. (Shim (1997))

5. DRAG DISK METERS

The drag disk is a very simple device capable of measuring the force exerted by the fluid flow on a portion of the pipe cross section.

The disk can have different geometry and dimension; when the target is a disk less than 10% of the pipe cross- section is also know as a target flowmeter.

The flow range of the strain gage target flow meter is determined by the target size. By changing targets the flow range can be altered.

Largely used in the past, is not popular today, the only type actually produced is the body-target-type meter, that detect the force exerted by the flow using a strain gauge circuitry (www.venturemeas.com).

The dynamic force of fluid flow, or velocity of the approaching stream, is sensed as a drag force on a target (disc) suspended in the flow stream. This force is transmitted via a lever rod and flexure tube to an externally bonded, four active arm strain gage bridge. This strain gage bridge circuit translates the mechanical stress due to the sensor (target) drag into a directly proportional electrical output. Translation is linear. The drag force itself is usually proportional to the flow rate squared. The electrical output is virtually unaffected by variations in fluid temperature or static pressure head within the stated limitations of the unit.
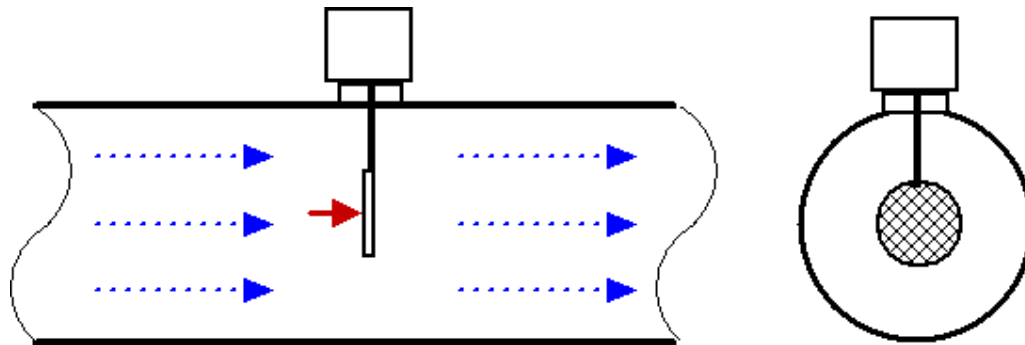
Fig. 16: Drag disk scheme

General performance characteristics

The main performance characteristics are:

- Sizes, range from 12.5 to 203 mm, and up to 1.2 m for probe design.
- Maximum measurement capacities range from 3.785 l/m to 28 l/m and from 1kg/h to practically every flow rate for probe type. One manufacturer (Target Flowmeter, Venture measurement Co. LLC, Spartanburg, SC, www.aaliant.com (2010)) offers devices for pipe sizes from 0.5 inches to 60 inches diameter (1.27 cm to 152.4 cm). The drag body size for the 0.5 inches diameter pipe is 0.4 inches diameter (1.016 cm) and the drag coefficient is around 4.5. It produces about 2 lb (8.9 N) of drag force at maximum flow. Drag bodies for larger pipe sizes take up a smaller fraction of the pipe cross section and have a drag coefficient of about 1.5; the maximum drag force is about 10 lb (44.5 N).
- Accuracy is $\pm 0.5\%$ of full scale, and $\pm 5.0\%$ for probe type.
- Repeatability is $\pm 0.15\%$ of rate
- The turndown ratio is approximately 15:1 (www.engineeringtoolbox.com/target-flow-metersd_ 497.html (2010)).
- Response time: from 0.002 to 0.1 sec
- Operating temperature ranges up to 150^oC, but special type meter can operate up to 649°C.
- Operating pressure ranges up to 20.70 MPa.
- Flow direction: Unidiretional/Bidiretional

Theory

A body immersed in a flowing fluid is subjected to a drag force given by:

$$F_d = \left(\frac{1}{2} C_d \cdot A_{t\arg et} \cdot \rho V^2 \right)$$

where C_d is the drag coefficient and A is the cross section area of the pipe.

The force sensed by the meter is proportional to the square of the velocity for Re>4000; in the laminar regime the results are not so predictable (Ginesi (1991)).
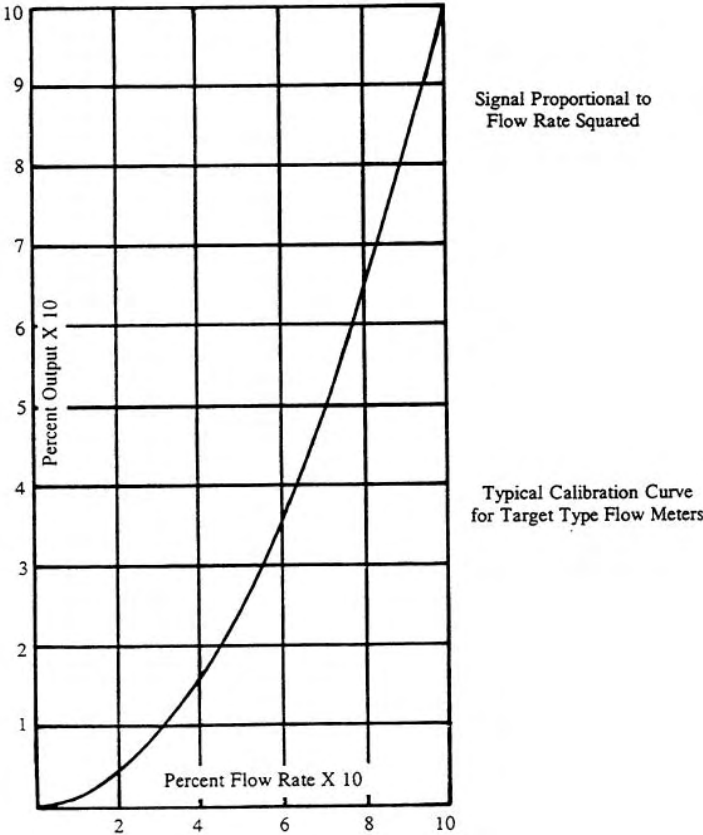
Fig. 17: Typical Calibration Curve for Target flow Meters

If, at the low end of the flow range, Re is between 1000 and 2000, the output for that part of the flow range may be affected by viscosity. Laminar flow exists below Re = 400 and a transition range exists between 400 and about 2000. The drag coefficient of the target, C_d, may vary in an unpredictable manner when Re is in the transition or laminar regions. The low Re can be brought about by low flow, high viscosity or both.

The drag coefficient is almost constant in a wide range of Re; Hunter and Green (1975) demonstrated that the variation in C_d over a Re number range of 2000-250000 is from about 0.97 to 1.93.

They suggested the following curve to fit the C_d values:

$$C_d = C_0 + C_1 \left(\frac{a}{A}\right) + C_2 \left(\frac{a}{A}\right)^2 + C_3 \left(\frac{a}{A}\right)^3 + C_4 \left(\frac{a}{A}\right)^4$$

where a is the area of the target and A the cross section of the pipe. They didn't introduce any term depending on the Re number.

Anderson was found that a full-flow drag plate of the type shown in Fig. 4 yielded a constant drag coefficient over a large Reynolds number range ($10^4 - 10^7$).
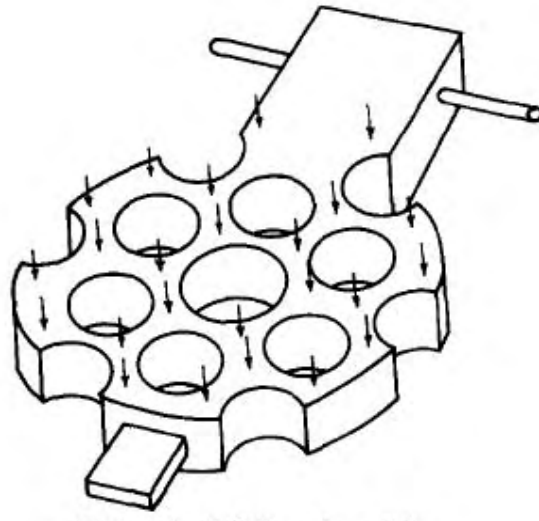
Fig. 18: Full-flow drag disk

Averill and Goodrich using a circular disc plate, found a coefficient C_d as in figure.

10^4

10^3

10^2

10^1

1

10^{-1}

Drag/coefficient, C_D

10^{-2} 10^{-1} 1 10^1 10^2 10^3 10^4 10^5 10^6 10^7

Reynolds number, $R = Vh/\nu$ INEL-A-12 384
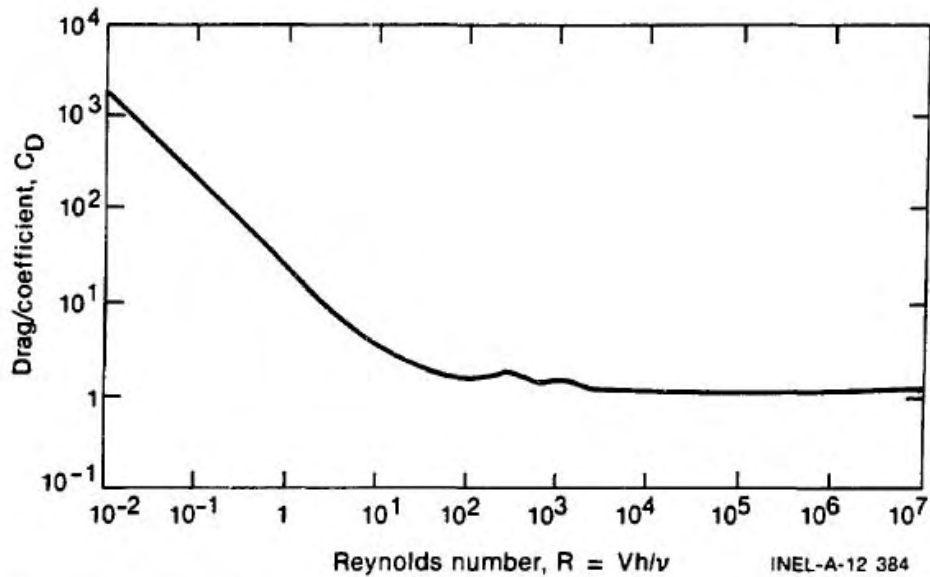
Fig. 19: Drag coefficient of circular and square plates (in normal flow) as a function of Re
(Averill and Goodrich)

Calibration, Installation and Operation for drag-target meter

The flow range of the instrument may be varied, within certain limits, by the installation of a new target or, by readjusting the amplifier gain.

A flowmeter can be calibrated with one fluid and then used with another fluid without loss of precision if the data are corrected for density change and the viscosities of both fluids are closely similar to keep Re within the same range. With all other factors constant, electrical output will vary directly with fluid density.

The two important parameter considered for calibration are: the target diameter and the force factor.

The effect of the drag is to produce a force on the target support rod, resulting in an electrical output signal from the strain gage transducer in the flowmeter. The relationship of the force on the rod to the signal is called the force factor and is a measure of the system sensitivity.

On bidirectional targets, both the upstream and downstream edges should be measured.

70

The meter should be installed on the upstream side of any flow controls or shut off valves to insure complete immersion of the target in the fluid at all rates of flow.

The small tube meters must be preceded by at least ten diameters of straight, uninterrupted flow line and followed by a minimum of five diameters. Do not precede the instrument with flexible corrugated tubing. Pipe, wafer or probe types should be preceded by a minimum of twenty diameters and followed by a minimum of ten diameters of straight uninterrupted flow line.

Sheppard et all (1975) have demonstrated that, in two-phase flow, if the drag meter is installed in a spool piece, with a turbine meter, accurate calculated measurements were attained only when the drag disc is positioned upstream the turbine and a flow disperser is installed.

A possible explanation is that the rotational motion of the turbine meter separates the phases and induces an annular flow rather than a dispersed flow.

If a bidirectional flow measuring unit has been ordered, the flowmeter should have 20 diameters of straight pipe on each side of the flowmeter unless the reverse flow accuracy is less important.

The use of steam traps, while at the option of the user, is strongly recommended in saturated steam systems, because minimizes the accumulation of condensate in the bottom of the pipe. This accumulation changes the effective cross-sectional area of the pipe, introducing an error in the indicated flow rate.

Flow surges may exceed the maximum rated electrical output by 100% for the Mark V (Aliiant productor) before a permanent zero shift is noted. Since the force sensing element is linear, the zero point need only be reset.

Except for extreme conditions, no recalibration is generally required.

Temperature effect

Averill and Goodrich during the Loss-of-Fluid Test at the LOFT facility   at the Loss-of-Fluid Test (LOFT) facility, EG&G Idaho, Inc., (at the Idaho National Engineering Laboratory, have measured the mass flow rates with the drag-disc turbine transducer (DTT).

The drag disc, used in the LOFT facility, is temperature sensitive; therefore, the authors proposed the following correction:

$$\rho U^2 = \left(Z_0 + Z_1 T \right) \frac{S_0 + S_1 T}{D_1} + \left(S_0 + S_1 T \right) V(t)$$

Where:

Z_0 is the zero offset from the zero offset temperature equation

Z_1 is the change in the zero offset with temperature

S_0 is the zero offset from the slop calibration temperature equation

S_1 is the change in slope calibration with temperature

D_1 is the full flow calibration at ambient temperature.

Hardy and Smith (1990), showed that the influence of the temperature induced changes on the resistance of the wires that connected the sensor to the control room could have influenced negatively the signal reading; a dedicated system to negate these effects was studied in order to avoid this issue.

The Drag body was tested under load cycles from 25% to 100% of the rated load and to thermal shock from 220 ºC to 25 ºC with no significant shift in zero.

The apparent strain due to thermal effects was measured at various temperatures under no load condition. The average thermal output was ±0.02 N/ºC. This correspond to an uncertainty for thermal effects of ±0.1% FS.

The combined effect of nonlinearity, hysteresis and repeatability was less than ±0.02% FS.

The Drag body was calibrated in air, steam and water single phase flow condition. The signal is effectively proportional to the square of the velocity with a scatter of the data equal to ± 10%.

Two-phase flow measurement capability and modeling

The use of two-phase full-flow drag devices has been described by several authors but all the research are relative to the years from 1960 to 1990. Actually the drag flow meter is not very used.

To obtain the momentum flux from the drag force, an accurate value of C_d is necessary.

For two-phase applications, a drag disk cannot easily be used because of the variation in momentum flux in the cross section due to void migration to the centre of a tube. Even with full-flow drag devices, it is difficult to determine the

correct value of the momentum flux to be applied. The only known parameters are the cross-sectional void fraction obtained from measurements and the individual-phase mass flows. Anderson developed a simple model with cross-sectionally averaged properties. Using a two-velocity separated flow model, he assumed that the forces on the drag body were equal to the sum of the individual forces due to both phases.

After some algebraic manipulation, the drag force was shown to be equal to

$$F_d = \frac{1}{2} C_D \cdot A_{t\arg et} \left[\alpha \cdot \left(\rho V^2 \right)_g + (1-\alpha) \cdot \left(\rho V^2 \right)_l \right]$$

where A is the test-section cross-sectional area and mg and mf are the superficial mass flow rates of gas and liquid, respectively.

Anderson claimed that the use of this technique resulted in mass flow measurements with an accuracy of better than 5%.

This model is the same used by Aya to analyse the behaviour of a turbine meter and a drag meter in a SP.

Drag coefficient C_d in two phase flow, can be correlate with the mass flux G:

$$C_{dTP} = C_{dMP} \left(1 + a \cdot (\alpha G) + b (\alpha G)^2 \right)$$

Where a and b are experimental coefficient, that are dependent from void fraction and flow pattern.

In transient analysis the Kamath and Lahey model (1981) can be used.

Kamath and Lahey's Model for Transient two phase flow

The equation of motion of a linear (or pivoted) drag-disk under the influence of spring, damping, drag and virtual mass forces is given by,

[The Rate of Change of linear (angular) Momentum of the Disk] = [Sum of External forces (torques) on the Disk due to spring, damping, drag and virtual mass effects]

To make the analysis applicable to both linear and pivoted disks, the equations can be written in terms of a generalized displacement function, r.

Hence,

[Rate of Change of Momentum of the Disk] $= \dfrac{I}{bg_c} \dfrac{d^2 r}{dr^2}$

73

$$F_{spring} = -k_s \frac{r}{b}$$

$$F_{damping} = -\xi \frac{dr}{dt} b$$

$$F_{drag} = \frac{C_{l_d} C_{D_l} A \cdot b}{2g_c} \left[\rho_l (1-\alpha) \left(v_l - \dot{r} a \right) \left(\left| v_l - \dot{r} a \right| \right) \right] + \frac{C_{g_d} C_{D_g} A \cdot b}{2g_c} \left[\rho_g \alpha \left(v_g - \dot{r} a \right) \left(\left| v_g - \dot{r} a \right| \right) \right]$$

Where the cross-sectional average of $\alpha_k \left(v_k - \dot{r} a \right) \left(\left| v_k - \dot{r} a \right| \right)$ has been expressed

in terms of the product of the averages using the correlation coefficient (C_{kd}), defined by:

$$C_{k_d} = \frac{\left\langle \alpha_k \left(v_k - \dot{r} a \right) \left(\left| v_k - \dot{r} a \right| \right) \right\rangle}{\left\langle \alpha_k \right\rangle \left\langle \left(v_k - \dot{r} a \right) \right\rangle \left\langle \left(\left| v_k - \dot{r} a \right| \right) \right\rangle}$$

It has been found in this study that the two-phase drag coefficient is not very different from the single-phase value of 1.13. However, the effective drag coefficient can be expected to be somewhat different due to the presence of the stem which holds the disk. In addition, the correlation coefficients, C_{ld} and C_{gd} for the non-uniform velocity profile due to the presence of the shroud, are different from unity.

Thus the value of the effective drag coefficient, which is the product of C_{Dk} and C_{kd}, was obtained from single-phase calibration runs to be unity. This value was used for all single and two-phase flow evaluations.

The force due to virtual mass effects can be written as,

$$F_{drag} = \frac{C_m \left\langle \rho \right\rangle D^3 b}{3g_c} \frac{d}{dt} \left[U_m - \dot{r} a \right]$$

This term arises because of the acceleration of the two-phase mixture relative to the disk. The center-of-mass velocity,

$$U_m = \frac{\rho_l (1-\alpha) v_l + \rho_g \alpha v_g}{\rho_l (1-\alpha) + \rho_g \alpha} = \frac{G}{\rho}$$

has been taken to be the appropriate velocity of the two-phase mixture. The virtual volume of a disk, $D^3/3$, has been previously obtained from a potential flow analysis (Lyle and Lai, (1972)). The virtual mass coefficient, C_m, is known to depend on the geometry of the disk and the fluid properties.

Substituting these expressions into the equation of motion, one obtains:

$$
\frac{dv_l}{dt} = \left\{ \frac{S-1}{(S+\phi)(1+\phi)} \left[\phi \left(\frac{1}{\rho_l} \frac{d\rho_l}{\rho dt} - \frac{1}{\rho_g} \frac{d\rho_g}{dt} \right) - \frac{\rho_l}{\rho_g} \frac{1}{\alpha^2} \frac{d\alpha}{dt} \right] - \frac{1}{(S+\phi)} \frac{dS}{dt} \right\} v_l +
$$

$$
- \left(\frac{C_{l_d} C_{D_l}}{C_m} \right) \left(\frac{3A}{2D^3} \right) \left(\frac{\phi}{S+\phi} \right) \left(v_l - r\,\dot{a} \right) \left(\left| v_l - r\dot{a} \right| \right) +
$$

$$
- \left(\frac{C_{g_d} C_{D_g}}{C_m} \right) \left(\frac{3A}{2D^3} \right) \left(\frac{S^2}{S+\phi} \right) \left(v_l - \frac{r\,\dot{a}}{S} \right) \left(\left| v_l - \frac{r\dot{a}}{S} \right| \right) +
$$

$$
+ \frac{3g_c k_s r}{C_m \left(D^3 b^2 \right)(S+\phi)\rho_g \alpha} + \frac{3g_c \dot{\xi} r}{C_m \left(D^3 \right)(S+\phi)\rho_g \alpha} +
$$

$$
- \left(\frac{1+\phi}{S+\phi} \right) \frac{r^2}{b} \sqrt{1-a^2} + \left[\frac{3I}{C_m \left(D^3 b^2 \right)(S+\phi)\rho_g \alpha} + a \left(\frac{1+\phi}{S+\phi} \right) \right] \ddot{r}
$$

The above equation can be integrated using the GEAR algorithm. Once (v_l) is known, the instantaneous mass flux is readily calculated from

$$
G(t) = \left[\rho_l (1-\alpha) + \rho_g \alpha S \right] v_l
$$

The dynamics of a pivoted type drag-disk were evaluated numerically, using the a sinusoidal forcing function of the form,

$r(t) = 0.011 \sin \left(2\pi ft \right)$

Pressure = 6.89 MPa,

α = *constant (0.2 and 0.3)*

The transient liquid phase velocity, calculated, and the quasi-steady values, obtained by setting all the time derivatives to zero,

75

$$v_l = \pm \left[\frac{3g_c k_s |r|}{Ab^2 \left(C_{D_l} C_{l_d} \rho_l (1-\alpha) \right) + C_{D_g} C_{g_d} \rho_g \alpha S^2} \right]^{1/2}$$

were calculated. The corresponding mass fluxes were determined using the $G(t)$ expression, and their modulus ($G(t) = |G| e^{1[2\pi f t + \beta]}$ where $|G|$ is the modulus and β is the phase angle) are compared in Fig. 20. For frequencies less than about 10 Hz, the transient terms are obviously not important.

The range 10-50 Hz is seen to contain a resonance. As can be seen in the expression for the un-damped natural frequency,

$$\omega_n^2 = \left[\frac{g_c k_s}{I + \frac{1}{3} C_m D^3 b^2 a \alpha} \right]$$

the frequency at which the resonance occurs depends on the magnitude of the spring stiffness, and the mass (moment of inertia) of the moving parts and the fluid density (hence the dependence on the void fraction).

In the region above 50 Hz, transient effects are obviously important.

Summarizing the results, it is seen from Fig. 20 that, for the drag-disk analyzed, the quasi-steady equation is valid below about 10 Hz. Above this frequency transient effects must be taken into account.

Fortunately, for many cases of practical significance a 10 Hz frequency response is adequate, and thus equations above can normally be employed to calculate the transient mass flux.
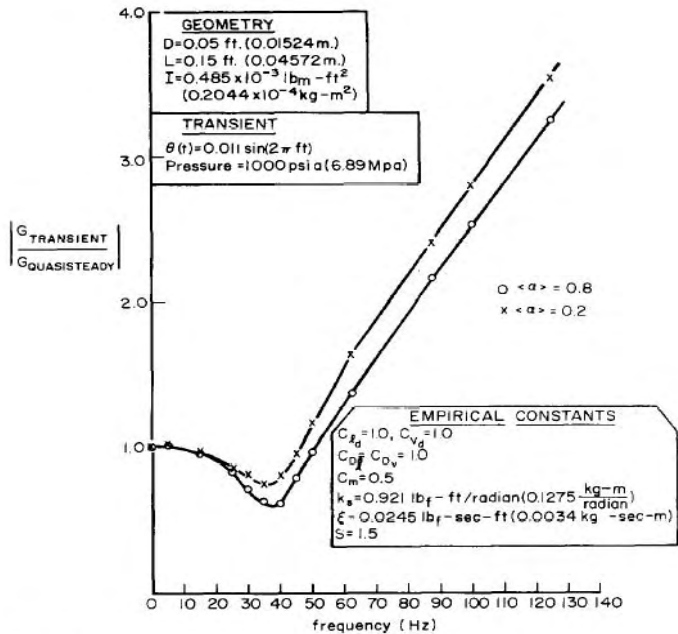
Fig. 20: Drag disk frequency response

Two phase flow applications

Because it is a momentum-sensing device, the drag meter has been used in conjunction with volume-sensing flowmeters, or with densitometer to allow density and mass flow to be deduced in a large number of nuclear loss-of-coolant experiments.

Hardy (1990) developed two strain-gauge-based drag transducers designed to make two-phase flow measurements in simulated LOCA environments.

One transducer, a drag body (DB), was designed to measure the bidirectional average momentum flux passing through an end box. The second drag sensor, a breakthrough detector (BTD). was designed to sense liquid downflow from the upper plenum to the core region.

The DB had a rangeability of over 200 to 1 with a resolution of 0.1% of FS. The overall measurement uncertainty during transient conditions is less than ±5% of reading. This uncertainly value included thermal effects, gage factor variations, lead wire effects, signal-conditioning electronics errors, hysteresis, nonlinearity, and repeatability.

77

The BTD had a resolution of 1.0% FS and an overall uncertainty of ±10% FS. For the DB the thermal effects, especially apparent strain, were reduced to acceptable limits by hand-selecting matched pairs of strain gages and employing them in a four-active-gauge bridge arrangement. The four active gages also increased the transducer output, which raised the signal-to-noise ratio lo a reasonable value. The BTD used two active strain gages and two dummy gauges for temperature compensation, which resulted in sufficient accuracy for its detection requirement. Rigorous acceptance testing results showed that the DB and BTD designs are capable of surviving the severe environment of high-temperature steam/water mixtures, the thermal shocks, and the

mechanical shocks induced by condensation. With the exception of the high-cycle fatigue problem, the drag transducers functioned very well in the foreign experimental test facilities. The data produced were of high quality and aided substantially in understanding the two-phase flow phenomena that occur during the refill/reflood stages of LOCAs in PWRs.

Hardy (1982) tested a SP where the drag have been coupled with a string probe.

Instrumentations have been devised and calibrated for two phase mass flux measurement under simulated pressurized-water reactor reflood conditions.

The drag disk and the string probe were positioned in three locations in the Japanese Slab Test Facility downcomer.

Fluid phenomena studied in the downcomere were:

- condensation-induced flow (oscillating liquid level)
- emergency core cooling (ECC) penetration.

The drag disk used in this experiment was bidirectional and forced calibrated in both direction.

The calibration constant may be a function of sensor orientation, flow velocity, and flow regime.

During this research Hardy determined the calibration constant with the final goal to provide a mass flow algorithm to predict fluid flow in the downcomer.

This spool gave mass flux estimation between + 40% and -30%, using the simplest model: homogeneous model.

Experiments were performed in both single and two phase flow, and correlations has been determined.

The first step in the calibration in single air and water flow.

For liquid calibration the velocity value of the water was determined in the following manner:

$$V_{dd} \quad \left(\frac{\overline{\rho_{TP} V^2_{DD}}}{\rho_l} \right)^{1/2}$$

And then the mass flow rate was:

$$\dot{m} = 1.242 \rho_l V_{dd}^{1.02}$$

For the vapour calibration a correcting term was required:

$$\dot{m} = 1.166 \rho_g V_{dd}^{1.056} \left(\frac{\rho_l}{\rho_g} \right)^{0.528}$$

In two phase flow, two distinct correlations were required to fit the data obtained. The reason of this can be a flow pattern transitin: from droplet mist to froth flow. But other possible reasons were:

flow disturbances and changing slip ratio.

The two correlation has been defined for mist and froth flow; the major criterion that delineates between the curves has been found in the void fraction value. If the void fraction was above 0.92 the flow was in mist regime, while at lower values the flow was froth.

Then the two correlations were:

$$\dot{m} = \left(3.654 \cdot 10^{-6} \right) \left(\rho_{SP} \right)^{1.645} \left(\rho_l \right)^{1.645} \left(V_{dd} \right)^{3.29} \quad \text{for froth regime } (\alpha \leq 0.92)$$

$$\dot{m} = 0.3884 \left(\rho_{SP} \right)^{0.567} \left(\rho_l \right)^{0.567} \left(V_{dd} \right)^{1.134} \quad \text{for mist regime } (\alpha > 0.92)$$

For $\alpha = 0.92$ and $\rho_l \left(\rho_{SP} V_{dd}^2 \right)^{1/2} \geq 300$ the liquid correlation was used instead of the froth flow algorithm. See Fig. 21.
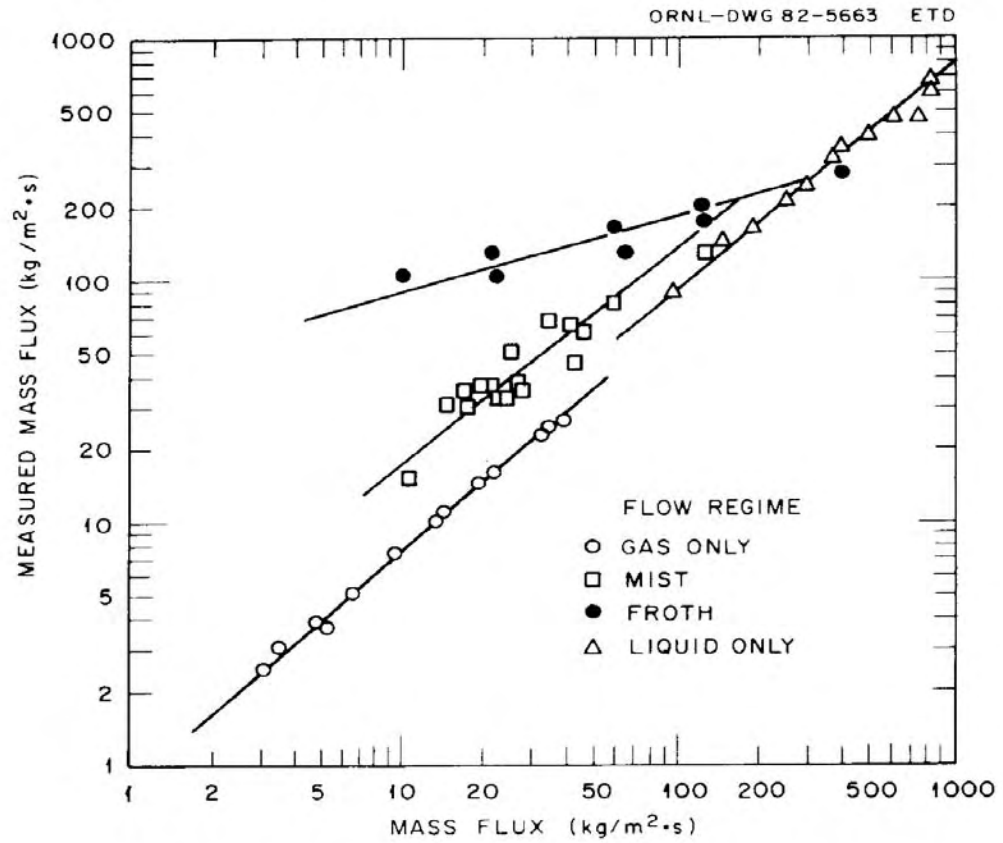
Fig. 21: Drag disk and string probe data vs. measured mass flux for single and two phase flow (Hardy (1982))
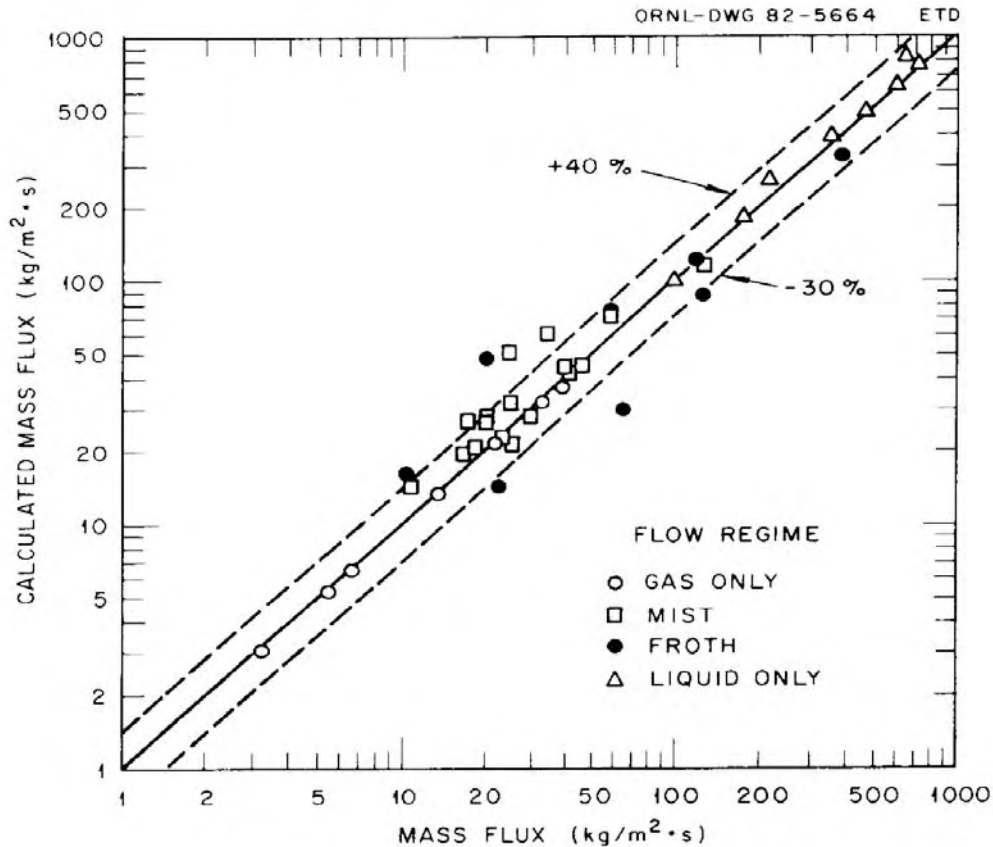
Fig. 22: Comparison of calculated with actual mass flux for single and two phase flow
(Hardy (1982))

Hardy and Smith (1990) studied a Drag body installed in order to monitor the momentum passing in both directions through the tie plate. The environmental conditions of the test facilities were: pressure up to 2.1 MPa and temperature up to 300ºC. Thermal transients up to 40ºC/s where expected The results were compared to the Δp measured across the plate, which is likewise proportional to flow momentum. Almost all the data fell in the uncertainty band ±20%. The scatter was due to the low sensitivity of the differential pressure device for values of Δp around 20 mm of water (see Fig. 23).
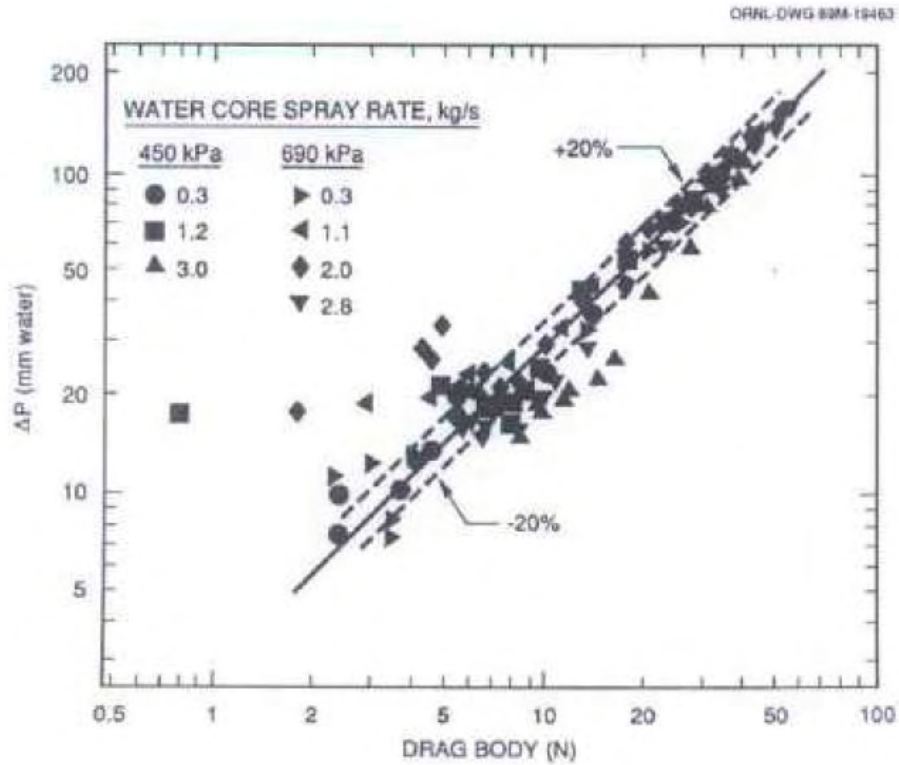
Fig. 23: Comparison of differential pressure and drag body measurements across the tie plate, (Hardy and Smith (1990))

A second comparison was performed with the momentum flux evaluated from the known input flow rates:

82
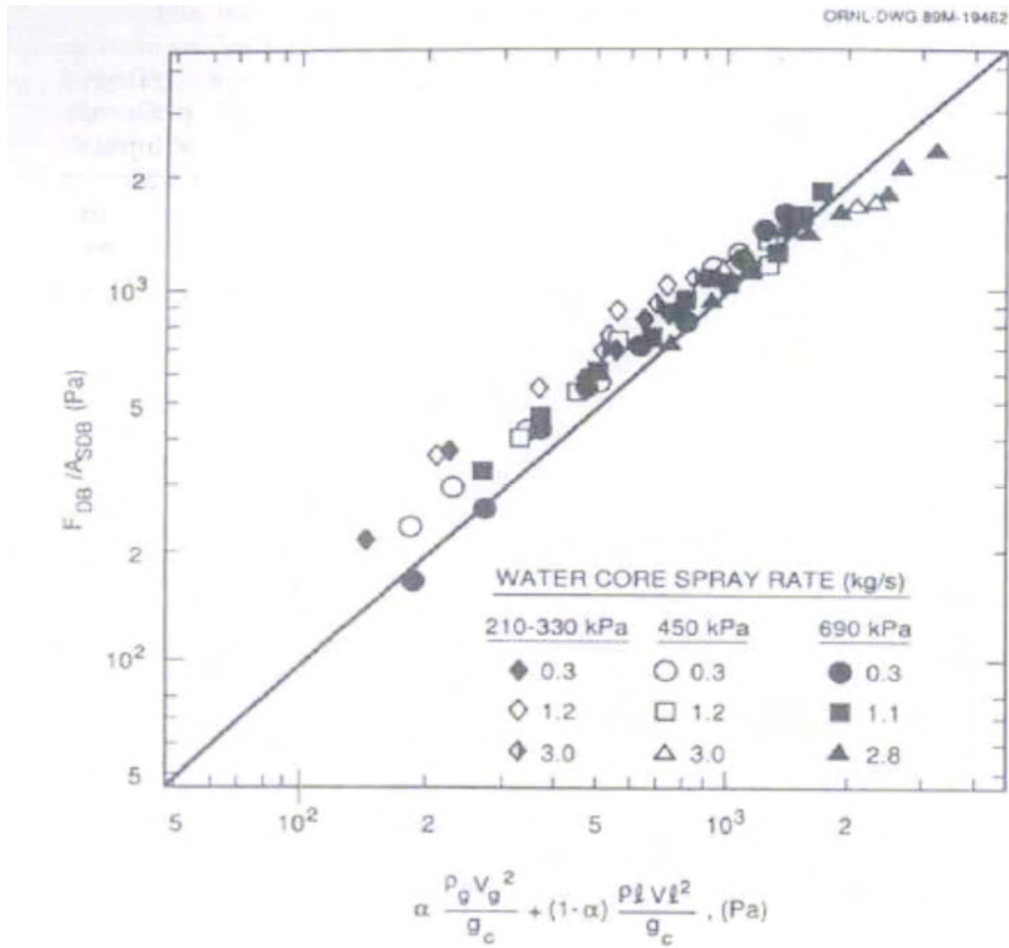
Fig. 24: **Comparison of momentum flux measured by the drag body with momentum flux calculated from measured data, Hardy and Smith (1990)**

In order to calculate the two-phase mass flow rate, the momentum measured with the drag plate was combined with the velocity detected by a turbine flow-meter:

$$\dot{m} = \left(\frac{\left(\rho V^2\right)_{DD}}{V_T} \right) \rho V$$

where DD indicates the Drag plate data and T the turbine flow-meter data. The results are showed in Fig. 25. The data provide a good estimate of the mass flow rate; almost all the data fell in an error band $\pm 20\%$.
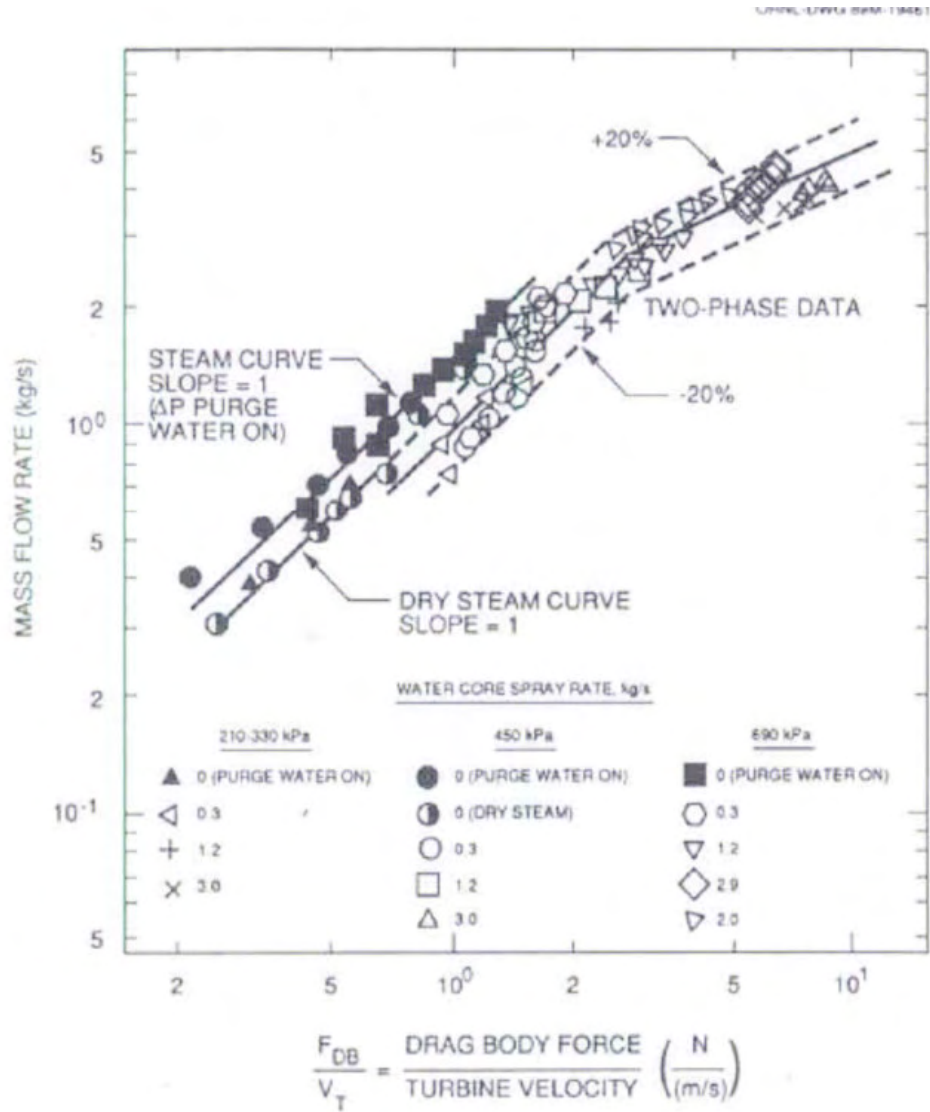
Fig. 25: Comparison of mass flow rate from measured inputs with a mass flow model combining drag body and turbine meter measurement, Hardy and Smith (1990)

6. DIFFERENTIAL PRESSURE METERS

The calculation of fluid flow rate by reading the pressure loss across a pipe restriction is perhaps the most commonly used flow measurement technique in industrial applications. The pressure drops generated by a wide variety of geometrical restrictions have been well characterized over the years, and, these primary flow elements come in a wide variety of configurations, each with specific application strengths and weaknesses. Different geometries are used for different measurements, including the orifice plate, flow nozzle, segmental wedge, V-cone, and Venturi tube. In this section general performance and characteristics are reported for the different designs.

Theory of differential flowmeter in single phase flow

In the 18th century, Bernoulli first established the relationship between static and kinetic energy in a flowing stream. As a fluid passes through a restriction, it accelerates, and the energy for this acceleration is obtained from the fluid's static pressure. Consequently, the line pressure drops at the point of constriction. Part of the pressure drop is recovered as the flow returns to the unrestricted pipe.
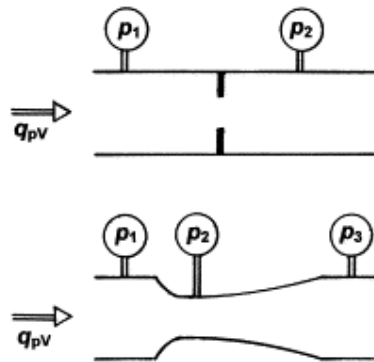
Fig. 26: Flow through an orifice (top) and a Venturi tube (bottom) with the positions for measuring the static pressure (Jitshin (2004))

A general equation for differential pressure flow meters is given by:

$$Q = CA_2 \left(\frac{2\Delta p}{\rho\left(1-\beta^4\right)} \right)^{0.5}$$

Q = flow rate through pipe and meter,

C = discharge coefficient for the particular meter, dimensionless,

A_2 = constricted area perpendicular to flow,

$\Delta p = p_1 - p_2$

p_1 = undisturbed upstream pressure in the pipe,

p_2 = Pressure in the pipe at the constricted area, A_2 ,

$\beta = D_2/D_1$ = (diam. at A_2/pipe diam.),

ρ = fluid density,

If also compressibility and thermal expansion effects are considered the equation became (Oliveira et all. (2008):

$$Q = \left[CA_2 \left(\frac{2\Delta p}{\rho\left(1-\beta^4\right)} \right)^{0.5} \right] \cdot F_a \cdot Y$$

F_a thermal expansion correction factor
Y compressibility coefficient.

The numerical values of F_a for orifice plates given in ISO5167 are based on data determined experimentally. For nozzles and Venturi tubes they are based on the thermodynamic general energy equation.
For liquids (uncompressible fluids), is always $F_a = 1$
For steam and gases (compressible fluids) $1 < F_a$
Is calculated with different formulas depending on the device geometry.
For example for a orifice plate, ISO5167-1:1991(E) section 8.3.2.2 gives on the following formula:

$$F_a = 1 - \left(0.41 + 0.35 \cdot \beta^4\right) \frac{\Delta p}{kp_1}$$

Where k is the isentropic exponent, a "Fluid property" that depends on fluid pressure and temperature. Is related with adiabatic expansion of the fluid in the bore zone.

The discharge coefficient C is influenced by the Reynolds number and by the "beta ratio," the ratio between the bore diameter of the flow restriction and the inside diameter of the pipe.

Additional parameters or correction factors can be used in the derivation of C, depending on the type of flow element used. These parameters can be computed from equations or read from graphs and tables available from the American National Standards Institute (ANSI), the American Petroleum Institute (API), the American Society of Mechanical Engineers (ASME).

The discharge coefficients are determined by laboratory tests that reproduce the geometry of the installation. Published values generally represent the average value for that geometry over a minimum of 30 calibration runs. The uncertainties of these published values vary from 0.5% to 3%. By using such published discharge coefficients, it is possible to obtain reasonably accurate flow measurements without in-place calibration. In-place calibration is required if testing laboratories are not available or if better accuracy is desired than that provided by the uncertainty range noted above. The relationship between flow and pressure drop varies with the velocity profile, which can be laminar or turbulent as a function of the Reynolds number (Re), which for liquid flows can be calculated using the relationship:

At low Reynolds numbers (generally under Re = 2,000), the flow is laminar and the velocity profile is parabolic. At high Reynolds numbers (well over Re = 3,000), the flow becomes fully turbulent, and the resulting mixing action produces a uniform axial velocity across the pipe.

The transition between laminar and turbulent flows can cover a wide range of Reynolds numbers; the relationship with the discharge coefficient is a function of the differential flow meter.

For example for a orifice plate, the formula used by ISO5167-1:1991 section 8.3.2.1 is:

$$C = 0.5959 + 0.0312\beta^{2.1} - 0.184\beta^8 + 0.0029\beta^{2.5} \cdot \left(\frac{10^6}{Re_D}\right)^{0.75}$$

$$+ 0.09 L_1 \beta^4 \left(1 - \beta^4\right)^{-1} - 0.0337 L_2' \beta^3$$

87

Where L'_1 and L'_2 are geometrical parameters of the orifice plate as described on same page of the document; and Re_D is the Reynolds number for up stream flow. Jitschin (2004) performed some experiments using a classical venture tube and a thin orifice in gas flow. He found that the discharge coefficient C_d approaches the value 1 at large Reynolds numbers (in agreement with DIN 1952 and EN ISO 5167-1), which gives the result C_d=0.990±0.005 (depending on wall roughness) at Re>2×10^5. The discharge coefficient becomes significantly smaller than 1 with decreasing Reynolds numbers. The reason for this behaviour is, for the author, an increasing importance of friction at the walls.

The data in Fig. 27 essentially follow an universal curve with considerable scatter. A closer look at the scatter reveals that even discharge coefficients of two nozzles with the same nominal dimensions differ significantly from each other, as can be seen, for example, by comparing the upward and downward triangles symbolising the data of the nozzles with 1.6 mm throat diameter. Thus, one obvious reason for the scatter are manufacturing tolerances. Apparently, Venturi tubes with the same nominal dimensions are not equal.

In order to get some more insight into the flow inside the Venturi tube, the author also measured the throughput in the classical Venturi tube operated in the reverse direction, with 8° conical confusor and 21° conical diffuser (Fig. 28). In the reverse direction, the discharge coefficients are substantially smaller than in the normal direction, particularly at small Reynolds numbers. This behaviour is to be expected. In the reverse direction, the entrance section of the Venturi tube is considerably longer, leading to much more wall friction.
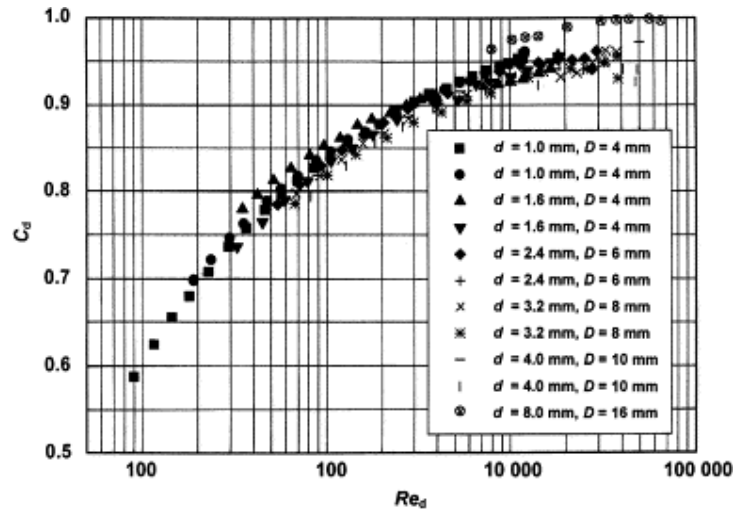
Fig. 27: Discharge coefficient of classical Venturi tubes with given throat diameters vs. Reynolds number. (Jitschin (2004))
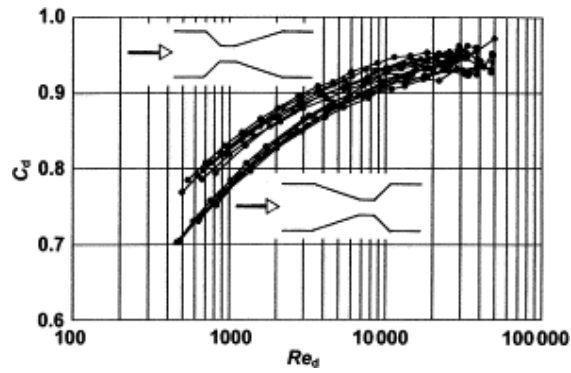
Fig. 28: Discharge coefficient of 6 Venturi tubes operated in normal direction (upper curves) and reversed direction (lower curves). (Jitschin (2004))

89

Table 3: Primary or "Head Flow" Element Comparisons					
PRIMARY ELEMENT	RECOMMENDED SERVICE	MINIMUM RE LIMITS	SIZES	ADVANTAGES	LIMITATIONS
Square edge concentric orifice plate	Clean liquids, gases, steam	≥ 2000	≥ 1/2 in	Easy to install Low cost Easy to replace	Relaxation piping requirements High head loss Accuracy affected by installation and orifice condition
Conical/quadrant edge concentric orifice plate	Viscous liquids	≥500	1 to 6 in	Easy to install Low cost Easy to replace	Relaxation piping requirements High head loss Accuracy affected by installation and orifice condition
Eccentric/segmental orifice plate	Liquids and gases containing secondary fluid phases	›10,000	4 to 14 in	Easy to install Low cost Easy to replace	Relaxation piping requirements High head loss Accuracy affected by installation and orifice condition Higher uncertainties of discharge coefficient data
Integral orifice	Clean liquids, gases, steam	›10,000	1/2 to 2 in	Easy to install No lead lines Low cost	Relaxation piping requirements Proprietary design requires calibration High head loss More prone to clogging than standard orifice plate
Venturi/flowtube	Clean & dirty liquids, gases, steam; slurries	›75,000	1/2 to 72 in	Low head loss 2 to 9 times less relaxation piping than orifice Higher flow capacity than orifice for the same differential pressure Accuracy less affected by wear and installation conditions than orifice	High initial cost
Nozzle	Clean liquids, gases, steam	›50,000	›2 in	Higher flow capacity than orifice for the same differential pressure Accuracy less affected by wear and installation conditions than orifice Good for high temperature and high velocity applications Mass transfer standard for gases	Harder to replace than orifice High head loss
Segmental wedge	Dirty liquids, gases, steam; slurries; viscous liquids	›500	≥1/2 in	No lead lines Minimal clogging potential 40% less head loss than orifice Minimal relaxation piping	Proprietary design needs calibration High initial cost Requires remote seal differential pressure transmitter, harder to zero
Venturi cone	Clean & dirty liquids, gases, steam; viscous liquids	None cited	1 to 16 in	Minimal relaxation piping Low flow capability	Proprietary design

Tab. 4: Differential pressure meter comparison

Accuracy and Rangeability

Bernoulli's equation states that the pressure drop across the constriction is proportional to the square of the flow rate. Using this relationship, 10 percent of full scale flow produces only 1 percent of the full scale differential pressure. At 10 percent of full scale flow, the differential pressure flowmeter accuracy is dependent upon the transmitter being accurate over a 100:1 range of differential pressure. Differential pressure transmitter accuracy is typically degraded at low differential pressures in its range, so flowmeter accuracy can be similarly degraded. Therefore, this non-linear relationship can have a detrimental effect on the accuracy and turndown of differential pressure flowmeters.

Because of the nonlinear relationship between flow and differential pressure, the accuracy of flow measurement in the lower portion of the flow range can be degraded. Accuracy can also be degraded when Reynolds number is low.

Flow element precision is typically reported in percentage of actual reading (AR) terms, whereas Δp cell accuracy is a percentage of calibrated span (CS). A Δp cell usually provides accuracy of ±0.2% of the calibrated span (CS). This means that, at the low end of a 10:1 flow range (at 10% flow), corresponding to a differential pressure range of 100:1, the flowmeter would have an error of ±20% AR. For this reason, differential producing flowmeters have historically been limited to use within a 3:1 or 4:1 range (Omega Handbook (1995))..

Flowmeter rangeability can be further increased without adverse effect on accuracy by operating several Δp flowmeters in parallel runs. Only as many runs are opened at a time as are needed to keep the flow in the active ones at around 75-90% of range. Another option is to stack two or more transmitters in parallel onto the same element, one for 1-10%, the other for 10-100% of full scale (FS) Δp produced. Both of these techniques are cumbersome and expensive. Intelligent transmitters offer a better option. The accuracy of intelligent transmitters is usually stated as ±0.1% CS, which includes only errors due to hysteresis, rangeability and linearity. Potential errors due to drift, temperature, humidity, vibration, overrange, radio frequency interference and power supply variation are all excluded. Including them, inaccuracy is about 0.2% CS. Because intelligent Δp transmitters can based on their own measurements automatically switch ranges between two calibrated spans (one for 1-10%, the other for 10-100% of FS d/p), it should be possible to obtain installations with 1% AR inaccuracy over a 10:1 flow range (Omega Handbook (1995)).

In some applications (as gas flow rate measure or in presence of pressure and temperature variations) the flowmeter should be designed carefully because changes in operating pressure and operating temperature can dramatically affect the flow measurement. In other words, the fluid density can vary significantly during operation. As a result, the differential pressure produced by the flowmeter can also vary significantly during operation. Failure to compensate for these effects can cause flow measurement errors of 20 percent or more in many applications (Omega Handbook (1995)). In these applications, a flow computer

can be used to calculate the corrected flow measurement using actual pressure, temperature and flow measurements.

Errors due to incorrect installation of the meter can be substantial (up to 10%). Causes of such errors can be the condition of the mating pipe sections, insufficient straight pipe runs, and pressure tap and lead line design errors.

Under turbulent flow conditions, as much as 10% of the Δp signal can be noise caused by disturbances from valves and fittings, both up- and downstream of the element, and by the element itself. In the majority of applications, the damping provided in Δp cells is sufficient to filter out the noise. Severe noise can be reduced by the use of two or more pressure taps connected in parallel on both sides of the Δp cell.

Pulsating flow can be caused by reciprocating pumps or compressors. This pulsation can be reduced by moving the flowmeter away from the source of the pulse, or downstream of filters or other dampening devices. Pulsation dampening hardware can also be installed at the pressure taps, or dampening software can applied to the Δp cell output signal. One such filter is the inverse derivative algorithm, which blocks any rate of change occurring more quickly than the rate at which the process flow can change (Omega Handbook (1995)).

Piping, Installation and Maintenance

Installation guidelines are published by various professional organizations (ISA, ANSI, API, ASME, AGA) and by manufacturers of proprietary designs. These guidelines include such recommendations as:

When, in addition to measuring the flow, the process temperature or pressure is also to be measured, the pressure transmitter should not be installed in the process pipe, but should be connected to the appropriate lead line of the flow element via a tee.

Similarly, the thermowell used for temperature measurement should be installed at least 10 diameters downstream of the flow element, to prevent velocity profile distortions.

In order for the velocity profile to fully develop (and the pressure drop to be predictable), straight pipe runs are required both up and downstream of the Δp element. The amount of straight run required depends on both the beta ratio of the installation and on the nature of the upstream components in the pipeline. For

example, when a single 90° elbow precedes an orifice plate, the straight-pipe requirement ranges from 6 to 20 pipe diameters as the diameter ratio is increased from 0.2 to 0.8.

In order to reduce the straight run requirement, flow straighteners can be installed upstream of the primary element.

The size and orientation of the pressure taps are a function of both the pipe size and the type of process fluid. The recommended maximum diameter of pressure tap holes through the pipe or flange is 1/4" for pipes under 2" in diameter, 3/8" for 2" and 3" pipes, 1/2" for 4 to 8" and 3/4" for larger pipes. Both taps should be of the same diameter, and, where the hole breaks through the inside pipe surface, it should be square with no roughness, burrs, or wire edges. Connections to pressure holes should be made by nipples, couplings, or adaptors welded to the outside surface of the pipe.

The Δp transmitter should be located as close to the primary element as possible. Lead lines should be as short as possible and of the same diameter. Both lead lines should be exposed to the same ambient conditions and be shielded from sunlight. In clean liquid or gas service, the lead lines can be purged through the Δp cell vent or drain connections, and they should be flushed for several minutes to remove all air from the lines. Entrapped air can offset the zero calibration.

Differential flowmeter types
Orifice Plate

A flat plate with an opening is inserted into the pipe and placed perpendicular to the flow stream. As the flowing fluid passes through the orifice plate, the restricted cross section area causes an increase in velocity and decrease in pressure. The pressure difference before and after the orifice plate is used to calculate the flow velocity.
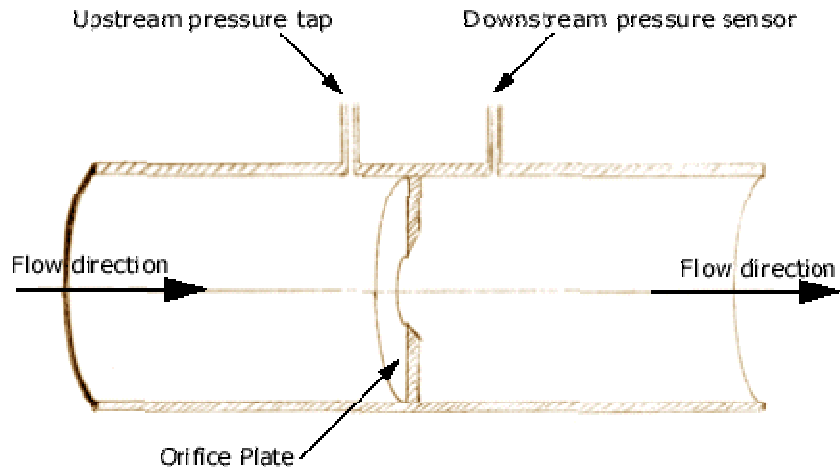
Fig. 29: Orifice Flowmeter

The orifice plate is commonly used in clean liquid, gas, and steam service. It is available for all pipe sizes, and if the pressure drop it requires is free, it is very cost-effective for measuring flows in larger pipes (over 6" diameter).

The orifice plate can be made of any material, although stainless steel is the most common. The thickness of the plate used (1/8-1/2") is a function of the line size, the process temperature, the pressure, and the differential pressure. The traditional orifice is a thin circular plate (with a tab for handling and for data), inserted into the pipeline between the two flanges of an orifice union. This method of installation is cost-effective, but it calls for a process shutdown whenever the plate is removed for maintenance or inspection. In contrast, an orifice fitting allows the orifice to be removed from the process without depressurizing the line and shutting down flow. In such fittings, the universal orifice plate, a circular plate with no tab, is used.
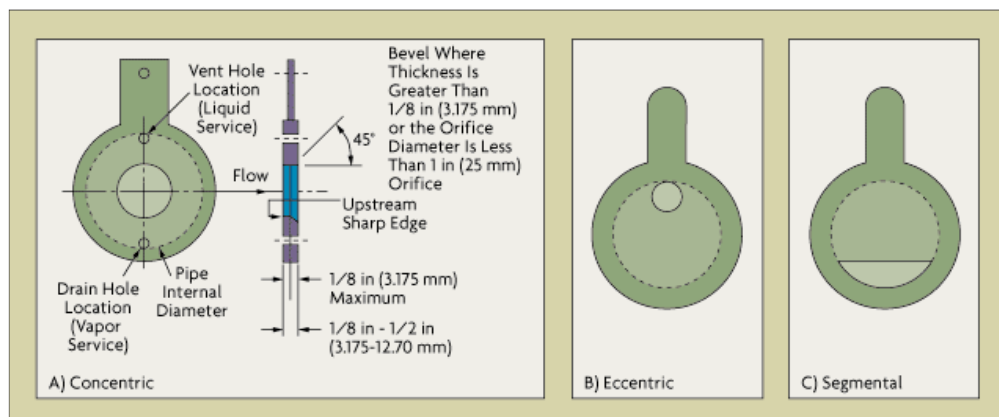
Fig. 30: Orifice Plate types ((Omega Handbook (1995)).**

The concentric orifice plate (Fig. 30) has a sharp (square-edged) concentric bore that provides an almost pure line contact between the plate and the fluid, with

94

negligible friction drag at the boundary. The beta (or diameter) ratios of concentric orifice plates range from 0.25 to 0.75. The maximum velocity and minimum static pressure occurs at some 0.35 to 0.85 pipe diameters downstream from the orifice plate. That point is called the vena contracta (Fig. 31) . Measuring the differential pressure at a location close to the orifice plate minimizes the effect of pipe roughness, since friction has an effect on the fluid and the pipe wall.

Flange taps are predominantly used in the United States and are located 1 inch from the orifice plate's surfaces. They are not recommended for use on pipelines under 2 inches in diameter. Corner taps are predominant in Europe for all sizes of pipe, and are used in the United States for pipes under 2 inches. With corner taps, the relatively small clearances represent a potential maintenance problem. Vena contracta taps (which are close to the radius taps, Fig. 30) are located one pipe diameter upstream from the plate, and downstream at the point of vena contracta. This location varies (with beta ratio and Reynolds number) from 0.35D to 0.8D.

The vena contracta taps provide the maximum pressure differential, but also the most noise. Additionally, if the plate is changed, it may require a change in the tap location. Also, in small pipes, the vena contracta might lie under a flange. Therefore, vena contracta taps normally are used only in pipe sizes exceeding six inches.

Radius taps are similar to vena contracta taps, except the downstream tap is fixed at 0.5D from the orifice plate. Pipe taps are located 2.5 pipe diameters upstream and 8 diameters downstream from the orifice. They detect the smallest pressure difference and, because of the tap distance from the orifice, the effects of pipe roughness, dimensional inconsistencies, and, therefore, measurement errors are the greatest.

Figure 2-1: Orifice Plate Pressure Drop Recovery
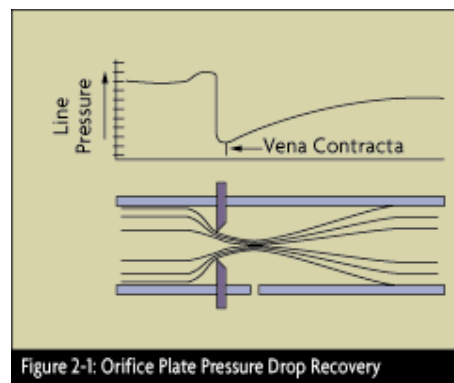
Fig. 31: Vena-contracta for orifice meter (Omega Handbook (1995))

Because of the abrupt constriction in an orifice meter, it has more frictional head loss than a venturi meter and a lower value for its discharge coefficient, C. A typical value for an orifice meter discharge coefficient is between 0.58 and 0.65.

Orifice Types, Performance and selection for two phase flow
The concentric orifice plate is recommended for clean liquids, gases, and steam flows when Reynolds numbers range from 20,000 to 10^7 in pipes under six inches. Because the basic orifice flow equations assume that flow velocities are well below sonic, a different theoretical and computational approach is required if sonic velocities are expected. The minimum recommended Reynolds number for flow through an orifice varies with the beta ratio of the orifice and with the pipe size. In larger size pipes, the minimum Reynolds number also rises.

Because of this minimum Reynolds number consideration, square-edged orifices are seldom used on viscous fluids. Quadrant-edged and conical orifice plates are recommended when the Reynolds number is under 10,000. Flange taps, corner, and radius taps can all be used with quadrant-edged orifices, but only corner taps should be used with a conical orifice.

Concentric orifice plates can be provided with drain holes to prevent buildup of entrained liquids in gas streams, or with vent holes for venting entrained gases from liquids. The unmeasured flow passing through the vent or drain hole is usually less than 1% of the total flow if the hole diameter is less than 10% of the orifice bore. The effectiveness of vent/drain holes is limited, however, because they often plug up.

Concentric orifice plates are not recommended for multi-phase fluids in horizontal lines because the secondary phase can build up around the upstream edge of the plate. In extreme cases, this can clog the opening, or it can change the flow pattern, creating measurement error. Eccentric and segmental orifice plates are better suited for such applications. Concentric orifices are still preferred for multi-phase flows in vertical lines because accumulation of material is less likely and the sizing data for these plates is more reliable.

The eccentric orifice is similar to the concentric except that the opening is offset from the pipe's centerline. The opening of the segmental orifice is a segment of a circle. If the secondary phase is a gas, the opening of an eccentric orifice will be located towards the top of the pipe. If the secondary phase is a liquid in a gas or a slurry in a liquid stream, the opening should be at the bottom of the pipe. The

drainage area of the segmental orifice is greater than that of the eccentric orifice, and, therefore, it is preferred in applications with high proportions of the secondary phase.

Although it is a simple device, the orifice plate is, in principle, a precision instrument. Under ideal conditions, the inaccuracy of an orifice plate can be in the range of 0.75-1.5% AR. Orifice plates are, however, quite sensitive to a variety of error-inducing conditions. Precision in the bore calculations, the quality of the installation, and the condition of the plate itself determine total performance. Installation factors include tap location and condition, condition of the process pipe, adequacy of straight pipe runs, misalignment of pipe and orifice bores, and lead line design. Other adverse conditions include the dulling of the sharp edge or nicks caused by corrosion or erosion, warpage of the plate due to water-hammer and dirt, and grease or secondary phase deposits on either orifice surface. Any of the above conditions can change the orifice discharge coefficient by as much as 10%. In combination, these problems can be even more worrisome and the net effect unpredictable. Therefore, under average operating conditions, a typical orifice installation can be expected to have an overall inaccuracy in the range of 2 to 5% AR.

Venturi

A section of tube forms a relatively long passage with smooth entry and exit. A Venturi tube is connected to the existing pipe, first narrowing down in diameter then opening up back to the original pipe diameter. The changes in cross section area cause changes in velocity and pressure of the flow.
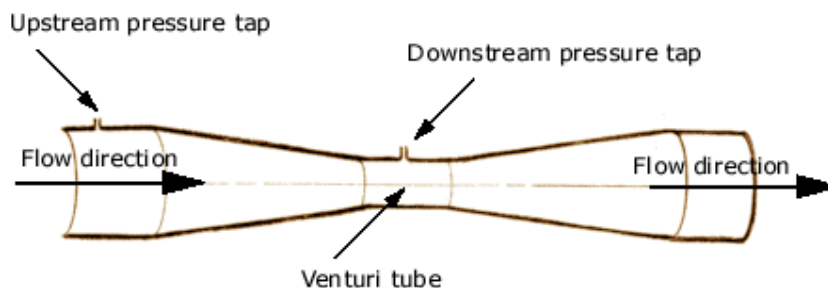
Fig. 32: Venturi tube

97

Venturi tubes are available in sizes up to 72", and can pass 25 to 50% more flow than an orifice with the same pressure drop. Furthermore, the total unrecovered head loss rarely exceeds 10% of measured pressure drop.

The entrance to a venturi meter is a converging cone with a 15° to 20° angle. It converges down to the throat, which is the point of minimum cross-sectional area, maximum velocity, and minimum pressure in the meter. The exit portion of the meter is a diverging cone with an angle of 5° to 7°, which completes the transition back to full pipe diameter. The diagram at the left shows a typical venturi meter configuration with the parameters, D_1, D_2, P_1 and P_2 identified. Because of the smooth gradual transition down to the throat diameter and back to the full pipe diameter, the friction loss in a venturi meter is quite small. This leads to the value of a venturi meter discharge coefficient, C, being nearly one. Typical discharge coefficient values for a venturi meter range from 0.95 to as high as 0.995 in liquid flow (Omega handbook (1995)).

Venturis are insensitive to velocity profile effects and therefore require less straight pipe run than an orifice. Their contoured nature, combined with the self-scouring action of the flow through the tube, makes the device immune to corrosion, erosion, and internal scale build up. In spite of its high initial cost, the total cost of ownership can still be favorable because of savings in installation and operating and maintenance costs.

The classical Herschel venturi has a very long flow element characterized by a tapered inlet and a diverging outlet. Inlet pressure is measured at the entrance, and static pressure in the throat section. The pressure taps feed into a common annular chamber, providing an average pressure reading over the entire circumference of the element. The classical venturi is limited in its application to clean, non-corrosive liquids and gases.

In the short form venturi, the entrance angle is increased and the annular chambers are replaced by pipe taps (Fig. 33-A). The short-form venturi maintains many of the advantages of the classical venturi, but at a reduced initial cost, shorter length and reduced weight.

Pressure taps are located 1/4 to 1/2 pipe diameter upstream of the inlet cone, and in the middle of the throat section. Piezometer rings can be used with large venturi tubes to compensate for velocity profile distortions.
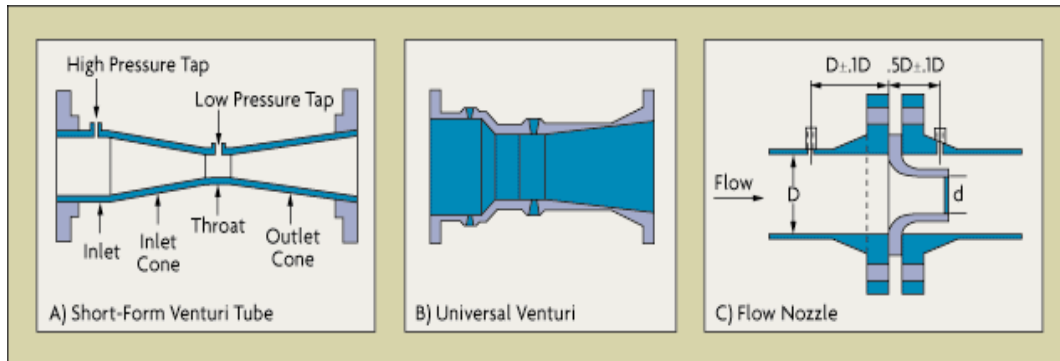
Fig. 33: Venturi flowmeter types

As long as the flow is stable, the DP signal is stable too and correlates to the flowrate according to the Bernoulli formula. However, the DP generated by the Venturi meter fluctuates due to not only the mechanical vibration of the pipe line but also the irregular disturbances of the micro-structures inside the fluid. Time histories of two typical DP signals of a Venturi meter used for liquid flow and gas flow are shown in Fig. 34 (a) and (b), respectively. As the fluctuation of the DP signal does not contribute to the measurement of the flowrate, it is commonly filtered out by specially designed pressure taps or by the DP transmitter. For example, the capacitance-based DP transmitter is generally insensitive to vibrations above 10 Hz. More details on the calibration, design and application of Venturi meter can be found in (Reader-Harris (2005), EN ISO 5167-1 (1997), Jitschinet al. (1999) Kanenko et al. (1990) , Xu et all (2003)).
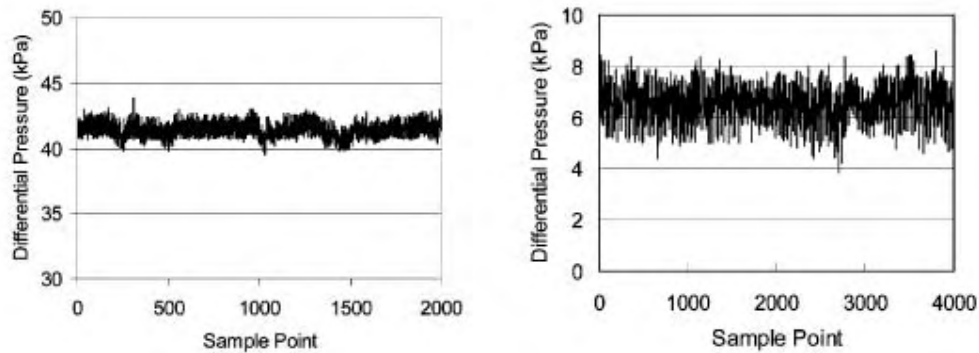
Fig. 34:**Fluctuation of the DP signal of Venturi meter for single-phase flow obtained on the experimental setup (measured by a Si-element transmitter; the sample rate is 260 Hz). (a) Liquid flowrate is 13.04 m3/h, static pressure is 0.189 MPa and the temperature is 48.9 °C. (b) Gas flowrate is 98.7 m3/h, static pressure is 0.172 MPa and the temperature is 24.6 °C. (Xu et all (2003))**

There are several flowtube designs which provide even better pressure recovery than the classical venturi. The best known of these proprietary designs is the universal venturi (Fig. 33-B). The various flowtube designs vary in their contours, tap locations, generated Δp and in their unrecovered head loss. They all have short lay lengths, typically varying between 2 and 4 pipe diameters. These flowtubes usually cost less than the classical and short-form venturis because of their short lay length. However, they may also require more straight pipe run to condition their flow velocity profiles.

Flowtube performance is much affected by calibration. The inaccuracy of the discharge coefficient in a universal venturi, at Reynolds numbers exceeding 75,000, is 0.5%. The inaccuracy of a classical venturi at Re > 200,000 is between 0.7 and 1.5%. Flowtubes are often supplied with discharge coefficient graphs because the discharge coefficient changes as the Reynolds number drops. The variation in the discharge coefficient of a venturi caused by pipe roughness is less than 1% because there is continuous contact between the fluid and the internal pipe surface.

The high turbulence and the lack of cavities in which material can accumulate make flow tubes well suited for slurry and sludge services. However, maintenance costs can be high if air purging cannot prevent plugging of the pressure taps and lead lines. Plunger-like devices (vent cleaners) can be installed to periodically remove buildup from interior openings, even while the meter is online. Lead lines

can also be replaced with button-type seal elements hydraulically coupled to the d/p transmitter using filled capillaries. Overall measurement accuracy can drop if the chemical seal is small, its diaphragm is stiff, or if the capillary system is not temperature-compensated or not shielded from direct sunlight.

Flow Nozzles

A nozzle with a smooth guided entry and a sharp exit is placed in the pipe to change the flow field and create a pressure drop that is used to calculate the flow velocity.
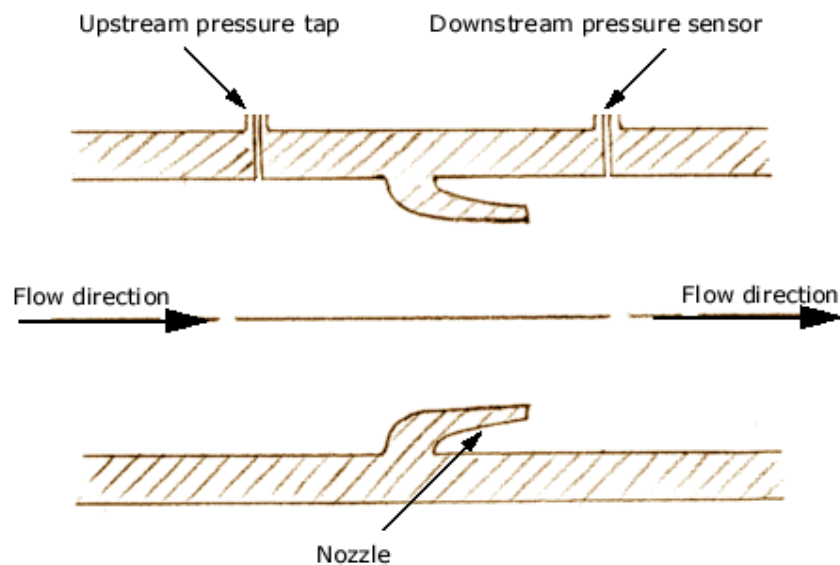
Nozzle shrinks down the cross-section area of the pipe and create pressure differential.

Fig. 35: Nozzle flowmeter

The flow nozzle is dimensionally more stable than the orifice plate, particularly in high temperature and high velocity services. It has often been used to measure high flowrates of superheated steam. The flow nozzle, like the venturi, has a greater flow capacity than the orifice plate and requires a lower initial investment than a venturi tube, but also provides less pressure recovery. A major disadvantage of the nozzle is that it is more difficult to replace than the orifice unless it can be removed as part of a spool section.

The low-beta designs range in diameter ratios from 0.2 to 0.5, while the high beta-ratio designs vary between 0.45 and 0.8. The nozzle should always be centered in the pipe, and the downstream pressure tap should be inside the nozzle exit. The throat taper should always decrease the diameter toward the exit. Flow nozzles are not recommended for slurries or dirty fluids. The most common flow nozzle is the flange type. Taps are commonly located one pipe diameter upstream and 1/2 pipe diameter downstream from the inlet face.

Flow nozzle accuracy is typically 1% AR, with a potential for 0.25% AR if calibrated. While discharge coefficient data is available for Reynolds numbers as low as 5,000, it is advisable to use flow nozzles only when the Reynolds number exceeds 50,000. Flow nozzles maintain their accuracy for long periods, even in difficult service. Flow nozzles can be a highly accurate way to measure gas flows. When the gas velocity reaches the speed of sound in the throat, the velocity cannot increase any more (even if downstream pressure is reduced), and a choked flow condition is reached. Such "critical flow nozzles" are very accurate and often are used in flow laboratories as standards for calibrating other gas flowmetering devices.

Nozzles can be installed in any position, although horizontal orientation is preferred. Vertical downflow is preferred for wet steam, gases, or liquids containing solids. The straight pipe run requirements are similar to those of orifice plates.

The frictional loss in a flow nozzle meter is much less than in an orifice meter, but higher than in a venturi meter. A typical flow nozzle discharge coefficient value is between 0.93 and 0.98 (efunda.com (2010)).

Segmental Wedge Elements

A wedge-shaped segment is inserted perpendicularly into one side of the pipe while the other side remains unrestricted. The change in cross section area of the flow path creates pressure drops used to calculate flow velocities.
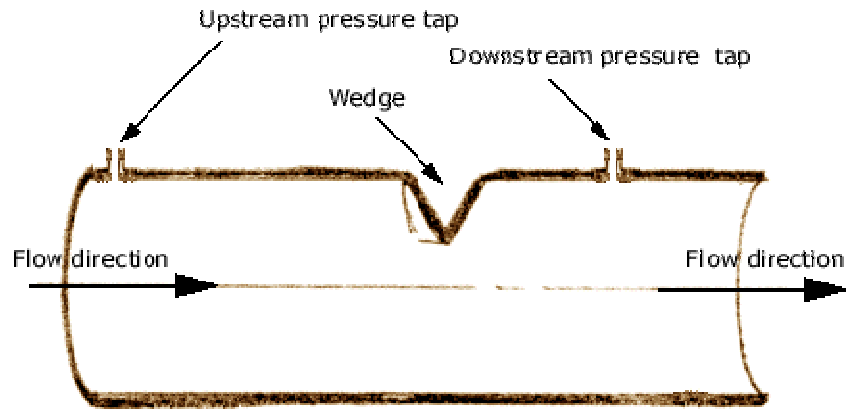
Fig. 36: Segmental Wedge element flowmeter

The segmental wedge element (Fig. 36) is a device designed for use in slurry, corrosive, erosive, viscous, or high-temperature applications. It is relatively expensive and is used mostly on difficult fluids, where the dramatic savings in maintenance can justify the initial cost. The unique flow restriction is designed to last the life of the installation without deterioration.

Wedge elements are used with 3-in diameter chemical seals, eliminating both the lead lines and any dead-ended cavities. The seals attach to the meter body immediately upstream and downstream of the restriction. They rarely require cleaning, even in services like dewatered sludge, black liquor, coal slurry, fly ash slurry, taconite, and crude oil. The minimum Reynolds number is only 500, and the meter requires only five diameters of upstream straight pipe run.

The segmental wedge has a V-shaped restriction characterized by the H/D ratio, where H is the height of the opening below the restriction and D is the diameter. The H/D ratio can be varied to match the flow range and to produce the desired Δp. The oncoming flow creates a sweeping action through the meter. This provides a scouring effect on both faces of the restriction, helping to keep it clean and free of buildup. Segmental wedges can measure flow in both directions, but the d/p transmitter must be calibrated for a split range, or the flow element must be provided with two sets of connections for two d/p transmitters (one for forward and one for reverse flow).

An uncalibrated wedge element can be expected to have a 2% to 5% AR inaccuracy over a 3:1 range. A calibrated wedge element can reduce that to 0.5% AR if the fluid density is constant. If slurry density is variable and/or unmeasured, error rises.

Venturi-Cone Element

A cone shaped obstructing element that serves as the cross section modifier is placed at the center of the pipe for calculating flow velocities by measuring the pressure differential.
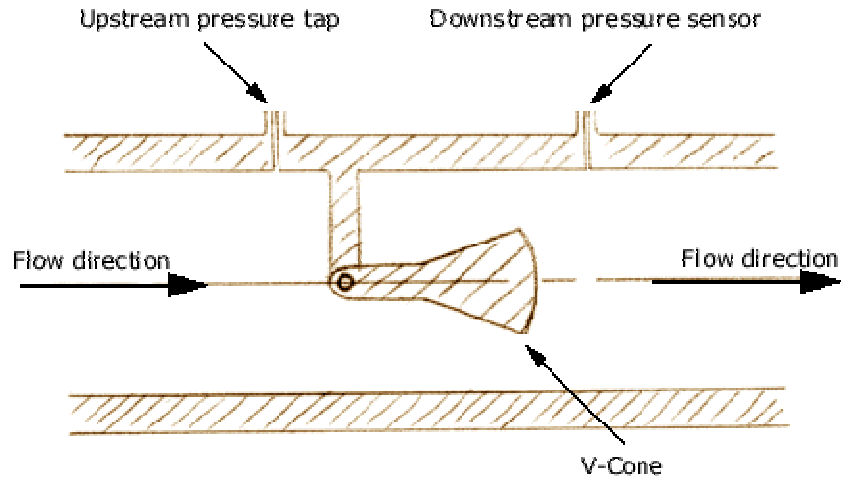
Fig. 37: V-cone flowmeter

The venturi-cone promises consistent performance at low Reynolds numbers and is insensitive to velocity profile distortion or swirl effects. Again, however, it is relatively expensive. The V-cone restriction has a unique geometry that minimizes accuracy degradation due to wear, making it a good choice for high velocity flows and erosive/corrosive applications.

The V-cone creates a controlled turbulence region that flattens the incoming irregular velocity profile and induces a stable differential pressure that is sensed by a downstream tap. The beta ratio of a V-cone is so defined that an orifice and a V-cone with equal beta ratios will have equal opening areas.

$$\beta = \left(D^2 - d^2 \right)^{0.05/D}$$

where d is the cone diameter and D is the inside diameter of the pipe.

With this design, the beta ratio can exceed 0.75. For example, a 3-in meter with a beta ratio of 0.3 can have a 0 to 75 gpm range. Published test results on liquid and gas flows place the system accuracy between 0.25 and 1.2% AR (Omega handbook (1995)).

Pitot Tubes

A probe with an open tip (Pitot tube) is inserted into the flow field. The tip is the stationary (zero velocity) point of the flow. Its pressure, compared to the static pressure, is used to calculate the flow velocity. Pitot tubes can measure flow velocity at the point of measurement.
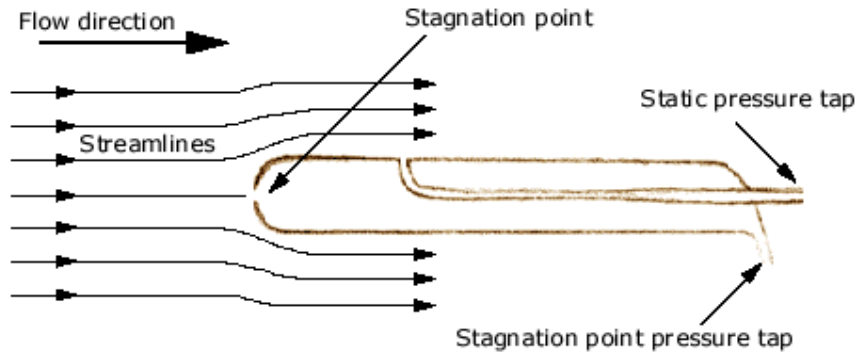
Fig. 38: Pitot tube

While accuracy and rangeability are relatively low, pitot tubes are simple, reliable, inexpensive, and suited for a variety of environmental conditions, including extremely high temperatures and a wide range of pressures.

The pitot tube is an inexpensive alternative to an orifice plate. Accuracy ranges from 0.5% to 5% FS, which is comparable to that of an orifice. Its flow rangeability of 3:1 (some operate at 4:1) is also similar to the capability of the orifice plate. The main difference is that, while an orifice measures the full flowstream, the pitot tube detects the flow velocity at only one point in the flowstream. An advantage of the slender pitot tube is that it can be inserted into existing and pressurized pipelines (called hot-tapping) without requiring a shutdown.

Pitot tubes were invented by Henri Pitot in 1732 to measure the flowing velocity of fluids. A pitot tube measures two pressures: the static and the total impact pressure. The static pressure is the operating pressure in the pipe, duct, or the environment, upstream to the pitot tube. It is measured at right angles to the flow direction, preferably in a low turbulence location .

The total impact pressure (P_T) is the sum of the static and kinetic pressures and is detected as the flowing stream impacts on the pitot opening. To measure impact pressure, most pitot tubes use a small, sometimes L-shaped tube, with the opening directly facing the oncoming flowstream. The point velocity of approach (V_P) can

be calculated by taking the square root of the difference between the total pressure (P_T) and the static pressure (P) and multiplying that by the C/ρ ratio, where C is a dimensional constant and ρ is density:

$$V_p = \frac{C\left(P_T - P\right)^{1/2}}{\rho}$$

When the flowrate is obtained by multiplying the point velocity (V_P) by the cross-sectional area of the pipe or duct, it is critical that the velocity measurement be made at an insertion depth which corresponds to the average velocity. As the flow velocity rises, the velocity profile in the pipe changes from elongated (laminar) to more flat (turbulent). This changes the point of average velocity and requires an adjustment of the insertion depth. Pitot tubes are recommended only for highly turbulent flows and, under these conditions, the velocity profile tends to be flat enough so that the insertion depth is not critical. Pitot tubes should be used only if the minimum Reynolds number exceeds 20,000 and if either a straight run of about 25 diameters can be provided upstream to the pitot tube or if straightening vanes can be installed

A calibrated, clean and properly inserted pitot tube can provide ±1% of full scale flow accuracy over a flow range of 3:1; and, with some loss of accuracy, it can even measure over a range of 4:1. Its advantages are low cost, no moving parts, simplicity, and the fact that it causes very little pressure loss in the flowing stream. Its main limitations include the errors resulting from velocity profile changes or from plugging of the pressure ports. Pitot tubes are generally used for flow measurements of secondary importance, where cost is a major concern, and/or when the pipe or duct diameter is large (up to 72 inches or more).

Averaging Pitot Tubes

Similar to Pitot tubes but with multiple openings, averaging Pitot tubes take the flow profile into consideration to provide better over all accuracy in pipe flows.
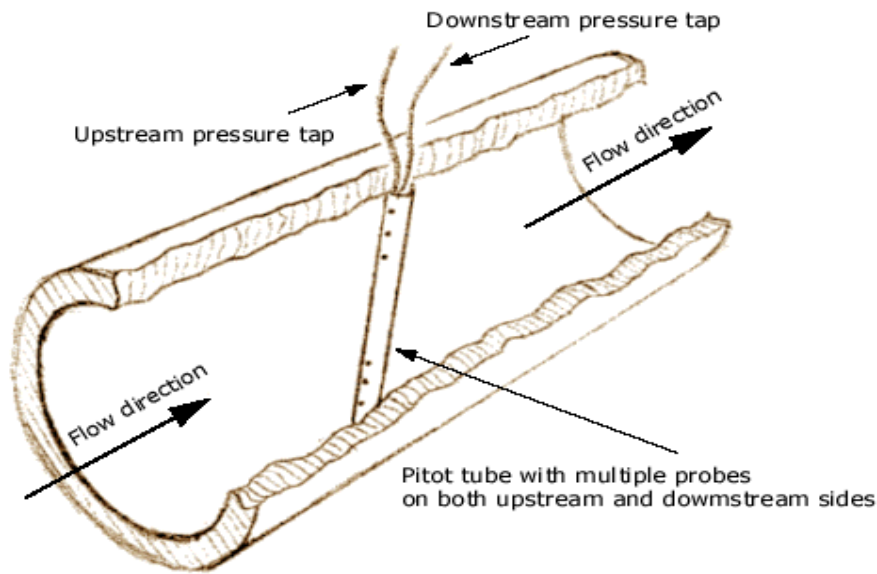
Fig. 39: Averaging Pitot Tube

Averaging pitot tubes been introduced to overcome the problem of finding the average velocity point. An averaging pitot tube is provided with multiple impact and static pressure ports and is designed to extend across the entire diameter of the pipe. The pressures detected by all the impact (and separately by all the static) pressure ports are combined and the square root of their difference is measured as an indication of the average flow in the pipe (Fig. 39). The port closer to the outlet of the combined signal has a slightly greater influence, than the port that is farthest away, but, for secondary applications where pitot tubes are commonly used, this error is acceptable.

Elbow

When a liquid flows through an elbow, the centrifugal forces cause a pressure difference between the outer and inner sides of the elbow. This difference in pressure is used to calcuate the flow velocity. The pressure difference generated by an elbow flowmeter is smaller than that by other pressure differential flowmeters, but the upside is an elbow flowmeter has less obstruction to the flow.
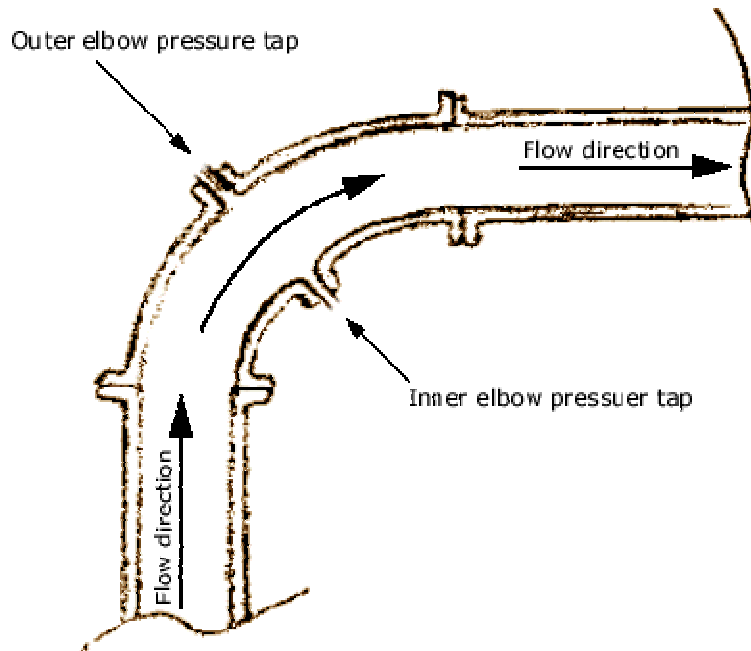
Fig. 40: Elbow type flowmeter (efunda.com (2010))

Recovery of Pressure Drop in Orifices, Nozzles and Venturi Meters

After the pressure difference has been generated in the differential pressure flow meter, the fluid pass through the pressure recovery exit section, where the differential pressure generated at the constricted area is partly recovered.
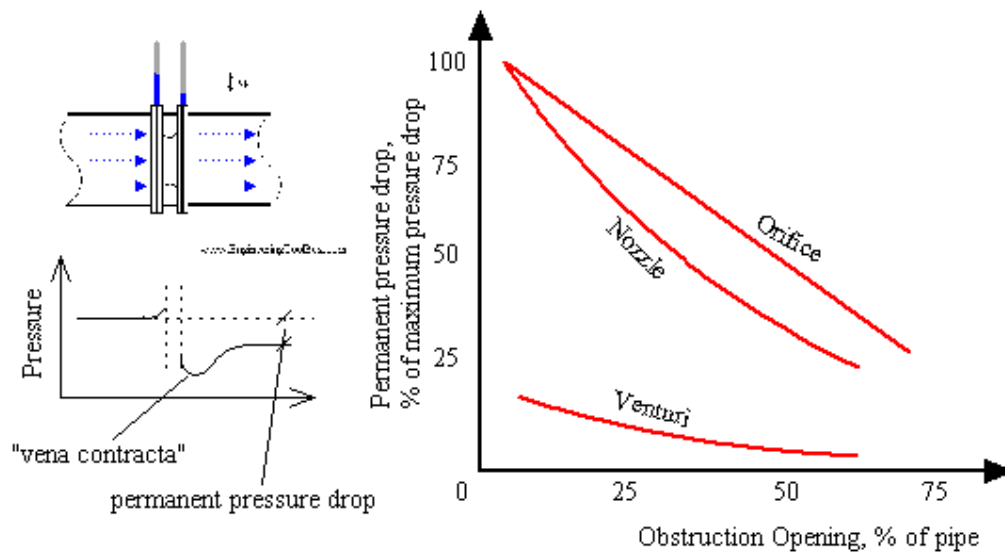
Fig. 41: Permanent pressure drop in differential flowmeter (EngineerinToolBox.com (2010))

As we can see in Fig. 41, the pressure drop in orifice plates are significant higher than in the venturi tubes.

The ISO standards provide an expression for pressure loss across an orifice plate. A typical value for the pressure loss is about 0.73Δp, where Δp represents the differential pressure across the meter.

The value of pressure loss across the Venturi meter is about 0.05-0.2 Δp, where Δp represents the differential pressure between the entrance and the throat, so it is much lower than the one for the orifice plates.

Differential flowmeters in two phase flow

In the last decades, many investigations focused on air-water or steam-water two-phase flow measurement using orifices and venturi meters.

The modern preference is to ignore the orifice meter as an instrument to measure the two-phase flow, since it acts as a dam for the liquid flow rate. It's advisable to use instead a Venturi flow meter instead as it is less likely to cause blockage to the liquid phase (Steven (2006)).

Compared with other kinds of differential pressure devices, Venturi has little influence on flow regimes (Lin, 2003), the smallest pressure loss, and the shortest straight pipe upstream and downstream.

The basic model is based on the "**Homogeneous flow correlation (Meng (2010))**".

It is assumed that the gas and the liquid phases are mixed homogeneously, have the same velocity, and are in thermal equilibrium. Then the density of two-phase flow is defined by:

$$\rho_h = \frac{1}{\left(\dfrac{x}{\rho_g} + \dfrac{1-x}{\rho_l}\right)}$$

And the total mass flow rate can be obtained by:

$$\dot{m} = K\sqrt{\Delta p_{TP}\rho_h}$$

Separated flow correlation (Meng (2010)):

$$\dot{m} = K\sqrt{\rho_{TP}\Delta P_{TP}}$$

$$\rho_{TP} = \alpha\rho_g + (1-\alpha)\rho_l$$

Where

$\dot{m}$	Two-phase mass flow rate [kgs^{-1}]
ΔP_{TP}	Two-phase pressure drop [Pa]
ρ_{TP}	Two-phase mixture density [kgm^{-3}]
ρ_l	Liquid density [kgm^{-3}]
ρ_g	Vapor density [kgm^{-3}]
α	Two-phase mixture void fraction

K I   Calibration coefficient of the flowmeter.

The proportionality constant K can be extrapolated from single-phase flow literature (provided the meter is single-phase standard design) and tailored on the basis of preliminary in-situ testing.

Some authors suggested two-phase flow correlation to correct the reading of a differential pressure flow-meter, usually applied just to the measurement of single-phase flow, in order to obtain the correspondent mass flow rate in two phase flow.

The presence of the two phase mixture causes an increase in the measured differential pressure and results in the differential flowmeter over-reading the actual amount of flow rate passing through the meter.

Fincke (1999) shows that a Venturi meter used to measure two-phase flow, by the single-phase formulation, over predicts the effective flow rate. This is due to an increase in the pressure drop in two-phase condition, because of the interaction between the gas and the liquid phase.

This over-reading is usually 'corrected' using available correlations derived from experimental data to determine the actual gas mass flowrate. This trend is observed in all differential-pressure meters.

To use an differential meter with two phase flow, there are three approaches (Baker (2000)):

a. adjusting the value of density to reflect the presence of a second component.

b. adjusting the discharge coefficient to introduce the presence of the second component

c. relating two phase pressure drop to that which would have occurred if all the flow were passing either as a gas or as a liquid.

In 1949, Lockhart and Martinelli researched the pressure drop and the liquid holdup of two-phase flow across the pipe, which became an important basis for the differential pressure method in two-phase flow measurement research.

Later, many researchers studied the relationship between the mass flowrate of gas-liquid flow and the differential pressure across the flowmeter. Many flowrate measurement correlations were reported by:

Murdock (1962),

James, (1965),

Bizon (reported by Lin (2003)- Meng (2010))

Lin (1982).

Chisholm, (1974),

And recently:

de Leeuw (1997)

Steven(2005)

Xu and al. (2003),

Moura and Marvillet (1997).

The correlations currently available for correcting the over-reading have been derived from a limited set of data and may only be suitable to cover restricted ranges of the flowmeter parameters, for example, a specific diameter ratio and are closely dependent on experiment conditions such as pressure, temperature, medium, devices, etc.

Use of correlations outside the conditions used to define them can result in large errors in the calculation of the gas mass flowrate.

Most of the available correlations for two-phase flow are valid only for low (x<0.1) or very high (x>0.95) steam quality.

The wet-gas flow is defined (in Steven (2006)) as a two phase flow that has a Lockart-Martinelli parameter value (X) less or equal to 0.3, where X is defined as:

$$X = \sqrt{\left(\frac{dp}{dz}\right)_l \bigg/ \left(\frac{dp}{dz}\right)_g}$$

Where

$$\left(\frac{dp}{dz}\right)_k$$

represents the pressure gradients for single-phase gas and liquid flow as fractions of the total two-phase mass flow rate, respectively (Whalley (1987)). According to Collier and Thome (1996), the Lockart-Martinelli parameter can be written as (if both the gas and the liquid flow are turbulent):

$$X = \left(\frac{1-x}{x}\right)\left(\frac{\rho_g}{\rho_l}\right)^{0.5}$$

Grattan et al. (1981) gave experimental pressure loss data for orifice tests with an empirical curve:

$$\phi_{lo}^2 = 1.051 + 291x - 3796x^2 + 74993x^3 - 432834x^4$$

for *0.00005<x<0.1*

The scatter in Fig. 42 is an indication of the limited value of such an empirical curve and of attempts to predict flowmeter performance in two-phase flows.
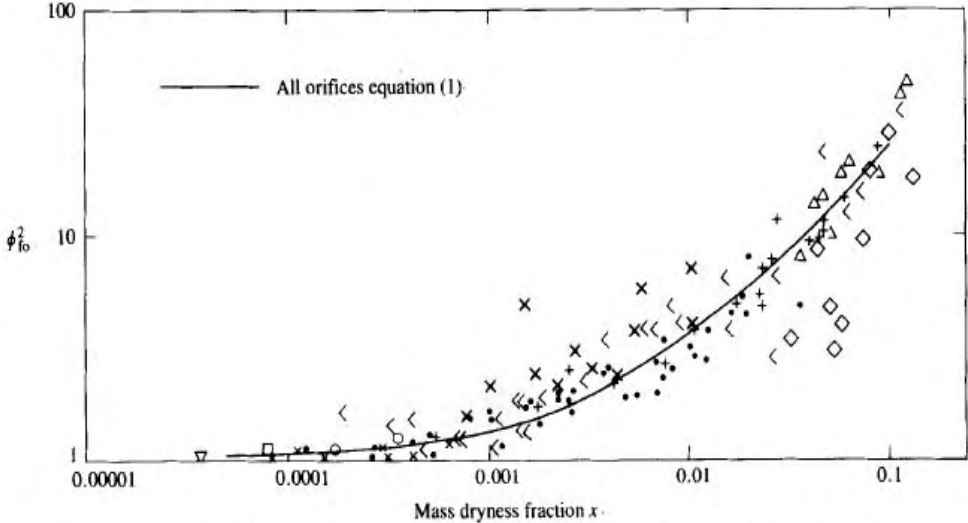
Fig. 42: Experimental pressure loss data for orifice tests (from Grattan et al. (1981)   (Baker (1991)).

Fig. 43 show the effect of increasing the oil content on each meter.
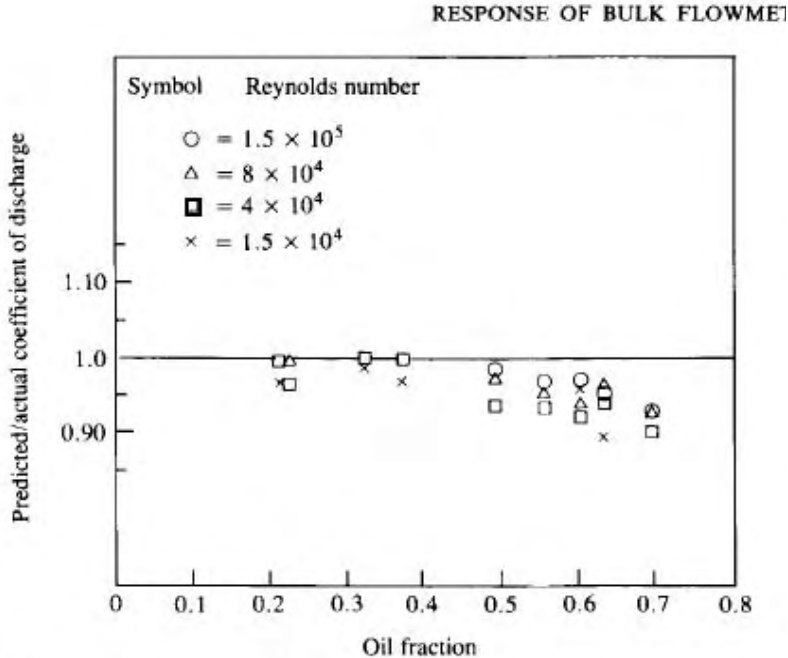
Fig. 43: Performance of orifice meter in an oil-water emulsion (from Pal and Rhodes (1985)) (Baker (1991))

113

All the research's work, searched to define the most important parameter that influence the flow meter behaviour.

Harris and Shires (1973) (Baker (1991)) tested a venturi in a horizontal steam/water flow in a 105 mm bore pipe. Steam quality varied from 0 to 0.55. Their results lay between the two extremes of a homogeneous model without slip and a maximum slip model. Lee and Crowe (1981) (Baker (1991)) numerically analysed gas particle flow in a venturi with apparently good agreement with experimental data as a function of the Stokes number. Crowe (1985) reported tests over a wide range of Stokes number.

Pascal (1984) (Baker (1991)) tested two orifices in series and the critical flow in a convergent-divergent nozzle. Azzopardi et al. (1989) reported tests on annular flow in a venturi.

Whitaker and Owen (1990) (Baker (1991)) obtained experimental results of the behaviour of an annular venturimeter in a homogeneous horizontal water/air flow up to void fractions of 30 per cent. They suggested a relationship between discharge coefficient and Reynolds number to allow for a change in the discharge coefficient of about 5 per cent and obtained a two-phase multiplier for a particular void fraction.

Tang et al. (1988) obtained flowrates at each phase of gas/solid flows to sufficient accuracy for industrial applications from an extended-length venturi.

Whitaker and Owen (1990) also obtained data for a spring-loaded variable-area orifice meter in a horizontal water/air flow with a void fraction up to 40 per cent.

Some of the most important effects of the two-phase flow to the response of a Venturi meter are reassumed by Steven (2006). He highlights that:

• The meter reading increases as the liquid load increases (i.e. the Lockart-Martinelli parameter increases (x axis in Fig. 44)). The effect is higher if the gas/liquid density ratio is lower (see Fig. 44).

• If the gas Froude number increases, for fixed gas to liquid density ratio, the over reading increases.

The gas Froude number is defined as the square root of the ratio between the gas inertia (if the gas flows alone) and the gravity force on the liquid phase:

$$Fr_g = \sqrt{\frac{J_g^2 \rho_g}{gD(\rho_l - \rho_g)}},$$

where Jg is the superficial velocity of the gas phase, and D is the pipe diameter.
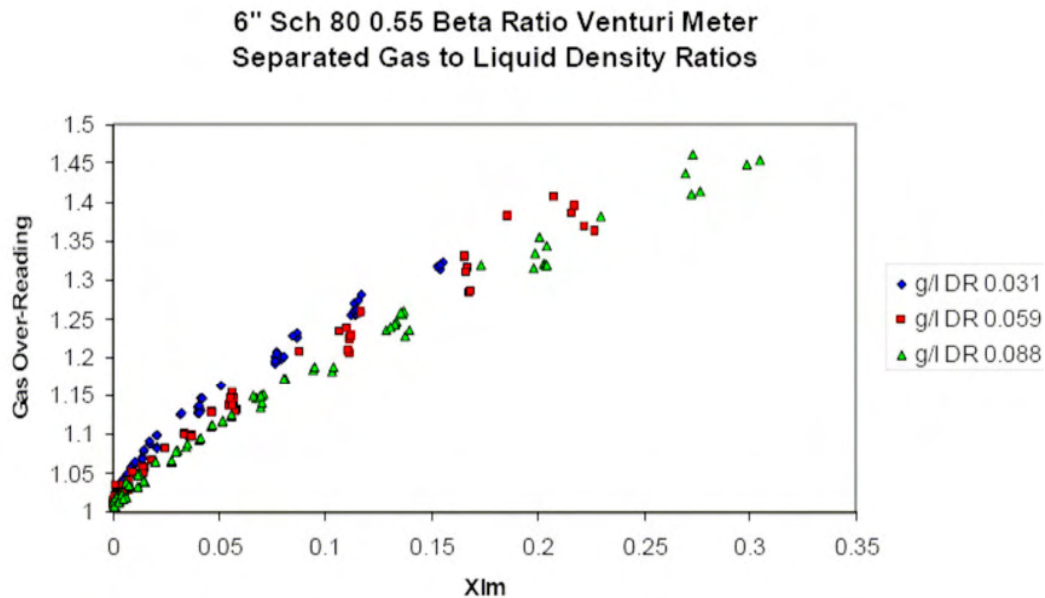
Fig. 44: X effect on the performance of a Venturi in two phase flow (Steven (2006))

- If the gas Froude number increases, for fixed gas to liquid density ratio, the over reading increases.

The gas Froude number is defined as the square root of the ratio between the gas inertia (if the gas flows alone) and the gravity force on the liquid phase:

$$Fr_g = \sqrt{\frac{J_g^2 \rho_g}{gD\left(\rho_l - \rho_g\right)}} \, ,$$

where Jg is the superficial velocity of the gas phase, and D is the pipe diameter.

- If the liquid density ratio and the Lockart-Martinelli parameters are fixed, the gas Froude number is higher if the superficial gas velocity is higher. With an increase in the gas superficial mass velocity the differential pressure across the meter is increasing, too. (See Fig. 45). Steven reported some results obtained by in the 2003. Stewart presented the response of a Venturi meter to wetgas flow for two fluids (nitrogen and kerosene). The gas to liquid density ratio (i. e. the pressure) and the gas Froude number were fixed.

Different sets of data were collected for different β ratio.

115
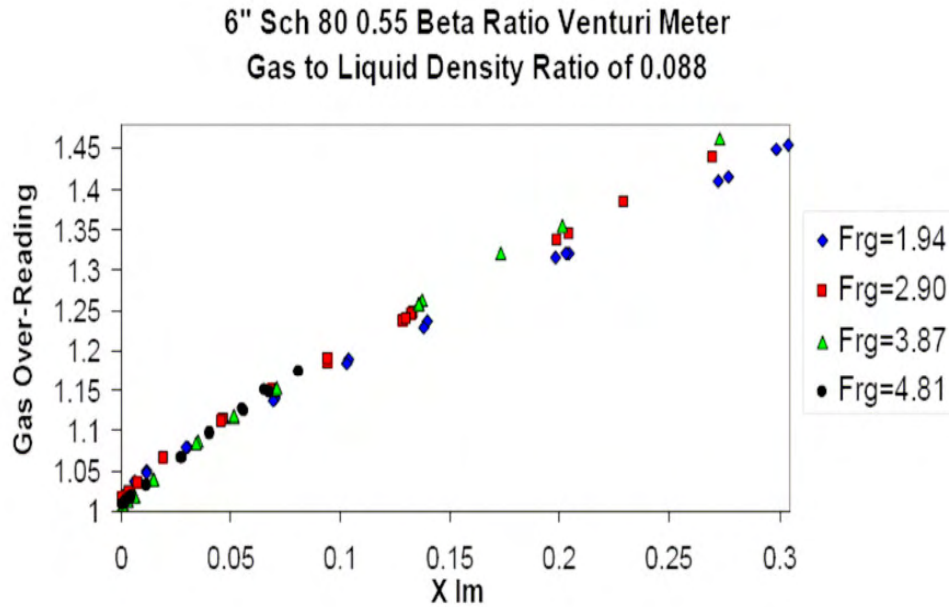
Fig. 45: Fr number effect on the performance of a Venturi in two phase flow (Steven (2006))

The Venturi meter over reading decreases if β increases (see Fig. 46). The response of the Venturi meter in two-phase flow is likely to be influenced by the liquid properties. Reader-Harris tested a 4'' Venturi meter with two different values of gas to liquid density ratio (0.024 and 0.046). At low gas flow rates (i.e. at low gas Froude number) there was not significant liquid property effect, but at higher gas Froude number it was found that the water wet gas flow would have a lower increase in the reading in comparison with kerosene wet gas flow under the same flow conditions (Steven (2006a), Reader-Harris (2005)). Other experiments by Steven (2006) supported the results obtained by Reader-Harris. Steven also postulated that the different results obtained with different liquid property are a direct consequence of the flow pattern that can be different for similar flow parameters, but different liquid properties.

Taitel and Dukler claim that fluid properties affect flow pattern. They proposed two different flow pattern maps for air and water at atmospheric conditions and for natural gas and crude oil (Taitel and Dukler (1976)).
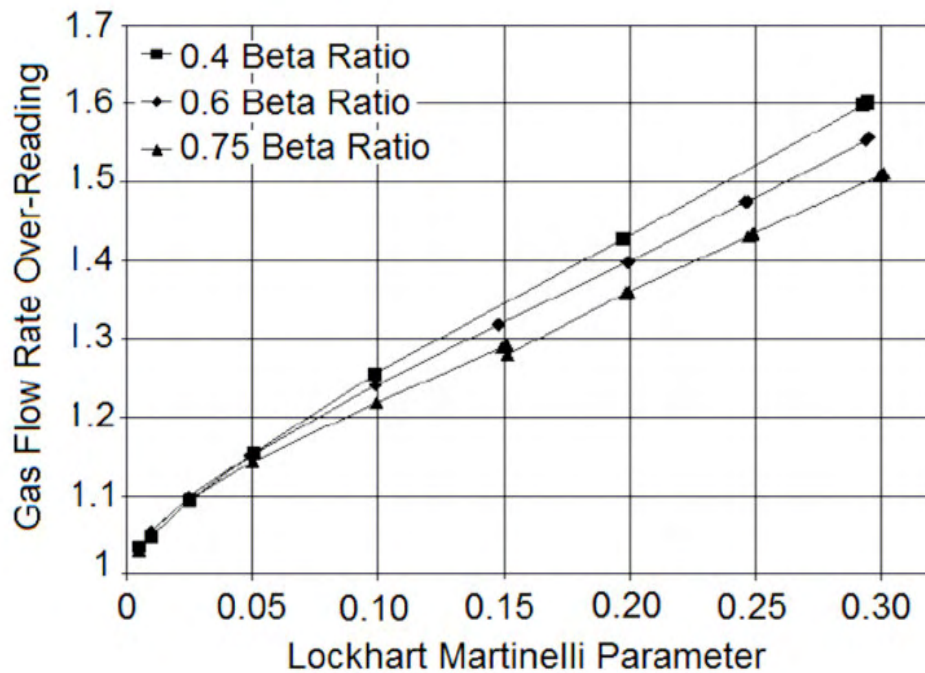
Fig. 46: Over reading of a Venturi meter measuring a wet gas flow at 15 bar and Fr = 1.5, for different β (Steven (2006)

- Steven (2006) indicated also a possible diameter effect on Venturi meter wet gas over reading. He presented the comparison of two data sets for two different Venturi diameters (the devices were tested in two testing campaigns by NEL (National Engineering Laboratory, UK) and CEESI (Colorado Engineering Experiment Station, Inc.)) The meter tested by NEL was a 4'' diameter, Sch. 80, β = 0.6 Venturi meter. The second meter (used by CEESI) was a 2'' diameter, Sch. 80, β = 0.6 Venturi meter. The gas to liquid density ratio and the gas Froude number in the two experiments were very close to each other. The device with the bigger diameter registers the higher over reading (see Fig. 47). Steven concluded that the difference in the over reading is due to the different flow regimes established inside the pipes. The larger meter has more entrainment (is more in the annular mist region) than the smaller meter. These observations need to be confirmed by a more detailed testing of the Venturi meter with various diameters.
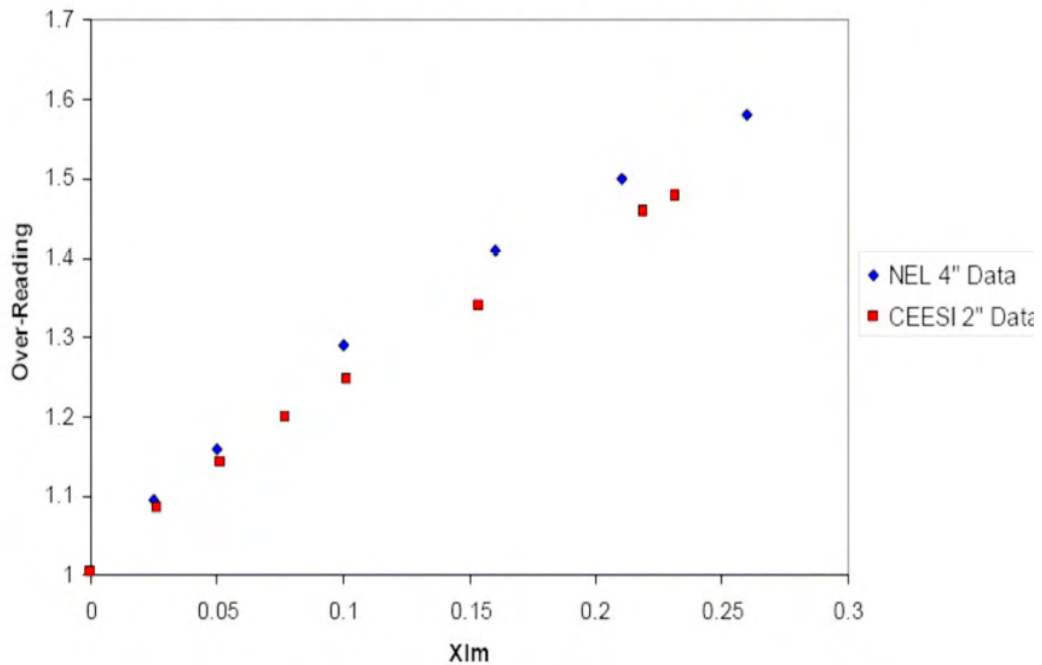
Fig. 47: Comparison between the Venturi meter response obtained by NEL and by CEESI
(Steven (2006))

Venturi and Orifice plate two phase's models

James' Correlation (1965)

It is a modification of the homogenous correlation:

$$\dot{m}_{James} = K \sqrt{\Delta P_{TP} \bigg/ \left(\frac{x^n}{\rho_g} + \frac{(1-x)^n}{\rho_l} \right)}$$

Where n =1.5.

Murdock's Correlation (1962):

Murdock derived a correlation to predict the behavior of an orifice plate in two-phase flow, horizontal mounting (Murdock (1962)). The experimental data were not restricted to wet gas flow only.

118

They ranged in the following intervals:

o 31.8 mm < pipe diameter < 101.6 mm

o 1.01 bar < pressure < 63 bar

o 0.025 bar < pressure drop < 1.25 bar

o 0.11 < x < 0.98

o 0.2602 < β = d/D < 0.5

o 13000 < Re_g < 1270000

Murdock's experiments were based on different types of liquid-gas combinations (liquid phase: water, salt water or natural gas distillate; gas phase: steam, air or natural gas). The correlation is expressed as:

$$\dot{m}_g = \frac{\dot{m}_{g,Apparent}}{1+1.26X}$$

where $\dot{m}_{g,Apparent}$ is the uncorrected value of the gas mass flow rate as detected by the orifice and $\dot{m}_g$ is the corrected value. The constant (1.26) is an empirical value. X_m is the modified Lockart-Martinelli parameter, defined as:

$$X = \frac{\dot{m}_l}{\dot{m}_g}\sqrt{\frac{\rho_g}{\rho_l}\frac{k_g}{k_l}}$$

where k_g and k_l are the gas and liquid flow coefficient, respectively.
Each of them is the product of the velocity of approach, the discharge coefficient and the expansibility factor:

$$k_k = \left(1-\beta\right)^{-1/2} F_a K$$

Where

$\left(1-\beta\right)^{-1/2}$ is velocity of approach

K is the discharge coefficient; defined as the ratio between the real volumetric flow rate and the ideal volumetric flow rate (if the flow is considered without losses).

It takes into account the permanent pressure loss through the meter and the presence of the *vena contracta* (the actual cross section of the flow after the contraction is smaller than the pipe diameter).

The expansibility factor (F_a) provides an adjustment to the coefficient of discharge that allows for the compressibility of the fluid, if the meter is used in gas flow.

If the flow is approximated as incompressible and the discharge coefficient for the liquid and the gas phase is the same, the modified Lockart-Martinelli parameter reduces to the standard Lockart-Martinelli parameter.

The correlation is dependent only on X, while the influence of the flow pattern is not considered; the author model the flow as two-phase stratified flow pattern.
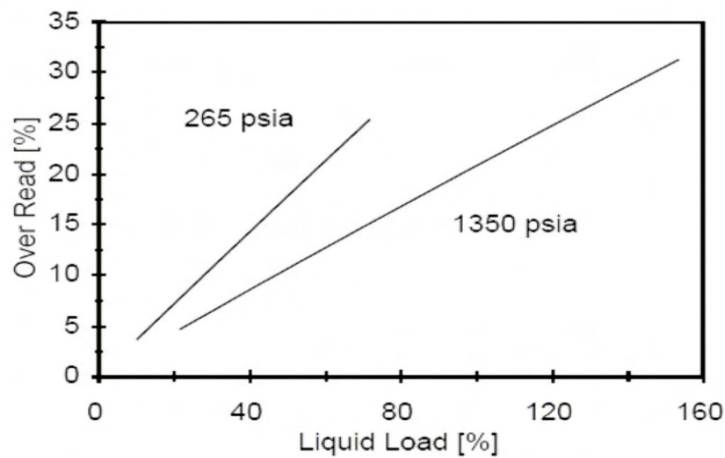
Fig. 48: Orifice meter over read as predicted by Murdock's correlation, Kegel (2003).
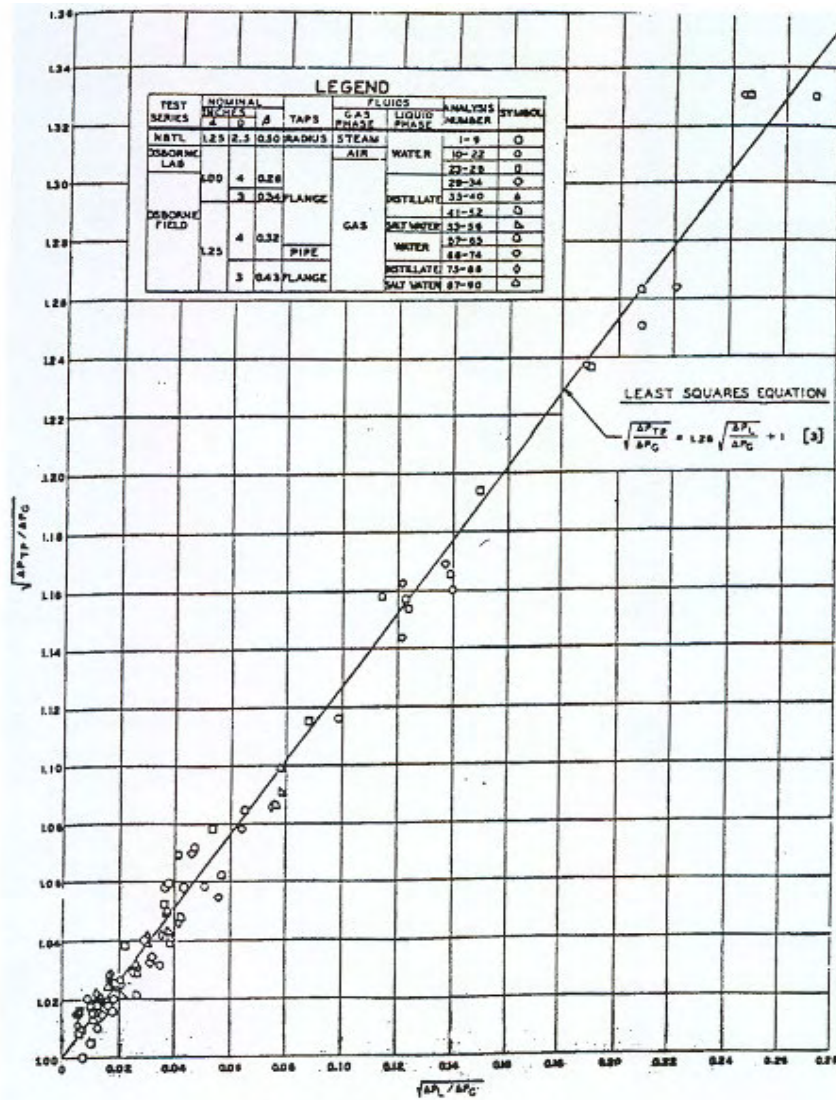
Fig. 49: The original Murdock Two-Phase Flow Orifice Plate Meter Data Plot (Stenven (2006))

The pressure drop in single phase gas flow is lower than the pressure drop in two-phase, wet steam flow, so the value detected by the orifice meter, without correction, tends to overestimate the gas mass flow rate.

Using the Murdock correlation the total flow rate is given by:

$$\dot{m}_{Murdock} = K\sqrt{\Delta P_{TP}}\Bigg/\left(\frac{x}{\sqrt{\rho_g}}+1.26\frac{1-x}{\sqrt{\rho_l}}\right)$$

Some author proposed modifications of Murdock correlation:

- **Bizon's Correlation (Meng 2010- Lin (2003))**

Bizon added one more parameter to the Murdock correlation and got the following correlation:

$$\dot{m}_{Bizon} = K\sqrt{\Delta P_{TP}} \bigg/ \left(a \frac{x}{\sqrt{\rho_g}} + b \frac{1-x}{\sqrt{\rho_l}} \right)$$

Where a and b are experimental values.

- **Collins's Correlation (1971)**

$$\dot{m}_{Collins} = K\sqrt{\Delta P_{TP}} \bigg/ \left(a \frac{x}{\sqrt{\rho_g}} + b \frac{1-x}{\sqrt{\rho_l}} + c \frac{\sqrt{x(1-x)}}{\sqrt[4]{\rho_l \rho_g}} \right)$$

Where a, b and c are experimental values.

- **Lin's Correlation (1982)**

It was originally developed for orifice meter, it considers the influence of the pressure and of the liquid mass content on the meter over reading.

$$\dot{m}_{Lin} = K\sqrt{\Delta P_{TP}} \bigg/ \left(\frac{x}{\sqrt{\rho_g}} + \vartheta \frac{1-x}{\sqrt{\rho_l}} \right)$$

Where ϑ is correlate with the density ratio:

$$\vartheta = 1.48625 - 9.26541\left(\frac{\rho_g}{\rho_l}\right) + 44.6954\left(\frac{\rho_g}{\rho_l}\right)^2 - 60.6150\left(\frac{\rho_g}{\rho_l}\right)^3$$

$$-5.12966\left(\frac{\rho_g}{\rho_l}\right)^4 - 26.5743\left(\frac{\rho_g}{\rho_l}\right)^5$$

Miller (1996) suggests the Murdock equation for two-phase flow both in an orifice meter and in a Venturi meter.

Hewitt (1978) lists many other references for the study of the pressure drop across Venturi meters and orifice in two-phase flow; but Fincke (1999) also proves that the Murdock correlation is not sufficient to adjust the apparent reading to the reference flow rate value; the gas flow rate evaluated with the correlation is affected by an error that can reach 20% of the reading (see Fig. 50 and Fig. 51).

It could be concluded that the application of the Murdock correlation to a data set detected by a Venturi meter is somewhat questionable, since Murdock's correlation has been firstly studied to be applied to orifice plate data set.

Fincke (1999) obtained the following performance using an extended throat nozzle to measure the two-phase flow rate of low pressure (15 psi-1bar) air-water mixtures and of high pressure (400 psi-27.6 bar, 500 psi-34.5 bar) natural gas-Isopar mixtures:

o Accuracy of ±2% of reading for $m_l/m_g < 10\%$

o Accuracy of ±4% of reading for $10\% < m_l/m_g < 30\%$

The studied interval corresponds to $0.95 < \alpha < 1.0$. During measurement the ratio between the liquid flow rate and the gas flow rate was known.

Based on the Venturi meter measurements and derived set of equations, the gas flow rate was calculated.
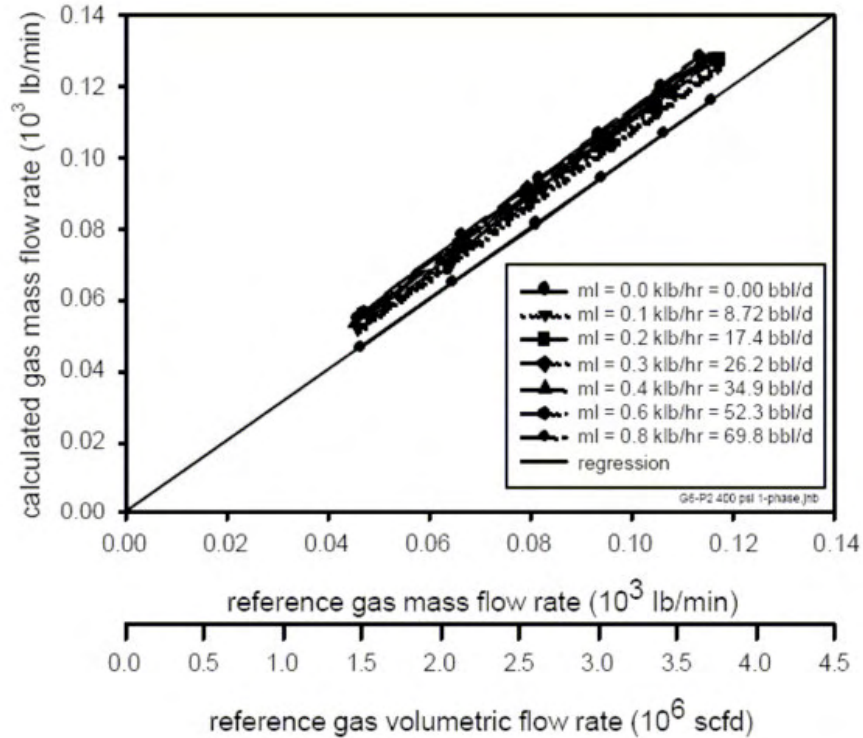
Fig. 50: Venturi performance using Murdock correlation (Fincke (1999))
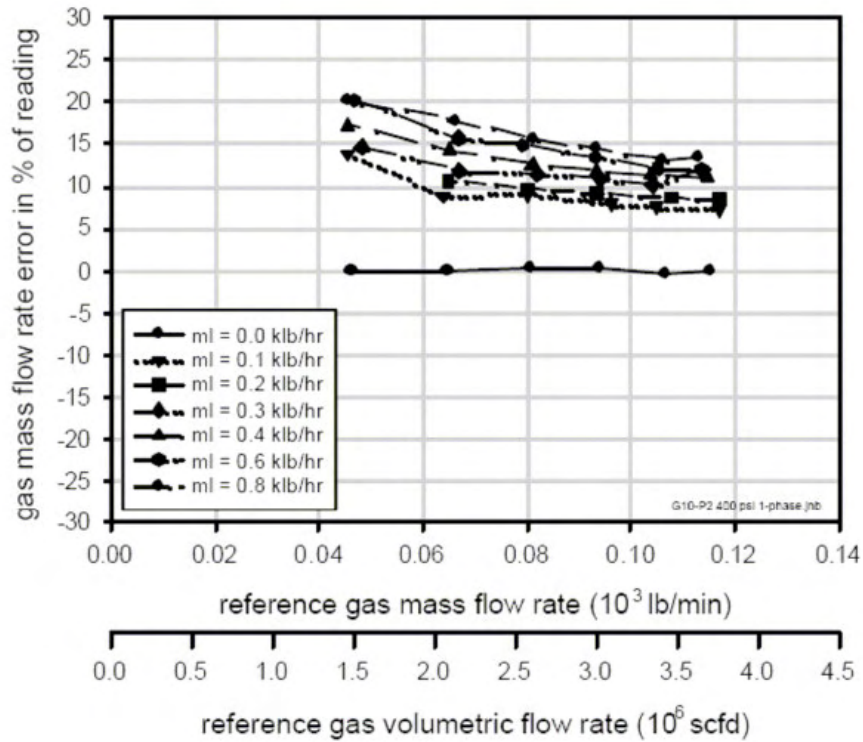
Fig. 51: Gas mass flow rate error using Murdock correlation (Fincke (1999))

Chisholm's Correlation

Chisholm (1969) developed a two-phase flow correlation, considering the slip between the fluids. It was assumed to be an incompressible two-phase flow, with negligible upstream momentum, no phase change, irrelevant drag forces in the wall when compared to the interfacial forces between the phases, and a constant void fraction across the differential pressure device. Chisholm's correlation is defined by:

$$\dot{m}_g = \frac{\dot{m}_{g,Apparent}}{\sqrt{1\left[\left(\dfrac{\rho_g}{\rho_l}\right)^{1/4}+\left(\dfrac{\rho_l}{\rho_g}\right)^{1/4}\right]X_m + X_m^{\ 2}}}$$

He concluded that the orifice meter response to wet steam, two phase flow in horizontal mounting does not only depend on the modified Lockart-Martinelli parameter (X_m), but also on the gas-liquid density ratio (and then on the pressure).

For both the Murdock's and the Chisholm correlation it is supposed the knowledge of the liquid flow rate or of the quality is necessary, since the calculation of the Lockart-Martinelli parameter is based on the single phase pressure drop evaluation. Thus the coupling of an orifice plate/venturi and

a quality (or liquid phase) detecting device is necessary for the calculation of the total mass flow rate.

Meng et al. (2010) proposed an experimental study where a venture was coupled with a ERT (Electrical Resistance Tomography) sensor.

Experimental work was carried out on the horizontal pipelines using air and tap water. The water flowrate was varied between 0.1 m^3/h and 16 m^3/h while the air flowrate ranged from 0.1 to 20 m^3/h.

Two groups of experiments were undertaken on two different pipelines with inner diameters of 25 mm and 40 mm respectively. Four typical flow patterns such as annular flow, bubble flow, stratified flow and slug flow were created. The diameter ratios of the Venturi meters was 0.68 (DN 25 mm) and 0.58 (DN 40 mm), respectively.

In the experiments the operation pressure was measured to be 0.3 MPa, the temperature was around 20 ,C, and the mass quality of air-water two-phase flow was less than 0.1.

The ERT sensor used in this work was a plexiglass pipe with 16 evenly spaced stainless steel electrodes of a diameter 2.8 mm. The electrodes were mounted around the pipe.

The authors in this work make a comparison between the different correlation reported above for the venture meter; the parameters in these correlations are optimized through experiments for different flow patterns as summarized in Tab. 5.

Correlations	Parameters	Parameters for different flow patterns			
		Annular flow	Bubble flow	Stratified flow	Slug flow
James	n	1.2530	0.9617	1.3371	1.0619
Murdock	M	1.7129	1.0847	2.0931	1.3752
Bizon	a	1.4008	9.7331	1.2585	3.8176
	b	1.5187	1.0220	1.8202	1.1480
Collins	a	0.9891	1.9463	0.2926	0.1566
	b	1.2778	0.9681	0.9096	0.9460
	c	0.6692	1.5116	1.9622	1.8327
Chisholm	m	0.2811	0.2500	0.2908	0.2500
	n	0.5310	0.5737	0.5828	0.5345

Parameters in Lin correlation are not optimized, because the limited range of density ratio in our experiments makes the optimization meaningless. The parameters in Eq. (13) are used.

Tab. 5: Parameters used in the flowrate measurement correlations for different flow patterns (Meng (2010))

In order to compare the performance of the above flowrate measurement correlations The root mean square error (RMSE) is used:

Correlations	RMSE for different flow patterns			
	Annular flow	Bubble flow	Stratified flow	Slug flow
Homogeneous	0.369	0.0601	0.436	0.160
Separated	0.224	0.175	0.302	0.210
James	0.129	0.0544	0.160	0.0802
Murdock	0.0604	0.113	0.0853	0.0816
Bizon	0.0183	0.0501	0.0841	0.0286
Collins	0.0137	0.0203	0.0703	0.0168
Chisholm	0.0259	0.0246	0.0754	0.0277
Lin	0.0432	0.0970	0.0681	0.0706

Tab. 6: Comparison results of flowrate measurement correlations for different flow patterns (Meng (2010))

The results have shown that the root mean square error of the total mass flowrate is no greater than 0.03 for bubble flow, 0.06 for slug flow, 0.12 for annular flow and 0.13 for stratified flow, respectively. Most of the relative errors of total mass flowrate are less than 5% for bubble flow and slug flow, and less than 10% for annular flow and stratified flow.

The annular flow and the stratified flow occur mostly at the low mass flowrate, and their measurement errors are larger compared to the bubble flow and the slug flow for reasons mentioned above.

The Collins correlation performs a little better than the Chisholm correlation.

Compared with the conventional differential pressure methods, the flow pattern information is introduced in the measurement process, so the influence of flow pattern is minimized and the measurement performance is improved.

De Leeuw's Correlation (1997)

The most commonly used correlation for Venturi tubes is that of de Leeuw published in 1997.

He used data collected from a 4-inch, 0.4 diameter-ratio Venturi tube and fitted the data using a modification of the Chisholm model. This research found that the wet-gas over-reading was dependent on the Lockhart-Martinelli parameter, the gas-to-liquid density ratio and the gas Froude number, but this correlation did not include geometrical effects of the differential meter and effect of the liquid properties (Steven (2008)).

126

The correlation is valid only for gas with a small amount of liquid (the Lockhart-Martinelli parameter has to be less than 0.3):

$$\dot{m}_g = \frac{\dot{m}_{g,Apparent}}{\sqrt{1 + CX + X^2}}$$

$$C = \left(\frac{\rho_g}{\rho_l}\right)^n + \left(\frac{\rho_l}{\rho_g}\right)^m$$

$$n = 0.606\left(1 - e^{-0.746Fr}\right) \text{ if } Fr \geq 1.5$$

$$n = 0.41 \text{ if } 0.5 \leq Fr < 1.5$$

$\dot{m}_{g,Apparent}$ is the uncorrected value of the gas mass flow rate as detected by the meter, $\dot{m}_g$ is the corrected value and Fr is the gas Froude number.

The difference between the de Leeuw formulation and the Chisholm formulation for orifice plates is the values of the n exponent. De Leeuw showed that n was a function of the gas Froude number, a parameter that was not considered in the previous Chisholm correlation.

De Leeuw stated that the value of n is dependent on the flow regime.

For stratified flow (for $Fr < 1.5$) n is constant and equal to 0.41. As the flow pattern changes from stratified to annular mist and on towards mist flow, the over reading for a set value of the quality will increase. He practically implied that below $Fr = 1.5$ the gas dynamic forces were too weak to produce flow patterns other than stratified flow. He claimed that for that meter geometry, for a known value of the liquid flow rate and within the test matrix parameters of the data set used, this correlation is capable of predicting the gas mass flow rate with ±2% uncertainty.

The knowledge of the β ratio influence on the Venturi meter response limits the application of the de Leeuw correlation to those cases in which the actual β ratio is very close to the value of the original experiment. If the correlation is applied to higher values of β (β > 0.401), there will be a systematic over correction of the actual over reading.

The Venturi meter sensibility (in two phase flow) to the changes in the diameter could lead to the restriction of the de Leeuw correlation to only those cases in

127

which the device diameter is close to the diameter of the Venturi meter employed in the original experiment.

Steven's Correlation (2005)

This correlation has been developed for wet-gas flow in a 4in. And 6 in., 0.75 beta ratio cone meters with gas/light hydrocarbon liquids:

$$\dot{m}_g = \frac{\dot{m}_{g,Apparent}}{\left(\dfrac{1+AX+BFr}{1+CX+BFr}\right)}$$

Where for $\rho_g / \rho_l \geq 0.027$:

$$A = -0.0013 + \frac{0.3997}{\sqrt{\rho_g / \rho_l}} \;\; ; \;\; B = 0.0420 - \frac{0.0317}{\sqrt{\rho_g / \rho_l}} \;\; ; \;\; C = -0.7157 + \frac{0.2819}{\sqrt{\rho_g / \rho_l}} \;\; ;$$

and for $\rho_g / \rho_l < 0.027$:

$A = 2.431 \;\; ; \;\; B = -0.151; \;\; C = 1$.

Zhang's Correlation (1992 et 2005)

To take into account the two-phase flow occurrence, Zhang et al. (1992) suggested the introduction of the K_L parameter to summarize the necessary corrections for correlating the twophase mass flow rate, to the two-phase pressure drop:

$$\dot{m}_{TP} = \left[C_{TP} A_2 \cdot F_a \cdot Y \cdot \left(\frac{2\rho_l \Delta p}{\left(1-\beta^4\right)} \right)^{0.5} \right] K_L$$

C_{TP} = discharge coefficient for the particular meter, dimensionless,

A_2 = constricted area perpendicular to flow,

$\beta = D_2/D_1$ = (diam. at A_2/pipe diam.),

ρ_l = liquid fluid density,

F_a thermal expansion correction factor

Y compressibility coefficient

$$K_L = \left[x^{1.25 + .25 x^{1/3}} \left(\frac{\rho_l}{\rho_g} - 1 \right) + 1 \right]^{-1/2}$$

This correlation has been developed for low quality (x<1%) air-water flow through orifice plates.

In 2005 Zhang proposed a new correlation based on experiments with low quality (x < 2%) oil–air flow through a venturi. These authors measured the void fraction by means of tomography. They proposed semi-empirical correlations to predict, and x, through modifications to the homogeneous model. They attempted to include the influence of the slip ratio by means of constants.

$$K_L = \left[c \left(\frac{\alpha}{1 - \alpha} \right)^n \left(\frac{\rho_l}{\rho_g} \right)^m + 1 \right]^{-1/2}$$

$$X = c' \left(\frac{\alpha}{1 - \alpha} \right) \left(\frac{\rho_g}{\rho_l} \right)^H$$

where *c, n, m, c'* , and *H* are constants which are dependent on the flow regimes and on the test conditions. For bubbly and slug flow, they are equal to 0.50, 0.95, 0.02, 0.51, and 0.65, respectively.

Oliveira et al. (2009) tested this formula in a SP using venturi and orifice plate coupled with a void fraction sensor.

Water mass flow rates of up to 4000 kg/h and air mass flow rates up to 50 kg/h were used. Pressure in the control volume ranged from 2 to 3 bar, void fraction from 2% to 85% and the quality

used was up to almost 10%. After the void fraction sensor calibration, tests with a venturi and an orifice plate with corner taps were carried out in the horizontal and upward vertical direction. The pipe inner diameter, D, was 21 mm and the throat (or orifice) diameter to pipe diameter ratio was 0.5. The electrodes of the void fraction sensor were located at a distance of 75D from the last section change, and the flow meters, venturi or orifice plate, were located at a distance of 95D.
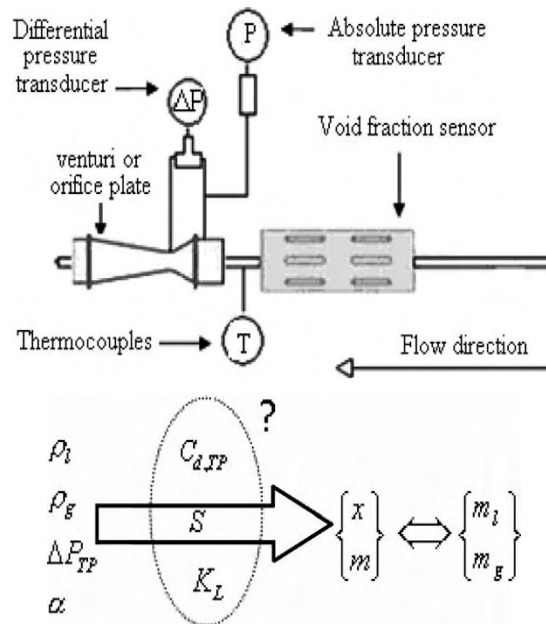
Fig. 52: Measurement system scheme and Experimental procedure flow map (Oliveira et al. (2009)).

Fig. 53 shows, in a logarithmic graph, the comparison between the experimental quality values and those predicted through the x-S-alpha correlation, assuming the non-slip condition (S = 1), and Zhang (2005) correlation.

The quality predicted assuming the non-slip condition (S = 1) was underestimated for most values. The performance was good for bubbly and slug regimes, but when the transition to churn and annular occurred, and mean void fractions over 0.7 and quality over 1% were reached, the predicted quality values deviated from the reference line. The fractional RMS deviation values were 43.8%.

The results obtained using the Zhang correlation overestimated the experimental values. The correlation, created with an oil–air flow data set, did not obtain satisfactory results, and fractional RMS deviation values over 200% were reached.
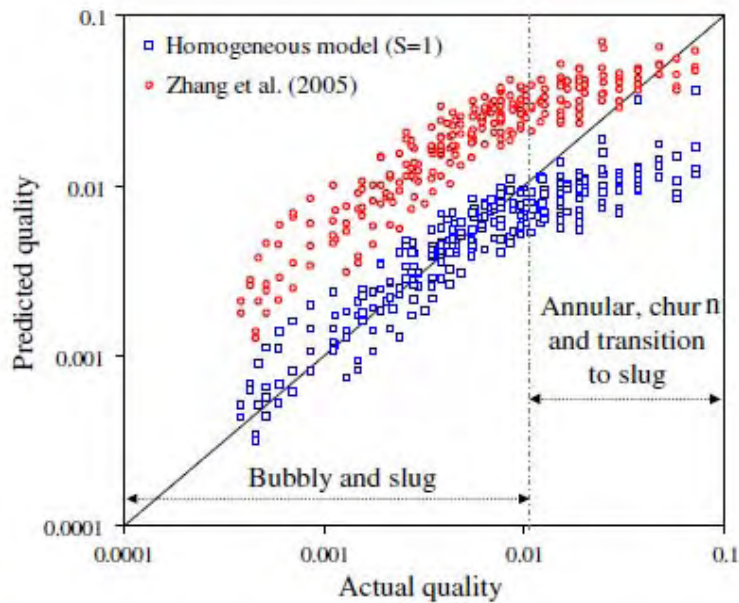
Fig. 53: Comparison between experimental and predicted quality using homogeneous and

Zhang model

(Oliveira et al. (2009))

The authors make a comparison also with other correlation. (see Fig. 54). Higher values for the RMS deviation were obtained for the orifice plate. The experimental points presented good accuracy, but not precision. The presence of this meter causes important disturbance in the two-phase flow and its use in the homogeneous model appears inappropriate.

As with the homogeneous model, Chisholm's correlation achieved better results with the venturi. A deviation of 6.8% was obtained for this meter in the vertical direction. Higher deviations were observed for the orifice plate. It should be noted that Chisholm's correlation had the best performance of all the tested correlations.

The correlation of Zhang et al (1992) overestimated the two-phase mass flow rate when used for the venturi meter. Also, high deviation values were obtained. For the orifice plate, however, deviations close to 9% were observed. This better result is to be expected, since the correlation was created using experimental data obtained with an orifice plate.

The correlation of Zhang et al. (2005) had a reasonable performance in predicting the two-phase mass flow rate. However, better results were found for the orifice plate. This was not expected, since this correlation was created with experimental

data obtained through measurements with a venturi in an oil–air two-phase flow.
A deviation of 5.5% was obtained for the orifice plate in the vertical direction.
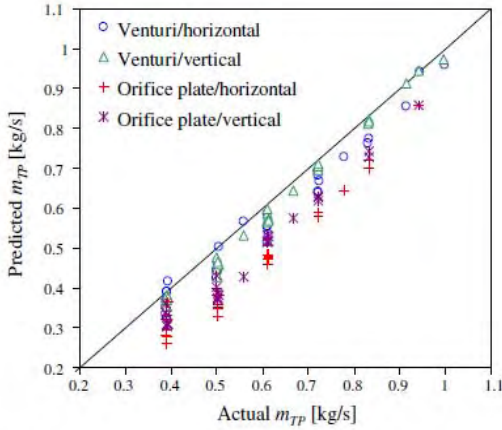
Fig. 10. Comparison between experimental two-phase mass flow rate and that predicted by the homogeneous model.
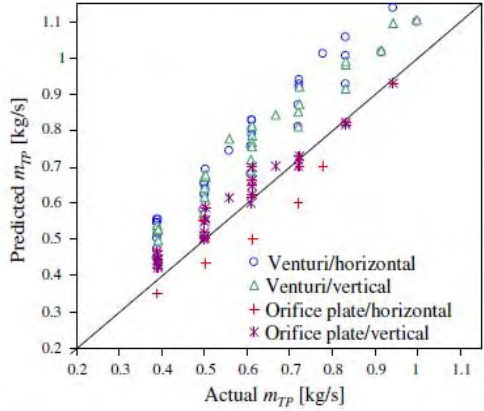
Fig. 12. Comparison between experimental two-phase mass flow rate and that predicted according to Zhang et al. [5].
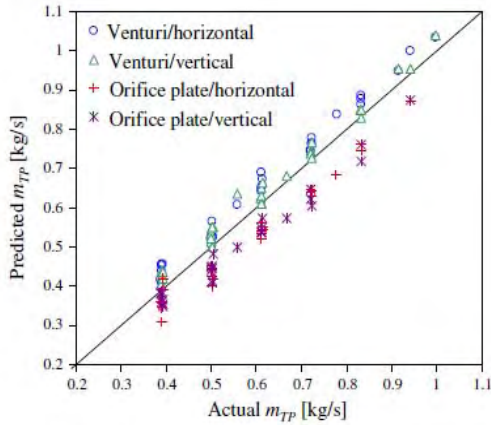
Fig. 11. Comparison between experimental two-phase mass flow rate and that predicted according to Chisholm [10].
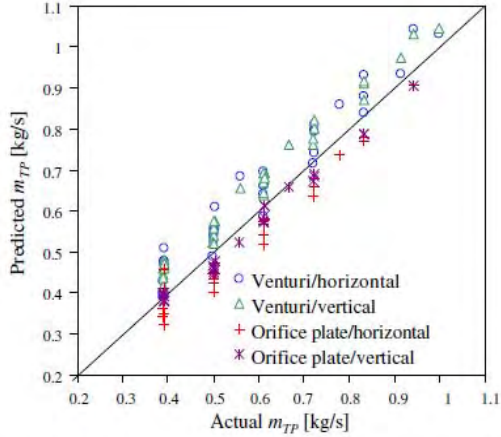
Fig. 13. Comparison between experimental two-phase mass flow rate and that predicted according to Zhang et al. [7].

Fig. 54: Comparison between experimental two phase flow rate and that predicted from correlations (Oliveira et al. (2009))

Steven (2002) compared the results of seven correlations for the correction of the Venturi meter response to wet gas flow:

• Homogeneous model
• Murdock correlation
• Chisholm correlation
• Lin correlation

132

- Smith & Leang correlation (Steven (2002), Smith and Leang (1975)): it was developed for orifice plates and Venturi meters, it introduces a blockage factor that accounts for the partial blockage of the pipe area by the liquid. The blockage factor is a function of the quality only.

- the modified Murdock correlation: it was developed by Phillips Petroleum. The Murdock constant M has been replaced by a new value (1.5 instead of 1.26), to adapt the formula to Venturi meter over reading.

Some of them (Murdock, Chisholm, Lin and Smith & Leang correlations) were studied for the orifice plate response in two-phase flow, but they were extensively used in the natural gas industry for Venturi meter applications.

The modified Murdock and the de Leeuw correlations were instead studied for the Venturi meter reading correction.

The meter studied was an ISA Controls standard North Sea specification 6'', $\beta = 0.55$ Venturi and it was tested with a nitrogen and kerosene mixture. The experiment was conducted for three pressure values (20 bar, 40 bar and 60 bar) and four values of the volumetric gas flow rates (400 m^3/h, 600 m^3/h, 800 m^3/h and 1000 m^3/h).

The difference between the actual mass gas flow rate and the mass gas flow rate evaluated with the seven correlations was expressed as the root mean square fractional deviation:

$$d = \sqrt{\frac{1}{n} \sum_{i=1}^{n} \left(\frac{m_{g,corrected,i} - m_{g,experimental,i}}{m_{g,experimental,i}} \right)^2}$$

The data are listed in the following table (Tab. 7). The d value was calculated for the whole data set and then for each pressure value separately.

All pressures	d		40 bar	d
de Leeuw	0.0211		de Leeuw	0.0193
Homogeneous	0.0237		Homogeneous	0.0220
Lin	0.0462		Murd, M=1.5	0.0410
Murd, M=1.5	0.0482		Lin	0.0448
Murd, M=1.26	0.0650		Murd, M=1.26	0.0589
Chisholm	0.0710		Chisholm	0.0658
Smith & Leang	0.1260		Smith & Leang	0.1199
20 bar	d		60 bar	d
de Leeuw	0.0279		de Leeuw	0.0140
Homogeneous	0.0285		Homogeneous	0.0202
Lin	0.0449		Murd, M=1.5	0.0287
Murd, M=1.5	0.0677		Lin	0.0479
Chisholm	0.0793		Murd, M=1.26	0.0504
Murd, M=1.26	0.0823		Chisholm	0.0675
Smith & Leang	0.1159		Smith & Leang	0.1401

Tab. 7: Root mean square fractional deviation for the whole data set (all pressures) and for each individual pressure, Steven (2002).

The results were also represented in a graph as predicted/actual gas flow rate ratio versus quality. In the following figures (Fig. 55, Fig. 56 and Fig. 57) the data related to the three values of pressure are showed.
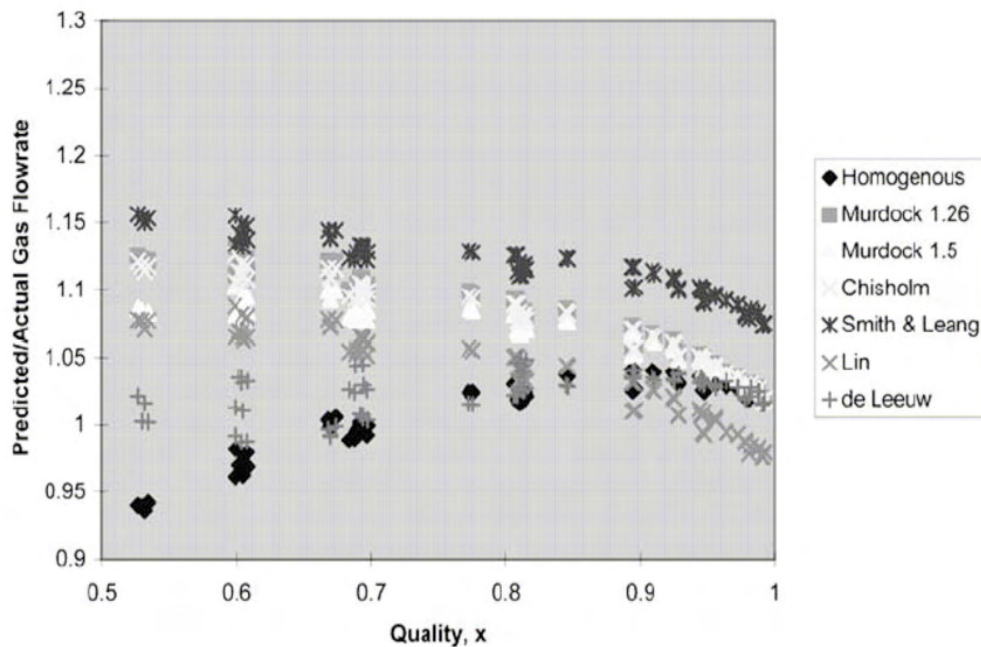
Fig. 55 : Comparison of correlations at 20 bar, Steven (2002),
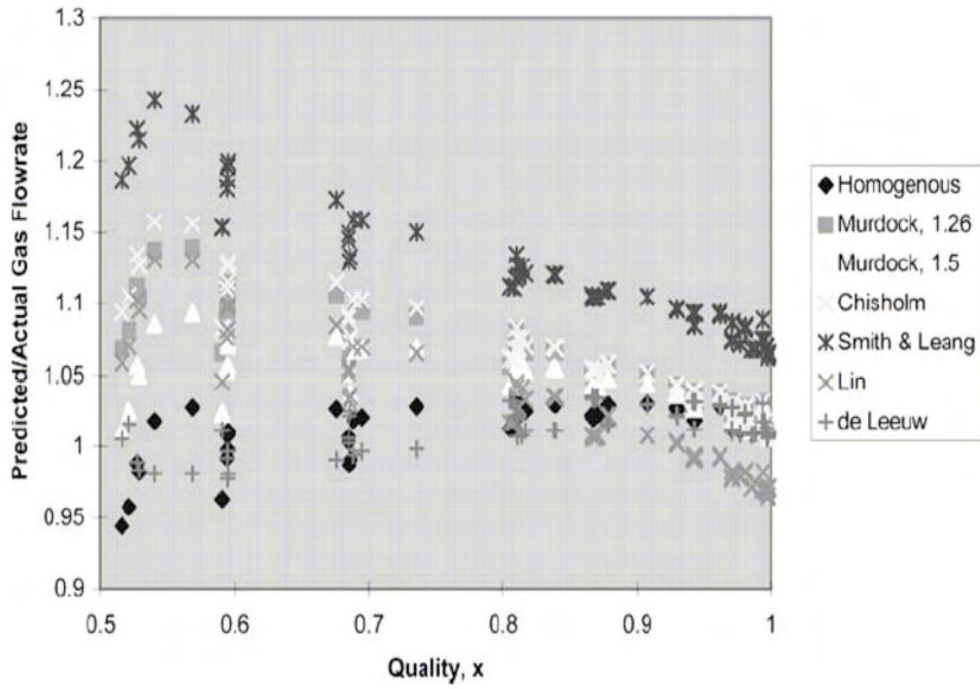
Fig. 56 : Comparison of correlations at 40 bar, Steven (2002).
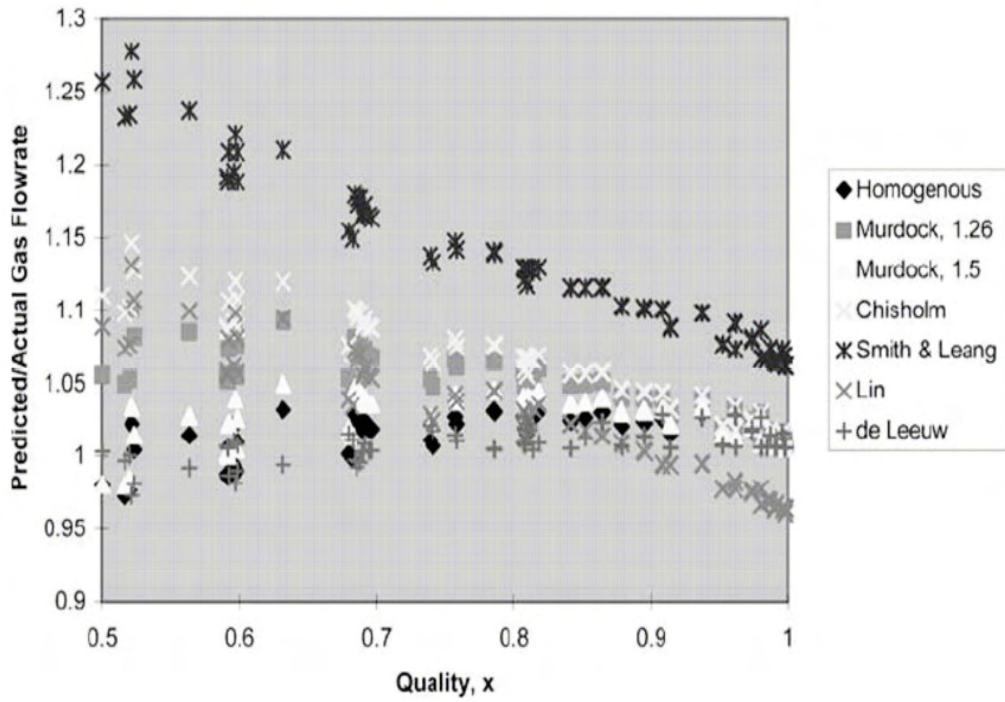
Fig. 57 :Comparison of correlations at 60 bar, Steven (2002).

The most important observations are:

- de Leeuw correlation has the best performance and is the best choice for correcting the Venturi meter over reading in wet steam. It takes into account the influence of the pressure (gas to liquid density ratio), of the gas volumetric flow rate and of the flow patterns. These are in fact three important effects for the changes in the Venturi meter over reading.

- The homogeneous model predicts the exact mass flow rate with a surprising little error in comparison to the other models. This model does not take into account the effect of the flow pattern and it should be therefore less accurate. The most important assumptions of the homogeneous model are the absence of slip ratio and the perfect homogenization of the two phases. The author deduced that the good agreement between this model and the actual mass flow rate should have been dictated by the similarity of the flow conditions in the experiment and the assumption of the model. The model performances are in fact increasing with the pressure and it is generally assumed that the greater the pressure, the larger is the amount of water in suspension in the gas flow (with a more homogenized flow pattern).

- The modified Murdock correlation, despite studied on purpose for the correction of the Venturi meter over reading, gives the worst agreement with the actual gas mass flow rate. This formula has been developed by Phillips Petroleum and the conditions in which it was validated are unknown. The author stated that the failure of the correlation should be referred to the difference between the conditions in which the formula was validated and the actual test conditions.

- The Chisholm, the Lin and the Smith & Lang correlations gives all poor results in this context.

Disturbance to the Flow

Pressure recovery of orifice plates is limited in single phase flow (typically 20-30%). Much higher pressure recovery can be obtained with Venturi meters in single phase flow, but the extrapolation to two-phase flow is not straightforward (pressure recovery with Venturi meters in single-phase flow relies on boundary layer theory, which is of little use in two-phase flow). So the hydraulic resistance of differential meters can be significant, and the overall disturbance to the flowing mixture can be remarkable.

Oliveira et all (2009) for the same meter, venturi or orifice plate, described above, studied the pressure drop. In the upward vertical and horizontal direction the authors showed that no significant differences exist as a result of disturbances in the flow due to gravity acceleration.

Fig. 58and Fig. 59 show the pressure drop for horizontal flow in the venturi and in the orifice plate, respectively, as a function of the water and air mass flow rates. The graphs for the vertical flow are similar.

According to the experimental results observed in these figures, even for very low qualities (x < 0.011), for a fixed water mass flow rate, small enhancements in the air mass flow rate can amplify significantly the two-phase pressure drop.

For a fixed air mass flow rate, the two-phase pressure drop increased with the water mass flow rate increase. For an air mass flow rate of around 1.6 and 3.9 kg/h, the behaviors of the twophase mass flow rate and the two-phase pressure drop were similar to the water single-phase flow behavior.

The mean ratio between the pressure drop in the orifice plate and the pressure drop in the venturi, considering the flow in the horizontal and upward vertical directions, was 1.81.

For the same meter, the mean ratio between the pressure drop with vertical flow and that with horizontal upward flow was close to one. Asymmetries in the phase distributions caused by gravity

did not influence considerably the pressure drop in the meters for slug and bubbly patterns in the horizontal and upward vertical flows.
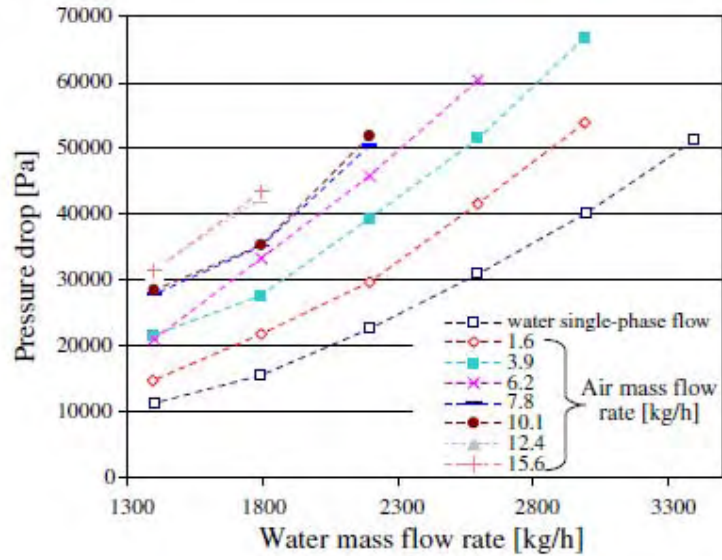
Fig. 58 Pressure drop in the Venturi, horizontal flow (Oliveira et al. (2009))
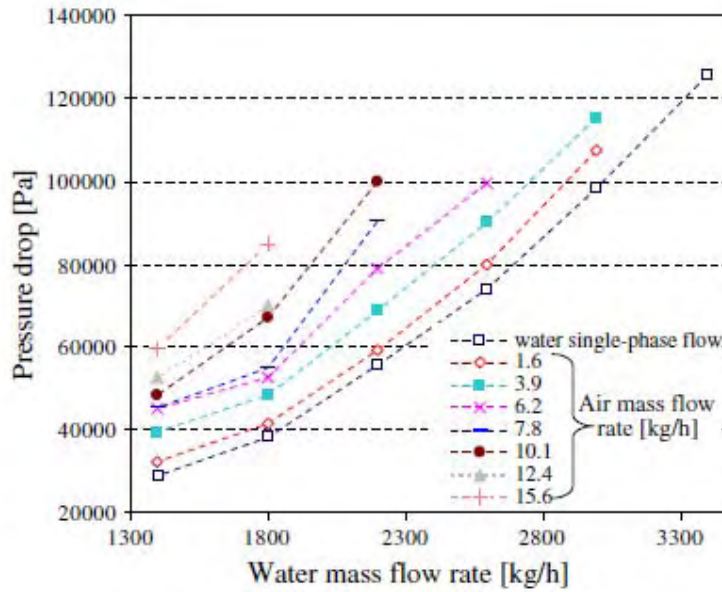
Fig. 59: Pressure drop in the orifice plate, horizontal flow (Oliveira et al. (2009))

Transient Operation Capability (time response)

Orifice plates and Venturi meters are typically designed for steady state applications. Fast transient response requires special care in the design and may require the correction of the signal on the basis of the modelling of the meter, which is doable but not straightforward.

If the flow is not steady, but pulsating, the measurement error will increase because of different reasons (Baker, 2000):

1. *square root error*

2. *resonance*

3. *limitations in the pressure measurement device.*

The first one is connected to the capability of a fast response of the pressure meter, the second to the possibility of a correspondence between the pulsating frequency and the resonance frequency of some components.

The response is highly influenced by the length of transmission pipe lines and the medium used (gas or liquid).

The only research found in literature about dynamic response is proposed by Xu et al. (2003).

Xu Model for dynamic differential pressure signal of Venturi for wet gas metering (2003): the author starting from the Li's correlation for static modelling, obtained, in relation to the fluctuation of the DP signal, a dynamic model.

The dynamic model is proposed in such a way that a monotonous relation between the relative fluctuation of the DP signal and the quality can be obtained. He write the basic equation as:

$$\frac{\Delta p_m}{\left(W_m\right)^2} = \left(kx+b\right)^2$$

where

Δp_m is the Dp generated by the Venturi

W_m is the mass flow rate of the wet gas

x is the quality of the wet gas

k,b are coefficients. They will be constant only if the static pressure remain unchanged.

Provided that the transient values of the DP are denoted by Δp^i_m:

$$\frac{\Delta p^i_m}{\left(W^i_m\right)^2} = \left(kx^i + b\right)^2$$

The root mean square (RMS) deviation of Δp^i_m can be described as:

$$\delta = \left[\frac{1}{n}\sum_{i=1}^{n}\left(\Delta p^i_m\right)^2 - \left(\Delta p_m\right)^2\right]^{1/2}$$

where n is the length of the observations. The value of δ reflects the fluctuating extent of the DP signal. If a function of δ that is monotonous with x can be found, it will provide a new valuable relationship between δ and the parameters to be measured.

Then the author found:

$$\frac{\delta}{\left(W_m\right)^2} = \left[\frac{1}{n}\sum_{i=1}^{n}\left(kx_i + b\right)^4 - \left(kx + b\right)^4\right]^{1/2}$$

He defined the normalized parameter of δ as:

$$I = \frac{\delta}{\Delta p_m}$$

And then combining the equations:

$$I = \frac{\left[\frac{1}{n}\sum_{i=1}^{n}\left(kx_i + b\right)^4 - \left(kx + b\right)^4\right]^{1/2}}{\left(kx + b\right)^2}$$

When the static pressure that determines the gas–liquid density ratio is unchanged, k and b can be considered as constants. Thus, I expresses the fluctuating feature of xi around x. However, as can be seen from Fig. 5, the relationship between I and x is not monotonous.

Experimental results show that I is also influenced by Wm and the static pressure, and then by the density of the gas phase.

He defined:

$$I' = I\left(W_m\right)^{\xi}\left(\rho_g\right)^{\zeta} = f(x)$$

Then it need to found ξ, ζ to make I monotonously relate to x.

$$I = f(x)\left(W_m\right)^{-\xi}\left(\rho_g\right)^{-\zeta}$$

That is the dynamic equation of the venturi.

The author proposed a experimental studies to find the value of ξ and ζ so that the relation is monotonous.

The inner diameter of the pipeline is 50 mm. The gas and liquid phases are natural gas and water, respectively. the flow can be treated as homogeneous. In addition, the volumetric flow fraction of gas phase is greater than 95%, thus the regime of the mixture flow can be treated as mist or annular-mist. Measurement of the DP across the Venturi meter is carried out by a DP transducer with range of 0–240 kPa. Owing to the adoption of silicon sensing element, the dynamic response of the transducer can approach several hundred Hz. After the mixer, there was a straight pipe section of 7 m length to make the flow fully developed. Before the experimental section, there was a 500 mm long transparent pipe so that the flow pattern can be inspected. The inner diameter at the inlet is 50 mm and the diameter ratio is 0.45. The convergence angle is 21° and the expansion angle is 15°.

Experiments have been carried out in vertical section only.

Experimental conditions were as follows:

- volumetric flowrate of gas between 50 and 100 m^3/h
- range of the quality between 0.06–0.412;
- static pressure inside the pipeline between 0.3–0.8 MPa.
- the sample frequency was 260 Hz and the sample time was 120 s.
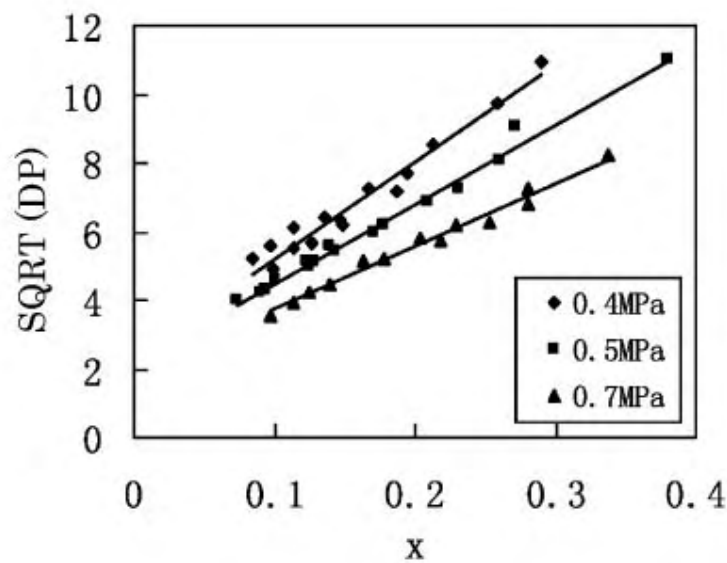
Fig. 60: Relationship between $\sqrt{\Delta p}$ and x (Xu et al. (2003))

141

Fig. 60 shows the relationship between $\sqrt{\Delta p}$ and x at different static pressures. As expected, the relationship can be fitted with a straight line, demonstrating that Lin's equation is applicable within the test conditions. The deviation of test points from their fitting lines is due to the fluctuation of the DP signal. In addition, it can be seen that values of k and b vary with static pressure. This is due to the density of the gas increasing with the static pressure. The values of k and b are listed in Tab. 8.
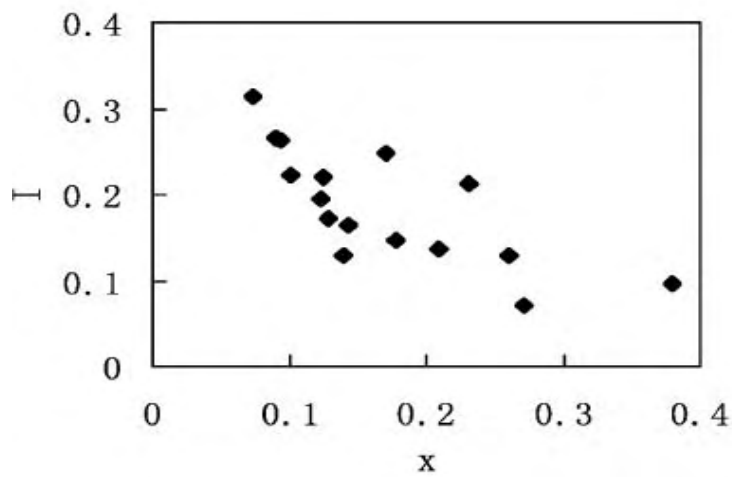
Fig. 61: Relationship between *I* and *x* at 0.5 MPa (Xu et al. (2003))

Table 1
Values of k and b under different static pressures

Static pressure (MPa)	k	b
0.4	28.032	2.4394
0.5	23.27	2.148
0.7	18.391	1.8743

Tab. 8: k and b values (Xu et al. (2003))

Fig. 61 displays the relationship between I and x at 0.5 MPa. It can be seen that the relationship between I and x is not monotonous. The author suggest that I is related to both Wm and x and decreases with either of them. The hold-up of the liquid decreases with the quality of the mixture and hence the fluctuation of the

DP signal decreases too. If we keep the quality unchanged, the higher the mass flowrate, the nearer the flow pattern to the homogeneous mist flow, the less the relative deviation of the DP and hence the less the value of I.

The relation between I' and x is shown in Fig. 6, where $\xi = -1$. It can be seen that the modified relative fluctuation of the DP signal is monotonously correlated to x and decreases with x.
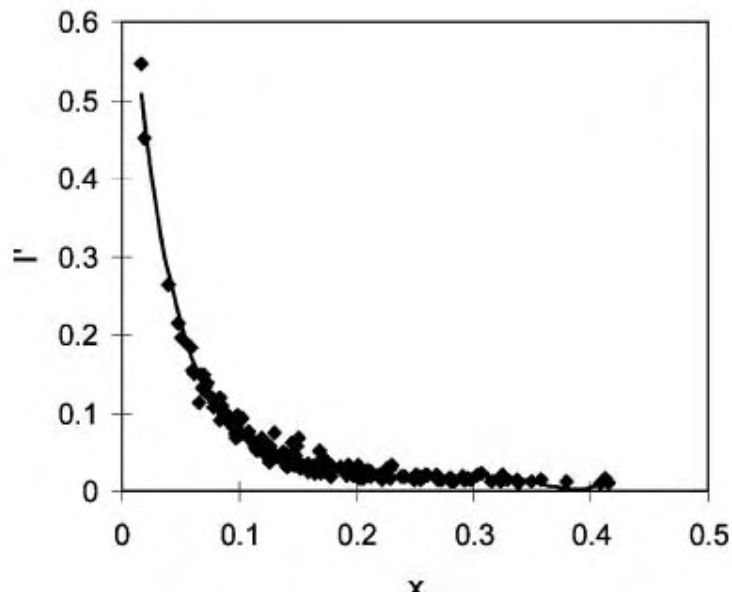
Fig. 62: Relationship between I' and x at all pressures (from 0.3 to 0.8 MPa) (Xu et al. (2003))

The tendency line is a good approximation of these data and monotonously maps x to I' except at data points with quality larger than 0.38. The tendency line can be represented by the following polynomial with a degree of 6:

$$I'(x) = 5494.4x^6 - 7933.3x^5 + 4590x^4 - 1365.7x^3 + 222.89x^2 - 19.499x + 0.7769$$

The average fitting error is 0.028. Experiments on repeatability showed that this relationship is well repeatable and the average fitting error is better than 0.03. The results obtained for these data display that within the range of the quality from 0.06 to 0.38, provides a monotonous functional relation between the relative fluctuation of the DP signal and the quality of wet gas. In addition, the dynamic model imply that the fluctuation of the DP signal carries information on both mass flowrate and quality of the wet gas.

143

It should be noted that the equation proposed by Xu is obtained from the same Venturi meter, that is to say, one device provides two independent equations. This equation can be used as auxiliary information on the wet gas flow.

In addition, the author suggest that, one may argue that the fluctuation of the DP signal is perhaps influenced by the size of the liquid droplets although experimental validation is difficult. If Wm and x are kept unchanged, the larger the size of the liquid droplet, the sparser the distribution of the droplet.

Accretion of the droplet size enlarges the fluctuation of the DP signal, on one hand; decrease of the droplet concentration will reduce the fluctuation on the other and vice versa. Both sides of this effect will compensate the influence of the variation of the droplet size with each other. As a result, the model might be less influenced by the droplet size within a certain range.

Bi-directional Operation Capability

Differential meters are typically one-directional. Bi-directional capability can be obtained either with a modified design (which could reduce the extrapolability of literature material) or with in-situ testing of a one-directional meter in reverse flow conditions.

7. IMPEDANCE PROBES

The void fraction is one of the most important parameter used to characterize two-phase flow. It is the physical value used for determining numerous other important parameters, (density and viscosity, velocity of each phase etc…) and it is fundamental in models for predicting flow patter, flow patter transition, heat transfer and pressure drop.

Various geometric definition are used for specifying the void fraction: local, chordal, cross-sectional and volumetric.

The local refers to that at a point (or very small volume): if P(r, t) represent the local instantaneous presence of vapour (or gas) or not at some point r at the time t, the local time-averaged void fraction is defined as:

$$\alpha_{local}(r) = \frac{1}{t}\int_t P(r,t)dt$$

The chordal void fraction is defined as:

$$\alpha_{chordal} = \frac{L_G}{L_G + L_L}$$

Where L_G is the length of the line through the vapour/gas phase and L_L is the length of the line through the liquid phase.

The cross-sectional void fraction is defined as:

$$\alpha_{cross-sectional} = \frac{A_G}{A_G + A_L}$$

where A_G is the area occupied by the vapour/gas phase and A_L is the area occupied by the liquid phase.

The volumetric void fraction is:

$$\alpha_{volumetric} = \frac{V_G}{V_G + V_L}$$

where V_G is the volume occupied by the vapour/gas phase and V_L is the volume occupied by the liquid phase.

Void fraction can be measured using a number of techniques, including radiation attenuation (X or γ-ray or neutron beams) for line or area averaged values, optical or electrical contact probes for local void fraction, impedance technique using

capacitance or conductance sensors and direct volume measurement using quick-closing valves.

The use of the different techniques depends on the applications, and whether a volumetric average or a local void fraction measurement is desired.

The radiation attenuation method can be expensive and from a safety aspect difficult to implement, while intrusive probes disturb the flow field. On the other hand, the impedance measurement technique is practical and cost-effective method for void fraction measurement.

Impedance sensors have been used successfully to measure time and volume averaged void fraction, and its instantaneous output signal has been used to identify the flow pattern.

Another solution for the void fraction measures is the coupling of a velocity sensing flow-meter and a momentum sensing flow-meter. The ratio of the momentum, ρv^2 , and the velocity, v , provides the mass flow rate value, as described previously. These techniques are frequently referred to as multiple sensor method or spool piece method, because the different meters are installed in the same portion of the line.

Table 1
Summary of parameters to be measured and applicable measurement techniques

Parameter to be measured	Measurement technique
Cross-section averaged void fraction	Gamma densitometer (wide beam)
Line-averaged void fraction distributions	Gamma densitometer (narrow beam)
Macro- and micro-photo-graphic analog and digital images	High speed video, digital flow visualization
Local void fraction distributions	Hot-film anemometer
Droplet size	Hot-film anemometer
Dispersed bubble and droplet velocity	Hot-film anemometer Laser Doppler velocimeter
Simultaneous bubble and liquid velocity	Laser Doppler velocimeter

Tab. 9: void fraction measured with different techniques

In two-phase flow research, the impedance (conductance or capacitance) technique has been applied for almost four decades in void fraction measurements, especially in laboratory experiments.

The fast response of the impedance meter makes it possible to obtain information about virtually instantaneous void fractions and their distributions across a pipe section. The impedance void-meter is a low-cost device. The economic feature makes it a more attractive approach than other techniques. In addition, the void-meter can be constructed easily in a non-intrusive structure.

It was realized that the relationship between void fraction and impedance depends on flow regime. To overcome the difficulty, a number of alternative probe designs have been investigated.

A variety of probe geometries has been applied, including those in which the ground and emitter are placed in opposite test section walls, and those which are completely immersed in the two-phase flow.

The impedance method is based on the fact that the liquid and gas phases have different electrical conductivities and relative permittivities.

The measurements of void fraction with impedance sensor are quasi-local, the sensor determines the percentage of both phases not strictly in a selected cross section of the pipe but in a certain volume, based on the electrodes height (except that for wire sensor that are installed inside the pipe and perpendicular to the flow). The exact boundary of this volume cannot be precisely drawn due to fringe effects. To minimise the non-local effects, the height of the electrodes measured along the pipe should be as short as possible, but the effect of the fringe field cannot be eliminated. Short electrodes have, however, small capacitance and low sensitivity, and in this case a compromise is needed. The sensor was shielded to minimise the distortion effects due to outer objects and electromagnetic fields. The shield dimensions should be as large as possible in order to minimise stray capacitance.

Because of the electric properties of the fluid, the impedance consist of capacitive and of resistive components. The simplest model consist of a capacitance and o resistance in parallel.

The measurements of capacitance of a capacitor filled with a conducting liquid, like water, are difficult because equivalent resistance of the liquid, which is usually low, is connected in parallel with capacitive component of the admittance, provided the water component is the continuous phase in the mixture. For low

147

frequencies, this resistance is like a 'short-circuit' to the capacitance. To cut-off the effect of the resistance, the sensor admittance has to be measured in high frequency range.

It's better to operate at high frequencies to obtain capacitance domination, because the liquid conductivity can change by orders of magnitude with the temperature and the ion concentration, whereas the dielectric constant varies less. Stott et al. (1985) tested external and internal capacitance of a sensor but only for low frequency of 1.6 kHz. Abouelwafa and Kendall (1980) used a radio-frequency bridge operating at the frequency of 1 MHz, however, it was still too low to overcome the liquid conductance component of the sensor capacitance. Huang et al. (1988) excited the capacitance sensor with frequency of up to 5 MHz. The frequency of 80 MHz for excitation of a capacitance sensor used in laboratory tests of void fraction measurement was proposed by Jaworek (1994 in Jaworek (2004)). The method of oscillation frequency deviation was used by the author for determination of the sensor capacitance.

The frequency of 80 MHz was also used for determination of capacitance variation by Jaworek et all (2004) in a water/steam mixture using two electrodes mounted outside a pipe operating at RF frequencies.

Electrode System

Many different types of electrodes configuration where studied by a number of authors.

The different geometries can be classified in four general type; within each type there are only minor differences related to the specific environment of the probe or the number of the electrodes:

- *Coaxial*
- *Parallel flat plates*
- *Wire grid*
- *Wall flush mounted circular arc*

Selecting the optimum shape is a non simple task. The coaxial system permit to have a quasi-uniform electric field; however Olsen reports that this type is very sensitive to void distribution and flow pattern.

One of the most interesting to overtake the problem of non homogeneous configuration of the flow pattern was studied by Hetsroni (1982), Merilo et al.

(1977). Six electrodes are mounted flush with the tube wall and respective pairs of these are energized by oscillators such that the electric field vector rotates. The results obtained tacking the average of the three values is a better approximation of the void fraction.

Elkow and Rezkallah (1996) compared the performance of concave and helical type sensors and determined that the problems associated with helical type sensors, including the nonlinear response, poor sensitivity and poor shielding, can be eliminated by using the concave type sensors. The accuracy of the concave parallel sensors can be improved by having both electrodes of equal length to decrease the non-uniformity of the electric field between the two electrodes and eliminate the non-linear response. Based on several tests, they also recommended that the distance between the electrodes and the shield should be large relative to the separation distance between the two electrodes in order to improve the immunity to stray capacitance.

Ahmed (2007) presented, a systematic method for the design of capacitance sensors for void fraction measurement and flow pattern identification.

Two different configurations of the sensors are considered: concave and ring type (Fig. 63). For the ring types sensor each electrode covers the entire circumference, except for a small gap to facilitate the installation of the sensor around the tubes, and are separated in the axial direction of the tube, while in the concave sensor, two brass strips are mounted on the tube circumference opposite to each other. The difference in the electrode geometry results in different electric fields within the measurement volume and hence in the sensitivity and response of the sensors. The two geometries are analyzed for the signal to noise ratio and the sensitivity to the void fraction and flow pattern. Experiments were performed to validate the design theory and to evaluate the sensor characteristics using air-oil two-phase flow in a horizontal pipe.

a) Ring type   b) Concave type
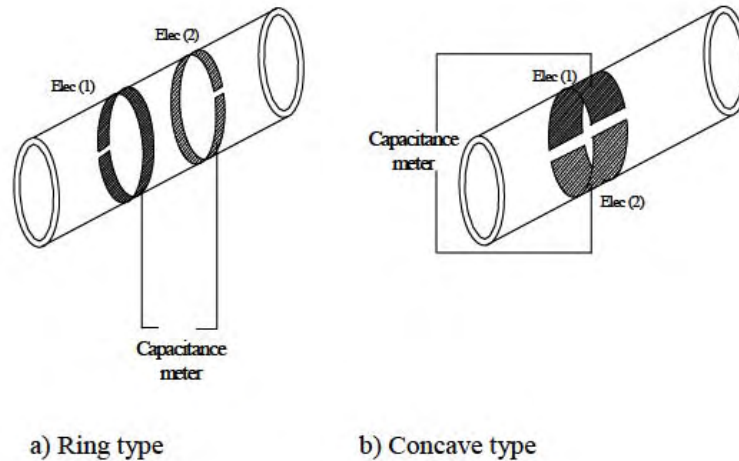
Fig. 63: Scheme of ring and concave type sensor

Signal Processor

The diversity of the signal processor design to measure the impedance of the mixture is comparable to that of the electrode systems. The principals methods are:

- *Comparator circuits*
- *Resonant circuits*
- *Bridge*
- *Voltage drop of a resistor in series with fluid cell impedance.*

In all these methods the fluid impedance is an integral part of the signal processor. The range of the electric field frequencies varies widely from a few kHz to a few MHz. Apart from the elimination of the electrochemical reactions, the choise of the frequencies reflect the intent to measure either the resistive or the capacitive component of the impedance. The measurement of one or the other serves only an academic purpose (Bernier (1982)) which is to verify the validity of the analytical solutions.

Theory: Effective electrical properties of a Two phase mixture

This type of instruments operates on the principle that the electrical impedance of a mixture is usually different from the impedance of each component.

A correlation between the void fraction and the mixture impedance is possible if the two constituents have dissimilar electrical properties.

Gas are generally poor conductor with a low dielectric constant, while liquids if not good conductors will a least assume a higher value of the dielectric constant due to a larger concentration of dipoles.

The measurements of the impedance takes place in a volume defined by the lines of an electric field associated with the electrode system.

There are, however, several disadvantages of the impedance technique, which are sometimes difficult to resolve. For example, the capacitance measurement is sensitive to the void fraction distribution or flow regimes due to the non-uniformity of the electrical field inside the measuring volume. This, however, can be compensated by first identifying the flow pattern. The measurement is also sensitive to the changes in electrical properties of the two phases due to temperature. The noise due to the electromagnetic field around the sensor and connecting wires can significantly affect the signal and needs to be minimized through proper design of the sensor shield. As mentioned by Olsen (1967) the polarization effect due to the ions in the liquid introduces an additional impedance localized in the vicinity of the liquid-electrode interface. This parasitic impedance can be removed by a proper choice of the electric frequency. If insulated electrodes are used, a proper model on the cell impedance should include the capacitive effect of the insulator.

The relation between the admittance of the mixture and the void fraction is not bijective and for a single admittance value there could be different void fraction values, based on different flow patterns.

The analytical treatment has been first done by Maxwell. His solution is obtained by considering a dilute suspension of spheres having a conductivity ε_i in a continuous medium of conductivity ε_o.

Maxwell found the following equation:

$$\frac{\varepsilon_{TP}}{\varepsilon_o} = 1 - \frac{3\alpha}{\left(\dfrac{2\varepsilon_o + \varepsilon_i}{\varepsilon_o - \varepsilon_i}\right) + \alpha}$$

For the case of air bubbles in water the equation reduces to

$$\frac{\varepsilon_{TP}}{\varepsilon_l} = 1 - \frac{3\alpha}{2 + \alpha}$$

Because $\varepsilon_l \gg \varepsilon_g$

And the effective dielectric constant became

$$\frac{\varepsilon_{TP}}{\varepsilon_W} = 1 - \frac{3\alpha}{2+\alpha}$$

Wagner (1914) gave the original derivation of the electric field through an array of distributed spheres, based on Maxwell's equation, and Van Beek (1967) gave a more general form of this equation:

$$\frac{\varepsilon_{TP}}{\varepsilon_l} = \left[1 + \frac{n\alpha\left(\varepsilon_g - \varepsilon_l\right)}{\varepsilon_g + (n-1)\varepsilon_l} \right]$$

Where n is a function of particle shape: 3 for spheres correspond to Maxwell's equation. For oblate spheroids is ~ 1 and for prolate spheroids is >3.

Bernier (1982) proposed a model that consider the "true" void fraction as a function of the relative capacitance (α_C) and a "dispersion factor" (m)

$$\alpha_T = f\left(\alpha_C, m\right)$$

With

$$\alpha_C = \frac{C_{liq} - C_{mix}}{C_{liq} - C_{gas}}$$

Where C is the capacitance of the fluid and m is the dispersion factor.

m is determined by the shape and distribution of the dispersed phase which, at high void fraction, is usually liquid. By definition :

$$\frac{C_{liq}}{C_{gas}} = \varepsilon_{liq}$$

$$\frac{C_{mix}}{C_{gas}} = \varepsilon_{mix}$$

And $\varepsilon_{gas} = 1$ is the dielectric constant for the gas phase.
Rewriting the equation:

$$\alpha_C = \frac{\varepsilon_{liq} - \varepsilon_{mix}}{\varepsilon_{liq} - \varepsilon_{gas}}$$

The relationship between relative capacitance and void fraction is described by Winner's equation:

$$1 - \alpha_T = \left(1 - \alpha_C\right) \left[\frac{\varepsilon_{liq} + m\left(\varepsilon_{gas}\right)}{\varepsilon_{liq}\left(1 - \alpha_C\right) + \varepsilon_{gas}\left(m + \alpha_C\right)} \right]$$

Note that m = 2 corresponds to Maxwell's theoretical equation.

Javorek (2004) proposed different models that can be applied to the situation of two phase flow.

These models calculate the equivalent permittivity of the mixture:

- plate voids placed perpendicularly to the electrodes, which can be reduced to two capacitances connected in parallel. The effective relative permittivity can be calculated as:

$$\varepsilon_{TP} = \varepsilon_g \alpha + \varepsilon_l (1-\alpha)$$

  where ε_g is the relative permittivity of the gaseous phase, ε_l the relative permittivity of the liquid phase.

- plate voids placed parallel to the electrodes, which can be reduced to two capacitance connected in series:

$$\varepsilon_{TP} = \frac{1}{\dfrac{\alpha}{\varepsilon_g} + \dfrac{(1-\alpha)}{\varepsilon_l}}$$

- a continuous medium (water) with cylindrical voids placed parallel to the electrodes, which could be a model for annular flow:

$$\varepsilon_{TP} = \frac{(2\alpha-1)(\varepsilon_g - \varepsilon_l) + \sqrt{(2\alpha-1)^2 (\varepsilon_g - \varepsilon_l)^2 + 4\varepsilon_g \varepsilon_l}}{2}$$

- a continuous medium with spherical voids, that could be a model for bubble flow:

$$\varepsilon_{TP} = \frac{2(\alpha\varepsilon_g + (1-\alpha)\varepsilon_l) - (\alpha\varepsilon_l - (1-\alpha)\varepsilon_g) + \sqrt{2(\alpha\varepsilon_g + (1-\alpha)\varepsilon_l) - (\alpha\varepsilon_l - (1-\alpha)\varepsilon_g)^2 + 8\varepsilon_g \varepsilon_l}}{4}$$

In Fig. 64 is represented the effective relative permittivity of the precedent models as a function of the void fraction.
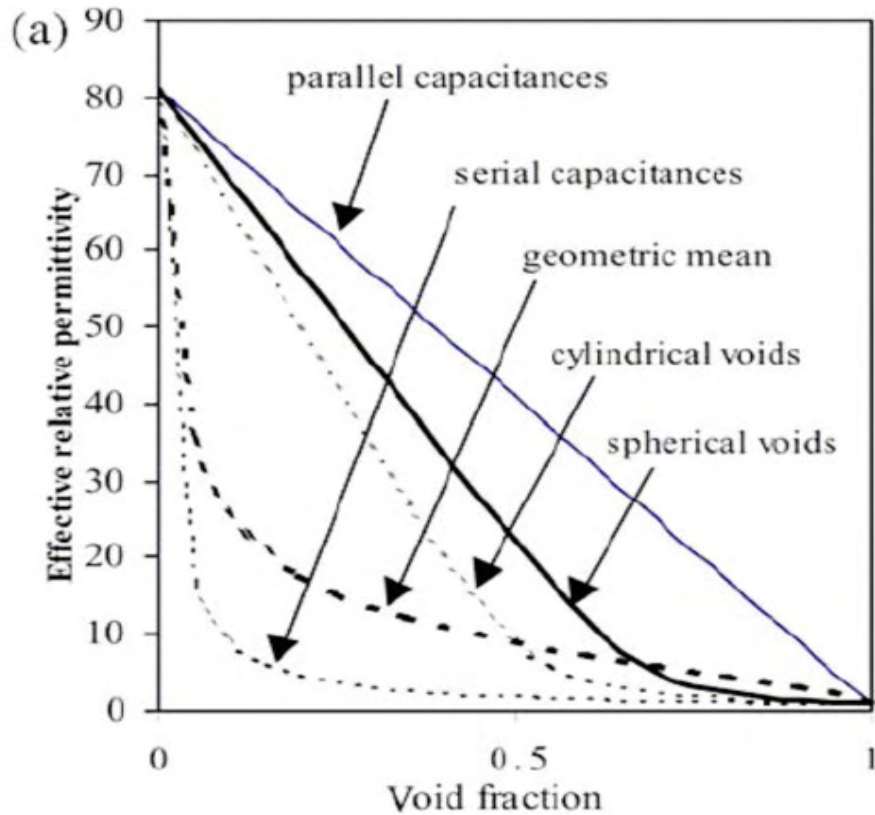
Fig. 64: Effective relative permittivity as a function of the void fraction

The formula that relates the dielectric constant (or relative permittivity) ε and the capacitance C for a parallel plate capacitor with a surface area A and the distance between the plates equal to d is:

$C \approx \varepsilon A/d,$

provided that $A \gg d^2$.

Ahmed (2007) show that the relationship between the capacitance and the void fraction is dependent on the dielectric values of the two phases, but also on the cross-sectional area of the sensors, and the separation distance between the two electrodes. He compare ring and concave type sensor as show previously.

Ring Type Sensors

The electric field can be assumed approximately constant in the axial direction and the two rings equivalent to parallel flat disks. In this method, the two phases are modelled as series or parallel capacitors between the electrodes. This equivalent circuit is based on the distribution of the two phases inside the channel.

a) Series circuit   b) Parallel circuit

Fig. 65: Capacitance circuit equivalent to two-phase flow distribution.

a) Annular flow   b) Stratified flow

c) Bubbly flow   d) Slug Flow

Fig. 66: Equivalent capacitance circuits for typical flow regimes (Adapted from Chang *et al.*)

## Concave Type Sensors

(a)   (b)   (c)

Fig. 67: Geometrical simplification of the concave type capacitance sensor. Equivalent capacitance circuit for annular and core flow regimes

155

(a) Elongated bubble simulation   b) Equivalent circuit

Fig. 68: Geometrical simulation of elongated bubble in ring type sensor. Equivalent capacitance circuit.

The above schematic analysis may be used to estimate the capacitance of such a sensor by substituting the permittivity of the free space and the dielectric constant of the liquid as well as the geometrical parameters as a function of the void fraction.

Time constant

The definition of the time constant of the capacitance sensor here is referred to the time interval required for the sensor-meter to change 70% from one state or condition to another. The time constant for both types of capacitance sensors was obtained experimentally by applying a unit step signal and recording the sensor response. Ahmed (2007) found that, fro ring and concave type, the time constant is approximately 40 μs, corresponding to a dynamic response of 25 kHz.

$$\frac{Y_t - Y_{initial}}{Y_{max} - Y_{initial}} = 1 - e^{T/\tau}$$

Sensitivity

The sensitivity, S, of the sensor can be defined as:

$$S = \frac{C_{liq} - C_{gas}}{\alpha_{liq} - \alpha_{gas}} = C_{liq} - C_{gas}$$

and needs to be maximized. The sensitivity depends on the geometrical shape and gap between the electrodes, which also affects the spatial resolution of the sensor.

Ahmed (2007) shows that for the ring type sensor, the main dimension that affects the sensitivity is the spacing between the electrodes (d). The results show that the sensitivity increases as the spacing decreases Fig. 69, which also results in a better spatial resolution, with the only limitation being in the fabrication of the sensor. For the concave sensor, the sensitivity increases as the electrode separation (z) decreases Fig. 70, and the electrode length increases. However, increasing the electrode length leads to a poor spatial resolution as shown in Fig. 71. In general, the sensitivity of the ring type sensor is found to be higher than the concave type for the same spatial resolution. The sensitivity of the ring sensor was found to be approximately 0.75 *pF*, while for the concave sensor it was 0.6 *pF*. The effect of the flow regime on the sensitivity of the capacitance sensor can be estimated.

It should be noted that the sensitivity is also affected by the electrode spacing and for the ring type sensor an electrode spacing of less than 2 mm is required for a high sensitivity. For this electrode spacing the sensor gives an approximate volumetric void fraction equal to the cross sectional value for bubbly flow.

Both types of sensors, used by Ahmed (2007), were fabricated and tested in an air-oil flow loop. The void fraction predictions from the theoretical models for the sensor design are within 15% of the experimental data.

The total flow rate through the test section was maintained within +2% of the average value while the void fraction measurements were taken. The main source of uncertainty in the void fraction measurement was the noise in the sensor signal from the surrounding equipment such as the oil pump and the biases of the voltage signal, sensor spacing and position. This uncertainty was calculated to be in the range of +6% over the entire range of void fraction.
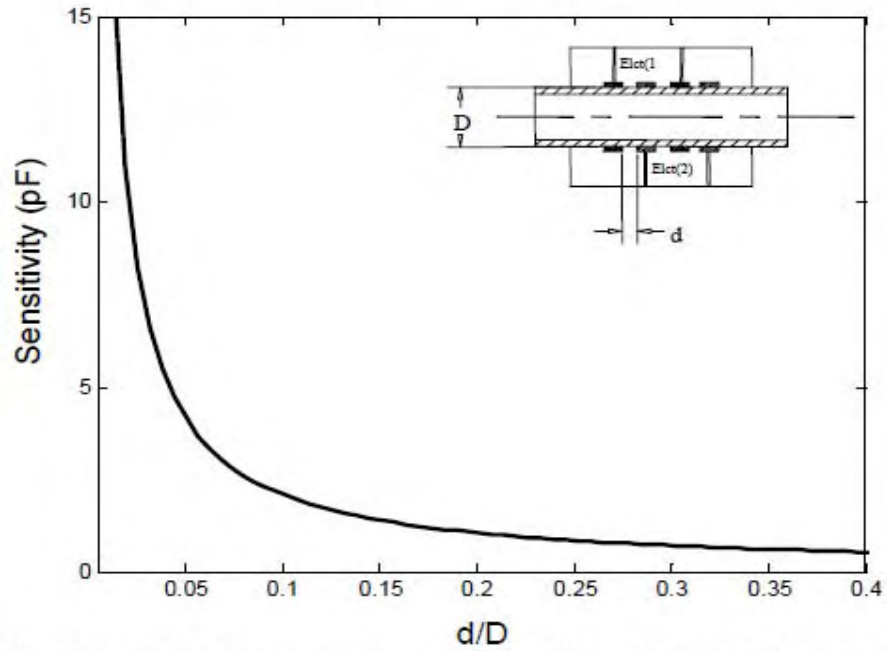
**Fig. 69: Effect of the electrode spacing on the sensitivity of the ring type sensor**
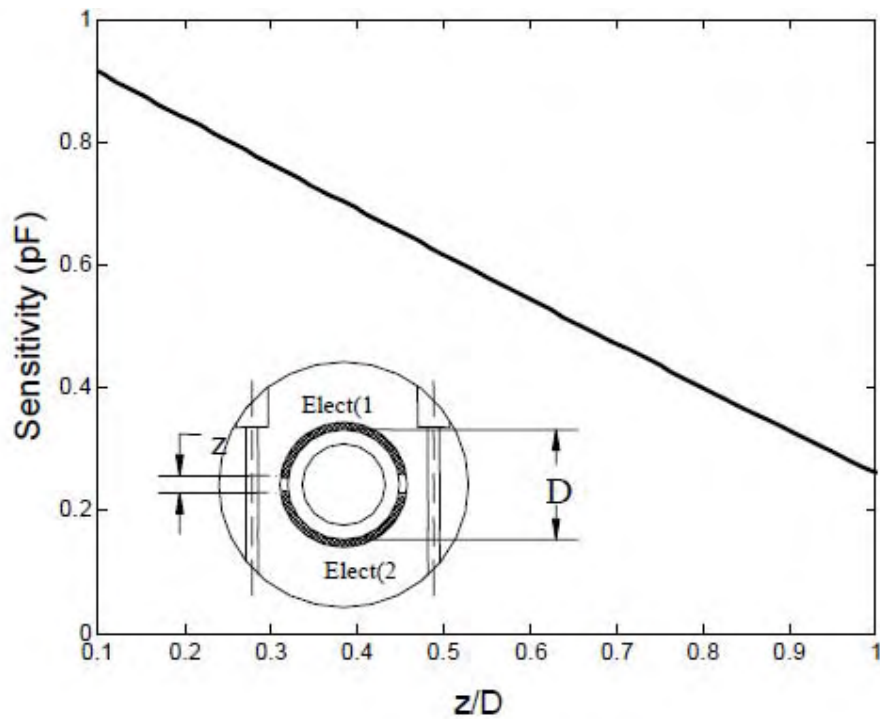
Fig. 70: Effect of the electrode separation on the sensitivity for concave type sensor
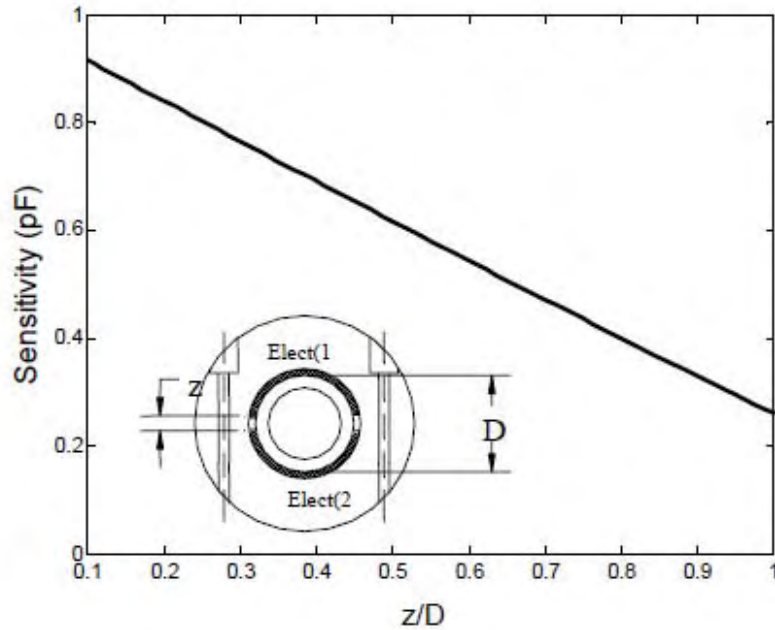
Fig. 71: Effect of the sensor dimensions on the sensitivity for concave type sensor

Fossa (1998) tested two sensors built whit different designs: ring electrodes and plate electrodes. In both cases their shape was very thin and they were positioned on the inner side of the pipe, adherent to the surface. It can be supposed that the influence on the flow was very little.

Two different configurations for the test section were used. The first one (A) is a pipe made of Plexiglas, 70 mm internal diameter, 480 mm long, equipped with three flush ring electrodes located 14 mm and 24 mm apart. The second one (B) is a cylinder made of PVC, 14 mm internal diameter, 70 mm long, used only for annular flow. It's equipped with two ring electrodes (width 1 mm, located 9 mm apart) and two plate electrodes (3 mm diameter, located 9 mm apart in the pipe axis direction.

The void fraction measurements were compared with the theoretical formulas from Maxwell (1882), Coney (1973), Tsochatzidis et al (1992), for the prediction of the conductance of a two phase flow characterized by the presence of a liquid film (the geometry of the electrodes, the electrical conductivity of the layer, the void fraction and the wetted length of the electrodes are known; these formulas were used for stratified and annular flow).

A preliminary set of experiments was carried out to find some reference values for the conductance (e.g. the conductance of the pipes filled with water).

In this case the first configuration showed a good repeatability, while the scatter of the data related to the second configuration was remarkable.

Micro air bubbles deposited on the small plate electrodes influenced negatively the response of the probe, furthermore, when the surface of the electrode is very small (like in the case of the plate electrodes) and the liquid film very thin, the liquid resistance could be of the same order of the impedance of the cable carrying the signal, resulting in a difficult recording of the data.

The conductance was measured for different flow patterns and probe geometry and then normalized with respect to the conductance of the pipes full of liquid. The data collected were plotted against the mean liquid fraction and compared to the theoretical formulas.

The mean liquid fraction was obtained using a method based on differential pressure measurements; a differential manometer detected the differential pressure between two pressure taps located 260 mm apart. The ratio between this value and the pressure of a water column 260 mm tall represented the mean volumetric void fraction.

For the section A under stratified conditions the scatter between the theoretical data and the measured value is within 8%. The agreement increased with a bigger spacing between the electrodes (24 mm instead of 14 mm) (see Fig. 72).
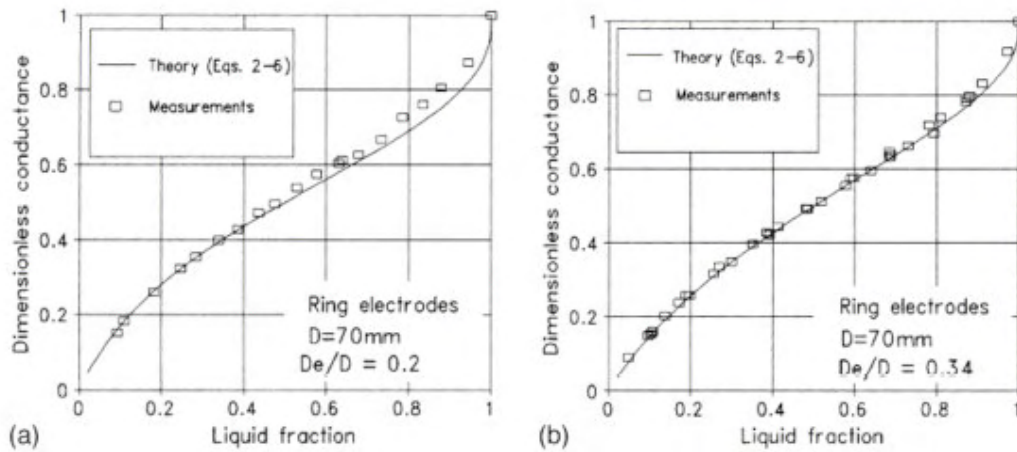
Fig. 72: Measured and theoretical dimensionless conductance for two different electrode spacing, ring electrodes under stratified flow conditions, Fossa (1998)

The same analysis was conducted on the data obtained from section A, under bubbly flow regime, for void fraction from 0.74 to 1. Maxwell (1882) equation corresponds almost perfectly with the data obtained from the two electrodes positioned 24 mm apart, while the data from the 14 mm spaced electrodes shown a worse agreement (see Fig. 73).
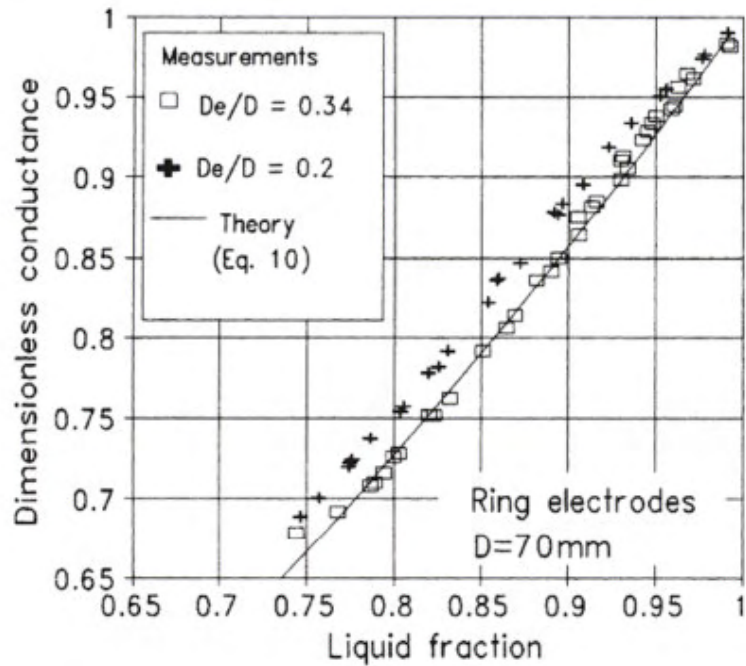
Fig. 73: Measured and theoretical dimensionless conductance for two different electrode spacing, ring electrodes under bubbly flow conditions. De indicates the distance between the electrodes, Fossa (1998)

The response under annular flow conditions was evaluated using both section A and B. Section A presents results that follows the predicted trends with a maximum error of 10%. The theory can take in account differences in the electrodes spacing. Section B (ring electrodes) is analyzed under the same condition and shows a scatter of the measured data of 15% with respect to the theoretical values.
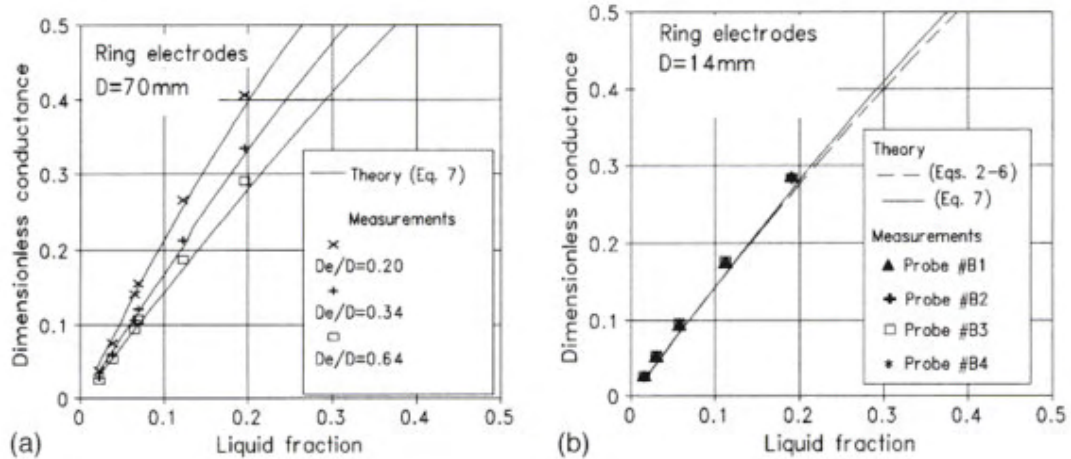
Fig. 74: Measured and theoretical dimensionless conductance for two probe geometries: (a) ring electrodes D=70 mm, (b) ring electrodes D=14 mm. De indicates the distance between the electrodes, annular flow, Fossa (1998).

This validates the procedure of introducing the adequate ratio (higher) between De (ring electrode spacing) and D (pipe diameter) to describe properly the influence of the distance between the plates in the theoretical analysis. No analytic formulas are available for the investigation of the behaviour of plate electrodes, so just a comparison with the response from ring electrodes was performed; the plate electrodes show a great sensitivity to the changes in liquid fraction and are frequently affected by the presence of surface pollutants (e.g. air bubbles), so calibration is strictly recommended before a set of measurements.

Effect of fluid flow temperature variation on the void fraction meters response

In gas–liquid flows through test loops, the fluid temperature increases, causing a change in the dielectric properties, mainly of the liquid component, which interferes with the response of capacitive void fraction meters. This phenomenon causes, for example, deviations of about 4% in the meter response for each 10 °C variation of temperature in the air–water flow.

Therefore, if the capacitive device is calibrated at a given temperature and the flow temperature changes during operation in the field, an error is introduced in the two-phase void fraction measurement.

Emerson dos Reis, Goldstein (2005) proposed a corrective technique to take in account this behaviour.

During the calibration stage, when the fluids temperature is constant and equal to *To*, a polynomial function *α(To)* = *f (Vo)*, called the calibration function, where *α(To)* is the flow void fraction and *Vo* is the electric voltage level on the transducer output with fluids at *To*, is determined by fitting the calibration data points. However, when the fluid temperature is *T*, different from the calibration temperature *To*, the output voltage *V* is different from *Vo* and, if *V* is applied directly in the calibration curve, a void fraction value with a bias error, *α(T)*, is obtained. As a consequence, it becomes necessary to correct from *V* to *Vo* before the calibration function can be properly applied.

If the capacitance transducer circuit has no baseline drift, its output voltage *V* is a function only of the capacitance *C*, which depends on the effective dielectric permittivity of the media among the electrodes, *εm* (quantity and local distribution of each component: gas, liquid, pipe material among the electrodes),which, in turn, depends on the system geometrical configuration and on the system conditions, such as its temperature. For a given flow configuration, the effective permittivity becomes a function only of the flow temperature. Consequently, the capacitance *C* and the output transducer voltage *V* are also functions only of the flow temperature *T*.

$$\frac{dV}{dT} = \frac{dV\left(\varepsilon_m(T)\right)}{dT}$$

Yang et al. (1994) observed that the response of the capacitance transducer circuit, *V* = *V(C)*, was basically linear, with a coefficient of correlation about 0.9999. A linear dependence was also found for the relation between the capacitance and the dielectric permittivity (D. Halliday (1997)), so d*V*/d*εm* can be assumed constant, then integrating:

$$V_0 = V - \alpha\left[\varepsilon_m(T) - \varepsilon_m(T_0)\right]$$

Where

$$\frac{dV}{d\varepsilon_m} = \alpha$$

The effective dielectric permittivity, $\varepsilon_m(T)$, is related basically to the volumetric concentration of each component, liquid and gas, and the pipe material has a minimal influence if the electrodes are mounted flush on the internal pipe wall. In this case the authors assumed:

$$\varepsilon_m(T) = \varepsilon_g(T)\alpha(T_0) + \varepsilon_l(T)\left[1 - \alpha(T_0)\right]$$

$$\varepsilon_m(T) \cong \varepsilon_l(T)\left[1 - \alpha(T_0)\right]$$

Because the little variation of the gas permittivity and because $\varepsilon_l \sim 80\,\varepsilon_g$.

Substituting:

$Vo = V - a[1 - \alpha(To)][\,\varepsilon_L(T) - \varepsilon_L(To)]$.

This equation can be solved iteratively for Vo using, for example, the Newton–Raphson method, knowing the calibration curve $\alpha(To) = f(Vo)$, and the value of a, obtained experimentally.

The relative dielectric permittivity of water as a function of temperature is calculated from empirical equations available in the literature:

$\varepsilon_L(T) = A\,\exp(BT)$

where

$A = 87.8149$

$B = -0.004558951$

which, according to the authors, is valid from 0 to 100 °C, with differences smaller than 0.1% relative the experimental data for pure water.

This analysis does not take into account the effect of the spatial distribution of the materials on the effective electrodes capacitance, which can be a major effect.

High temperature materials for impedance probes

At the Oak Ridge National Laboratory (Eads (1978)), a number of different materials have been tested in air and water to establish design requirements for both the film and impedance probes, for high-temperature experiments.

The results of several tests during the development of high-temperature materials have shown varying degrees of possibilities. However, a material has not been

identified that will withstand the severe thermal transients of 300°C/sec without cracking after a minimum of quenching tests.

Moorhead and Morgan, in this document, explain that the electrical insulation used in the film and impedance probes must be able to withstand exposure to hot steam , 950°C, and severe thermal transients, 300°C/sec in the PKL facility. Commonly used ceramic materials such as aluminum oxide and beryllium oxide will survive the hot steam but cannot withstand the thermal shock. Materials such as quartz, diamond, and boron nitride may survive the shock but are subject to some dissolving or leaching in hot water.

Several ceramic systems have been found which are impervious to thermal shock and appear able to survive in the hot steam.

The thermal shock requirement means that the ceramic must have a very low (near zero) coefficient of thermal expansion or sufficient strength to withstand the thermal-gradient-induced stress. The adequacy of thermal shock resistance of candidate ceramics was tested by quenching from high temperature in water. Although higher temperatures were used initially, it was concluded that quenching from 500°C in to hot water would provide a sufficiently rigorous test.

The approximate rate of cooling, determined by attaching a thermocouple to the specimen and recording the temperature with a digital transient recorder, was around 600°C /sec. The effect of thermal shock was evaluated on the basis of the appearance of microscopically visible cracks. Dye penetrant tests were not used since many of the ceramics tested were porous.

Materials evaluated include alumina and beryllia pieces for comparison.

The tests include pieces from three ceramic systems that have very low thermal expansion: Cordierite , Al_2O_3 , MgO, SiO_2,Rosolite, Li_2O and Ta_2WO_8 and Hf-Ta_2WO_8 .

A special type of cermet prepared by hot-pressing Al_2O_3 powder with small metal globules on the particle surfaces was tested. The globules were deposited in situ. Samples of these and other ceramics were subjected to a series of ten quenchings; the results and conditions are described in Tab. 10.

Several of the specimens (hot-pressed Ta2WOe, Hf-Ta_2WO_8, Cordierite, Rosolite, Al_2O_3-Fe and Al_2O_3-Pt cermets, and quartz) had no cracks, while the Si_3N_4 had only small cracks at the periphery. The quartz may not be usable since it is soluble in high-temperature water and the Al_2O_3-Fe slowly oxidizes. Other specimens are

being tested in a stream of high-temperature, superheated steam; preliminary results indicate a very slow etching. The authors highlight that some materials that are unaffected by steam may be vulnerable to hot water leaching.

The evaluation results indicate that many of the materials in Tab. 10 would be satisfactory. The only problem is that the materials that survived the thermal shock tests are slightly porous and will absorb a certain amount of water, thus changing the electrical properties.

Preliminary measurements have indicated that the effect of these changes on the overall instrument performance can be held to a tolerable level by using appropriate electrical measurement circuits.

Material	Coefficient of thermal expansion ($\Delta l/l \times 10^{-6}$/K)	Density (% of theoretical)	Results of thermal shock tests[a]
Aluminum oxide[b]	6.5	99+	Microscopic cracks visible after 1 quench
Beryllium oxide	8	99+	Microscopic cracks visible after 1 quench
Beryllium oxide	8	80+	Cracks visible after 2 or 3 quenches
Cordierite (Alsimag 701) $2MgO, 2Al_2O_3, 5SiO_2$	3.3	99	Cracks visible after 2 or 3 quenches
Cordierite (Alsimag 447)	1.5	85+	No cracks after 30 quenches
Rosolite ($Al_2O_3, 4SiO_2, 9Li_2O$)	<1	80	No cracks after 30 quenches
Rosolite	<1	99	Microscopic cracks visible after 2 quenches
$Al_2O_3 - 5\%$ Fe	7	85	No cracks after 10 quenches
$Al_2O_3 - 1\%$ Pt	6.5	85	No cracks after 10 quenches
$Al_2O_3 - 1\%$ Pt	6.5	99	Cracks appeared after 3 quenches
Ta_2WO_8	−2.1	90+	No cracks after 10 quenches
$Hf-Ta_2WO_8$	0	60	No cracks after 10 quenches
Si_3N_4	2.8	90+	Small cracks near edge after 10th quench
Quartz	19	100	No cracks after 10 quenches
MACOR (Corning glass ceramic)	9.4	100	Broke into pieces after second quench

[a] Quenching from 500°C (932°F) into hot water.

[b] Several types of Al_2O_3 were tested (including sapphire); all cracked.

Tab. 10: Material tested for thermal shocks (Moorhead and Morgan (1978)

Impedance probes works

The impedance method proposed by Ma et al. (1991) and Wang et al. (1991) measured the area-averaged void fraction using copper electrodes flushed with a 32 mm diameter acrylic tube.

In this impedance method, the performance of the probe was found to be very sensitive to the void fraction and flow pattern. This shortcoming can be partially alleviated by using a small probe. Andreussi et al.(1988) showed that the theory developed by Maxwell and Bruggman for dispersed flow can be adapted to describe the electrical behaviour of their ring-electrode design. In the development of impedance sensor design, ORNL/NUREG-65 report presented two Pt-30%-Rh probes to measure the void fraction. However, because of the probe shape, only the line-averaged void fraction could be obtained from the impedance of the water–vapor mixture.

Ma et al. (1991) described two methods of measuring void fraction. An impedance probe was connected to a signal processing circuit which gave a linearized output with a fast response:

When the void fraction measured by this arrangement was compared with that deduced from fast closing valves, the results agreed to within 20%. They also deduced void fractions below 0.8 to within 20% by measuring the static pressure in a vertical test section and assuming that the total pressure drop was dominated by it. Wang et al. (1991) report on the use of this impedance probe to determine flow pattern transitions for air and water in vertical 50.8 mm diameter tubes

Costigan and Whalley (1996) developed and tested a design of conductivity based void fraction meter (see Fig. 75) and they found to be accurate to within +0.1 over the whole range of void fraction. Two of these meters have been used together to record dynamic void fractions at 108 data points (covering water superficial velocities from 0 to 1.0 m/s and air superficial velocities from 0.05 to 37 m/s in a 32 mm diameter tube). Cross-correlation of the void meter signals has provided statistical data on slug and bubble lengths and void fractions whit good results.
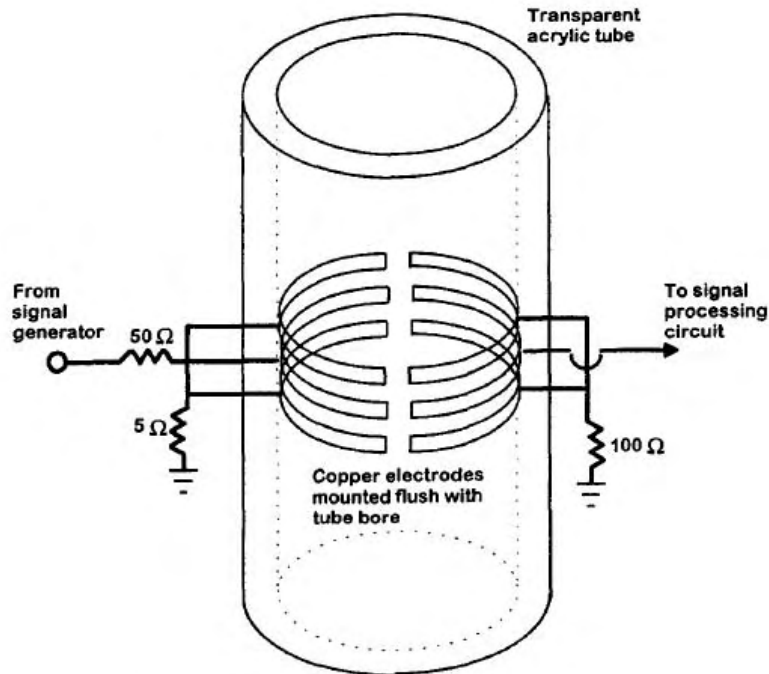
Fig. 75: Void fraction conductivity probe arrangement (G. COSTIGAN and P. B. WHALLEY (1996))

Hardy (1982) describes two different types of experiments conducted in the Slab Core Test Facility (SCTF) and in the Cylindrical Core Test Facility (CCTF):

•   Installation of a drag disk-string probe combination in different locations of the STCF in order to monitor the void fraction trend during the last phases of the blowdown and the refill and reflood phases of a LOCA. Two measurement sites were foreseen in the lower part of the downcomer to monitor the inlet and outlet mass flux (measurement of the vertical flow); one measurement site was installed in the upper part to detect the bypass from the intact cold leg to the broken cold leg (measurement of the horizontal flow). The string probe consisted of a stainless steel frame with two stainless steel wires strung to form eight pairs of electrodes across the frame. The wires were isolated from the frame by cermet. The electrical impedance across the electrodes was measured and its signal converted in an output voltage. Using water-only and air-only calibration points and the magnitude and phase of the impedance signal, the capacitative portion of the impedance can be determined. One of the available models to reconstruct the void fraction of the mixture is to connect linearly the variation in the capacitance with the variation in the void fraction. The same type of string probe was used by Hardy and Hylton (1983).

169

- A string probe of the same type, and a turbine flow-meter were installed at a vent valve location in the CCTF in order to monitor the mass flow rate passing through the valve. The combination of the two instruments measured only the 7% of the total volumetric flow (covering only the 7% of the cross section area), so to calculate the total mass flow rate the measured flow has to be multiplied by a suitable factor; assuming that the flow is well homogenized.
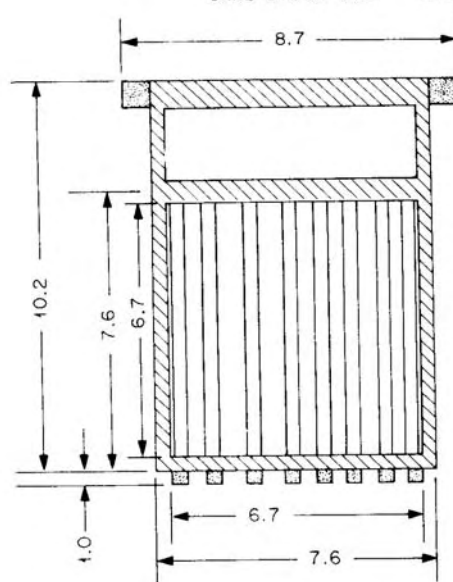

Fig. 76: SCTF downcomer probe

The drag disk-string probe combination was calibrated for both air only flow or water only flow, in a velocity range of, respectively, 2.6- 31.0 m/s and 0.095-0.85 m/s, respectively.

The same combination was then calibrated for two phase flow measurements. Two correlations were required to fit the data obtained from the calibration facilities. The most important parameter to choose one correlation over the other is the flow pattern: the transition from droplet mist to froth flow seems to dictate different responses from the drag disk-string probe device. Other effects are also probable, such as the flow disturbances and variation in the slip ratio (see Fig. 77).
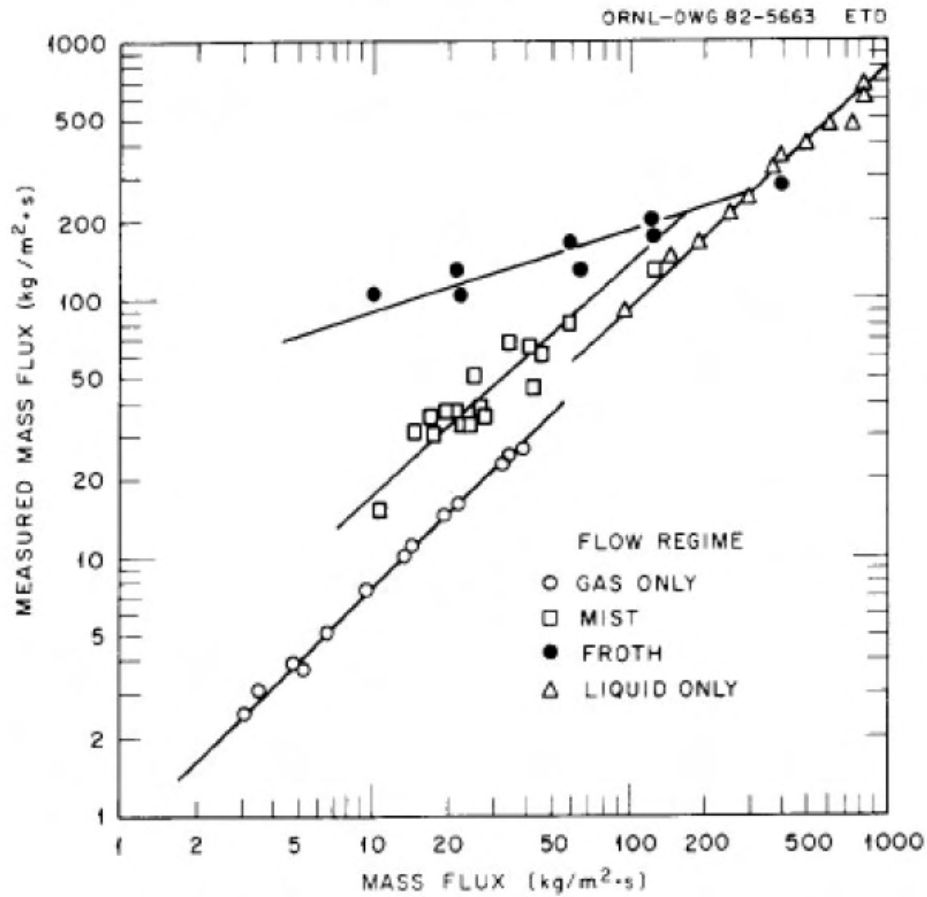
Fig. 77: Drag disk and string probe data vs actual the mass flow rates for both single phase and two-phase flow (Hardy (1982))

The correlations evaluate the actual mass flux to within +40% and - 30% for 85% of the data. The selection of the right correlation depends on the location of the sensor in the downcomer and on the flow regime (see Fig. 77).
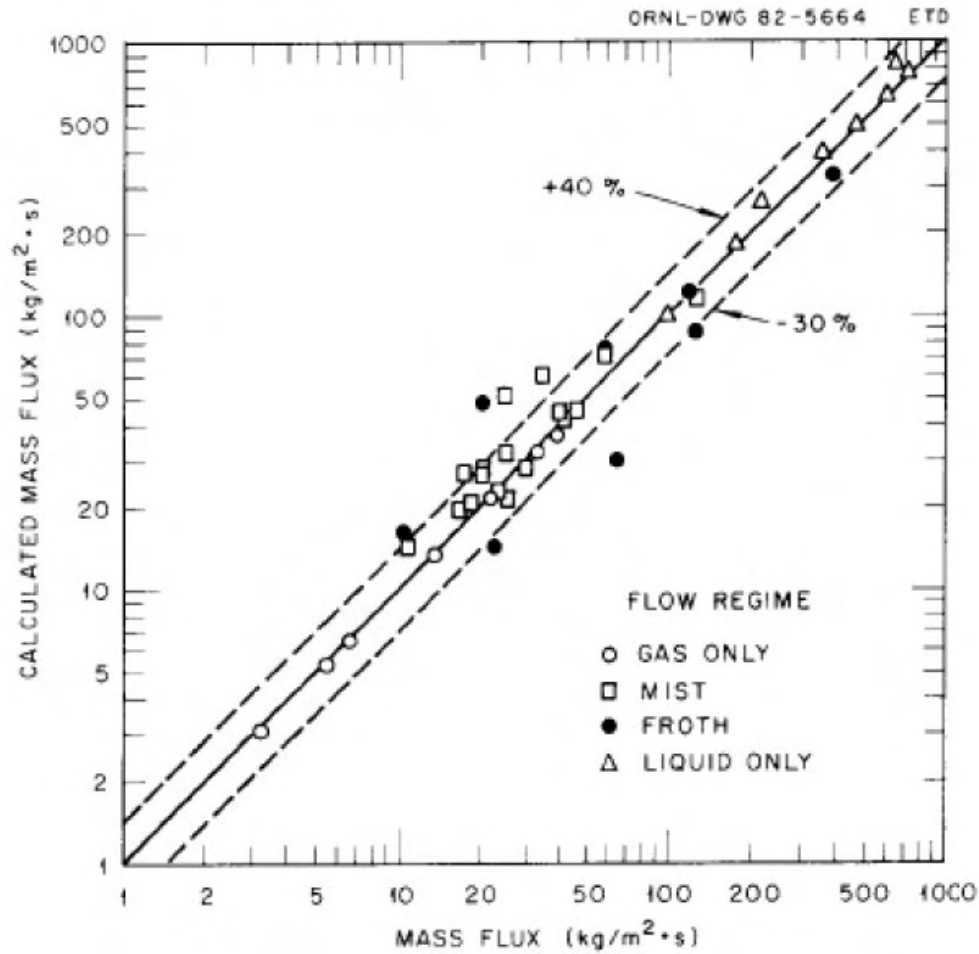
Fig. 78 : Comparison between the mass flux calculated with the calibration correlations and the actual mass flux for both single and two-phase flow (Hardy (1982))

The comparison between the values from the string probe and those from the gamma densitometer show a good agreement for $0.4 < \beta < 0.85 \ (0.15 < \alpha < 0.6)$.

For liquid fraction $\beta < 0.4 \ (\alpha > 0.6)$ the string probe underestimates the results from the gamma densitometer; then the two values seem to converge again, and finally diverge for $\beta < 0.01 \ (\alpha > 0.99)$ (see Fig. 79).

For condition of $\beta > 0.4 \ (\alpha < 0.6)$ the flow is slug or bubble: in both cases the bubbles distribution is almost homogeneous, and the values from the gamma densitometer and the string probe correspond fairly well. For liquid fraction $\beta < 0.4$ and $\beta > 0.1 - 0.2$ the flow regimes are froth or annular and both tend to collect a film of water close to the pipe wall. The three beam gamma densitometer

172

averages the entire cross section, where the string probe is more influenced by the high void fraction central region. For $\beta \sim 0.01-0.02$ $(\alpha \sim 0.98 - 0.99)$ the annular-mist flow regime occurs and the film on the wall is no more continuous, resulting in a more uniform distribution of voids. Finally the limit of the sensitivity of the three beam gamma densitometer is reached near $\beta \sim 0.01$ $(\alpha \sim 0.99)$ and below that value a scatter in the data is evident.
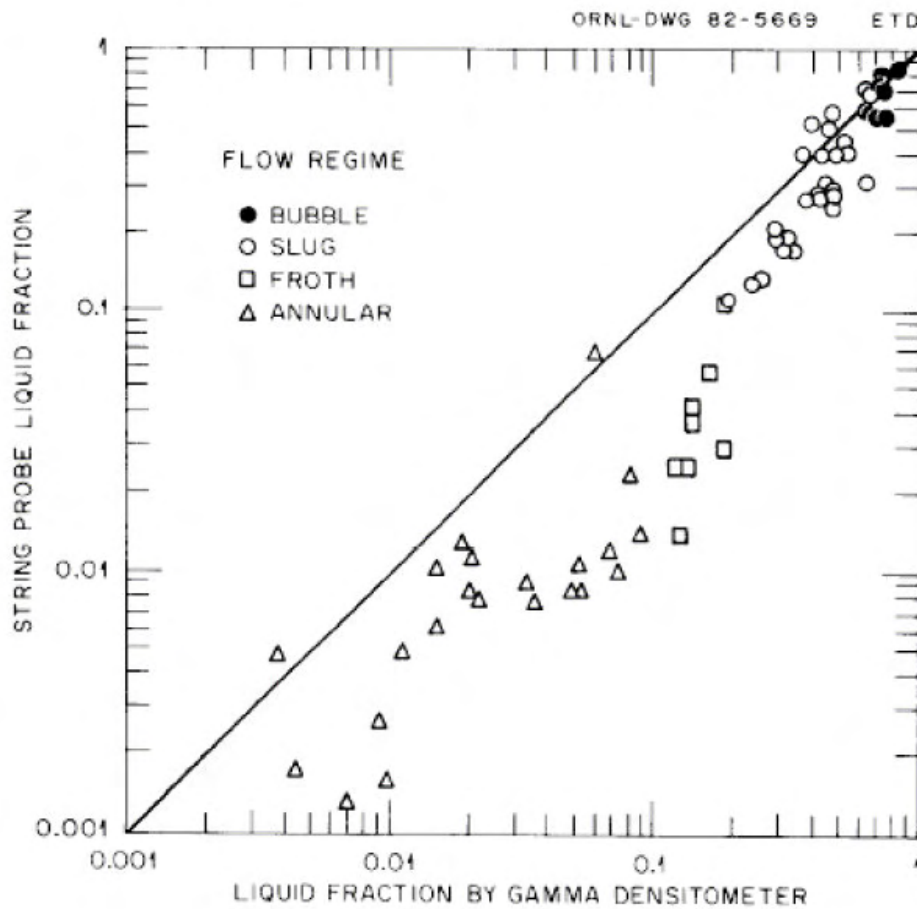

Fig. 79: Comparison of liquid fraction from string probe and three beam gamma densitometer (Hardy (1982))

In order to obtain a value for the mass flow, the homogeneous model was adopted. Two curves were fitted to the data (Fig. 80), above and below a break point equivalent to 5.0 kg/s for the mass flow rate:

173

- For the mass flow points >5 kg/s nearly all the data fell within ±30% of the calculated curve.
- For the mass flow points <5 kg/s the scatter was remarkable and only two thirds of the data fell within ±30% of the calculated curve.
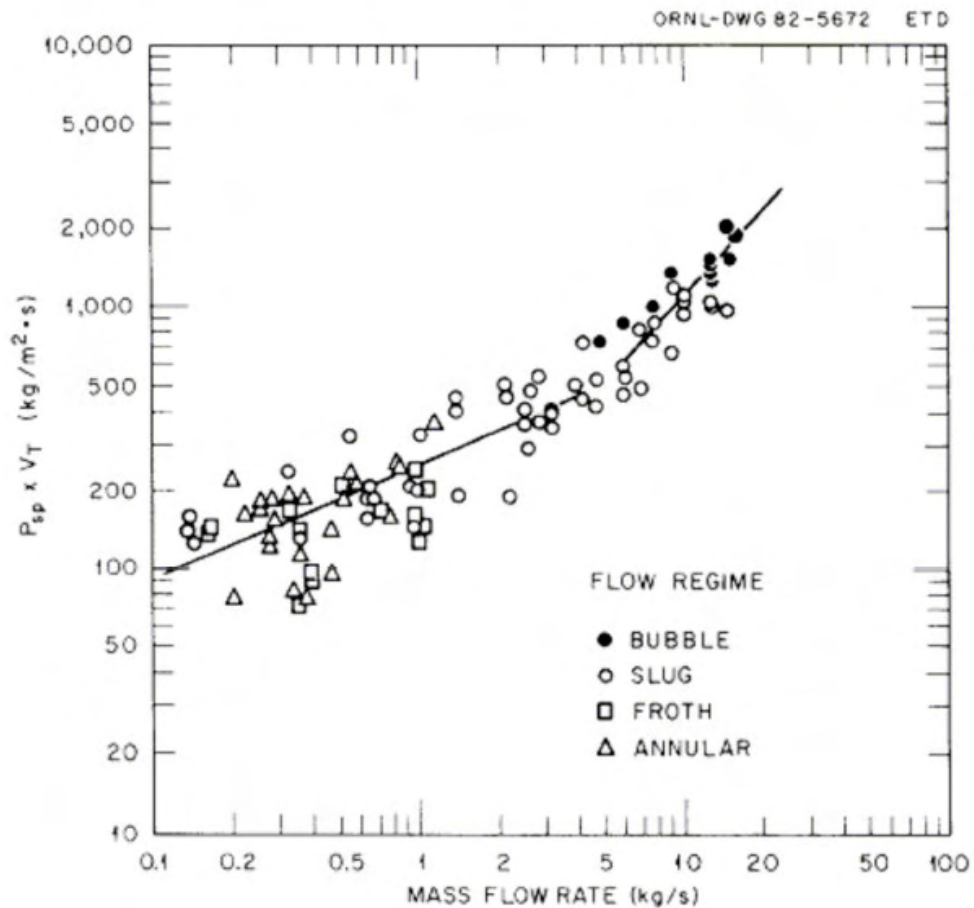
Fig. 80: Actual mass flow rate compared with the mass flow rate calculated with the homogeneous model (Hardy (1982))

These two calibration equations were used to convert all the measurements obtained from the turbine flow-meter/string probe combination into the mass flow rate (see Fig. 80).

For mass flows > 2 kg/s, 80% of the data fell within ±30% of actual mass flow rate.

Below 2 kg/s, considerable scatter appear: the data fell within ±70% of the actual flow rate.

174

In 1983 Hardy and Hylton used a double-layer string probes for measure void fraction and velocity.

The probe consisted in a pair of steel wires (electrodes) strung back and forth across a rectangular stainless steel frame. There were two electrodes layers to allow the measurement of the velocity. They were characterized by an axial spacing of 1.90 cm and an electrode to electrode spacing of 0.25 cm . Two wires were strung per layer, creating a pair of electrodes. The wires were electrically insulated from the frame by a cermet (ceramic-metal material).
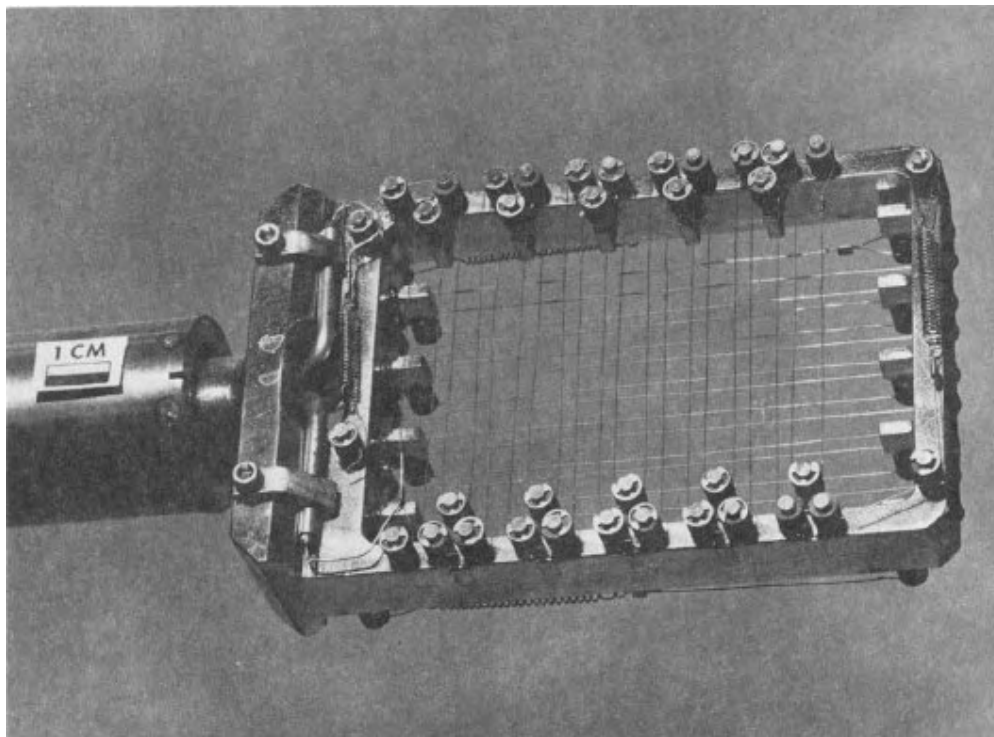
Fig. 81: String probe used by Hardy et all. (1983)

The probe was designed and fabricated to operate under severe thermohydraulic conditions: temperature up to 350ºC and thermal transient of 300ºC/s; and it was tested in three different loops:

• A test rig that operated at pressure up to 10 bar and temperature up to 170ºC with a wide range of steam and water flow rates.

• A full scale vertical section of an upper plenum to measure void fraction in air-water mixtures (temperature and pressure range is not available).

• A steam-water circuit that operated in the pressure range 2-7 bar (the temperature range is not available).

Concerning the *void fraction measurements*, the values obtained from the string probe positioned in the first experimental facility were compared with the measurements of a three beam gamma densitometer (that had an accuracy of ±5% of reading). The data from both the upper and the lower level of the probe agreed quite well with the densitometer measurement. The string probe void fraction slightly over-predicted the densitometer in the range from $\alpha = 0.5$ to $\alpha = 0.95$ (up to 0.1 at $\alpha_{\gamma\,dens} = 0.58$, up to 0.3 at $\alpha_{\gamma\,dens} = 0.86$) (See Fig. 82).
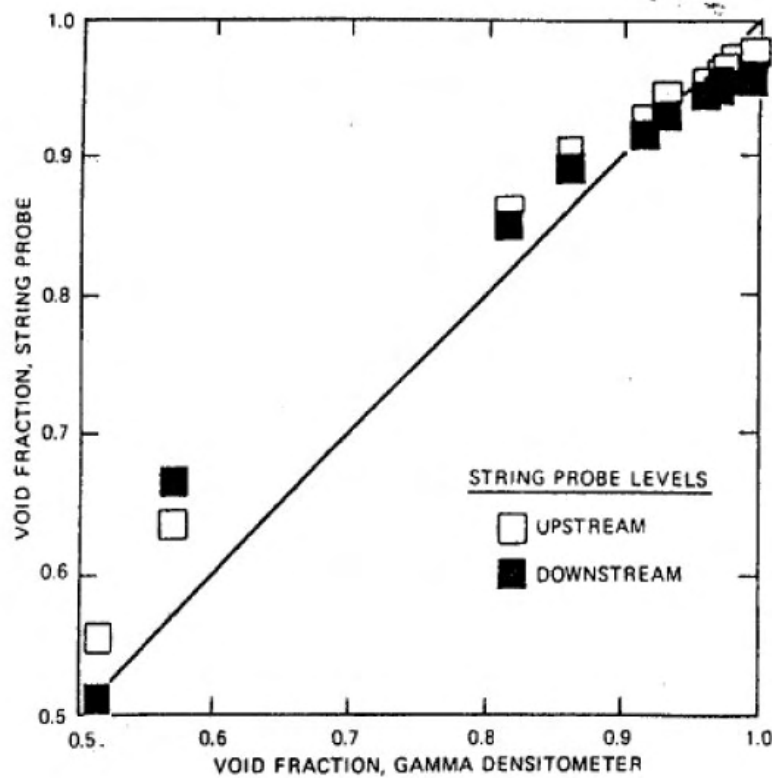
Fig. 82: Void fraction comparison for string probe and three beams gamma densitometer (both level of sensor presented), Hardy and Hylton (1983)

The probe was also tested in the second experimental facility and the obtained data were compared with the values from a gamma densitometer. There was a good agreement for α between 0.70 and 0.98. The string probe consistently measured a higher void fraction with respect to the gamma densitometer because of its position in the facility. The probe inspected the central part of the upper

plenum (where the void fraction was higher), while the densitometer gave an average of the void fraction from the vessel centerline to the wall, assuring a value more coherent with the real situation (water tended to collect on the side surfaces). Finally the probe was inserted in the last experimental device. The data was collected for a series of different pressure values (from 210 to 690 kPa) and for a wide range of liquid fraction $(0.0015 < \beta < 0.75)$, void fraction $0.25 < \alpha < 0.9995$.

For the *velocity measurements* the values obtained from the probe placed in the first experimental facility were compared to the ones measured by a turbine meter. The turbines are more sensitive to the gas phase velocity at high void fractions and to the liquid velocity at low void fractions, at intermediate void fractions some theories have been studied, but none of them is widely accepted.

The string probe measures a gas phase velocity in low void fraction and a liquid phase velocity in high void fraction. The comparison between the values sensed by the string probe and the turbine flow-meter is therefore difficult. For low values of velocity (slug flow) what is monitored by each instrument is not clear, but as the velocity increases (dispersed flow), the agreement becomes quite good because the string sensor is monitoring the droplets velocity and the turbine is sensing mainly the gas velocity, but the flow is almost homogenized and so the slip ratio approaches 1.

The values from the string probe were also compared against the results from a separate-flow model; at velocity below 6 m/s the probe is measuring a gas phase velocity that is greater than the real velocity of the two phase mixture, but for velocities above 6 m/s the agreement is quite good.

Other observations based on the analysis of the string probe velocity measurements confirm the theory that the string is approaching the turbine flow meter values at high and low velocities because the slip ratio in both cases is almost 1 (see Fig. 83).
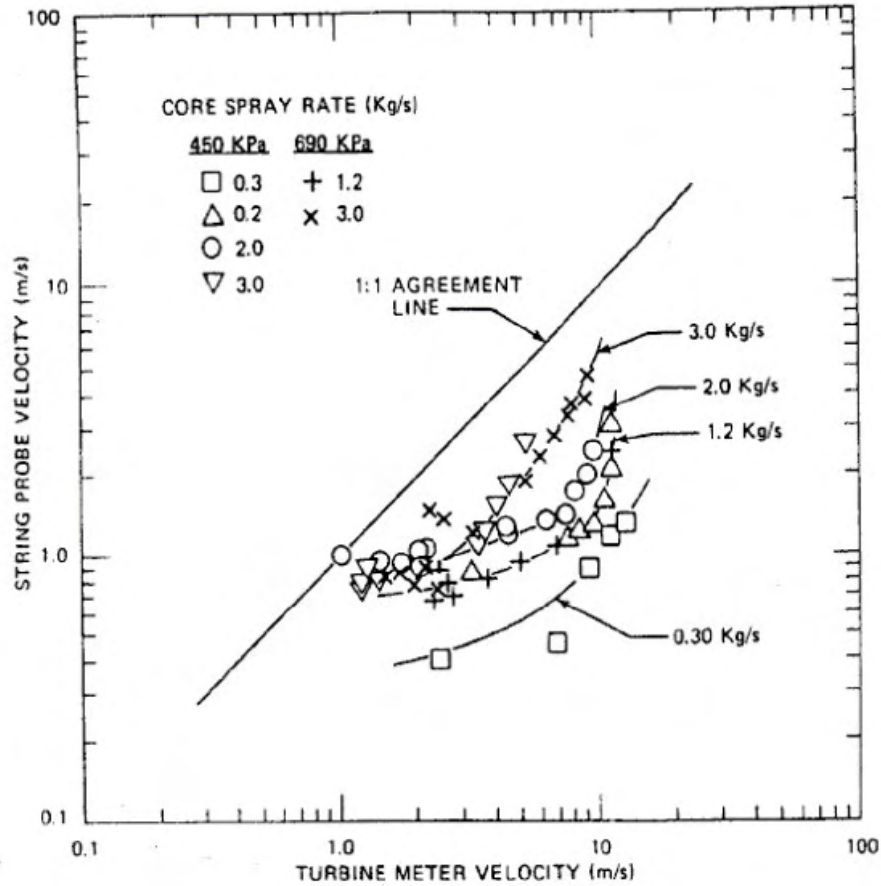
Fig. 83: Velocity comparison of the string probe and turbine meter (Hardy and Hylton (1983))

The probe tends to monitor vapour phenomena at low void fractions and liquid phenomena at high void fraction. It is able to measure a large range of flow velocities (1-17 m/s) and void fraction (0.25-0.99), with a good repeatability.

The probes were also used to detect the velocity of the two phase mixture, using a technique of analysis of random signal from two spatially separated impedance probes. The flow disturbances can be sensed at the two locations with a time delay τ. If the Fourier transform of the two signals is calculated, the transfer function between the signals will be simply a linear curve in the plane (frequency-phase). The slope of the curve will correspond to the dominant time delay. The velocity of the perturbation will be:

$V=D/\tau$,

where D is the separation distance between the probes. This type of measurements can detect the velocity of the disturbance source, but this does not always

178

correspond to the velocity of one phase. In pure bubble flow the method will measure an average bubble velocity (so the velocity of the gas

phase), in droplet flow an average droplet velocity will be detected, but in slug or froth flow the gas-liquid interface velocity are not necessarily the phase velocities. In annular-mist flow both the velocities of droplets and waves will be detected. A good knowledge of the existing flow pattern is therefore necessary to interpret correctly the results obtained with the velocity measurements.

With its highly deformable interface, gas/liquid flow is difficult to describe and thence model. It is more and more desirable to get instantaneous phase distributions with a high resolution in space and time.

The most ambitious goal is a resolution that allows us to identify individual gas bubbles and to determine their parameters (shape, volume, diameter etc.). For this purpose, the spatial resolution must be in the range of the dimensions of the lowest bubble fraction to be detected and the measuring volume must be well defined.

Another important dilemma encountered in multiphase flow measurements is that probes or instruments should be placed outside the flow domain so as not to disturb the flow itself; however, phase distributions cannot easily be measured from the boundary, as described above.

Concerning the impedance probes, it is clear that, one of the most important drawbacks of these sensors is the strong sensitivity to the flow pattern.

To solve these problems, in the last year tomographic image reconstruction using the impedance probes has been developed. In this way impedance probes are able to measure phases distributions inside the measured volume.

Two different technology are studied:

- Electrical tomography (capacitance and resistance)
- Wire Mesh sensor (capacitance and conductance)

Using these instruments is possible to know, at the same time the flow pattern and the void fraction value; obviously each technology offers certain vantage but also drawback or limitations.

Electrical tomography (ET) is a non-intrusive technique which can be used for imaging and velocity measurement in flows of mixtures of 2 non-conducting materials.

Developments over the last 15 years have made fast, accurate measurement systems available for laboratory research. Using ET can offer measurements unobtainable with other measurement technologies, but the interpretation of quantitative flow data requires a good physical model of the interaction of the materials with the electric field in the sensor and appropriate reconstruction and analysis algorithms.

With the wire-mesh sensor, which was first proposed for high-speed liquid flow measurements by Prasser et al(1998) there is a hybrid solution in between invasive local measurement of phase fraction and tomographic cross-sectional imaging, allowing the investigation of multiphase flows with high spatial and temporal resolution. The meter causes a fragmentation of the bubbles, but this effect is not sensed by the sensor, since it measures the undisturbed upstream flow structure (Prasser (2006)).

Wire-mesh sensors

Principle

The sensor is essentially a mesh of wire or bar electrodes (as in string probes descrived above), one plane of electrodes being the current emitter electrodes and another plane arranged orthogonal to the emitter plane being the current receiver electrodes. Between the emitter and receiver electrodes there is a gap of a few millimeters distance where conductivity is measured in the crossing points of the electrodes.
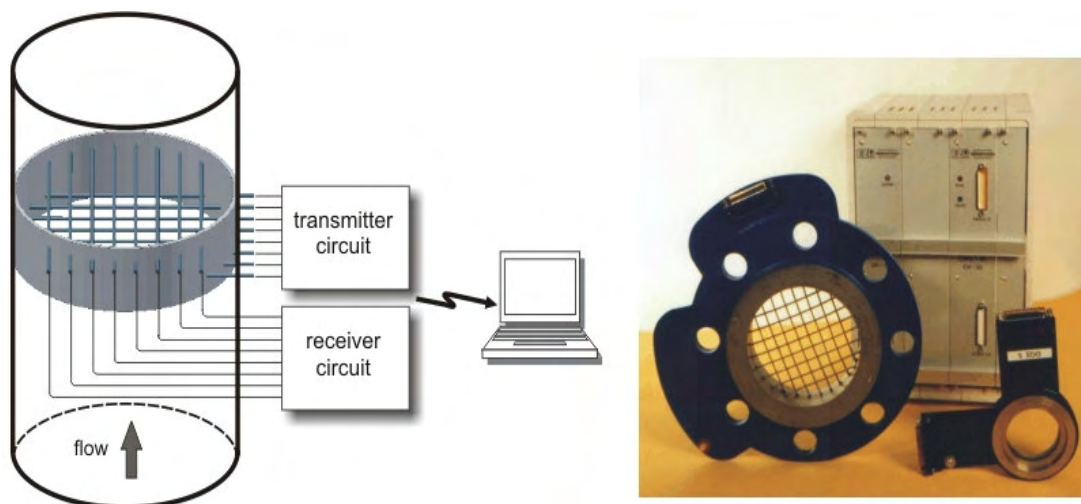

Fig. 84: (left) Principle of wire-mesh sensor having 2 x 8 electrodes. (right) Wire-mesh sensor for the investigation of pipe flows and associated electronics.

The transmitter electrodes are sequentially activated while all receiver electrodes are parallel sampled, in such a way, that an electrical property (conductivity or permittivity) of the fluid in each crossing point is evaluated. Based on those measurements the sensor is thus able to determine instantaneous fluid distribution across the cross-section, for instance, of a pipe. The following pictures show the three-dimensional representation of a slug flow and the results of the visualization of different flow regimes of a air-water vertical flow.
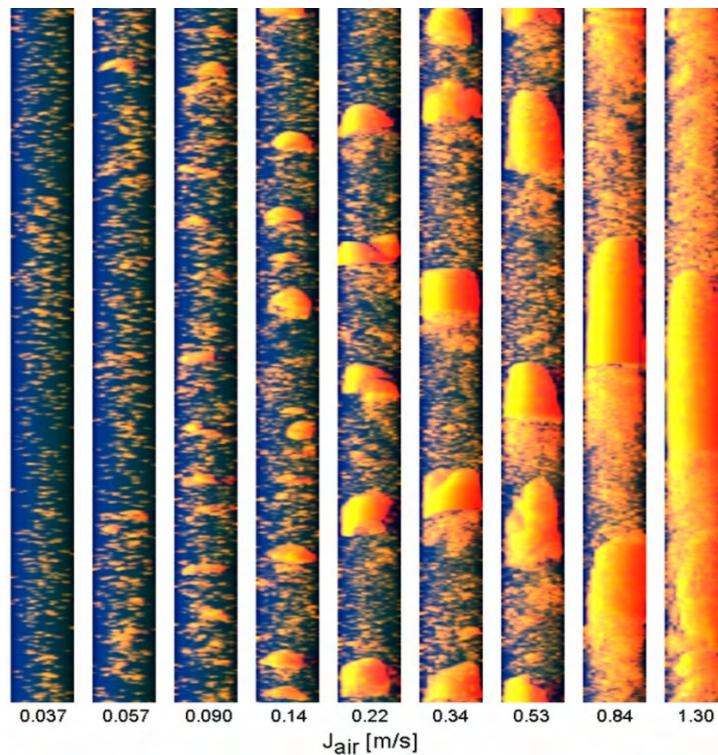
Fig. 85: 3D-Visualization of data acquired with a wire-mesh sensor in a vertical test section of air-water flow at the TOPFLOW test facility.

Data processing

The data of a wire-mesh sensor consists of a time sequence of digitally codes conductivity values for each mesh point. The first step of data processing is the determination of absolute conductivity values or alternatively an assignment of the relative conductivity values to the corresponding phase that is present in the flow. As a result it obtained the conductivity or phase distribution within the measurement plane at a contiguous sequence of temporal sampling points - thus a three-dimensional data volume.

The wire-mesh sensors can provide very detailed information about the distribution of the liquid and gas phase in two phase flow. Many flow parameters, such as gas volume

fraction or bubble size distribution, are encoded in these data but must be extracted with appropriate processing algorithms (see Prasser (1998) and Prasser (2001).

From data of gas-water two-phase flows it is possible to compute axial and radial gas fraction profiles and the integral gas fraction by proper integration of the gas fraction over certain cross-section areas.

For the determination of gas bubble size distributions from the raw data special data analysis algorithms were developed that can identify single bubbles by means of a filling algorithm and compute volume and equivalent bubble diameters accordingly. Further, it is possible to measure the velocity distribution of the gas phase by placement of two wire-mesh sensors with a small axial spacing in the flow. Since the conductivity distribution reaches the second sensor with only minor spatial structure modifications with a time shift that is determined by the flow velocity after having passed the first sensor, we can obtain the local velocity values within the measurement cross-section from a computational cross-correlation analysis of the two sensor signal.

Types of sensors

Wire-mesh sensors can be manufactured depending on application requirements in diversity of different cross-section geometry and operating parameters. Newest wire-mesh sensors can be employed in a environmental conditions range of up to 286 °C and 7 MPa (Pietruske and Prasser (2007)). Associated electronics for signal generation and data acquisition achieves a maximum temporal resolution of 10,000 Hz for the 16 x 16 wire mesh design and 2500 Hz for the 64 x 64 wire mesh design.

Conductivity wire-mesh sensors have been successfully employed in the investigation of two-phase flows in the past. Since the measuring principle requires at least one continuous conductive phase, wire-mesh sensors have almost exclusively been used for the investigation of air-water or steam-water systems. The field of application of conductivity wire-mesh sensors is, limited by the fact that at least one flow phase must have an electrical conductivity of $\kappa > 0.5$ μS/cm. For this reason the principle of the wire-mesh sensor was extended to applications with non-conducting fluids.

The main idea of the conductivity wire-mesh sensor has been maintained. One plane of wires is used as transmitter. The other one is used as receiver. During the measuring cycle, the transmitter wires are activated in a successive order while all

other wires are kept at ground potential. For each time slice a transmitter wire is activated, the receiver wires are sampled in parallel. However, while in the conductivity wire-mesh sensor a bipolar excitation voltage and a DC measuring scheme is employed, for the capacitance measurement is used an AC excitation and measuring scheme. Therefore a sinusoidally alternating voltage is employed for excitation and the receiver circuit must encompass a demodulator. For the capacitance measurement of the crossing points is employed an AC based capacitance measuring method, which is typical for many types of capacitance measuring circuits and has also been successfully used in electrical capacitance tomography.

A different number of sensor has been tested by Prasser's research group:

- 8x8

- 16x16

- 24x24

- 64x 64

The probe was presented with two different designs by Prasser et al. (1998):

 - Wire mesh sensor with 16 x 16 measuring points; 0.12 mm diameter wires.

 - Lentil shaped rods sensor with 8 x 8 measuring points or 16 x 16 measuring points.

The first design is characterized by 96% of free cross section for one grid; the pressure drop coefficient K is about 0.04 (single grid). The second design has a 73% of free cross section for one grid and the pressure drop coefficient K is around 0.2 (single grid). The pressure drop (single phase flow) is then calculated as:

$\Delta p = K \rho v^2$,

where ρ is the density and v is the velocity. In water flow with v $1m/s$ the pressure drop would be 40 Pa for the wire mesh design and 200 Pa for the lentil shaped rods design (Prasser et al. (1998)).

Prasser et al. (2002) tested a couple of 24 x 24 probes to sense the gas phase velocity distribution in a 50 mm diameter pipe. The two sensors were positioned with an axial distance of 37 mm. The visualization of the distribution of the air velocity inside the pipe was obtained.

The measurement of the liquid phase velocity could be feasible, but it has not been tested yet. It can be measured with the cross correlation technique if there are conductivity fluctuations in the liquid phase conductivity (Prasser (2008)). These fluctuations could be caused by changes in the liquid temperature. Prasser stated that the liquid velocity measurement can be much more unreliable than the gas velocity measurement, but it can help increasing the information about the flow (Prasser (2006)). Schleicher suggested adding a liquid tracer to cause a detectable modification in the liquid conductivity (Schleicher (2008)).

The experiment (Prasser et al. (2002)) with the measurement of the gas phase velocity was performed in the superficial gas phase velocity, J_{air}, range from 0.037 m/s to 0.835 m/s, while the liquid phase velocity J_{water} was kept constant at 1.02 m/s. The probe has been used for the measurement of the void fraction distribution in the J_{air} range from 0 to 12 m/s and in the J_{water} range from 0 to 4 m/s (Prasser et al. (2002)).

The cross correlation technique allows for the detection of the reverse flow condition for the measurement both of the gas and the liquid velocity (Prasser (2008)).

Schleicher underlines that the detection of bi-directional flow is not a common use of the cross correlation technique (Schleicher (2008)).

Calibration

The linear dependence between the void fraction and the conductivity of the mixture needs for the knowledge of two limit values: the conductivity as measured with the pipe filled with liquid only and the conductivity measured with the pipe filled with gas only. The liquid conductivity is dependent on the temperature and the temperature is varying during the transient experiment. It is therefore necessary to calibrate the instrument in order to take into account the changes in this limit value. Prasser (Prasser (2008)) suggests two ways to proceed:

• It is possible to perform a calibration of the sensor reading for a completely filled pipe as a function of the water temperature. A fast thermocouple mounted close to the sensor is then necessary to provide the correction of the limit value.

This method was implemented in some experiments at the CIRCUS facility in Delft. If there are periods when the pipe is filled completely, then the

measurements performed during these periods can be easily recognized and used for an online correction/adaptation of the calibration values.

• If there is a two-phase flow permanently present at each crossing point of the sensor, short-term PDFs (probability density functions) of the measured raw data can reveal the signal levels for liquid and gas without an explicit calibration.

The position of the maxima in the PDF can be used as calibration values.

The meter has been used for the detection of the mixture void fraction in the flow pattern range from bubble to annular flow (Prasser et al. (2002)). The meter is capable of detecting the presence of bubbles whose dimensions are bigger than the wire pitch. The wire mesh probes tested had a wire pitch that ranged from 2 mm to 3 mm; the diameter of the pipe ranged from a minimum of 42 mm to a maximum of 195 mm (Prasser et al. (1998), Prasser et al. (2000), Prasser et al. (2002), Prasser et al. (2005), Pietruske and Prasser (2007)).

A mesh sensor is very intrusive and would interfere with packing of a packed column and the column itself may also compromise / damage the sensor. Any reactions or flow observed after the sensor would also be altered by its intrusive nature, particularly, the separation effect of the mesh layer to the packed bed .

Not suitable for flow with small bubbles if the grid length is bigger than the bubble dimension.

Not suitable for fluid containing any particles (the mesh is very fragile and has the risk of sensor damage).

Electrical Impedance Tomography

Principle

The impedance measurements are taken from a multi-electrode sensor (typically 8 or 12; see Fig. 86) surrounding a process vessel or pipeline.

The working principle consists of injecting electrical current between a pair of electrodes and measuring the potential differences between the remaining electrode pairs. This procedure is repeated for all the other electrode pairs until a full rotation of the electrical field is completed to form a set of measurements.

Each dataset is interpreted by image reconstruction algorithms to compute a cross-sectional image corresponding to the electrical conductivity inside the sensor. The concentration of each phase can be computed based on the knowledge of the electrical conductivity of each phase, yielding the concentration tomogram.

The advantage of EIT lays in its excellent time resolution arising from the very fast measurements of electrical resistances.

The drawback of EIT resides in the relatively low spatial resolution, reported as being between 3 and 10% of the sensor diameter. In fact, electrical tomography is considered as a soft-field technique since the image is based on measurements at the periphery of the sensor and the image reconstruction involves resolution of a mathematically challenging inverse problem (Giguère et all. (2008).
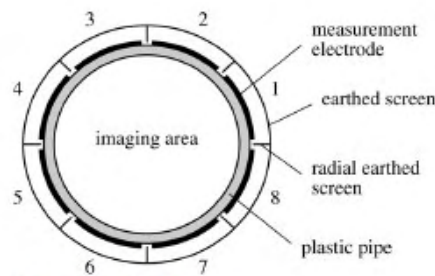

Fig. 86: EIT electrode configuration

Hung et all. (2008) (Gigère et all (2008)) used eight electrodes along the circumference of the tube to obtain a tomographic image of the two-phases.

The electrical capacitance tomography technique was also implemented recently by Gamio et all. (Gigère et all (2008)) to image various two-phase gas-oil horizontal flows in a pressurized pipeline. They emphasized the potential of this technique for real-time flow visualization and flow regime identification in practical industrial application at high pressure operating conditions.

Electrical Impedance Tomography (EIT) is also introduced in a recent patent by Wang (2006 and 2007) as a new signal processing method. The method is used on-line to obtain accurate estimates of the local disperse phase volumetric flow rate, the mean disperse and continuous phase volume fractions and the distributions of the local axial, radial and angular velocity components of the disperse phase.
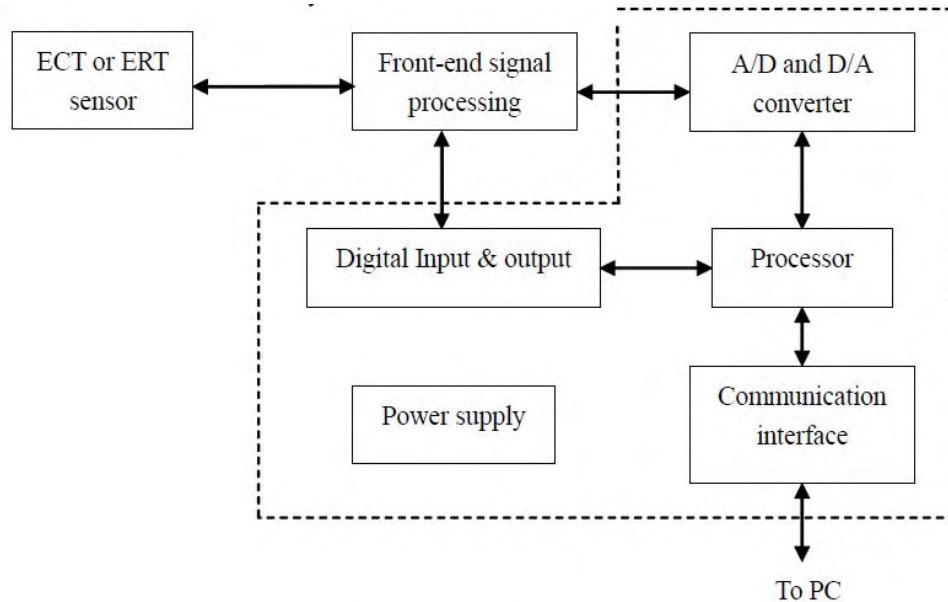

Fig. 87: Block diagram of ECT or ERT system

ECT and ERT's Characteristics and Image Reconstruction

ECT electrodes are normally mounted outside of a pipe or vessel. In this case, the ECT sensor is both non-intrusive and non-invasive, which is a preferred option in industrial applications. The ECT has been used to measure two-phase flows of materials with different permittivity values, such as gas-oil and gas-solids. The measurements are presented as a series of capacitance data.

In contrast, the ERT is non-intrusive but invasive.

In this case, the electrodes are mounted flush with the inside surface of a pipe (or vessel) wall and directly in contact with the fluids.

The operation of ERT systems is basically the same as ECT systems except that a high-impedance measurement frontend is needed for conductive loads. Forward and inverse problems for both modalities have many similar features.
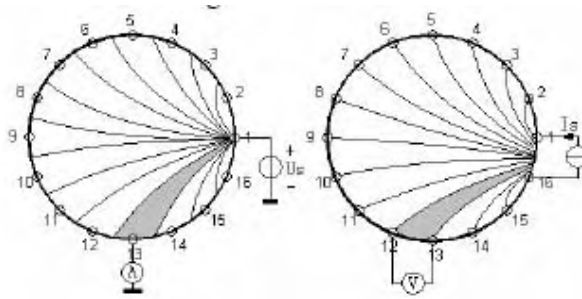

Fig. 88: Measuring principles of ECT (left) and ERT (right)

Cui and Wang (2009) noted that the ERT sensor is not a good choice for monitoring multi-phase flows in a horizontal pipe. This is because the ERT uses a sine-wave constant current as an excitation signal. The resulting voltage at current source end will be saturated to a square-wave when the excitation electrodes are covered by materials of low conductivity, e.g. gas, as shown in Fig. 89. Therefore, the acquired measurements become invalid and cannot be used for image reconstruction.

In Fig. 89, when the excitation signals are applied to electrode pairs of (1-2), (2-3), (3-4), (4-5), (5-6), (6-7), (7-8) and (8-9), the voltage at the excitation electrode will be saturated to a square-wave. Therefore, the reconstructed images with the measurements are no longer valid.
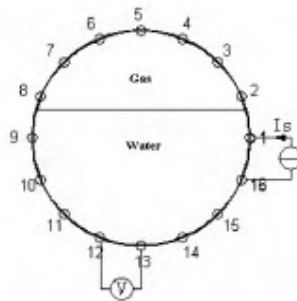

Fig. 89: ERT for water-gas flow (Cui and Wang (2009))

On the other hand, the ECT employs bipolar measurement methods and a voltage source. As the excitation signal is voltage, saturations will not occur if excitation electrodes are covered by non-conductive materials. Therefore, the ECT sensor remains valid and can provide images for flow regime identification and gas holdup computation.

The authors note that with the lower number of electrodes (8) in each plane for both ECT and ERT operations, the spatial resolutions are low for both modes. The system is hence unable to distinguish small bubbles in the flow. Increasing the number of electrodes in the system can help improve the spatial resolution at a certain degree.

However, the high data acquisition rate of electrical tomography can provide a relatively high temporal resolution compared to other tomography modalities.

Lemonnier (1997) analysed ERT algorithms and reported different studies; Andersen and Bernsten (1988), for example, have show that there is no sensitivity of the EIT to the conductivity at the center of the domain, the reconstructed conductivity is sensitive to noise, and the quality of the reconstruction deteriorates dramatically with the increase in the special resolution.

Lemmonier (1997) said that there is no potential in EIT for measuring phase velocities because the correlation techniques provides either wave velocities or interface velocities that almost always differ from material velocities. Moreover he said that because this methods require controlled operating conditions are very difficult to use outside laboratories. This opinion it's contrasting with other studies.

Wu and Wang (3rd WC of industrial Process Tomography) described the experiments carried out using the multiphase flow loop made of transparent glass at Institute of Particle Science and Engineering at University of Leeds, which is a 12 m gas-liquid flow loop with an inner diameter of 50mm, using a ERT sensor, to measure void fraction and the fluid velocity using the cross correlation technique.

The flow loop can run a maximum superficial liquid velocity of 1 m/s with Reynolds number about

58,500, and a superficial gas velocity larger than 30 m/s with Reynolds number above 100,000.

Measurements were performed at ambient temperature. By controlling the air flowrate at the air inlet, different flow patterns was generated in the flow loop.

The authors used the so-called adjacent electrode pair strategy (Brown, 1985), using a 10mA injection current at 9.6 kHz for flow regime recognition, and a 50mA current at 38.4 kHz for cross-correlation calculation. Data collection rates were 23.04 frames per second at the signal frequency of 9.6 kHz and 28.3 frames per second at the signal frequency of 38.4 kHz. Both single-plane and dual-plane ERT sensors were used in this study. Each ERT sensing plane consisted of 16 titanium-alloy rectangular electrodes (5mm×12mm).

The principle of the dual-plane strategy is based on a 'cross measurement between two correlated electrodes on two sensing planes' instead of 'plane by plane' measurement. SBP (sensitivity coefficient weighted back-projection) algorithm was used for online flow pattern recognition due to its fast image reconstruction speed. An off-line multi-step algorithm, known as SCG algorithm (the sensitivity theorem based inverse solution using generalised conjugate gradients methods with a method of error vector decomposition) (Wang, 2002), was utilized for the image reconstruction in the velocity implementation in order to reduce the error caused by the pointspread function in the use of the SBP algorithm. The SCG algorithm employs a multi-step approach with the sensitivity theorem based linear approximation and the differences between the relative changes in the measured and simulated boundary voltages at each step to solve the non-linear electric field inverse problem.

In this context they found:

First, the ERT technique is a suitable means for detecting the flow patterns of gas-liquid multiphase

flow in a vertical pipe. With a fast data collecting protocol and an effective iterative image

reconstruction algorithm, gas-phase and liquid-phase distribution and their dynamic variations in the pipe can be clearly quantified (Fig. 90).
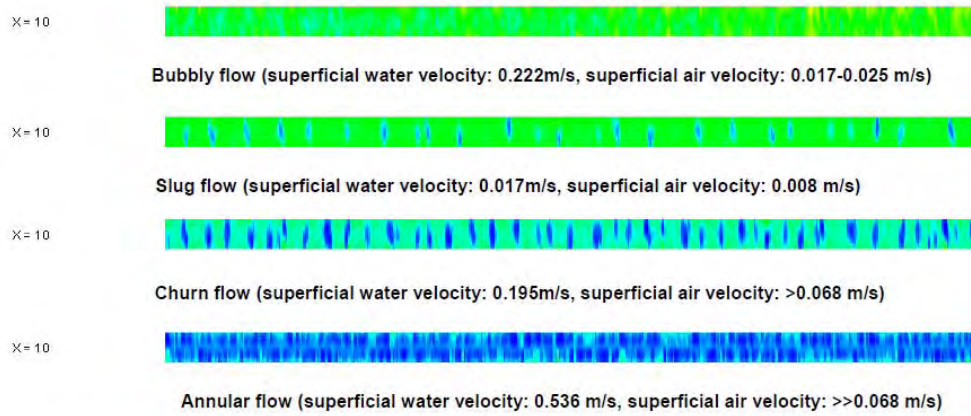
Fig. 90: Flow Pattern recognition (Wu and Wang)

Secondly, the time of cross-correlation can reveal the velocity magnitude of the interface of the gas phase and liquid-phase. The cross-correlation time interval of bubbly flow is longer than that of churn flow, and much longer than that of annular flow (Fig. 91). Based on the time interval (ERT data frames), the mean velocity of gas-liquid two-phase can be estimated. This may be important in the on-situ monitor of industrial processes.
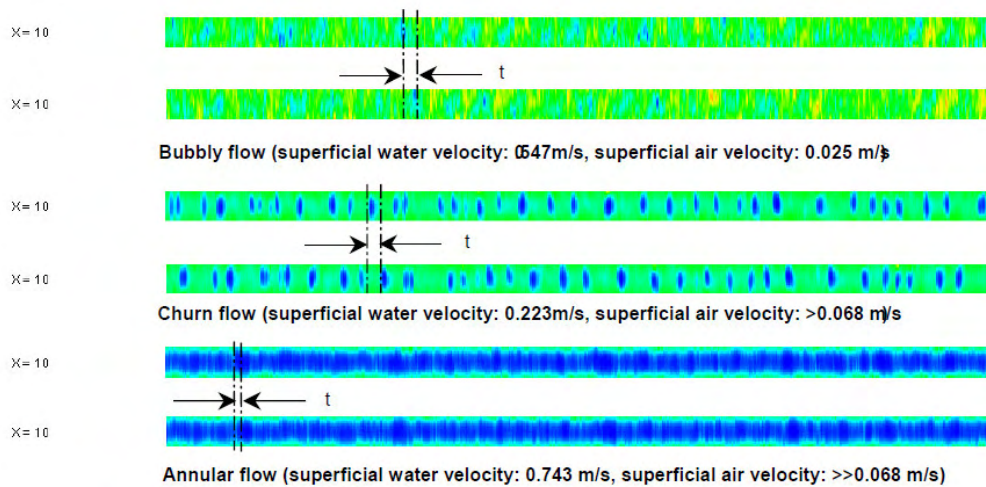

Fig. 91: Cross-correlation between two image obtained with dual-plane ERT sensor (Wu and Wang)

Thirdly, we can see that as gravity acts in the axial direction giving symmetry across the pipe cross-section.

Flow patterns tend to be somewhat more stable, but with slug and churn flows, oscillations and bubble roll in the flow can occur to destroy the symmetry. The degree of the cross-correlation of the flow state is good for bubbly flow and annular flow, but not so good for churn flow (Fig. 92). This can also be proven during the cross-correlation procedure. In a bubbly or an annular flow, the cross-correlation graphics can be obtained almost on every pixel, but only partially for churn flows.


(a) Bubbly flow (superficial water velocity: 0.141 m/s, superficial air velocity: <0.008 m/s)

(b) Churn flow (superficial water velocity: 0.419 m/s, superficial air velocity: >0.068 m/s)

(c) Churn-annular flow (superficial water velocity: 0.463 m/s, superficial air velocity: >>0.068 m/s)
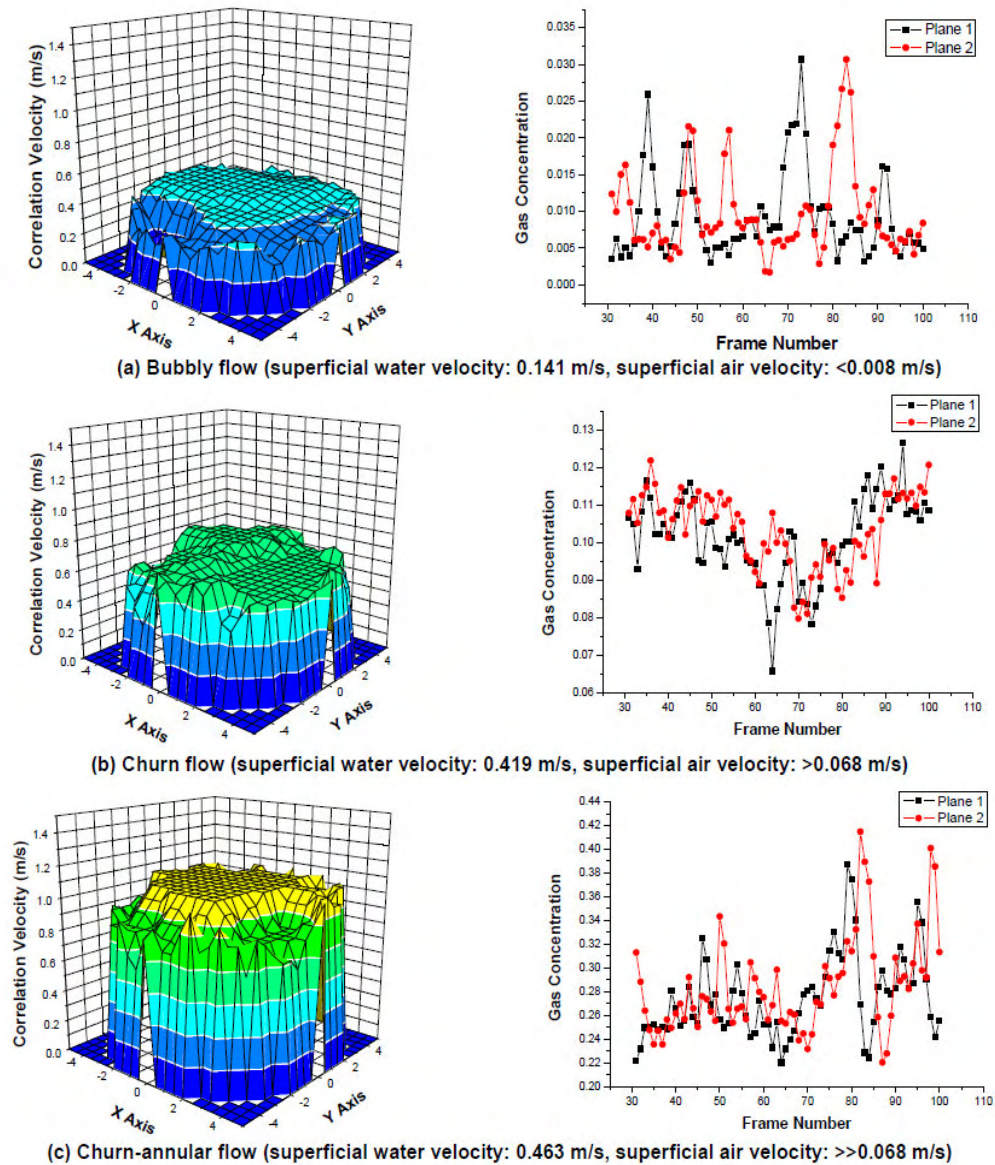
Fig. 92: Correlation local velocity distribution and mean cross-section gas concentration at different flow pattern. (Wu and Wang)

Fourthly, the velocity on the central part of the pipe is larger than that on the edge of the pipe at any flow pattern. For a churn flow (Fig. 92.b), large air bubbles rise upwards asymmetrically, which causes the distribution of velocities on a section of the flow loop also to be asymmetrical. While for a bubbly flow or an annular flow, it is almost symmetrical. As the amount of gas is increased the coalescence of smaller air bubbles forming larger bubbles gradually concentrates on the core of the pipe to transit to an annular flow at the end of the pipe. Lastly, for a churn flow or an annular flow, as the velocity is relatively high, the sampling frequency should be high, otherwise large errors will arise in the measured data. More noise points occur on the edge of the pipe with increasing gas content. For obtaining accurate value of flow parameters, much more care should be taken both on ERT hardware and software improvement, such as increasing the sampling frequency, reducing noise influence, developing better correlation algorithm to describe the three-dimensional velocity distribution of the flow field.

The most efforts concerning the EIT technology are concentred in the development of the computer algorithms used for reconstructing phase volume fraction profiles.

Knowing the phase distribution, the problem of finding the electrical potential and potential differences V between electrode pairs for a given current injection is called the *forward problem* and it is denoted:

$$V = F\left(\sigma \text{ or } \varepsilon\right)$$

where F is defined as the forward operator.

Finite element methods (FEM) are widely used to solve the forward problem in electrical tomography. Nowadays, many FEM implementations are available for this well-known Poisson equation problem necessitating a simple inversion of a linear system.

In the case of EIT, it provides an approximation of the potential differences for a given conductivity/capacitance distribution, denoted:

$$V_{\text{FEM}} = F_{\text{FEM}}(\sigma \text{ or } \varepsilon)$$

where F_{FEM} is called the FEM forward operator. The distribution is generally defined as a constant per element in the mesh, each discrete value corresponding to a pixel of the image.

Another forward operator can be derived from the linearization of the above equation. The change in voltage differences $V + \Delta V$ in response to a perturbation of distribution can be expressed by the Taylor expansion:

$$\Delta V = \frac{\partial F}{\partial (\sigma \text{ or } \varepsilon)} \Delta (\sigma \text{ or } \varepsilon) + \text{O}\left(\left(\Delta (\sigma \text{ or } \varepsilon) \right)^2 \right)$$

Neglecting the higher order terms, the equation is simplified to the linear form:

$$\Delta V = s \Delta (\sigma \text{ or } \varepsilon)$$

where $s = \dfrac{\partial F}{\partial (\sigma \text{ or } \varepsilon)}$ is the Jacobian matrix, also referred to in literature as the sensitivity matrix.

Finding the conductivity/capacitance distribution based on the voltages measurements V_M is called the *inverse problem* of EIT.

$$(\sigma \text{ or } \varepsilon) = F^{-1}(V)$$

In general, direct analytical solution for the inverse problem does not exist since F is a non-linear operator with more unknown values than known voltage measurements. In that context, only approximations of F^{-1} or S^{-1} can be found by numerical techniques, representing both challenges and limitations for EIT imaging.

Approximations of S^{-1} are commonly derived using an optimisation method by computing a conductivity distribution, which minimises the difference between the measured voltages and the simulated voltages.

Many reviews about electrical tomography image reconstruction techniques are available in the literature (Polydorides (2002), Yang (2003), Wang (2002), Isaksen (1996))

The choice of the approximation of S^{-1} leads to different image reconstruction algorithms summarized in Table 2.

The simplest choice is to use the transpose of S, which corresponds to the linear back projection (LBP) and Landweber method. The Newton–Raphson method (NRM) appears to be very sensitive to the noise in the raw measurements because of ill-conditioned Hessian matrix (Polydorides (2002), Yang (2003), Su et all.

(2000), Zhao et all. (2002), Lu et all (2005), Tibirna et all. (2006)). Therefore, a modified Newton–Raphson method (MNRM), which includes a regularization property, is commonly preferred. Depending on the choice of regularization matrix, the Tikhonov method or the Levenburg–Marquardt method can be obtained. In general, a large value of the regularization parameter λ tends to attenuate the presence of noise in data, but also reduces the precision of the reconstructed image (Yang (2003)). Thus, the choice of the regularization parameter λ is seen as a compromise between the noise level and the desired precision of the solution.

Single-value decomposition (SVD) can be used to solve the inverse problem but it is very sensitive to the noise as well, even in presence of very small singular values. Truncated single-value decomposition (TSVD) can alleviate the problem by filtering the singular values. With the MNRM and TSVD methods, some regularization parameters must be fitted as a function of the noise level, mostly by a trial-and-error method. The preconditioned conjugate gradient method can also be used to solve the inverse problem of EIT.

Approximations of S^{-1} in GIA

Algorithms	$\hat{S}^{-1}$
LBP/Landweber	S^{T}
Newton–Raphson	$(SS^{\mathrm{T}})^{-1}S^{\mathrm{T}}$
Tikhonov	$(SS^{\mathrm{T}}+\lambda I)^{-1}S^{\mathrm{T}}$
Levenburg–Marquardt	$(SS^{\mathrm{T}}+\lambda W)^{-1}$

Tab. 11: Numerical method for image reconstruction (Giguère et all. (2008))

George et all. (1998) have tested the EIT in a number of experiments with solid-liquid and gas-liquid flows and the results are compared with gamma-densitometry tomography (GDT).
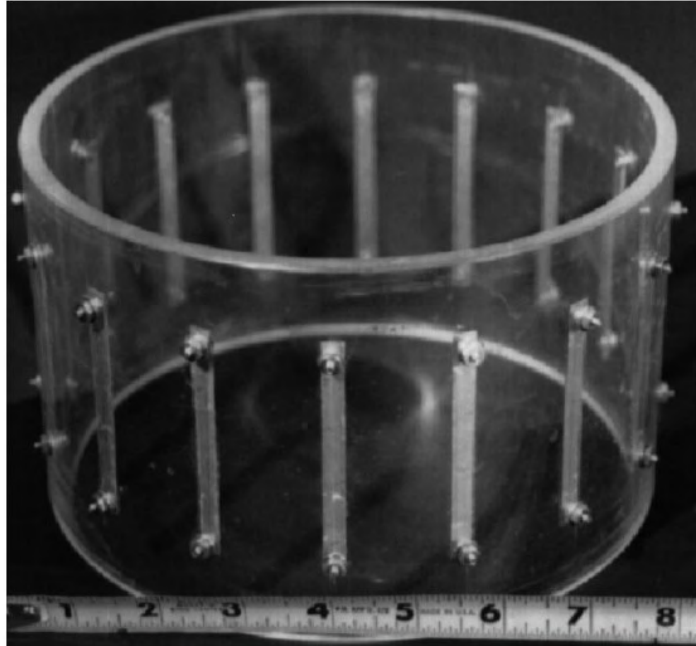
Fig. 93: EIT strip electrode array. The bottom scale is in inch (George et all (1998)

The reconstruction algorithm used in their experiments has been described in detail by Torczynski et al. (1996, 1997) and is based on the YWT method described by Yorkey et al. (1987). This method is summarized in Fig. 94.
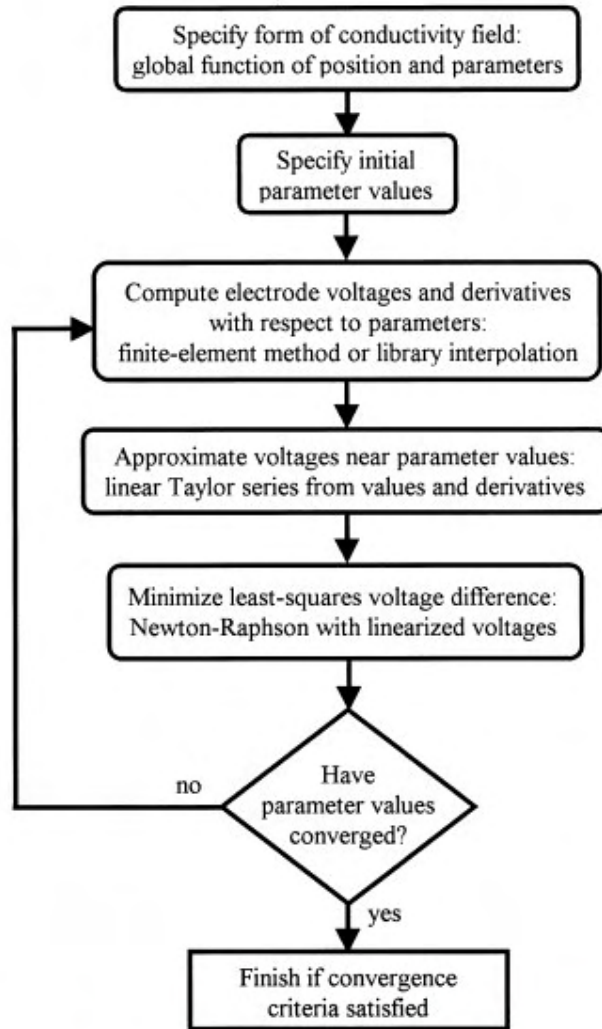
Fig. 94: Flow chart of EIT reconstruction algorithm (George et all. (1998))

In the solid-liquid flows, the average solid volume fractions measured by EIT are in good agreement with nominal values. In the gas± liquid flows, average gas volume fractions and radial gas volume fraction profiles from GDT and EIT are also in good agreement.

EIT was used to measure solid volume fractions of up to 0.05, with excellent agreement between EIT results and the nominal values determined from the mass of solids in each flow.

Gas-liquid bubble-column flows were measured with EIT and GDT; for cross-sectionally- averaged gas volume fractions up to 0.15, the average values and radial profiles from EIT and GDT agreed to within 0.01, despite large radial variations across the column. The Maxwell-Hewitt relations used to convert

197

conductivity information to conducting phase distributions were found to be accurate for cases where the assumptions inherent in their derivation were valid.
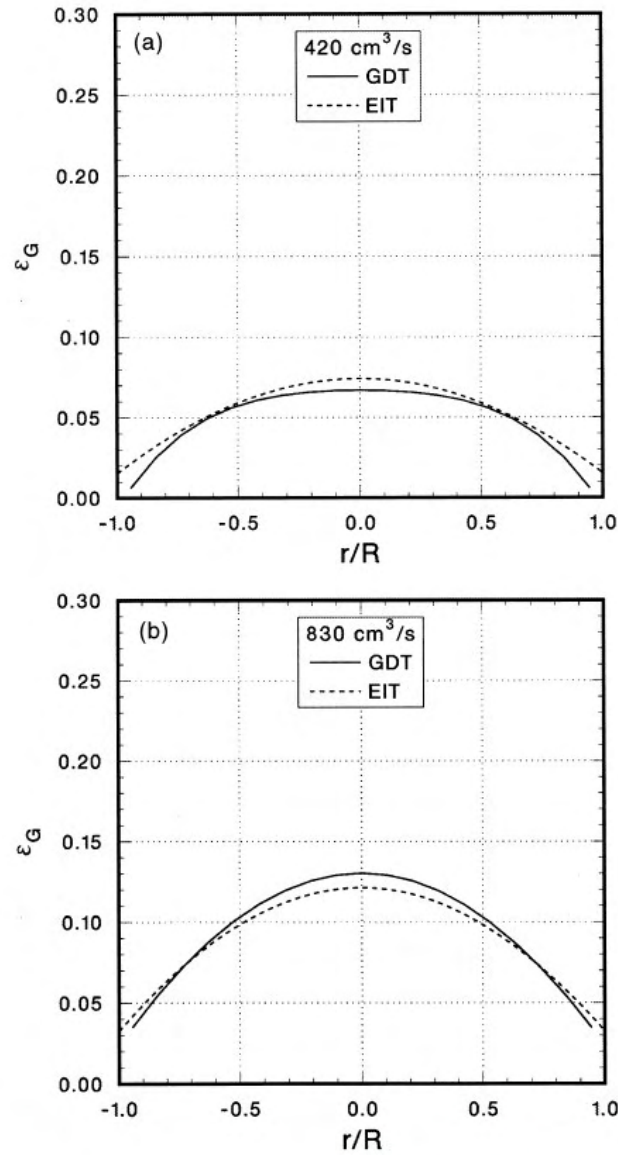

Fig. 95: Comparison of symmetric radial gas volume fraction profile from GDT and EIT (George et all. (1999))

A more complex reconstruction algorithm, based on a modified Hopfeld dynamic neural network optimization technique, has been developed by Warsito and Fan (2001). This algorithm is used to reconstruct the tomographic data to obtain the cross-sectional distribution of the gas holdup. The real-time flow structure and bubbles flow behavior in the two- and three-phase systems are discussed along with the effects of the gas velocity and the solid particles.

The authors have developed a new reconstruction algorithm based on an analog neural network multi-criteria optimization image reconstruction technique (NN-MOIRT) for imaging two-phase as well as three-phase flows using electrical capacitance tomography.

The reconstruction technique is a combination of multi-criteria optimization image reconstruction technique for linear tomography and the LBP technique.

The multi-criteria objective functions used are:

(a) the entropy function, (b) the least-weighted square error between the measured capacitance data set and the estimated capacitance from the reconstructed image, and (c) a smoothness function that gives a relatively small peakedness in the reconstructed image. The multi-criteria optimization image reconstruction problem is then solved using modified Hopfeld model dynamic neural-network computing. More details on the image reconstruction algorithm is described by Warsito and Fan (2001).

An example of the reconstructed results using the new algorithm is shown in Fig. 96 as compared to the results using other available techniques, i.e. linear back projection technique (LBP), iterative linear back projection (ILBP) and simultaneous image reconstruction technique (SIRT). LBP and ILBP are based on a commercial software packet developed by Process Tomography Ltd (1999) (PTL, UK). SIRT for ECT is based on the work of Su, Zhang, Peng, Yao, and Zhang (2000).

Fig. 96 shows the reconstruction results with Gaussian noise added (the noise intensity is up to 30 dB).

The first and second columns in Fig. 96 show model images (permittivity distributions in two-phase system). The subsequent columns show, respectively, the reconstructed images using LBP, ILBP, SIRT and NN-MOIRT.
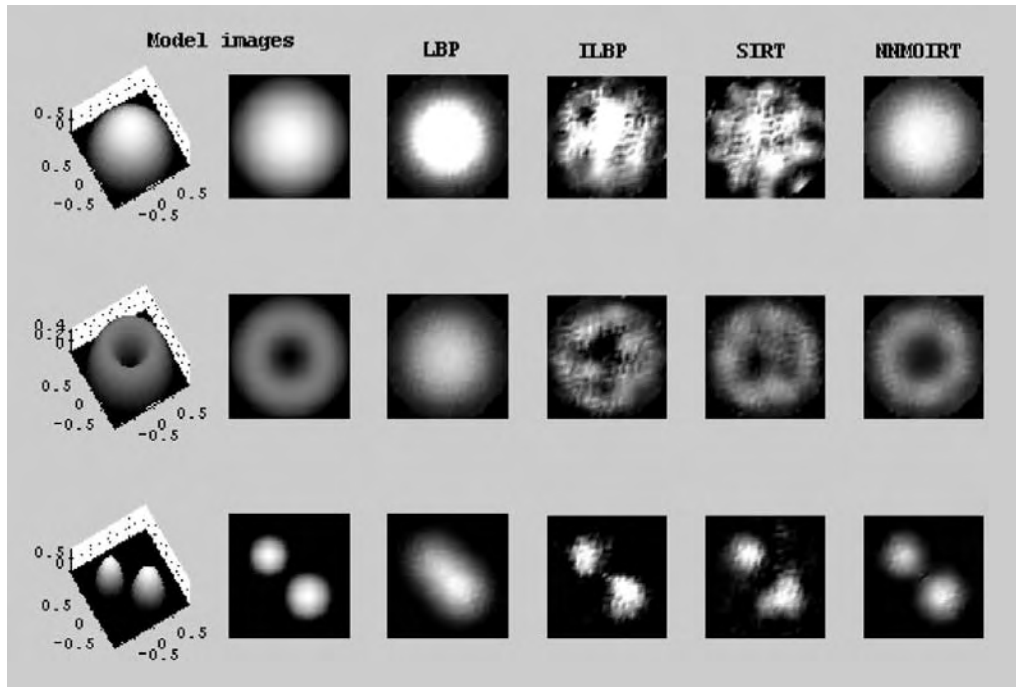
Fig. 96: Comparisons of reconstruction results using NN-MOIRT and other techniques (Warsito and Fan (2001))

The capacitance sensor array comprised a twin-plane sensor using 12 electrodes for each plane attached to the outside of the column wall but 10 and 15 cm above the distributors for plane 1 and plane 2, respectively. The length of each electrode was 5 cm. Two guard sensor planes were located below and above the measuring sensor planes to adjust the electrical field within the sensoring area. The data acquisition system used by Warsito and Fan (2001) was manufactured by Process Tomography Limited (UK) and is capable of capturing image data up to 100 frames per second.
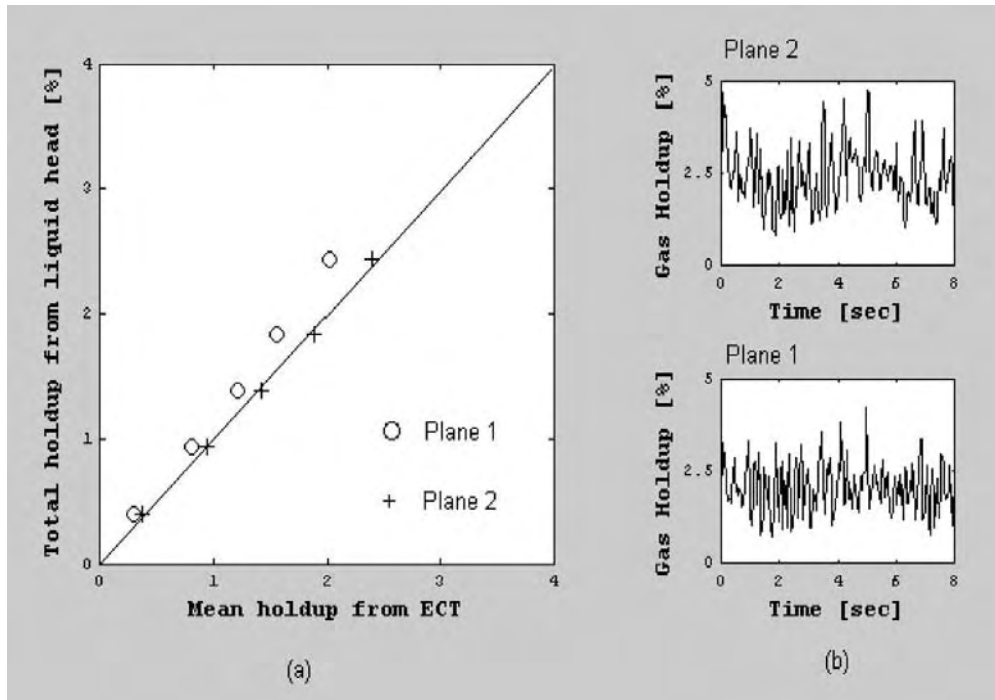
Fig. 97: Comparisons of time average cross-sectional mean gas holdup and time-variant cross-sectional mean holdup in gas–liquid system (liquid phase: Norpar 15, gas velocity=1 cm/s). (Warsito and Fan (2001))

However, the voidage measurement implemented by the conventional ECT technique usually needs a complicated and time-consuming image reconstruction algorithm to obtain a high quality cross-sectional image. Its real-time performance is not satisfactory.

Recently, interests have been shown on the rapid voidage measurement which estimates voidage directly from the electrical values obtained by EIT system (Wang and Li (2007) and (2006)). However, to overcome the influence of the flow pattern, these methods usually need the cross-sectional image to identify the real-time flow pattern of the two-phase flow (Wang and Li (2007) and (2006)).

The void fraction can be measured without any image reconstruction using flow pattern recognition techniques (Dong et all. (2003), Li et all. (2008)).

Support Vector Machine (SVM) is a new machine learning Method (Tan et all. (2007)) which has been used for solving pattern recognition and nonlinear function estimation problem with many successful applications (Vapnik (1998), Jain et all. (2000), Trafalis et all (2005), Cao et all (2003)).

 LS-SVM is a modified formulation of SVM and it can achieve the solution more quickly than the common SVM. In their work, Li et all. (2008) used the LS-SVM

to design the flow pattern classifiers and to develop the void fraction measurement model (nonlinear regression model between the voidage and the capacitance values).

The aim of this research work was to develop a new on-line voidage measurement method based on the capacitances obtained by ECT system and the LS-SVM technique, without any image reconstruction process.

Li et all. (2008) explain that the main idea of their work is to use the capacitances to identify the flow pattern and measure the voidage simultaneously.

In this context it is necessary to establish the flow pattern classifiers and the regression models between voidage and capacitances. They use the LS-SVM for either pattern classification and nonlinear regression.

Because the generation performance of LS-SVM deteriorates if the input data are highly collinear or somewhat irrelevant to the output data, it is necessary to reduce the dimensionality of the input data of LS-SVM. In this work, Partial Least Squares (PLS), which is an effective dimensionality reduction method, is adopted to extract the most useful information of the capacitances obtained by ECT system, both in flow pattern identification and in voidage measurement.

The scheme of the method adopted by Li et all. (2008) is presented in Fig. 98.
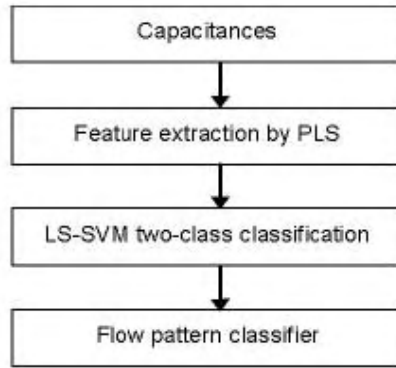
Fig. 3. Design of a flow pattern classifier.
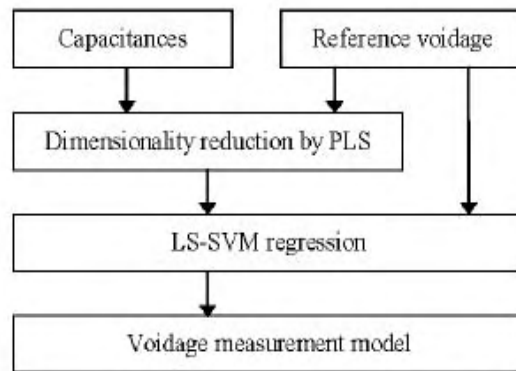
Fig. 4. Developing the voidage measurement model.

Fig. 98: Design of flow pattern classifier and Void fraction measurement model (Li et all (2008)

They used a 12-electrode ECT system, and they obtained 66 capacitances used to identify the flow-pattern; finally, a suitable voidage measurement model is selected according to the flow pattern identification result and the void fraction is calculated.
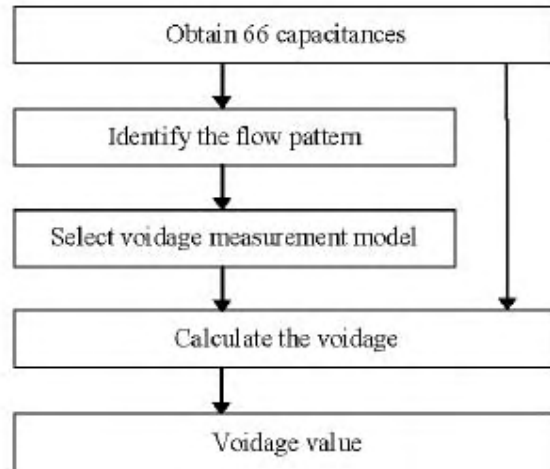
Fig. 99: Voidage measurement process (Li et all (2008)

The method was tested in static experiments, that simulated the geometric structure of gas-oil two phase flow (Li et all. (2008)).

Fig. 100 shows the good agreement between reference and measured void fraction.
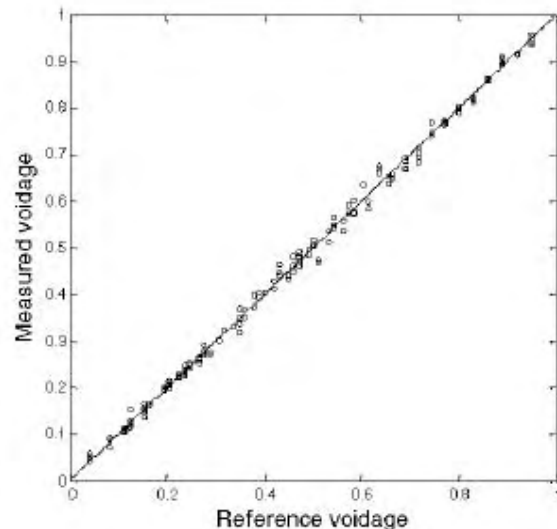
Fig. 100: Comparison between measured and reference void fraction (Li et all (2008)

The maximum errors of the voidage measurement were less than 3.60%, 3.4% and 3.3 % for bubble flow, stratified flow and annular flow respectively. Experimental result also indicates that the real-time performance of the proposed method is satisfactory.

The total voidage measurement time was less than 0.1 s.

Wire Mesh and EIT Comparing Performances

Azzopardi et all. (2010) compared the wire mesh sensor and the ECT sensor in gas-liquid flow (air-water and air-silicon oil).

An array of electrodes was arranged around the outside of the non-conducting pipe wall (see Fig. 101) and all unique capacitance pairs were measured using a Tomoflow R5000 flow imaging and analysis system. The instrument contains 16 identical measurement channels and 16 identical driven guard circuits and in the was operated with a twin-plane sensor.
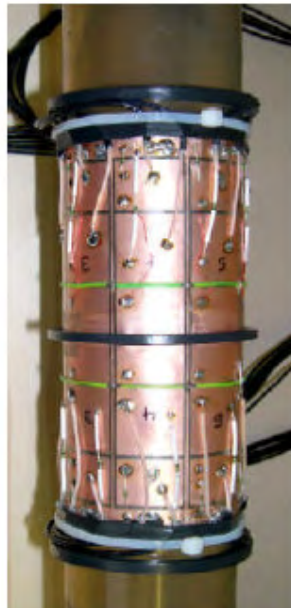

Fig. 101: ECT sensor mounted on transparent plastic pipe with electrical guard removed for clarity. (Azzopardi et all. (2010))

In this work, a 24×24 wire configuration sensor was used. The sensor comprises of two planes of 24 stainless steel wires of 0.12 mm diameter, 2.8 mm wire separation within each plane and 2 mm axial plane distance. The wires are evenly distributed over the circular pipe cross section. An acrylic frame supports the sensor and allows fixation in the test section. Fig. 102 shows a photograph of the sensor. The present electronics is able to generate up to 7,000 images per second.

Fig. 102: 24×24 wire-mesh sensor for pipe flow measurement. (Azzopardi et all. (2010))

Measurements have been made with the instrumentation described above for air superficial velocities in the range 0.05-6.0 m/s and 0-0.7 m/s for liquid phase. The ECT electronics were triggered from the WMS electronic so results were exactly simultaneous. The sampling rate for the WMS was 1 kHz.

That for the ECT was 200 Hz in the first campaign and 1kHz in the second.

Fig. 103 shows the mean void fractions from the two techniques taken in the first campaign. That for the second campaign is show in Fig. 104. The figures illustrate the agreement between the two methods of measurement. There are exceptions for the data taken from liquid superficial velocity of 0.2 m/s. This might due to those data having been obtained at a lower sapling frequency.
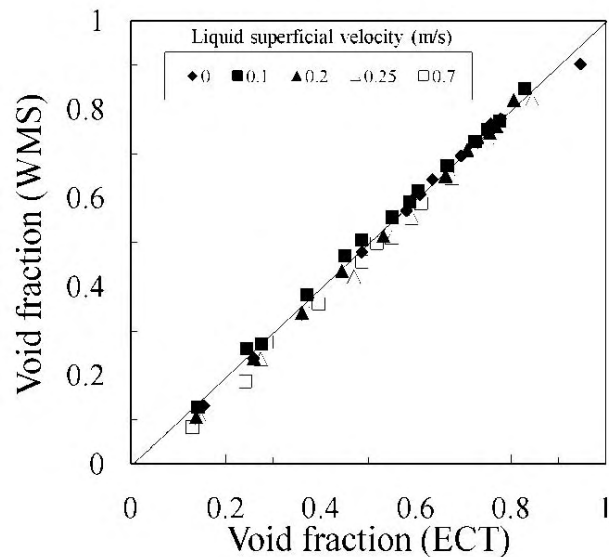

Fig. 103: Comparison of overall averaged void fraction from Wire Mesh Sensor and Electrical Capacitance Tomography (first campaign). (Azzopardi et all. (2010))

206

Some of the minor differences may be due to the fact that the ECT measures over a larger axial distance than the WMS.
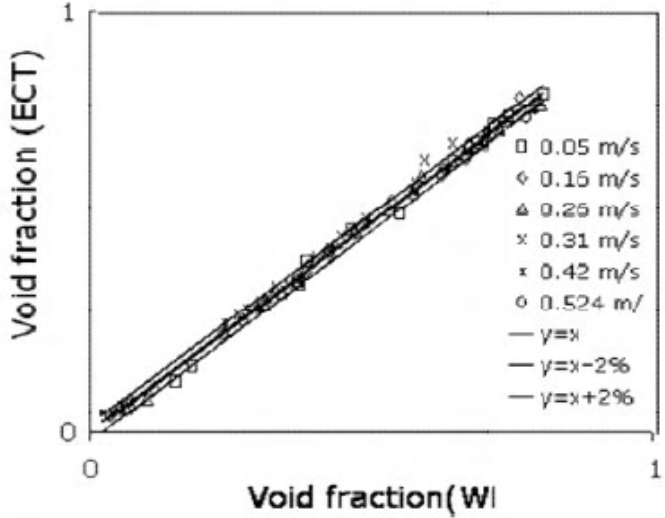

Fig. 104: Comparison of overall averaged void fraction from Wire Mesh Sensor and Electrical Capacitance Tomography (second campaign). (Azzopardi et all. (2010))

The output of the WMS has been tested against gamma ray absorption. The gamma beam was positioned just under individual wires. Obviously, as the gamma can only give integral measurements in time and along the chord, the data from the WMS have been analysed in a similar manner. Fig. 105 shows the good agreement between the two measurement techniques.
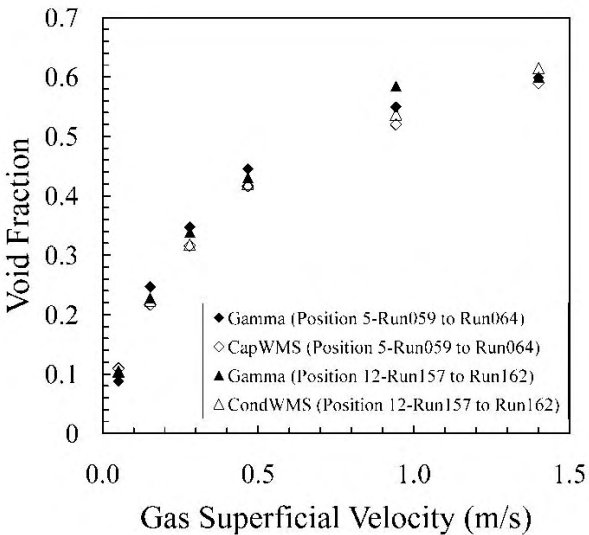

Fig. 105: Comparison between WMS (both conductance and capacitance) and gamma densitometry. Gamma beam placed just under individual wire of sensor. (Azzopardi et all. (2010))

207

The authors used the cross-sectionally averaged void fraction to do a comparison with different correlations of literature:
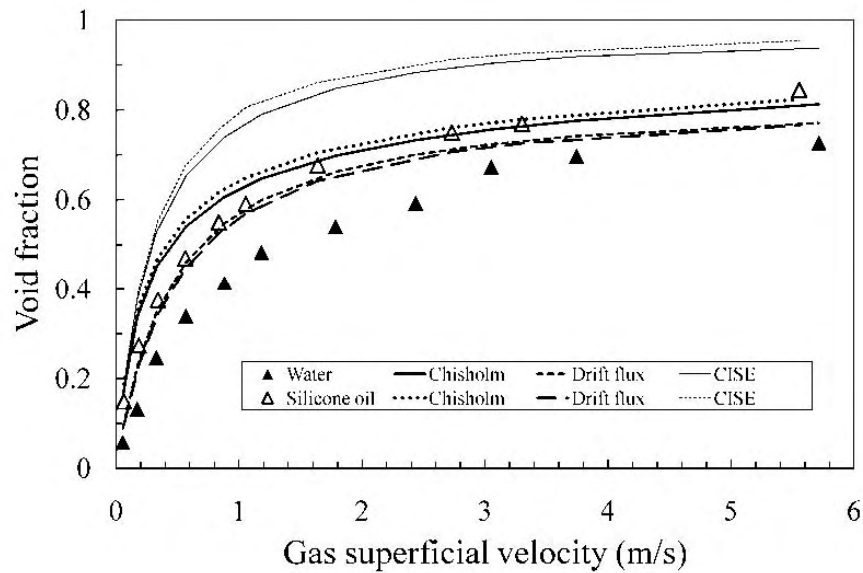
**Fig. 106: Mean void fraction – liquid superficial velocity =0.25 m/s - closed symbols – water; open symbols = silicone oil. (Azzopardi et all. (2010))**

They also tested the instruments to evaluate the influence of the pipe orientation, bends and sudden contraction in bubble size, radial void fraction profile and radial velocity distribution for air-water and air-oil flow, with very good results.

8. FLOW PATTER IDENTIFICATION TECHNIQUES

Traditionally, flow regimes have been defined according to visual observations performed by viewing the flow through transparent channels. The majority of all the reported data have been obtained in this manner.

However, at present there are some other methods of flow regime identification which employ a variety of signals and are based on two principally different approaches. These are (Rouhani et Sohal (1982)):

- Direct observation, including;

    Visual and high speed photography

    X-ray attenuation picture

    Electrical contact probe

    Multi-beam, gamma-ray density measurement.

- Indirect determination, including;

    Static pressure oscillation analysis

    X-ray attentuation fluctuation analysis

    Thermal neutron scattering 'noise' analysis

    Drag-disk signal analysis.

Direct observation methods

Visual and high speed photography viewing

As stated earlier visual observation has been used extensively as the only means of flow regime detection in many experiments. Tests have mostly been performed inside transparent channels at low pressures, or, in the case of boiling channels with metallic walls, some segments of transparent tubing were fitted at the exit of the metallic part in order to provide visibility of the flow. It is admitted, however, that ambiguities regarding the exact nature of flow patterns may exist in the interpretation of such visual observations, particularly at high flow velocities. In this connection, still pictures taken by high speed photography have been employed as a useful aid.

Even though such pictures may give a clear view of flow at a certain moment of time, their interpretation regarding the flow regime may be arbitrary or somewhat

subjective, depending on the observer. In fact some of the discrepancies in matching the data of different investigators against a given flow map may, to some extent, be attributed to the inexactness of such determinations.

Flash photography for flow regime observation has been employed by many investigators. Some of the earlier works of this kind were reported by Cooper et al. (1963), Staub and Zuber (1964), Bennett et al. (1965) and Hewitt and Roberts (1969).

High speed photography of two-phase flow regimes has indeed become a routine part of such studies even if other flow regime detection methods have been employed. One example of this kind is the work of Vince and Lahey (1980) in which photographs of flow regimes are shown side by side with the results of pattern indicators obtained by other means. Examples of this work will be described later.

There are also two other disadvantages associated with the direct visual observation method or highspeed photography.

These are: limitation on pressure that may be safe enough for using transparent channel walls and, more importantly, the difficulty of obtaining a clear view of the central parts of the flow cross section. The latter difficulty is due to the light defraction at all gas-liquid or vapor-liquid interfaces which, in some cases, would make the clear observations limited to only a layer of the mixture near the channel walls.

However, in spite of all these limitations, the direct visual observation approach has been used for its simplicity and inexpensiveness. It certainly has its everlasting merit as the best tool for simple experiments.

Electrical contact probe

Information on the alternative passage of gas/vapor and liquid at some points inside a channel may be obtained with the use of a thin electrical contact probe which is insulated from the channel walls. Both the probe and the channel wall are parts of an energized electric circuit which would close if a mass of electrically conducting liquid bridged the gap between the uninsulated tip of the probe and the channel wall. The electric circuit is equipped with appropriate current detection systems which record the signals indicating passage of liquid at that point. Bergles et al. (1968) used such an electric contact probe to study the flow regimes at the exit of boiling channels.

For the purpose of flow regime determination the probe tip was positioned at the center point of the channel cross section. Flow regime studies with this method were performed in round tubes and also in two subchannels of a heated four-rod bundle. The electrical signals registered by the contact probe for different flow regimes in those subchannels are shown in Fig. 107 which is reproduced from Bergles et al. (1968). The test facility used for these studies was also equipped with a transparent section at the channel exit for visual observation and flash photography.
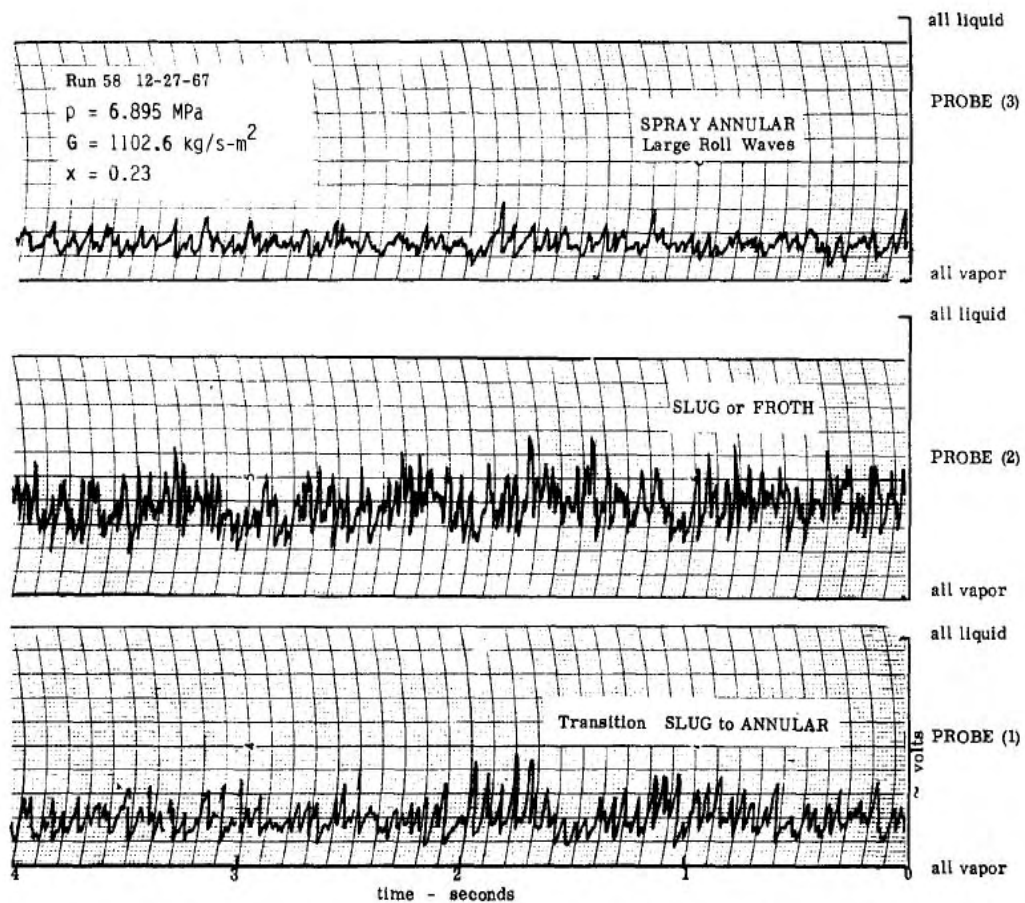

Fig. 107: Electric probe signals displaying different flow regimes
(Rouhani et Sohal (1982) from Bergels et al. (1968))

Indirect determining techniques

Determination of flow regimes through indices other than a direct view of the flow appearance, or of its density distribution picture, is possible and even preferable. Indirect methods of flow regimes detection are mostly based on some statistical analysis of the fluctuating character of the flow and are sometimes referred to as obtaining 'the flow regime signature'.

With the exception of the quiescent and very smooth two-phase flow in a horizontal pipe, all forms of two phase flow demonstrate a noticeable fluctuating character. This is true even in the case of so-called steady state flows whose average intensity does not vary in time. The most significant fluctuations are observed in the local pressure and in the instantaneous mixture ratios of vapor and liquid, or the local average density and its distribution over flow cross section.

Analysis of these fluctuations according to certain mathematical models have been shown to yield clear indications of the different flow regimes. These mathematical models are according to some statistical analysis of random fluctuations which include the calculation of Power Spectral Density (PSD) and Probability Density Function (PDF) as will be very briefly described in the following.

Autocorrelation and power spectral density

One of the first publications on the characterization of flow regimes by a statistical method was by Hubbard and Dukler (1966) in which they gave a description of statistical analysis of random fluctuations based on the developments in communication theory. Following is a short extract from their description.

The autocorrelation of a fluctuating function, $f(t)$ is defined as a function of some time interval $\tau = \Delta t$ in the following manner,

$$A_\infty(\tau) = \lim_{t_0 \to \infty} \frac{1}{2t_0} \int_{-t_0}^{t_0} f(t) \cdot f(t+\tau) \, dt$$

$A_\infty(\tau)$ depends strongly on the length of z if it is not very small compared to the dominating oscillation period of the function $f(t)$.

Application of this analysis would be in the treatment of a long series of instantaneous values of $f(t)$ sampled at short time intervals.

212

If the function *f(t)* is stationary so that it shows the same statistical properties over any period of time, then its auto power spectral density in terms of frequency to, is defined by

$$P_{\infty}(\omega) = \int_{-\infty}^{\infty} A_{\infty}(\tau) \cos(2\pi\omega\tau) d\tau$$

According to Hubbard and Dukler (1966) some errors may be introduced in the use of these equations if the total recorded sample is not adequately large compared to x.

The above described forms of A_{∞} and P_{∞} are then multiplied by a so-called spectral window, $Q(\omega)$ and integrated again to obtain the smoothed forms of these functions which in the case of power spectrum will be,

$$P_o(\omega) = \int_{-\infty}^{\infty} Q(\omega) P_{\infty}(\omega) d\omega$$

in which $Q(\omega)$ is the Fourier transform of a function, which is 1, if $\tau < \tau_{max} < 10\%$ of the total record length, and is zero if $\tau \geq \tau_{max.}$

Finally a normalized estimated power spectral density (PSD) P(ω) is calculated according to

$$\hat{P}(\omega) = \frac{P_0(\omega)}{\sum_{\omega=0}^{\omega_n} P_0(\omega)}$$

in which $\omega_n = 1/(2\varDelta\tau)$ is the maximum frequency that needs to be considered.

Analysis of wall pressure fluctuations

Hubbard and Dukler (1966) used the above described power spectral density analysis to their own recorded measurements of wall pressure fluctuations, for various flow regimes in a horizontal pipe, and concluded that there was a clear relationship between the observed flow regimes and normalized power spectral density (PSD) distribution, as a function of frequency.

However, this method did not find a wide acceptance for flow regime detection for the simple reason that the plots of PSD versus frequency would not only depend on the flow regimes alone, but also on the actual velocities of vapor and liquid which were not always known *a priori*. Such ambiguities in the interpretations of the PSD distributions would render the conclusions unreliable. This particular point was clearly demonstrated in the work of Vince and Lahey

213

(1980). However, further elaboration on the use of PSD, reported by Albrecht et al. (1982), shows that this is a powerful means for indicating change over from one flow regime to another.

Probability density function

As stated earlier, two-phase flows demonstrate considerable fluctuations particularly in their instantaneous average densities, or void, at any cross section of the channel.

The usefulness of signals from a sensor monitoring a dynamic parameter or phenomenon can be found in the significant work of Jones and Zuber (1975), which shows the applicability of statistical analysis techniques for flow pattern determination. They reported on the use of time traces of void fraction measured by X-ray density meters by analyzing its Probability Distribution Functions (PDF) of the fluctuations and using the plots of the PDF as an indicator of flow patterns. Their approach is described briefly in the following.

If the instantaneous values of void fraction or some other fluctuating feature of two-phase flow, at a certain point in a channel, are measured and recorded as a function of time, one would obtain a varying function, that may seem like the example curve shown in Fig. 15. Here α may represent the local void fraction, or some other quantity. According to Jones and Zuber (1975), if the probability that the void fraction is less than some specific value, α, is given by $P(\alpha)$, then $dP(\alpha)/d\alpha = P'(\alpha)$ represents the probability per unit void fraction that the void fraction lies between the

values of α and $\alpha + d\alpha$. As shown in Fig. 15, the timerecord of the measured void, α, may be divided in a number of equal increments of $\Delta\alpha_i$ and the time scale in equal increments of Δt_j. One may then express the relative number of times n_i that α is within $\Delta\alpha_i$ during a total time period of $t_N = N \Delta t_j$, by,

$$\frac{n_i/N}{\Delta\alpha_i} = \frac{1}{\Delta\alpha_j} \sum_{j=1}^{n_i} \frac{\Delta t_j}{t_N}$$
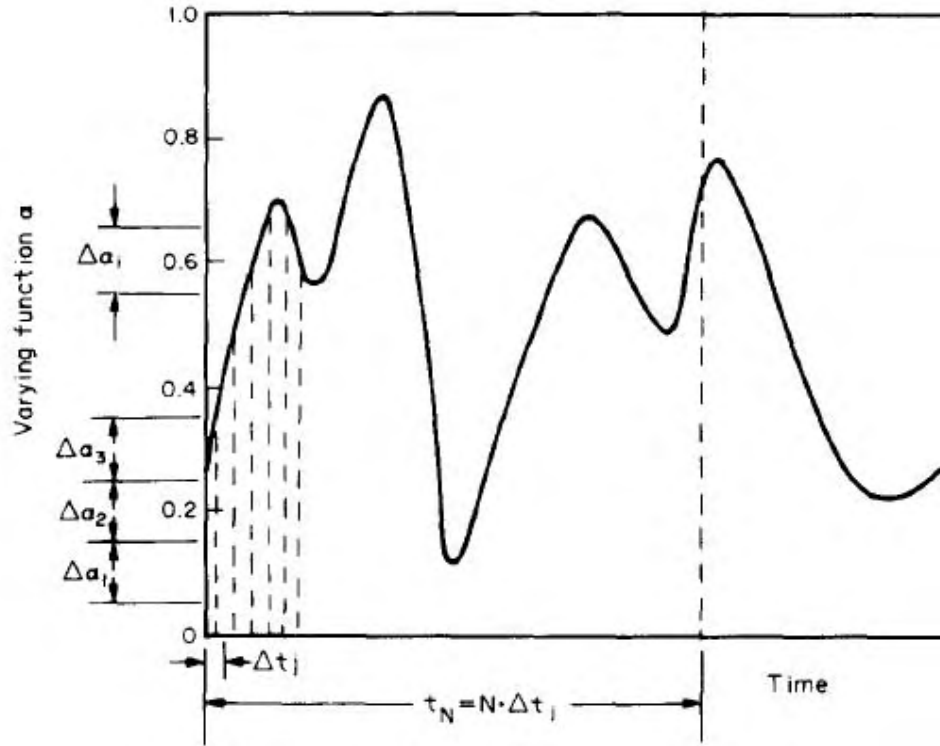
Fig. 108: Illustration of PD determination (Rouhani et Sohal (1982))

The summation $\dfrac{\Delta t_j}{t_N}$ represents the probability that the instantaneous value of α lies within the designated interval $\Delta\alpha_i$. Hence, at the limit when $\Delta\alpha_1{\sim}0$ the above summation gives,

$$\lim_{\Delta\alpha_i \to 0}\left[\frac{1}{t_N\Delta\alpha_i}\sum_{j=1}^{n_i}\Delta t_j \to P^{'}(\alpha)\right]$$

This represents the probability density function (PDF) of the particular record of α which is examined.

Jones and Zuber (1975) applied this analysis to their own recorded void fraction data that was obtained by X-ray through a rectangular channel, and complemented by high-speed motion picture of the actual flow patterns. They found clearly distinctive differences in the PDF versus average void profiles for different flow regimes. Some of these interesting findings are reproduced in Fig. 109, Fig. 110, Fig. 111.

As shown in Fig. 109 the bubble flow regime, which is photographed through the transparent channel wall , shows an X-ray trace of void fraction which is at a low level most of the time, but includes a number of sharp peaks with short duration. The PDF of this trace, which is also shown in the same figure, has a characteristic peak near zero void fraction with sharply reduced probabilities at higher void fractions.

One should note that the PDF profile extends somewhat to the left of 0.0 void fraction which may be interpreted as some probability for finding small 'negative voids'. This is actually due to the system noise of the X-ray machine and the attenuation detection electronics. In the absence of any voids the system noise would give a PDF profile with Gaussian distribution and its peak would be at 0.0 void fraction.

Fig. 110 shows the photographs, X-ray void trace and the PDF profile of slug flow regime. This so called double-humped PDF versus void profile is a distinctive characteristic of slug flow, as it has been observed in repeated experiments.

Fig. 111 shows the typical PDF profile of annular flow. Its main characteristic is the probability density peak at a very high average void fraction with a considerably lower probability at lower values of void fraction.

Similar studies are reported by Vince and Lahey (1980) who further demonstrated the usefulness of

PDF in flow regime identification. They performed void measurements using a specially developed, 6-beam, X-ray system, on the flow of air-water in a vertical tube of 2.54 cm diameter. They obtained a large number of PDF profiles of void fraction, using the diagonal beam signals, for a variety of liquid and air flow rates. An examples of these is reproduced in Fig. 112, showing pictures of the actual flow regimes side by side with their PDF and PSD signals. Here again the PDF profiles show different characteristic shapes for different flow regimes and, in this respect, they have a strong resemblance to the PDF profiles reported by Jones and Zuber (1975) for the respective flow regimes.

However, Vince and Lahey (1980) argued that the interpretation of the void fraction PDF is still a subjective method of flow regime indication, but their variance or the second moment around the mean value of the PDF distribution is a true objective means of flow regime identification.

The variance of a distribution f is defined by,

$$\sigma = \sum_{i=1}^{N} \left(f_i - \overline{f} \right)^2 P_i$$

Where

$\overline{f}$ is the mean value of f_i given by:

$$\overline{f} = \sum_{i=1}^{N} P_i f_i$$

Fig. 113, which is a reproduction from Vince and Lahey (1980), shows the PDF variance as a function of area-averaged void fraction. This was obtained from a number of PDF profiles gathered from a variety of flow conditions involving all the different patterns.

As may be seen in Fig. 113, the plots of PDF variance for all different chords (X-ray paths through the flow) show some discontinuities at a void fraction of about 0.30 and again at about 0.70. Vince and Lahey (1980) pointed out that these PDF variance discontinuities, both of which happen to occur at 0.04 variance, are the signs of flow regime transitions. The first one indicates transition from bubbly to slug flow and the second on from slug to annular flow. But they admit that transitions at a variance of 0.04 may be only a characteristic of their experimental facility and that such observations need further investigation before any generalization could be made.

It must be added that the suggested process of establishing the variance of the measured void fraction PDF curves is a rather lengthy approach for the determination of flow regime transitions, at least in engineering applications
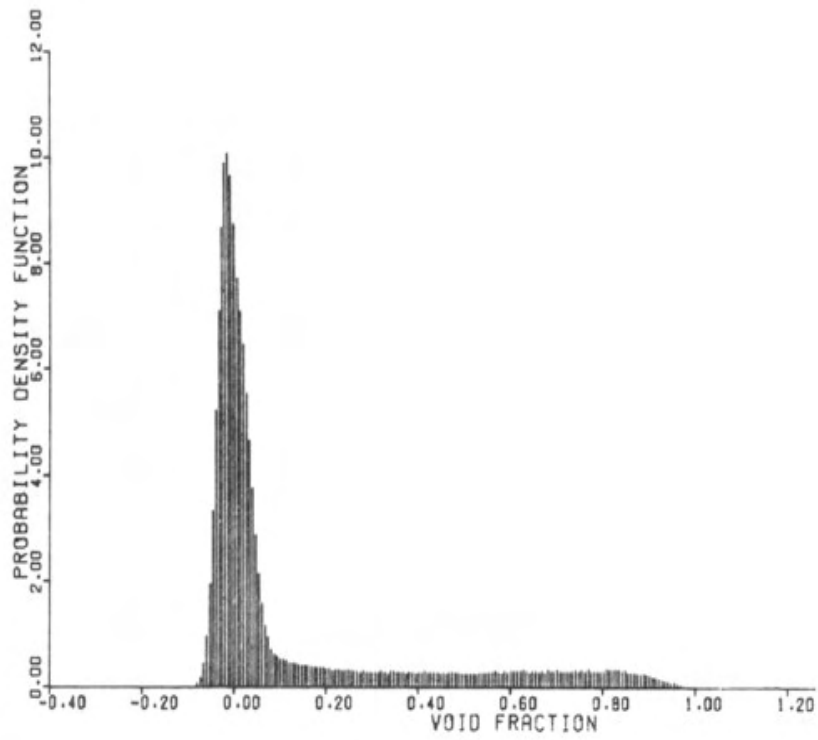
**Fig. 109: PDF of bubbly flow (Jones and Zuber (1975)).**
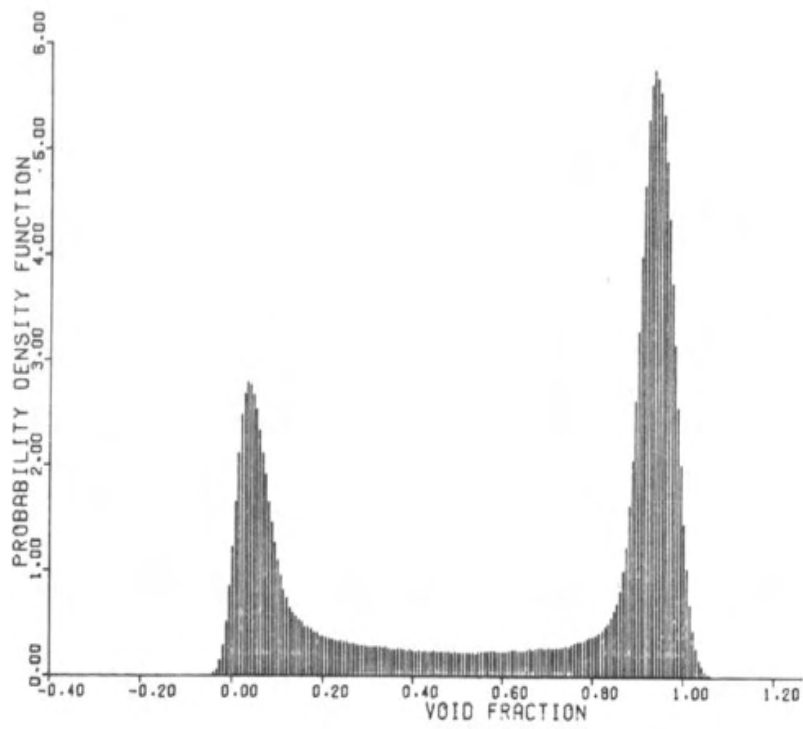

Fig. 110: PDF of slug flow (Jones and Zuber (1975)).
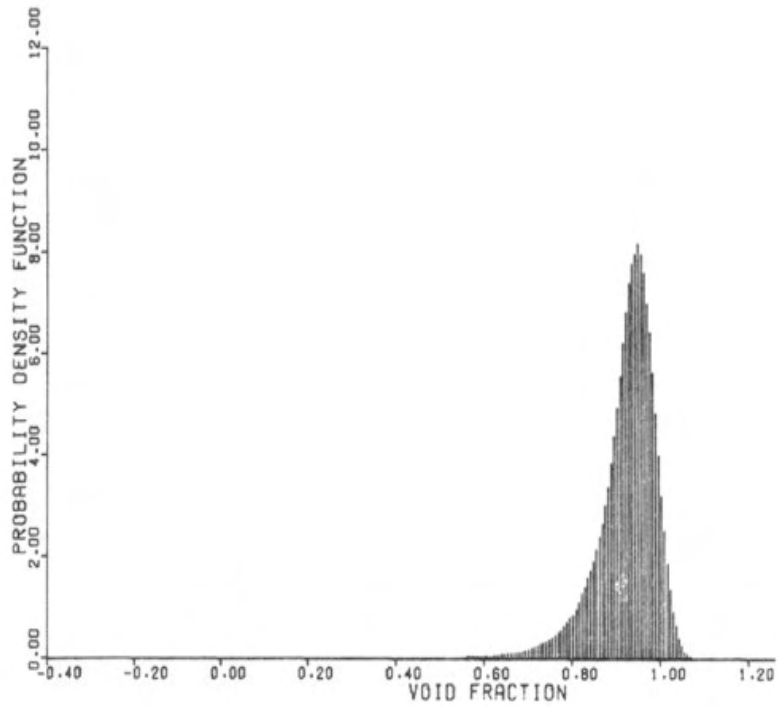
Fig. 111: PDF of annular flow (Jones and Zuber (1975)).
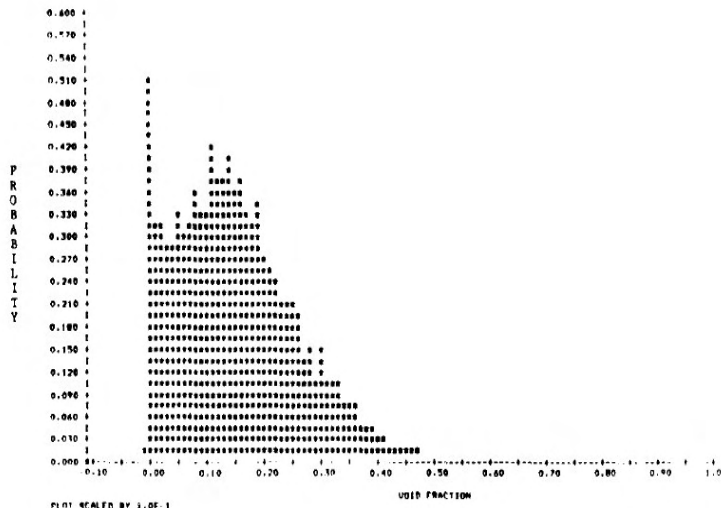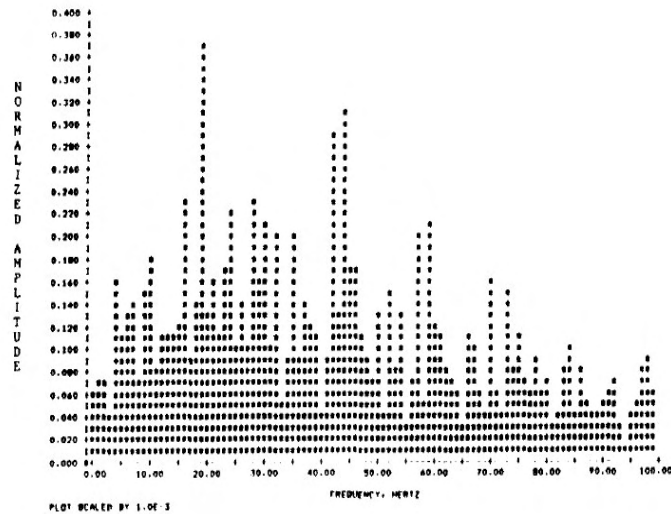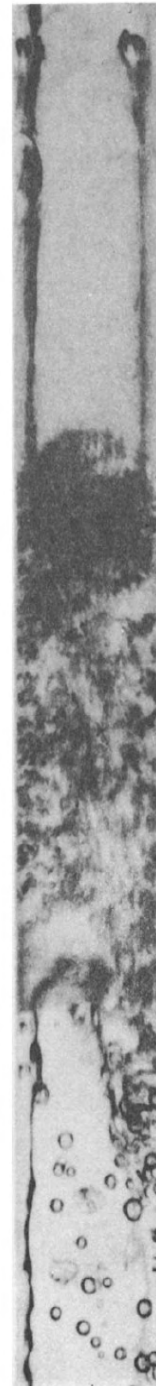
Fig. 112: PDF of bubbly flow. A photograph (a), diameter PDF (b), and diameter PSD (c) for 13% area-averaged void fraction, jl = 0.37 m/s, jg= 0.97 m/s (Vince and Lahey (1980))
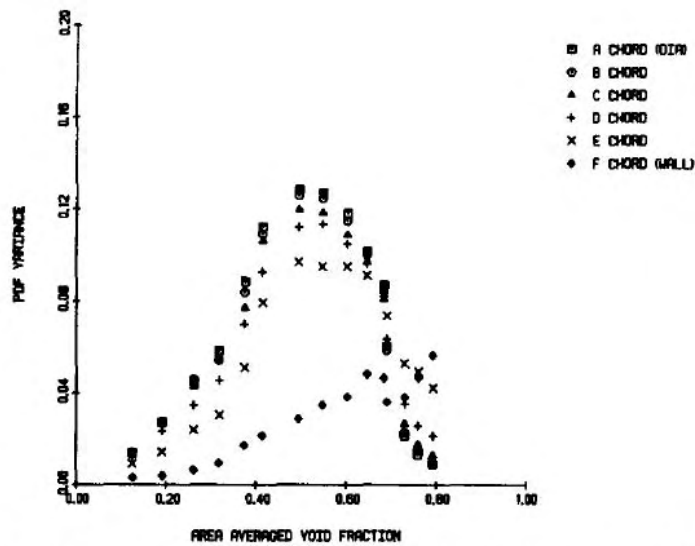
Fig. 113: PDF variance and indication of regime transition (Vince and Lahey (1980))

Drag-disk noise analysis

A drag-disk is a device for sampling the linear momentum carried by flow in a channel. Its structure is basically a small disk at the tip of a Supporting bar which protrudes from the channel wall into the flow. The bar transmits the impact force of the flow to a detection and measuring system outside of the flow channel. Since the flow momentum affecting the drag-disk is proportional to the local density around it, a continuous recording of the forces on a drag-disk will show a fluctuating nature similar to those obtained from traces of void or density measurements.

An analysis of drag-disk deflection fluctuations may be performed exactly in the same way as X-ray or neutronic techniques.

The statistical analysis could yield some PDF curves versus flow momentum (instead of cordal or average void fraction). No data from the application of drag disk in this capacity has yet been reported; however, drag-disk noise analysis is mentioned by Albrecht et al. (1982).

Keska (1992 and 1993) reports the results of laboratory experiments with respect to flow pattern determination and spatial and temporal distribution of the component concentration using capacitive systems. The author used a previously

developed capacitive system to measure in situ concentration with the ability to measure high frequency spatial concentration fluctuation by volume up to 1 kHz.

The experimental wave form images of concentration versus time were statistically evaluated and presented in the form of power spectral density (PSD) and cumulative power spectral density (CPSD) images. The author notes that there is a clear difference in both PSD and CPSD distribution due to a change in average solid particle size. The author explains that as the particle size decreases, the PSD and CPSD will be spread over a larger frequency range. A decrease in particle size will result in higher frequency fluctuations of the AC component of concentration. Additionally, increasing the particle size will lower the saturation frequency of the CPSD. The author concludes that this measurement method and system used in conjunction with statistical analysis (PSD, CPSD) of time traces is clearly a viable means for definition and determination of flow patterns in slurry flow.

The PDF and PSD functions were used to characterize the concentration signals in the amplitude and frequency domains. Authors (as Keska et all. (1992 and 1993), Nencini et Andreussi (1982), Ohlmer et all. (1984), Person (1984), Saiz-Jabardo et all. (1989) in (Keska (1998)) used non-intrusive resistive sensors mounted flush with the inside of the channel to monitor the concentration of the mixture.

Using statistical analysis techniques, PDF and PSD functions, these authors determined the character of flow patterns from bubble to annular flow and void fraction ranging from 0 to 0.6. All authors using resistive methods reported on the high potential and the high frequency of response of the resistive method in the determination of void fraction.

Keska (1998), based on a search of the literature, identified four different methods to measure fluctuations of concentration or other related signals, such as interfacial phenomenon, that can be used in flow pattern detection, which are the capacitive, resistive, optical, and pressure methods. The literature also demonstrates that the PDF and RMS functions may be used as flow pattern discriminators.

In particular the signals in the time domain from each of these methods can be seen as the superposition of the fluctuating component and the time averaged component. Many authors have shown that the fluctuating component alone or together with the average component of a signal can be observed in the time

domain, amplitude domain, and frequency domain to help identify flow regime based on characteristics of the signal shown in each domain. However, most authors use only one measurement system to measure the parameter of interest.

If all chosen methods can be used simultaneously in the same space and time to monitor each respective signal pertaining to the mixture flow, the comparison of each method's ability to determine flow pattern would be direct and adequate, even if the flow patterns themselves are not well defined.

The first stage of the Keska's research (1998) was to develop and build an experimental system capable of generating and controlling two-phase flow patterns, secondly, from literature determine the most commonly used flow pattern detection methods, third, develop and incorporate systems for each of these chosen measurement methods to allow each to simultaneously monitor, in the same space and time, their respective parameters related to mixture flow conditions, and finally, analyze the signals from each system for a direct comparison of each method's ability to determine flow patterns.

The experimental apparatus was developed and constructed to generate air±water mixture flow in a vertical channel under adiabatic conditions. In this work, the four most commonly used flow pattern detection methods, simultaneously and in the same space, measured mean and fluctuating components of signals related to flow patterns and, or concentration. Eight different flow patterns were analyzed in the time and amplitude domains in order to determine the ability of each method to recognize these flow patterns ranging from bubble to churn flow. To better understand and analyze the primary signals, the probability density function (PDF) and the cumulative probability density function (CPDF) were used on the signals from each method at eight different flow patterns. The in situ concentration and flow pattern, both, influence the results of the output when these functions are used to evaluate the character of each signal. Each method indicates different abilities and potential for use for flow pattern recognition. The capacitive and resistive signals are of similar nature and demonstrate a high potential for flow pattern recognition.

The pressure based system has some resolution, approximately half that of the capacitive and resistive systems. Additionally, the pressure system is influenced differently by the in situ concentration and flow pattern compared to the capacitive and resistive signals as interpreted from the variation of the local

223

maximums on the respective curves representing each system's RMS values. Overall, the pressure system demonstrates a lower potential for use for flow pattern recognition, compared to the capacitive and resistive systems. The optical system has very limited ability to be used for flow pattern recognition in low range of concentration, however, the optical method may have ability to determine flow patterns with concentration ranging above 70%.
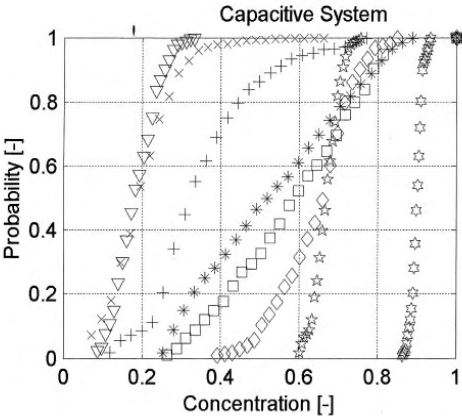

Fig. 6. Cumulative probability density function (CPDF) of concentration obtained from the capacitive signals for eight flow patterns.
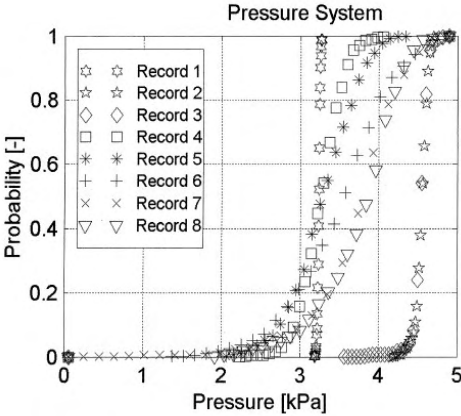
Fig. 8. CPDF of pressure (kPa) obtained from the pressure signals for eight flow patterns.
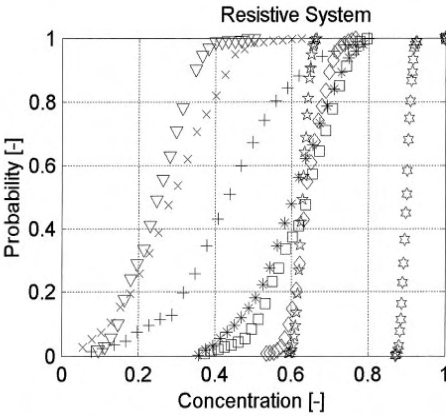
Fig. 7. CPDF of concentration obtained from the resistive signals for eight flow patterns.
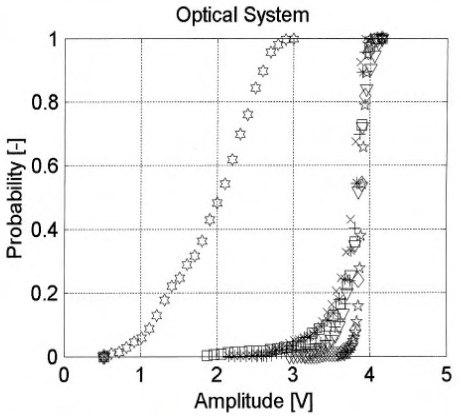
Fig. 9. CPDF of amplitude (V) obtained from the optical signals for eight flow patterns.

**Fig. 114: Cumulative PDF from different sensors analysis (Keska (1998))**
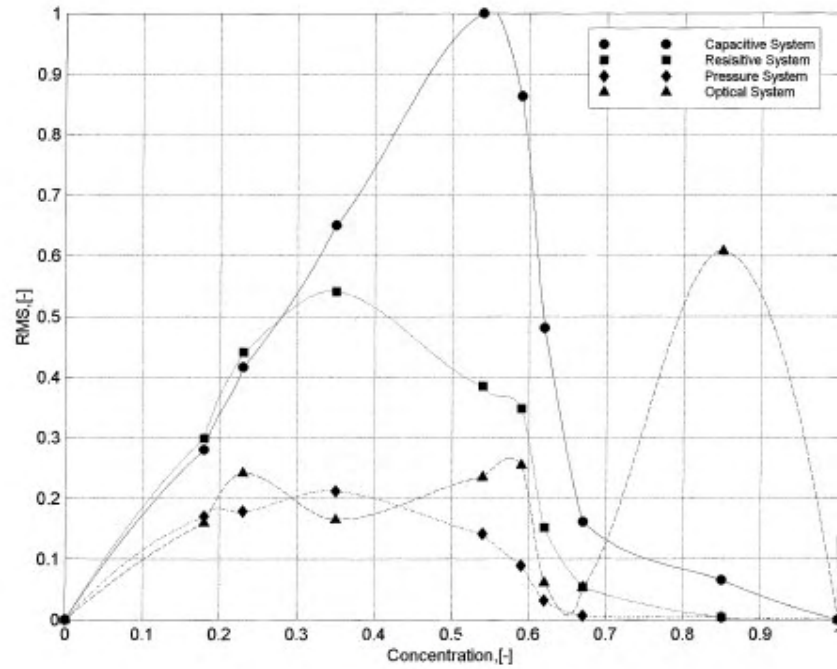
Fig. 115: Comparison of RMS values of each signal obtained from four methods at different flow pattern (Keska (1998))

A new method for flow pattern recognition is the tomographic impedance method, described at the end of the paragraph of impedance probe.

9. Conclusions

A careful measurement of the relevant two-phase flow parameters is the basis for the understanding of many thermohydraulic processes. Reliable two-phase instrumentation is therefore essential for the connection between analysis and experiment especially in the nuclear safety research where accident scenarios have to be simulated in experimental facilities and predicted by complex computer code systems.

In this work few instruments used in two phase flow measurement have been analyzed.

It's important to highlight the this research is not exhaustive, and a lot of works, concerning different devices are available in literature.

The choice of instruments to analyze has been made considering that most of the devices commercially available are not useable for nuclear accidents simulations.

Limitation in pressure, temperature or flow velocity reduce the number of instrument that could well perform in these situations.

Many instruments recently developed have not yet sufficiently experimental validations, and some of them are too fragile to operate at the conditions realizable during nuclear accident simulations (LOCA).

The main parameter that needs to be monitored during the simulation of the transient is the mass flow rate. Since the density of each phase is not known, it is necessary to measure both the velocity of the two-phase flow (with a flow-meter) and the density of each phase (with a densitometer).

The Spool Piece could be composed by two, or three instruments, able to measure the mass flow with a prescribed accuracy and able to avoid instrument breaks.

The meters must then be characterized of an high robustness, reliability and accuracy.

The meters analyzed are very robust devices, and are largely used in the past for thermohydraulic nuclear safety researches, with good results.

Also considering limits and drawback, Turbine, Drag Disk, Venturi tube and Impedance Probes can operate in accident situation with an acceptable performance.

Different combinations of them can be used to create different spool piece, more or less adapt to operate in different flow conditions. For this purpose, since the flow pattern can't be directly identified, sophisticate models must to be used, and in some case developed, to understand the instrument signal and then to convert it in a physical flow parameter.

Ambitious goals remain for instrument developers such as the development of:

- simple to use low and high flow measuring techniques,

- high void fraction local and averaged density measurements,

- automated signal interpretation and flow pattern identification.

10.   Bibliography

Baker O. (1954), Simultaneous flow ofoil and gas, Oil and Gas J. 53

Baker, C. R., (1991) Response of bulk flow meters to multiphase flow, Proc. I. Mech. E. Part C: J. Mech. Eng. S

Baker, C. R., (2000), Flow measurement handbook, Cambridge University Press
.
Dahl, Michelsen et all. (2005), HANDBOOK OF MULTIPHASE FLOW METERING Revision 2, March 200

Hetsroni, G., (1982) Handbook of multiphase systems, Hemisphere, Washington.

Hewitt G.F. (1981) Liquid-gas systems, in Handbook of Multiphase Flow (Editor Hetsroni G.), Chapter2, Hemis

Hewitt G.F. and Lovegrove P.C. (1976) Experimental methods in two-phase flow studies, AERE Harwell, Prepa

Hewitt, G. F., (1978), Measurement of two phase flow parameters, Academic Press.

Ishii M. (1977) One-dimensional drift-flux model and constitutive equations for relative motion between phases

lshii M. and Mishima K. (1980) Study of two-fluid model and interfaciai area, Argonne National Laboratory, AI

Miller, R. W., (1996), Flow measurement engineering handbook, McGrawHill

Rouhani and Sohal (1982), Two-Phase Flow Patterns: A review of research Results, Progress in Nuclear Energy

Taitel Y. (1977) Flow pattern transition in rough pipes, Int. J. Multiphase Flow 3.

Taitel Y. and Dukler A. E. (1976) A model for predicting flow regime transition iii horizontal and near horizonta

Taitel Y., Barnea D. and Dukler A. E. (1980) Modeling flow pattern transitions for steady upward gas-liquid flo

Whalley, P. B., (1987), Boiling, condensation and gas-liquid flow, Clarendon Press, Oxford

White, F. M., Fluid mechanics, (1994), McGRAW-HILL.

Yeung, Ibrahim (2003), Multiphase flows sensor response database, Flow Measurement and Instrumentation 14

Bibliography Turbine meters

Abdul-Razzak, M. Shoukri, and J. S. Chang, Measurement of two-phase refrigerant liquid-vapor mass flow rate

AGA Transmission Meas. Committee Rep. No. 7, Measurement of fuel gas by turbine meters, Arlington, VA:A(

ANSI/ASME MFC-4M-1986 (R1990), Measurement of gas flow by turbine meters, NY, Y:ASME.

ANSI/AWWA C701-88, Cold water meters - turbine type, for customer service, Denver, CO: Amer. Water Wor

ANSI/AWWA C708-91, Cold-water meters, multi-jet-type, Denver, CO: Amer. Water Works Assoc., 1991.

API MPM, Ch. 5.3, Measurement of liquid hydrocarbons by turbine meters, 3rd Ed., Washington, DC:API (Ame

Atkinson, A software tool to calculate the over-registration error of a turbine meter in pulsating flow, Flow Mea

Aya I. (1975), A Model to Calculate Mass flow rates and Other quantities of Two phase flow in a Pipe with a de

Baker, C. R., (1991) Response of bulk flow meters to multiphase flow, Proc. I. Mech.

Baker, C. R., (2000), Flow measurement handbook, Cambridge University Press.

Baker, C. R., and Deacon, J. E., (1983), Tests on turbine, vortex and electromagnetic flow-meters in two-phase

Ball et all (1977), Ball, J. M., (1977)*, Viscosity effects on the turbine flowmeter, Proc. Symp. On flow Measur

British Standard, BS ISO TR 3313:1998, Measurement of fluid flow in closed conduits—guidelines on the effec

Bronner, R.J. McKee, Cogen pulsation effects on turbine metering, Gas Research Institute, Report No. GRI-92/(

Cheesewright and C. Clark, Step response tests on turbine flowmeters in liquid flows, Proc. Instn. Mech. Engrs

Cheesewright, Bisset, C. Clark, Factors which influence the variability of turbine flowmeter signal characteristic

Cheesewright, D. Edwards and C. Clark, Measurements with a turbine flow meter in the presence of large, non-s

Cheesewright, K.N. Atkinson, C. Clark, G.J.P. ter Horst, R.C. Mottram and J. Viljeer, Field tests of correction p

Chen, N.C. J., Felde, D. K., (1982), Two phase mass flux uncertainty analysis for thermal-hydraulic test facility

Dijstelbergen, Rotameters and turbine flowmeters in pulsation flow measurement, Measurement Control (1970

Dowdell and A.H. Liddle, Measurement of pulsating flow with propeller and turbine type flowmeters, Trans. AS

Grey, Transient response of the turbine flowmeter, Jet Propulsion (1956)

Hardy, J. E., (1982), Mass flow measurements under PWR reflood conditions in a downcomer and at a core barr

Hetsroni, G., (1982) Handbook of multiphase systems, Hemisphere, Washington.

Hewitt, G. F., (1978), Measurement of two phase flow parameters, Academic Press Inc., London.

Hsu, Two-Phase Flow Instrumentation Review (1978)

ISA-RP 31.1, Specification, installation and calibration of turbine flowmeters, Research Triangle Park, NC: ISA

ISO 9951:1993, Measurement of gas flow in closed conduits - turbine meters, Geneva, Switz.: Int. Organization

Johnson, and S. Farroll, Development of a turbine meter for two-phase flow measurement in vertical pipes, Flow

Kamath, P. S., and Lahey, R. T., "A Turbine-Meter Evaluation Model for Two-Phase transients," NES-459. Ren

Lee and H.J. Evans, A field method of determining gas turbine meter performance, Trans. ASME J. Basic Eng (

Lee, and H. J. Evans, Density effect and Reynolds number effect on gas turbine flowmeters, Trans. ASME, J. Ba

Lee, D. C. Blakeslee, and R. V. White, A self-correcting and self-checking gas turbine meter, Trans. ASME, J. F

Lee, M.J. Kirik and J.A. Bonner, Gas turbine flowmeter measurement of pulsating flow, J. Eng. Power, Trans. A

Lee, R. Cheesewright and C. Clark, The dynamic response of small turbine flowmeters in liquid flows Flow Mea

Lee, R. V. White, F. M. Sciulli, and A. Charwat, Self-correcting self-checking turbine meter, U.S. Patent , 1981.

Lui, B. Huan, Turbine meter for the measurement of bulk solids flowrate, Powder Technol, 1995

Mark P.A., Johnson M.W., Sproston J.L., Millington B.C., The turbine meter applied to void fraction determinat

McKee, Pulsation effects on single- and two-rotor turbine meters, Flow Meas. Instrum (1992)

Minemura, K. Egashira, K. Ihara, H. Furuta, and K. Yamamoto, Simultaneous measuring method for both volun

Ohlmer, E. and Schulze, W. (1985), Experience with CENG full-flow turbine meters for transient two-phase flo

Olivier, and D. Ruffner, Improved turbine meter accuracy by utilization of dimensionless data, Proc. 1992 Nat. O

Ovodov, E.A. Raskovalkina and A.L. Seifer, Dynamic characteristics of turbine-type flowmeters for cryogenic f

Ower, On the response of a vane anemometer to an air-stream of pulsating speed, (1937).

Pate, A. Myklebust, and J. H. Cole, A computer simulation of the turbine flow meter rotor as a drag body, Proc.

Quick, Gas measurement by insertion turbine meter, Proc. 70th Int. School Hydrocarbon Meas., OK, 1995.

Rouhani, S., "Application of the Turbine Type Flow Meters in the Measurement of Steam Quality and Void," pr

Ruffner, and P. D. Olivier, Wide range, high accuracy flow meter, U.S. Patent, 1997.

Shim, T. J. Dougherty, and H. Y. Cheh, Turbine meter response in two-phase flows, Proc. Int. Conf. Nucl. Eng.

Silverman, S. and Godrich, L. D., (1977), Investigation for vertical, two-phase steam-water flow for three turbin

Stine G.H. (1977), Development of the turbine flowmeter, ISA transaction

Termaat, W. J. Oosterkamp, and W. Nissen, Nuclear turbine coolant flow meter, U.S. Patent, 1995.

Thompson, and J. Grey, Turbine flowmeter performance model, Trans. ASME, J. Basic Eng., 1970.

Van Der Hagen, Proof of principle of a nuclear turbine flowmeter, Nucl. Technol., 1993.

Wadlow D.(1998), Turbine flowmeters, Measurement, Instrumentation and Sensor Handbook

Wright, and C. B. McKerrow, Maximum forced expiratory flow rate as a measure of ventilatory capacity, 1959.

Zheng W. and Tao Z, Computational study of the tangential type turbine flowmeter, Flow Meas. Instrum (2007)

Bibliography Drag Disk Meters

Anderson, J. L. and Fincke, J. R. (1980): Mass flow measurements in air/water mixtures using drag devices and

Averill and Goodrich (1979): Design and performance of a drag Disc and Turbine transducer. For LOFT Experi

Aya (1975): A Model to Calculate Mass flow rates and other quantities of a two phase flow in a pipe with a Den

Baker (1991): Response of bulk flowmeters to multiphase flows. Review paper.

Chen and Felde (1982): Two phase mass flow uncertainty analysis for Therma-Hydraulic test facility instrument

Furrer M. (1986): Strumentazione, metodi e analisi impiegati per la misura della portata in massa in regime bifas

Ginesi (1991), Chosing the best flowmeter, Chem. Eng., NY, 98(4):88-100.

Hardy (1982): Mass flow measurements under PWR reflood conditions in downcomer and at a core barrel vente

Hardy and Smith (1990): Measurement of two phase flow momentum using force transducers

Kamath and Lahey (1981): Transient analysis of DTT rakes. NUREG/CR-2151. and also in Nuclear Engineerin

Kamath, Lahey and Harris (1983): Measurement of virtual mass and Drag coefficient of a disk oscillating sinusc

Lahey, R. T. (1978) Two phase flow phenomena in nuclear reactor technology. Quarterly report NUREG/CR-02

Reimann, John and Moller (1981): Measurement of two phase mass flow rate: a comparison of different techiqu

Sheppard, Long, Tong (1975): Apparatus for monitoring two phase flow . Oak Ridge National Laboratory repor

Sheppard, Thomas, Tong (1981): Effects of flow dispersers upstream of two phase flow monitoring instruments.

Solbrig and Reimann (1980): Behavior of Drag Disc Turbine transducers in steady-state two phase flow. IEEE T

Turnage (1980): Two-Phase Flow Measurements with Advanced Instrumented Spool Pieces. NUREG/CR-1529

Turnage and Jallouk (1978): Advanced Two-Phase Instrumentation Program Quarterly Progress Report. NUREG

Turnage, Davis and Thomas (1978): Advanced Two-Phase Flow Instrumentation Program Quarterly Progress R

www.venturemeas.com

www.engineeringtoolbox.com/target-flow-metersd_ 497.html

www.aaliant.com

Bibliography Differential Pressure Meters

Azzopardi, B. J., Memory, S. B. and Smith, P. (1989) Experimental study of annular flow in a venturi. Proceedi

Baker, C. R., (1991) Response of bulk flow meters to multiphase flow, Proc. I. Mech.E. Part C: J. Mech. Eng. So

Baker, C. R., (2000), Flow measurement handbook, Cambridge University Press.

Chisholm D. , 1969, Flow of incompressible two-phase mixtures through sharp-edged orifices. Journal of Mech

Chisholm D. Research note: Two-phase flow through sharp-edged orifices. Journal of Mechanical Engineering S

Chisholm, D. and Leishman, J. M. (1969) Metering of wet steam. Chem. Process Engng

Clark, C., (1992), The measurement of dynamic differential pressure with reference to the determination of puls

Collier J.G., J.R. Thome, Convective Boiling and Condensation, Oxford Science Press, New York, 1996.

Collins DB, Gacesa M. Measurement of steam quality in two-phase upflow with venrurimeters and orifice plate

De Leeuw R. Liquid correction of venturi meter readings in wet gas flow. In: North sea workshop, 1997.

Fang LD, Zhang T, Jin ND. A comparison of correlations used for Venturi wet gas metering in oil and gas indus

Fincke J. R. (1999), Performance Characteristics of an Extended Throat Flow Nozzle for the Measurement of H

Hewitt, G. F. (1978) Measurement of two-phase flow parameters (Academic Press).

James, R., 1965. Metering of steam-water two-phase flow by sharp-edged orifices. Proc. Inst Mech. Engrs,.

Jitschin W. (2004), Gas flow measurement by the thin orifice and the classical Venturi tube, Vacuum 76

Jitschin, Ronzheimer, Khodabakhshi, Gas flow measurement by orifices and Venturi tubes, Vacuum 53 (1999)

Kanenko, Svistunov, Prostakov, V.V. Lyubchenko, New Venturi tube designs for converter practice, Steel in the

Kegel, T., (2003), Wet gas measurement, 4th CIATEQ Seminar on Advanced Flow Measurement,Colorado Eng

Lin ZH. (1982), Two-phase flow measurements with sharp-edged orifices. International Journal of Multiphase F

Lin ZH. (2003), Gas_liquid two-phase flow and boiling heat transfer. Xi'an: Xi'an Jiaotong University Press

Lockhart RW, Martinelli RC. Proposed correlation of data for isothermal two- phase, two-component flow in pi

Meng , Huang, Ji, Li, Yan (2010), Air-water two phase flow measuremnt using a Venturi meter and an electrical

Miller, R. W., (1996), Flow measurement engineering handbook, McGrawHill

Moura, L.F.M., Marvillet, C., 1997. Measurement of Two-phase Mass Flow Rate and Quality Using Venturi and

Murdock JW. (1962), Two-phase flow measurement with orifices. Journal of Basic Engineering

Oddie, Pearson (2004), Flow-rate measurement in two-phase flow, Annual Reviews of Fluid Mechanics 36

Oliveira, Passos, Verschaeren, van der Geld, (2009) Mass flow rate measurements in gas–liquid flows by means

OMEGA (2005) Complete Flow and Level Measurement Handbook and Encyclopedia®, OMEGA Press

Reader-Harris MJ, Hodges D, Gibson J (2005), Venturi-tube performance in wet gas using different test fluids. I

Steven R (2008), Horizzontally installed cone differential pressure meter wet gas flow performance. Flow Meas.

Steven R. (2006), Horizontally installed differential pressure meter wet gas flow performance review. In: North

Steven R. Liquid property and diameter effects on venturi meters used with wet gas flows. In: International fluid

Steven, R.N., 2002. Wet gas metering with a horizontally mounted Venturi meter. Flow Measurement and Instru

Taitel Y, Dukler AE. (1976), A model for predicting flow regime transitions in horizontal and near horizontal g

Tang, L., Wene, C., Crowe, C. T., Lee, J. and Ushimann, K. (1988) Validation study of the extended length vent

Venturi meter for wet gas metering, Flow Measurement and Instrumentation 14 (2003)

Whalley P.B., Boiling, Condensation, and Gas–Liquid Flow, Oxford University Press, New York, 1987.

Xu L, Jian Xu, Feng Dong, Tao Zhang, On fluctuation of the dynamic differential pressure signal of Venturi me

Zhang, Lu, Yu, An investigation of two-phase flow measurement with orifices for low-quality mixtures, Internat

Zhang, Yue, Huang, Investigation of oil–air two-phase mass flowrate measurement using venturi and void fracti

See also:
ISO-5167:
ISO-5167-1:1991(E) Measurement of fluid flow by means of pressure differential devices.
ISO-5167-1:1991/Amd.1:1998(E) Amendment
ISO-5167: Measurement of fluid flow by means of pressure differential devices inserted in circular
cross-section conduits running full:
   −   Part1: General principles and requirements, Second edition, 2003-03-01, Ref. No.:
       ISO 5167-1:2003(E).
   −   Part2: Orifice plates, Second edition, 2003-03-01, Ref. No.: ISO 5167- 2:2003(E).

- Part3: Nozzles and Venturi Nozzles, Second edition, 2003-03-01, Ref. No.:ISO 5167-3:2003(E).
- Part4:Venturi tubes, Second edition, 2003-03-01, Ref. No.: ISO 5167- 4:2003(E).

Bibliography Impedance Probes

Abouelwafa, Kendall, The use of capacitance sensor s for phase percentage determination in multiphase pipeline

Ahmed and Ismail (2007), Innovative Techniques for two phase flow Measurements, recent Patents on Electrica

Andersen and Bernsten (1988), Quasi-static Profile reconstruction of a Circular Cylinder, Electromagnetic Wave

Andreussi P, Di Donfrancesco A, Messia M. An impedance method for the measurement of liquid hold-up in tw

Azzopardi, Abdulkareem, Sharaf, Abdulkadir, Ijioma (2010), Using Tomography to interrogate gas liquid flow,

Bernier R. J. N. (1982) , Unsteady two-phase flow instrumentation and measurement, PhD Thesis, California Ins

Cao, Chua and Chong (2003), A comparison of PCA, KPCA and ICA for dimensionality reduction in support v

Coney MWE. The theory and application of conductance probes for the measurement of liquid film thickness in

Costigan G. and Whalley P. B. (1996), Slug flow and Regime identification from Dynamic void fraction measur

Cui, Wang, Xu, Zhang (2009), An Integrated ECT/ERT Dual Modality Sensor, IIMT Conference 2009, Singap

Dong, Jiang, Qiao, Xu, 2003, Application of electrical resistance tomography to two-phase pipe flow parameters

Eads, et all (1977), Advanced Instrumentation for Reflood studies, Program Quartely Progress Report, October-

Elkow, Rezkallah (1996), Void fraction measurements in gas–liquid flows using capacitance sensors,Measurem

Emerson dos Reis and Leonardo Goldstein, Jr (2005), A procedure for correcting for the effect of fluid flow tem

Fossa, M., (1998), Design and performance of a conductance probe for measuring the liquid fraction in two-pha

Georgea, Torczynskia, Shollenbergera, O'Herna, Ceccioba (1998), Validation of electrical-impedance tomograph

Giguère, Fradette, Mignonb, Tanguy (2008), "ERT algorithms for quantitative concentration measurement of m

Halliday, Resnick, Walker, Fundamentals of Physics, 5th edition, J. Wiley & Sons, 1997.

Hardy and Hylton (1983), Double-layer impedance string probe for two-phase void and velocity measurements,

Hardy, J. E., (1982), Mass flow measurements under PWR reflood conditions in a downcomer and at a core barr

Hestrony G. (1982), Handbook of multiphase systems, McGraw-Hill.

Huang, Fielden, Green, Beck, A new capacitance transducer for industrial applications, J. Phys. E: Sci. Instrum.

Isaksen, Review of reconstruction techniques for capacitance tomography, (1996)

Jain, Duin and Mao (2000), Statistical pattern recognition: a review

Jaworek, A., Krupa, A. and Trela, M., (2004), Capacitance sensor for void fraction measurement in water/steam

Lemmonier H. (1997), Multiphase Instrumentation: The Keystone of Multidimensional Multiphase Flow Model

Li, Huang, Wang, Li (2008), A new method for the on-line voidage measurement of gas-oil two-phase flow, IEE

Li, Wang and Huang (2007), Application of PLSR to the voidage measurement of gas-oil two-phase flow

M. Wang, Inverse solutions for electrical impedance tomography based on conjugate gradients methods (2002)

Ma, Bei, Lin (1991), An Impedance method to determine void fraction for two phase flow, Nuclear Science. J.

Maxwell JC. A Treatise on Electricity and Magnetism. Oxford: Clarendon Press, 1882.

Merilo M, Dechene RL, Cichowlas WM. Void fraction measurements with a rotating electric field conductance

Olsen (1967), Theoretical and Experimental Investigation of Impedance Void Meter, Kjeller Research Establish

Pietruske, H. and Prasser, H.-M (2007), Wire-mesh sensors for high-resolving two-phase flow studies at high pr

Polydorides N. 2002, PhD thesis, Image reconstruction algorithms for soft-field tomography.

Prasser, H. -M., Böttger, A. and Zschau, J., (1998), A new electrode-mesh tomograph for gas–liquid flows, Flow

Prasser, H.-M., Krepper, E., Lucas, D., Zschau, J., Peters,D., Pietzsch,, G., Taubert, W., Trepte, M., (2000), Fast

Prasser, H.-M., Misawa, M. and Tiseanu, I., (2005), Comparison between wire-mesh sensor and ultra-fast X-ray

Prasser, H.-M., Zschau, J.,Peters, D., Pietzsch, G., Taubert, W., Trepte, M., (2002), Fast wire-mesh sensor for ga

Stott, Green, Seraji, Comparison of the use of internal and external electrodes for the measurement of the capaci

Su, Zhang, Peng, Yao, Zhang, (2000), The use of simultaneous iterative reconstruction technique for electrical c

Tan, Dong, Wu (2007), Identification of gas/liquid two-phase flow regime through ERT-based measurement and

Tibirna, Edouard, Fortin, Larachi, (2006), Usability of ECT for quantitative and qualitative characterization of tr

Tollefsen, Hammer, Capacitance sensor design for reducing errors in phase concentration measurements, Flow N

Trafalis, Oladunni and Papavassiliou (2005), Two-phase flow regime identification with a multiclassification Su

Tsochatzidis NA, Karapantios TD, Kostoglou MV, Karabelas AJ. A conductance method for measuring liquid fr
.

Vapnik V. N. (1998), Statistical learning theory, New York: Wiley

Wang et all. (1991), Research report: an improved EIT data protocols, UMIST

Wang M. (2002), Inverse Solution for EIT based on a Coniugate Gradients Methods, Measurement Science and

Wang M. (2007), Voidage Measurement of Gas-Oil two phase flow, Chemical Engineeering

Wang W. W. (2007), Voidage Measurement of Gas-Oil Two-phase Flow

Warsito, Fan (2001), Measurement of real-time flow structures in gas–liquid and gas–liquid–solid flow systems

Wu, Li, Wang and Williams, A Study on the Characterization of Air-water Two-phase Vertical Flow by Using E

Yang W.Q., Peng L. (2003), Image reconstruction algorithms for electrical capacitance tomography.

Yang, Stott, Beck (1994), High frequency and high resolution capacitance measuring circuit for process tomogra

Zhao, Fu, Li, Wang (2002), An image reconstruction algorithm based on a revised regularization method for ele

Bibliography Flow Pattern Recognition Techniques

Albrecht R. W. et al. (1982) Measurement of two-phase flow properties using the nuclear reactor instrument, Pro

Barnea D., Shoham O., Taitel Y. and Dukler A. E. (1980), Flow pattern transition for gas-liquid flow in horizont

Bennett A. W., Hewitt G. F., Kearsey H. A., Keeys R. K. F. and Lacey P. M. C. (1965), Flow visualization studi

Bergles A. E., Roos J. P. and Bourne J. G. (1968), Investigation of boiling flow regimes and critical heat flux, N

Cooper K. D., Hewitt G. F. and Pinchin B. (1963), Photography of two-phase flow, AERE-R4301
.
Delhaye J.M., Giot M and Reithmuller M.L. (1981) Thermohydraulics of Two-Phase Systems for Industrial Des

Dukler A. E. and Taitel Y. (1977) Flow regime transitions for vertical upward gas liquid flow: A preliminary ap

Hewitt G. F. and Roberts D. N. (1969) Studies of two-phase flow patterns by simultaneous X-ray and flash phot

Hubbard M.G. and Dukler A. E. (1966) The characterization of flow regimes for horizontal two-phase flow, Pro

Jones and Zuber (1975), The interrelation between void fraction and flow patterns in two-phase flow, Internation

Jones O. C. and Zuber N. (1975) The interrelation between void fraction fluctuations and flow patterns in two-ph

Jones O.C. and Zuber N. (1974) Statistical methods for measurement and analysis in two-phase flow, Proceeding

Keska J.K. (1993), Experimental investigation of spatial concentration spectra of a solid in a slurrying horizonta

Keska Jerry K. and Williams Brian E. (1998), Experimental comparison of flow pattern detection techniques for

Keska, Fernando, Hamer (1992), Experimental study of temporal fluctuation of physical parameters in an air±wa Nuclear Society, La Grange Park, Illinois

Keska, Fernando, Rohan, Hamer, Matthew (1992), Experimental investigation of average parameters for air±wa

Nencini F. and Andreussi P. (1982), Studies of the behavior of disturbance waves in annular two-phase flow, Th

Ohlmer, Fortescue, Riebold, Bors, Immink, Wesser (1984), Two-phase flow identification by calibration with s

Person, Application of an optical scatterer to the study of two-phase flow in vertical pipes, in: J.M. Delhaye, G.

Rouhani S.Z. and Sohal M.S. (1982), Two Phase flow patterns: A review of research results, Progress in Nuclea

Saiz-Jabardo and Boure (1989), Experiments on void fraction waves, International Journal of Multiphase Flow 1

Staub F. W. and Zuber N. (1964), A program of two-phase flow investigation, General Electric Co., Report, EUI

Taitel Y. (1977), Flow pattern transition in rough pipes, Int. J. Multiphase Flow 3, 597-601.

Taitel Y. and Dukler A. E. (1976), A model for predicting flow regime transition iii horizontal and near horizont

Taitel Y., Barnea D. and Dukler A. E. (1980), Modeling flow pattern transitions for steady upward gas-liquid flo

Vince M.A. and Lahey R.T. (1980), Flow regime identification and void fraction measurement techniques in two